Tyrosine Kinase Inhibitors in Triple Negative Breast Cancer.

A Thesis submitted for the degree of Ph.D.

by Brendan Martin Corkery, MB. BCh. BAO.

September 2010

The work in this thesis was carried out under the supervision of

Dr. Norma O'Donovan,
Prof. Martin Clynes & Prof. John Crown

National Institute of Cellular Biotechnology
School of Biotechnology
Dublin City University

I hereby certify that this material, which I now submit for assessment on the programme of study leading to the award of Ph D. is entirely my own work, that I have exercised reasonable care to ensure that the work is original, and does not to the best of my knowledge breach any law of copyright, and has not been taken from the work of others save and to the extent that such work has been cited and acknowledged within the text of my work.

Signed: _____ **ID No.:** 57117390

Date: _____

ACKNOWLEDGEMENTS

First of all, I would like to express my profound gratitude to my supervisors. Dr. Norma O'Donovan has been such a wonderful example of how to be a good scientist, and an excellent teacher. I have no doubt that the support and patience you have demonstrated over the last 4 years has been essential for my progress through this research. Your tirelessness in overseeing all aspects of this work, great and small, and helping me with all of my many questions, have been always appreciated. Prof. John Crown has been an inspiring and motivated mentor, and has demonstrated to me what it takes to be an outstanding clinician and researcher. I have gained a huge amount of experience in my ongoing medical education. My presentation skills – while still a work in progress, I might agree! – are certainly much the better for your advice. Furthermore, I am most grateful for the opportunity to carry out this research, and indeed I remember that it was your lectures while I was a student in St. Vincent's University Hospital that encouraged me to begin this journey in oncology. Prof. Martin Clynes also deserves great thanks for affording me the opportunity to be involved in research at the NICB, and has always been available for advice and support during the project. The positive experiences I have had at the NICB are a testament to the leadership you have given since you set up the centre.

Many people have contributed to aspects of this research. Dr. Annemarie Larkin provided contributed much advice and experience in carrying out the immunohistochemistry – through the good and the bad times! The know-how of Sandra Roche and Dr. Robert O'Connor in drug accumulation assays was of immense help. Dr. Paul Dowling supervised the proteomics experiments, and his expertise was vital in this aspect of the research. The assistance of many others when I was learning cell culture and experimental techniques should be acknowledged – Dr. Brigid Brown, Dr. Alex Eustace, Dr. Denis Collins, and Dr. Aoife Devery, in particular deserve acknowledgement in this regard.

As I've said, one of the very positive experiences I have had at the NICB has been the many friendships that have developed during my time here. So in addition to everyone mentioned above – colleagues and friends - I want to express my thanks to everyone that I have met at the NICB.

I have to acknowledge the support and love of my parents, John and Mary. You are in so many ways the reason I am able to sit here and write this acknowledgement. And also thanks to my brothers Dan, Fr. Seán, and my sister Patricia for informing so much of who am I.

I want to thank all of my friends that have supported me during this research. For being my friends when I needed it, and for putting up with me when I wasn't able to be around as much I would have liked. In particular, shout outs go to Eugene, John, Dolores (my Dublin mammy), David, Therese, and to the rest of you – I hope you know who you are.

And lastly, but not least, to Colum. You have been a greater support than you know. Thank you for all of the understanding, kindness and patience involved in getting me over the finish line!

Table of Contents

ABSTRACT

Basal-like breast cancers are generally negative for estrogen and progesterone receptor expression and HER-2 amplification ('triple negative' breast cancer, TNBC), and express basal cytokeratins 5/6, and EGFR (epidermal growth factor receptor). No targeted therapy options are currently approved for this subgroup of patients. The main aim of this study was to assess the potential role of selected inhibitors in TNBC, including the small molecule tyrosine kinases inhibitors of EGFR gefitinib and erlotinib, the monoclonal antibody against EGFR cetuximab, and the multi-target tyrosine kinase inhibitor dasatinib.

Significantly higher EGFR expression was detected in TNBC compared to HER-2 positive breast cancer cell lines. EGF treatment stimulated phospho-EGFR which was inhibited by gefitinib. Sensitivity to gefitinib was associated with decreases in P-MAPK and P-Akt, and G1 cell cycle arrest. Combined treatment with gefitinib and chemotherapy was more effective than either gefitinib or chemotherapy alone.

EGFR and P-EGFR expression were examined by immunohistochemistry in 101 breast tumours. Only 6 % were positive for EGFR and 3 % for P-EGFR. Sixteen of the tumours were triple negative, with 31 % and 6 % rates of positivity for EGFR and P-EGFR, respectively.

It has been reported that dasatinib preferentially inhibits growth in TNBC cell lines compared to other breast cancer subtypes. A dasatinib-resistant variant of the triple negative MDA-MB-231 cell line was established (231-DasB). A dose-dependent decrease in P-Src levels in response to dasatinib was observed in MDA-MB-231 but not in 231-DasB. Proteomic analysis identified 78 significantly altered proteins. Six proteins were uniquely altered in MDA-MB-231 and 9 proteins were uniquely altered in 231-DasB. ANXA1, which has been implicated in breast carcinogenesis previously, was significantly increased in the variant cell line in response to dasatinib. While ANXA1 siRNA knockdown decreased proliferation in MDA-MB-231, it did not significantly alter response to dasatinib.

ABBREVIATIONS

95 % CI	95 % Confidence Interval
ACN	Acetonitrile
ADCC	Antibody-Dependent Cellular Cytotoxicity
ATCC	American Type Culture Collection
ANOVA	Analysis of variance
ANXA1	Annexin A1
BCA	Bicinochoninic acid
BCRP	Breast Cancer Resistance Protein (ABCG2 gene)
BSA	Bovine serum albumen
Btf3	Basic transcription factor 3
BVA	Biological variation analysis
cDNA	complementary deoxyribonucleic acid
CAS	Crk-associated substrate
CBB	Coomassie Brilliant Blue
CCT3	Chaperonin containing TCP1, subunit 3
CHAPS	3-[(3-cholamidopropyl)dimethylammonio]-1-propanesulfonate
CI	Combination Index
Cis	Cisplatin
CK	cytokeratin
c-Src	Cellular Src
D	Docetaxel
DIA	Differential in-gel-analysis
DIGE	Difference in gel electrophoresis
DFS	Disease-free survival
DMF	Dimethylformamide
DMSO	Dimethyl sulfoxide
DNA	Deoxyribonucleic acid
DPX	Di(nbutyl) Phthalate in Xylene
DTT	Dithiothreitol
EDTA	Ethylenediaminetetraacetic acid
EGF	Epidermal Growth Factor

EGFR	Epidermal Growth Factor Receptor (erbB-1)
ELISA	Enzyme-Linked Immunosorbent Assay
EMT	Epithelial-to-Mesenchymal Transition
ENO1	Enolase 1
ER	Estrogen Receptor
FAK	Focal Adhesion Kinase
FCS	Fetal Calf Serum
FGFR3	Fibroblast growth factor receptor 3
G	Gefitinib
Grb	Growth Factor Receptor Bound
GLXR3	Glutaredoxin 3
H&E	Hematoxylin and eosin
HEPES	4-(2-hydroxyethyl)-1-piperazineethanesulfonic acid
HePC	Hexadecylphosphocholine
HER	Human Epidermal growth factor Receptor (erbB)
HER-2	Human Epidermal Growth Factor Receptor 2 (erbbB-2, HER-2/neu)
HR	Hazard Ratio
Hsp90	Heat Shock Protein 90
IC_{50}	Half maximal inhibitory concentration
IEF	Isoelectric focus
IHC	Immunohistochemistry
IMPDH2	Inosine monophosphate dehydrogenase 2
IP	Immunoprecipitation
IPF53	Trytophanyl-tRNA synthetase (WARS)
JAK2	Janus tyrosine kinase 2
Kd	Dissociation constant
KRAS	Kirsten rat sarcoma viral oncogene homolog
LC-MS	Liquid Chromatography tandem Mass Spectrometry
MALDI	Matrix-assisted laser desorption/ionisation
MAPK	Mitogen-activated protein kinase
MBC	Medullary Breast Cancer
MDR1	P-glycoprotein (P-gp), (ABCB1 gene)
mRNA	messenger Ribonucleic acid
MS	Mass Spectrometry

mTOR	Mammalian Target Of Rapamycin
NCBI	National Center for Biotechnology Information
NOS	Not otherwise specified
NSCLC	Non-small cell lung cancer
OR	Odds Ratio
P	Carboplatin
P-	Phosphorylated
p53	protein 53
PARP	Poly (ADP-Ribose) Polymerase
PBS	Phosphate-buffered saline
pCR	Pathological Complete Response
PDGFR	Platelet-derived growth factor receptor
PDK1	3'-phosphoinositide-dependent kinase 1
PH	Plekstrin homology
PI3K	Phosphatidylinositol-3-kinase
PKB	Protein Kinase B
PKC	Protein Kinase C
PLC-γ	Phospholipase C-gamma
PMSF	Phenylmethylsulfonyl fluoride
ppm	Parts per million
PR	Progesterone Receptor
PTEN	Phosphatase and tensin homolog gene/protein
RR	Relative Risk
RNA	Ribonucleic acid
RPMI-1640	Roswell Park Memorial Institute-1640 medium
SAM	Significant Analysis of Microarrays
SD	Standard Deviation
SDS	Sodium dodecyl sulfate
SHC2	Src homology 2
siRNA	Small interfering RNA
*t*BME	*tert*-Butyl Methyl Ether
TALDO1	Transaldolase 1
TEMED	Tetramethylethylenediamine
TFA	Trifluoroacetic acid

TMA	Tissue Microarrays
TNBC	Triple Negative Breast Cancer
TOF	Time of flight
TP53	Tumour protein 53 (also called p53)
TGF	Transforming Growth Factor
VEGF	Vascular Endothelial Growth Factor
VEGFR	Vascular Endothelial Growth Factor Receptor
YB-1	Y-box bind protein

Chapter 1

INTRODUCTION

1.1 BREAST CANCER

Cancer is the third commonest cause of death worldwide (estimated 11.8 % for women and 13.4 % for men in 2004), behind cardiovascular disease (31.5 % for women and 26.8 % for men) and infectious and parasitic diseases (15.6 % for women and 16.7 % for men) [1]. Breast cancer is the most common female malignancy in the Western world, and is the commonest cause of cancer death of women [2]. In Ireland, breast cancer is the most common invasive cancer in women (30 %) excluding non-melanoma skin cancer (www.ncri.ie). In 2007, there were 2463 cases of female breast cancer (16.9 % of all cancers in women). The most recent mortality data available is from 2005, when there were 696 deaths from breast cancer (all female). The average five year survival for women with breast cancer in Ireland for 2001 – 2006 was 82.5 % (95 % confidence interval 81.3 – 83.6).

1.2 TRADITIONAL CLASSIFICATION OF BREAST CANCER

The traditional cellular classification of breast cancer has been based on the histological appearances of the various breast tumour subtypes. A complete list of subtypes is given in Table 1.1. The main subtype is invasive ductal carcinoma which accounts for approximately 70 to 80 % of all primary breast cancers. This classification, based on histo-pathological characteristics, does not reflect disease outcome. However, this classification, combined with other information such as tumour size, lymph node involvement, and disease staging, is used to select adjuvant options following appropriate surgical intervention. For the past number of decades, adjuvant treatment has consisted of combinations of chemotherapy drugs. The recognition of the prognostic importance of hormone receptors (estrogen (ER) and progesterone (PR)), and the benefits of hormonal therapies such as tamoxifen in responsive tumours, has led to the routine analysis of these receptors in the clinical setting. More recently, HER-2, which is present in approximately 25 % of breast cancers, has been shown to confer a more aggressive breast cancer phenotype [3]. Trastuzumab, a monoclonal antibody against the extracellular domain of HER-2, has significantly improved outcomes for patients with HER-2 over-expressing breast cancer [4].

Table 1.1 Breast tumour subtypes adapted from AJCC Cancer Staging Manual (2002) [5]

	Carcinoma, NOS (not otherwise specified)
Ductal	Intraductal (*in situ*)
	Invasive with predominantly intraductal component
	Invasive, NOS
	Commedo
	Inflammatory
	Mucinous
	(colloid)
	Papillary
	Medullary with lymphocytic infiltrate
Lobular	Scirrhous
	Tubular
	Other
Nipple	Paget's disease,
	NOS
	Paget's disease with invasive ductal carcinoma
	Paget's disease with intraduct carcinoma
Other	Undifferentiated
Atypical	Phyllodes
	tumour
	Primary
	lymphoma
	Angiosarcoma

1.3 MOLECULAR CLASSIFICATION OF BREAST CANCER

In recent years, an evolution in the classification of breast cancer has been made possible by gene expression analysis. This approach involves hierarchical cluster analysis based on the expression pattern of a chosen set of genes. The initial work was reported in 2000 by Perou at al., who performed cDNA microarray profiling of 65 breast tumours from 42 individuals, including 20 paired pre- and post-treatment samples, and 2 tumours paired with lymph node metastases [6]. A primary distinction was made between ER positive and ER negative tumours. ER-positive tumours express ER, ER-responsive genes, and other genes that encode proteins characteristic of luminal epithelial cells, and are therefore usually referred to as the 'luminal' subgroup [6, 7]. ER-negative tumours were subdivided into three groups: HER-2 positive, basal-like tumours, and so-called 'normal breast-like' [6, 7].

HER-2 positive tumours express high levels of genes located in the HER2 amplicon on 17q21, including HER-2 and growth factor receptor-bound protein 7 (GRB7), a high level of nuclear factor (NF)-κB, and the transcription factor GATA4, and lack expression of ER and GATA3 [8, 9].

Basal-like tumours frequently lack ER and HER-2, and express genes characteristic of basal epithelial cells, including metallothionein 1X, fatty acid binding protein 7, FOXC2, activating transcription factor 3, CK5 and CK17, and P-cadherin [7].

The normal breast-like subgroup resembled normal breast tissue, with high expression of genes characteristic of adipose cells, and non-epithelial cell types [7].

Analysis of the ER positive/luminal tumours, has sub-classified these into A, B, and C [10]. The luminal A subtype (32 tumours) had the highest expression of the ERα gene, GATA binding protein 3, X-box binding protein 1, trefoil factor 3, hepatocyte nuclear factor 3α, and estrogen-regulated LIV-1. Luminal B (5 tumours) and luminal C (10 tumours) both showed low to moderate expression of the luminal-specific genes, including the ER cluster. Interestingly, luminal C was distinguished from A and B by

the high expression of a novel set of genes of unknown coordinated function, which they share with the basal-like and HER-2 subtypes.

This sub-grouping of breast tumours has been confirmed in other studies [11-16], and the molecular classification continues to be investigated and refined. For example, work by Herschkowitz *et al.* recently identified a fifth molecular group of human breast cancers. The authors characterised mammary tumour gene expression in 13 murine models. These were cross-compared with human breast microarrays (232 microarrays representing 184 primary breast tumours and 9 normal breast samples) [17]. In addition to the 4 human subtypes previously identified (basal-like, luminal, HER-2+/ER-, normal-like), a fifth subgroup was putatively identified ('claudin-low'), based on the murine models. Claudins are a family of proteins involved in tight junctions and cell-cell adhesion [18]. These tumours were phenotypically triple negative, but with characteristically decreased expression of claudin proteins. Hennessy *et al.* characterised this subgroup in 2009 [19]. The claudin-low breast cancer subtype are typically triple negative and are characterised by low expression of GATA3-regulated genes and of genes responsible for cell-cell adhesion with enrichment for markers linked to stem cell function and epithelial-to-mesenchymal transition (EMT) [19].

The basal-like and HER-2 positive breast cancer subtypes have been associated with the shortest survival times [10]. This review will focus on the basal-like subgroup of breast cancers.

1.4 IDENTIFICATION OF BASAL-LIKE BREAST CANCERS

The molecular profile of basal-like breast cancers was initially described by Perou *et al.* in 2000 [6]. Using a subset of 496 genes (the 'intrinsic' gene subset) the tumour samples were divided into ER positive (luminal, expressing luminal cell keratins 8/18 by immunohistochemistry) and ER negative subgroups. A subgroup of 6 ER negative tumours was found to express many genes characteristic of breast basal epithelial cells. This was confirmed by immunohistochemical analysis for basal cytokeratins (CK) 5/6

and 17. HER-2 positive tumours were identified as a separate subgroup of ER negative breast tumours.

A follow-up study from the same group sought to classify breast tumours based on variations in gene expression patterns [10]. 78 cancers, 3 fibroadenomas, and 4 normal breast tissues were analysed, using an intrinsic set of 456 cDNAs. This study also reported that these tumours could be classified as basal-like, HER2-overexpressing, and normal breast-like. At least two subgroups of luminal/ER-positive tumours were identified, which were reliably clustered in relation to a gene set reflecting the intrinsic properties of the tumours, and a gene set that correlated with patient outcome. The basal-like subgroup was characterised by low to absent gene expression of ER and several additional transcriptional factors expressed in the luminal/ER positive cluster, as well as high expression of keratins 5 and 17, laminin, and fatty acid binding protein 7.

TP53 status, which is associated with poor prognosis, and poor response to systemic therapy, was examined in 69 of the tumours used in this study, by gene expression [10]. A significant difference in mutation status was found between the subgroups ($p < 0.001$). Luminal A contained 13 % mutated tumours, whereas 9/11 (82 %) of the basal-like subgroup were TP53 mutated tumours, and 5/7 (71 %) of the HER-2 tumours. Of note, the TP53 gene was not included in the intrinsic set tested.

In the same study, Perou *et al.* used Significant Analysis of Microarrays (SAM, [20]) to correlate gene expression with patient survival. Using a list of 264 cDNAs, 71 of the 78 tumours could be organised into the same main subgroups with this approach as with the intrinsic subset of 456 clones (with 81 genes overlapping). Univariate analysis was performed on the resulting 5 hierarchical groups (49 patients), and Kaplan-Meier curves were produced (Figure 1.1). In summary, this study found that the basal-like and HER-2 subgroups had significantly shorter survival times [10].

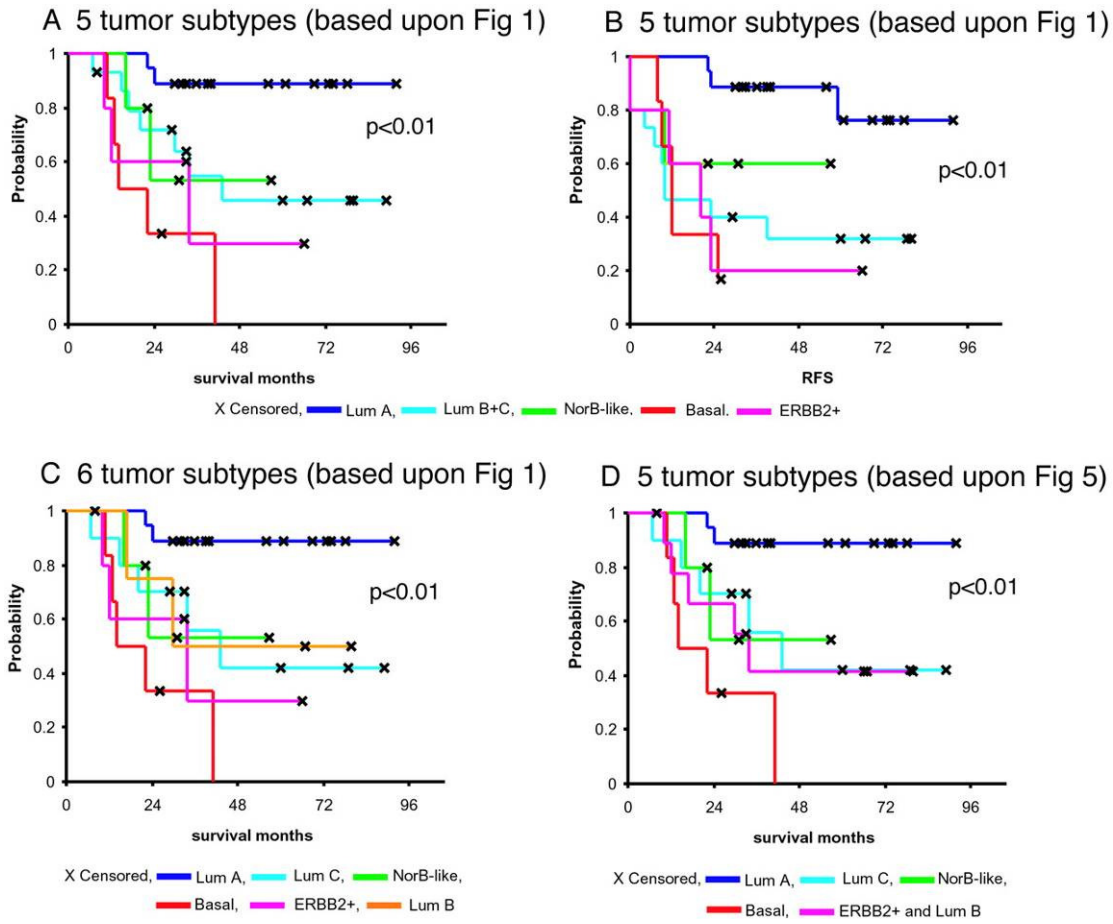

Figure 1.1 Overall and relapse-free survival analysis of the 49 breast cancer patients, uniformly treated in a prospective study, based on different gene expression classification. (A) Overall survival and (B) relapse-free survival for the five expression-based t tumour subtypes based on the classification (luminals B and C were considered one group). (*C*) Overall survival estimated for the six-subtype classification with the three different luminal subtypes presented (*D*) Overall survival based on the five-subtype classification presented (from Sørlie at al. [10]).

Further data from Sørlie *et al.* in 2003 again confirmed the robustness of this classification of breast cancers [21]. In this work, the authors used tumour samples from two independent studies of response to chemotherapy in locally advanced breast cancer [22, 23], an "extended Norway/Stanford cohort" which extended the samples used in their previous studies, and re-analysed data from two further independent studies [24, 25]. The tightest correlation in gene expression in the Norway/Stanford cohort and in the van't Veer *et al.* [24] data was in the basal-like subgroup. A significant observation in the van't Veer data was that all the tumours with BRCA1 mutations (18 carriers) were classified as basal-like. The hierarchy with the West *et al.* data [25] was less well correlated, although this may be due to the fact that only approximately half of the genes from the 'intrinsic' gene list used in the West *et al.* study was used in this study. Univariate analysis of clinical outcomes in this study confirmed that the basal and HER-2 groups showed much shorter disease-free survival. However, the West *et al.* data was not included in analysis of clinical outcomes based on subtype, as follow-up data were not available.

Expression of the basal cell keratins 5/6 and 17 have been found to be characteristic of the basal-like subgroup of breast carcinomas, and are associated with poorer clinical outcomes [13, 26]. Van de Rijn *et al.* examined basal cytokeratin expression in 564 breast tumours [26]. Sixteen percent (90/564) cases stained with either CK 5/6 and/or CK 17, and 51 of these 90 were positive for both. Follow-up data was available on 505 of the 564 cases (range 1 – 151 months, mean 65.9 months, median 63 months). The *absence* of cytokeratins 5 or 17 conferred a significantly better prognosis than the presence of either ($p = 0.012$). Expression of these "basal" cytokeratins was associated with a poor prognosis independent of tumour size, tumour grade, or staining for ER, HER-2, or GATA-3. Malzahn *et al.* have also reported that CK 17 expression in ER negative ductal breast carcinomas was associated with short overall and disease free survival [27]. Van de Rijn *et al.* found that in normal breast tissue, cytokeratins 5/6 and 17 stain the basal layer of breast ductal epithelium (while keratins 8 and 18 stain luminal cells)

Using high-throughput protein expression analysis of tissue microarrays El-Rehim *et al.* examined a panel of epithelial biomarkers in a series of 1,076 invasive breast cancers [13]. The specific basal phenotype markers included CK 5/6, CK 14, SMA,

and p63 ab-1. The authors classified the carcinomas into the broad categories previously described and 6 separate groups were assigned:

- Groups 1 (n = 336 (31.2 %)) and 2 (n = 180 (16.7 %)) were luminal and hormone receptor positive
- Group 3 (n = 234 (21.7 %)) was HER-2 driven, hormone receptor weak/negative, and MUC1 positive with altered E-cadherin expression
- Group 4 (n = 4 (0.4 %) was hormone receptor negative; expressed basal markers and had the highest levels of EGFR expression (however this group had only a small number of tumours, making generalisation difficult)
- Group 5 (n = 183 (17 %)) was p53-driven, hormone receptor negative, but in general basal marker positive
- Group 6 (n = 139 (12.9%)) was HER-2 positive, hormone receptor weak/negative, MUC1 weak/negative, E-cadherin strong.

HER-2 expression in group 5 was uncommon. BRCA1 alteration was a common feature in this predominantly basal-like group 5, (and in the 4 tumours in group 4). Expression of p53 protein was confined mainly to this group. It was noted that strong combined expression of both P53 and HER-2 was rare in the entire series analysed, suggesting possible parallel pathways with different, potentially overlapping mechanisms in breast carcinogenesis. The tumours in group 5 were also found to have the most aggressive phenotype of those studied, and to have a significantly younger age profile compared to the other groups ($p = 0.004$).

1.4.1 CLASSIFICATION OF BREAST CANCER CELL LINES

The gene expression profiling established by Perou, Sørlie and El-Rehim has been used primarily to categorise breast tumour tissues [6, 10, 13, 21]. Charafe-Jauffret *et al.* sought to use the established molecular classification of breast cancers to better characterise a panel of 31 breast cancer cell lines, primarily to discover potential new markers to apply to tumour analysis, with a particular focus on establishing new markers for the basal-like breast cancer subtype [28]. The authors combined the

intrinsic gene set of Sørlie *et al.* [10] with cell line marker studies by Perou *et al.* [6] and Ross *et al.* [29]. A resultant 364 set (centroid) of common genes was tested. Good correlation was observed with the results of their microarray analysis and the previously described breast cancer subtypes. The basal gene cluster included cytokeratins (KRT4, 5, 6A, 6B, 13, 14, 15, 16, 17), integrins (ITGA6, ITGB4, ITGB6) and other genes (LAMB3, LAMC2, TRIM29, S100A2, SLP1, ANXA8, COL17A1, BNC1). Eight cell lines were found to be basal (SUM-225, HME-1, MCF10A, 184B5, SUM-149, HCC38, HCC1937, BT20). Differential gene expression analysis between the basal and luminal subtypes was performed, and supervised analysis accurately predicted whether a cell line was in the basal, or luminal class ($p < 0.001$). Of 1,233 genes differentially expressed, 665 genes were over-expressed in the basal cell lines, including those coding for cytokeratins (KRT5, 6, 14, 17), tyrosine kinases (MET, EGFR, LYN), ERM protein moesin (MSN), transcription factor ETS1, transmembrane hyaluronate receptor CD44, CD10, caveolae proteins CAV1 and CAV2, GPI-anchored proteins CD14, CD58 and CD59, annexins, metalloproteinases, and WNT pathway inhibitor secreted Frizzled related protein-1 (SFRP1).

Importantly, four of the analysed cell lines were found to be mesenchymal (SK-BR-7, MDA-MB-157, MDA-MB-231, Hs578T). Charafe-Jauffret *et al.* found only 227 genes which discriminated between the mesenchymal and basal-like cell lines, whereas 1,309 genes were identified as discriminators between mesenchymal and luminal subtypes. This mesenchymal subtype has not been identified in tumour samples and was close to the basal-like subtype in terms of gene classification in these cell lines. One of the mesenchymal cell lines – Hs578T – was representative of this subtype, and was derived from the rare carcinosarcoma (also called metaplastic carcinomas, sarcomatoid carcinomas, or spindle cell carcinomas). These cells expressed basal and myoepithelial markers, suggesting they may represent epithelial-to-mesenchymal transition (EMT). The authors confirmed the profiles of the cell lines by comparing their data with that of Ross and Perou [6, 29] using a 364-gene set, and found perfect concordance for discriminating between luminal, basal, and mesenchymal gene clusters. Interestingly, Farmer *et al.* suggested that EMT of tumour epithelial cells is associated with increased stromal gene expression [30]. The authors suggested that this stromal 'metagene' cluster (represented by the gene DCN (decorin)) may be associated with increased chemoresistance.

Finak *et al.* derived a 26 gene stroma-derived prognostic predictor (SDPP) based on 53 primary breast tumours, and derived gene signatures based on clinical outcomes [31]. Interestingly, Wennmalm et al. combined the SDPP with a number of breast cancer datasets, and observed that 76 % of the poor outcome cluster (supervised analysis) were basal-like tumours [32] , as defined by Sørlie et al. [10]. The overlap was 91 % by unsupervised analysis. These data suggest that these genes may be associated with the basal-like subtype, although Finak *et al.* felt that it was incorrect to compare the Sørlie centroids with their stromal data as many of the genes identified by Sørlie *et al*. were epithelial [32].

1.4.2 BASAL-LIKE BREAST CANCER AND BRCA1

Familial breast cancer accounts for approximately 5 – 10 % of all breast cancers [33, 34]. Germline mutations of the tumour suppressor genes BRCA1 and BRCA2 have been shown to have a significant role in the majority of cases of familial breast cancer. Women with germline heterozygous mutations in BRCA1 or BRCA2 have an elevated risk of developing breast (up to 85 %), ovarian, and other types of cancer [35].
BRCA1-related breast cancers tend to be high grade [36], node negative [37] tumours that lack ER, HER-2 [38], $p27^{Kip1}$ [39], but are positive for p53 [40], cyclin E, and cytokeratins 5/6 [21, 41]. The association between high p53 expression and the basal-like subgroups of breast cancers has been frequently observed [6, 10, 13, 15, 24, 28, 42].

The relationship between high p53 expression, BRCA1 mutation, and the basal-like breast cancer phenotype was studied by Foulkes *et al.* [43], in a series of 309 consecutive cases of Ashkenazi Jewish women with primary, non-metastatic breast cancer. BRCA1 mutation status was assessed, and compared to CK5/6, and variables including cyclin E, p27, p53 and Glomeruloid-Microvascular-Proliferation (GMP) which are features of BRCA1 mutation. Adequate follow-up data were available for 247 women. There were 27 BRCA1 mutation carriers in this cohort, and 95 tumours expressed the basal markers CK5/6. CK5/6 expressing tumours were more likely to be ER negative, p53, GMP, and cyclin E positive, which was consistent with the basal

phenotype. A borderline correlation with HER-2 over-expression and lack of $p27^{Kip1}$ was noted. HER-2 expression did not vary with BRCA1 status overall. However, sub-analysis of the relationship between HER-2 over-expression and p53 expression found that it was much less likely in CK5/6 positive tumours (OR 1.9 (95% CI, 0.63 – 5.9, p = 0.25) than in CK5/6 negative tumours (OR 15.0 (95% CI, 4.2 – 54)). The authors concluded that basal tumours tend to have low HER-2 and high p53, as well as high levels of cyclin E and GMP, low expression of ER and p27.

Univariate analysis in this study showed associations between a significantly poorer disease-specific outcome and expression of CK5/6 ($p = 0.0045$), cyclin E ($p < 0.0001$), p53 ($p = 0.0002$), and lack of p27 ($p = 0.0046$). BRCA1 mutation did not have a significant impact on outcome ($p = 0.20$). Using multivariate analysis, GMP (any expression *versus* no expression) conferred the highest relative risk (RR) for breast cancer death (RR = 2.34; $p = 0.0002$). CK5/6 positive tumours were less likely to be node positive when large in size, even though they were associated with a worse outcome.

Of note in this study, p53 status was determined by immunohistochemistry (IHC) rather than cDNA sequencing. The failure of IHC to detect p53 mutations in 33 % of cases, and a 30 % false positive rate of 30 % for IHC have been reported [44]. These data suggest that determination of p53 status by IHC is suboptimal, and correlation of the p53 findings in this study should be interpreted with caution.

A population based study of 496 invasive breast cancer cases from the Carolina Breast Cancer Study reported a 25 % (84/496) frequency of p53 mutations by sequencing analysis [45]. The frequency of p53 mutations were higher in basal-like tumours (44 %) and HER-2 positive/ER negative tumours (43 %), compared to luminal A (23 %) and luminal A (15 %) subtypes. The difference in frequency was statistically significant for the basal-like compared to the luminal A subtypes ($p < 0.001$).

1.4.3 MEDULLARY BREAST CANCERS AS A SUBGROUP OF BASAL-LIKE CARCINOMAS

Medullary breast cancers (MBC), as traditionally defined, represent about 2% of all invasive breast cancers. MBCs have a high rate of p53 mutations [46]. As noted in section 1.4.3 above, p53 is characteristically over-expressed in basal-like breast cancers. A comparison of MBCs and basal-like cancers by Vincent-Salomon *et al.* [47] argued that MBCs are a subgroup of basal-like cancers. The authors used a series of 33 MBCs and 26 basal-like cancers. ER, PR, TP53, Erb-B2, EGFR, CK5/6, CK14, CK8/18, and CD117 (a KIT epitope) expression were measured by immunohistochemistry and sequence analysis was performed for TP53 mutations. No significant difference ($p > 0.05$) in the rate of p53 mutations was found between MBCs (77 %, 20/26) and basal-like cancers (83 %, 20/24). Also, no significant immunophenotypic differences were found between the groups for CK14, p53, CK8/18, EGFR and KIT. Of note, CK5/6 was significantly more frequently expressed in MBCs (94 %, 30/32) compared to basal-like breast cancers (56 %, 14/25), ($p = 0.0007$). There were a large number of chromosomal alterations in common in both groups. These data suggest that MBCs belong to the basal-like phenotype.

1.5 TRIPLE NEGATIVE BREAST CANCER (TNBC)

The molecular phenotyping of basal-like breast cancer is well established. The most relevant biological markers in the clinic at present are the estrogen and progesterone hormone receptors (ER, PR) and HER-2 (Erb-B2). It has been frequently observed that the so-called "triple negative" (ER, PR, HER-2 negative) breast cancer patients tend to have poorer outcomes compared to other groups of breast cancer. This observation correlates well with the poorer prognosis of basal-like breast cancers (which frequently lack ER, PR, HER-2 expression).

The question of whether the triple-negative phenotype and the molecular basal-like subgroup of breast cancers are equivalent is being addressed. Nielsen at al [15] sought to characterise basal-like breast cancers using immunohistochemistry, and to determine prognostic significance, with the aim of developing a clinically applicable assay for identification of basal-like tumours. Using a panel of 21 basal-like tumours from Sørlie *et al.* [21], a 'typical' profile of ER negativity, HER-2 negativity, basal cytokeratins, EGFR +/-, and c-KIT positivity was found by microarray analysis and immunohistochemistry. An additional 930 patient cohort of samples on TMAs were stained for ER, HER-2, CK5/6 and 17, EGFR, and c-KIT. A median follow-up of 17.4 years was available. Basal CK positivity was significantly associated with decreased survival (median survival 8.8 *versus* 13.2 years, $p = 0.015$). In lymph node positive patients, the presence of either basal cytokeratin was associated with significantly poorer outcomes ($p = 0.008$). A similar trend was seen in the lymph node positive patients but did not reach statistical significance. EGFR expression was present in 44.1 % (41/93) of cases positive for basal CKs, and was significantly less common in basal CK negative cases (7.9 % (41/521), $p < 0.001$) of negative cases. EGFR expression was an independent negative prognostic factor ($p = 0.017$, RR = 1.54). c-KIT expression was more frequent in basal-like tumours, but did not significantly affect outcomes. The authors concluded that testing for ER and HER-2 (negativity) along with EGFR and CK5/6 (positivity) can accurately identify basal-like tumours with a high degree of specificity.

Of note in the Nielsen *et al.* study, PR status was not tested. However, the existence of the ER negative/PR positive cohort of breast cancers is an ongoing debate. Using newer and more sensitive staining techniques, De Maeyer *et al.* [48] recently re-analysed a cohort of 32 patients with ER negative/PR positive patients. Twenty cases were ER positive/PR positive, 5 were false positive for PR, and 7 were considered false negative for ER. Therefore, on re-analysis none of the 32 cases were true ER negative/PR positive breast cancers. In contrast, Rakha *et al.* reported a 3.4 % rate of ER negative/PR positive tumours in their series of 1944 breast cancer cases, and argue that, while rare, this represents a distinct biological subtype with an aggressive clinical behaviour [49]. In response to De Maeyer *et al.* [48], Rakha *et al.* argued that factors such as staining whole tissue sections rather than TMAs, antibody sensitivity, and variations in qualitative and quantitative estimations of ER and PR staining are potential reasons for not detecting an ER negative/PR positive subgroup [7].

Kreike *et al.* generated gene expression profiles on 97 triple negative tumours using a group of 102 invasive breast cancers (ER+ and/or PR+ and/or HER-2 +) as controls [12]. The triple negative tumours were also characterised by immunohistochemistry for ER, PR, HER-2, p53, CK5/6, KIT, and EGFR [15]. Using hierarchical clustering, all of the triple negative tumours clustered as basal-like. Furthermore, 19 of the control tumours also clustered with the basal-like group (the remainder were either HER-2 over-expressing or luminal). The authors concluded that all triple negative breast tumours can be classified as basal-like, and that immunohistochemistry was sufficient to classify these tumours [50].

Thike *et al.* identified a cohort of 653 triple negative breast cancers, and used a panel of markers to identify basal-like tumours (including CK14, EGFR and 34 beta E12) [51]. The triple negative tumours were associated with adverse clinicopathological characteristics such as high grade and nodal metastases. They characterised 84 % of the triple negative tumours as basal-like. They concluded that the triple negative phenotype was a reliable means of identifying basal-like tumours (specificity 100 % and sensitivity 78 %). Overall, these data suggest that many, but not all, triple negative breast cancers are basal-like. However, at present in the clinical setting, the triple negative phenotype is a practical surrogate for the treatment of basal-like tumours.

1.5.1 CLINICAL CHARACTERISTICS OF THE TRIPLE NEGATIVE BREAST CANCER PHENOTYPE

Triple negative breast cancers tend to behave aggressively. Several series have shown poor clinical outcomes in this subgroup [13, 15, 26, 43]. Banerjee *et al.* reported poorer disease-free survival (DFS) and overall survival (OS) in basal-like breast cancers compared to other subtypes [52]. Higher rates of visceral rather than bony metastases [53, 54], a high rate of cerebral metastases [55], local recurrence [54], and earlier age of onset [53] have been reported in triple-negative breast cancer.

Dent *et al.* reported a 11.2 % (180/1608) rate of triple-negative breast cancers in a cohort of breast cancer patients in Toronto [56]. Patients with triple negative disease had a relatively poorer outcome up to 5 years (Hazard Ratio (HR) 2.9; 95 % CI: 2.1 – 3.9, p = 0.0001) compared to other types of breast cancer, but not after that (HR 0.5; 95 % CI: 0.2 – 1.1, p = 0.07). These patients were significantly more likely to have visceral metastases compared to other patients (HR 4.0; 95 % CI: 2.7 – 5.9, p < 0.0001), which may contribute to the poorer prognosis of this subgroup. However, even in very early breast cancers (T1N0) the risk of recurrence is higher in the triple negative tumours compared to HER-2 positive tumours (hazard ratio for recurrence 6.57 (95% CI = 2.34, 18.49) when adjusted for prognostic factors such as age, tumour size, and adjuvant treatment [57].

The triple negative phenotype is associated with lower median durations of survival following recurrence than the other breast cancer subtypes. In an analysis of 3726 early stage breast cancer patients, the median survival in the basal-like subgroup following distant recurrence was 0.5 years, compared to 2.2 years for the luminal A subgroup, and 0.7 years for the HER-2 amplified cohorts (p < 0.001) [58].

The triple negative phenotype is associated with earlier age on onset in comparison to other subtypes [53, 59].

There appears to be a higher incidence of the triple-negative breast cancer phenotype in African-American women (especially pre-menopausal) and Hispanic women of poorer socio-economic backgrounds [60, 61]. For example, an unselected cohort of

148 Nigerian women with breast cancer had an estimated 59 % (87/148) incidence of basal-like breast cancer [62]. Recently published is the first study examining molecular subtypes in a West African population [59]. In a cohort of 378 breast cancers, 27 % were classified as basal-like. These were predominantly large (mean 4.4 ± 2.0 cm), high-grade tumours (83 %) in advanced stages (72 % node positive) in younger women (mean age 44.8 ± 11.8 years).

In summary, triple negative breast tumours are generally more aggressive tumours, associated with earlier age of onset, and are associated with poorer outcomes compared to other subtypes of breast cancer,

1.5.2 CURRENT TREATMENT OPTIONS FOR TRIPLE NEGATIVE BREAST CANCER

Currently there is no specific recommended systemic regimen of treatment for triple-negative breast cancer. Given the lack of hormone receptors and HER-2, there is no role for hormone antagonists such as tamoxifen or aromatase inhibitors, nor trastuzumab, a monoclonal antibody against HER-2. Therefore, chemotherapy remains the only systemic therapy currently available for patients with triple negative breast cancer. Even so, there are no standard chemotherapy regimens for triple negative disease. For example, in an ongoing clinical trial comparing the VEGF inhibitor sunitinib with standard-of-care chemotherapy in recurrent of metastatic triple negative disease (NCT00246571), options for standard-of-care chemotherapy include capecitabine, vinorelbine, docetaxel, paclitaxel, or gemcitabine (www.clinicaltrials.gov).

Commonly used chemotherapy regimens in breast cancer include anthracyclines and taxanes. Carey *et al.* prospectively studied 107 patients given neoadjuvant anthracycline-based chemotherapy regimens (doxorubicin and cyclophosphamide) [63]. Using immunohistochemical staining for ER, PR, and HER-2, basal-like breast cancers were defined as ER negative/PR negative/HER-2 negative. The authors observed that basal-like and HER-2+/ER- tumours were more sensitive to neo-adjuvant anthracyline-based therapies (27 % pathological complete response (pCR) in basal-like, 36 % in HER-2+/ER-, 7 % in luminal, P = 0.01). Tumours which achieved

a pCR did favourably regardless of subtype. ER negativity [64] and high Ki-67 expression [65] are associated with response to neoadjuvant chemotherapy.

Tan *et al.* have reported, in a cohort of 245 breast cancer patients given standard anthracycline therapy in the adjuvant setting, that the chemotherapy did not alter the poor prognosis of triple-negative/basal-like breast cancers [14]. In a study of 474 patients with metastatic breast cancer, treated with paclitaxel, Harris *et al.* observed that patients with high p53 expression and triple negative tumours had a relatively shorter overall survival. None of the biomarkers tested correlated with response to paclitaxel, including HER-2, p53 status and hormone receptor status [66].

Given the frequency of high p53 expression and the possibility of defects in the BRCA1 DNA repair pathways in triple negative breast cancer [41, 43], the use of platinum drugs is a rationale approach. However the data regarding p53 status should be interpreted with caution, as it was determined by immunohistochemistry rather than cDNA sequencing, as discussed above. Platinum agents are among those being commonly tested in current clinical trials in triple negative breast cancer. These include a phase II non-randomised trial of cisplatin in metastatic disease (NCT00483223), and a phase III randomised crossover comparison of carboplatin and docetaxel in locally advanced/recurrent/metastatic disease (ISRCTN97330959) [67].

The lack of a targeted therapy has led to the search for druggable targets in triple negative breast cancer. Receptor and non-receptor tyrosine kinases represent rational targets for cancer as they are frequently dysregulated in cancer e.g. HER-2 in breast cancer. A number of tyrosine kinases which have been shown to be of particular importance in basal-like/triple-negative breast cancer, including EGFR, MAPK, Akt, Src, c-kit, FAK and MET, are reviewed in the next section.

1.6 TYROSINE KINASES IN TNBC

1.6.1 EPIDERMAL GROWTH FACTOR RECEPTOR (EGFR)

EGFR is one of a family of four transmembrane growth factor receptor proteins that share similarities in structure and function. These receptors are generally referred to as the c-erbB or HER (**h**uman **e**pidermal growth factor **r**eceptor) family of receptor tyrosine kinases. EGFR (HER-1, c-erbB-1) was the first member of this family described [68-70], and is a 170 kDa glycoprotein consisting of an extracellular domain (630 residues), a transmembrane region (23 residues), and an intracellular tyrosine kinase domain (260 residues) (Figure 1.2) [71, 72].

EGFR is activated by bind growth factors of the epidermal growth factor family that are produced by the same cells, e.g. tumour cells (known as autocrine secretion), or by surrounding cells (paracrine secretion) (Figure 1.3) [73]. Ligands for EGFR include EGF, transforming-growth factor α (TGF-α), amphiregulin, betacellulin, heparin-binding growth factor (HB-EGF) and epiregulin [74].

The extracellular domain of EGFR has four distinct subdomains (I-IV) (Figure 1.2). Regions II and IV are enriched in cysteine residues that form numerous disulfide bonds within each region [72, 75]. Subdomains I and III have a β-helical fold and are important for ligand binding. Direct receptor-receptor interaction is promoted by a dimerisation loop in subdomain II. In the crystal structure of EGFR bound to EGF, the dimerisation loop protrudes from EGFR and mediates interaction with another EGFR molecule leading to the formation of a dimer, composed of two 1:1 receptor/ligand complexes [76, 77]. EGFR appears to exist in two different binding affinities at the cell surface (Kd of ~0.1 nM (low affinity), and Kd of ~10 nM (high affinity)) [78]. It is thought that the ligand first binds to domain I only, in a low affinity state. This results in a conformational change in the extracellular domain by rupturing hydrogen bonds between domains II and IV, resulting in ligand interaction with domain III, in a high affinity manner [78]. This conformational change allows for formation of receptor dimers. Both homodimerisation with another EGFR, or heterodimerisation with another member of the EGFR family have been described [79, 80].

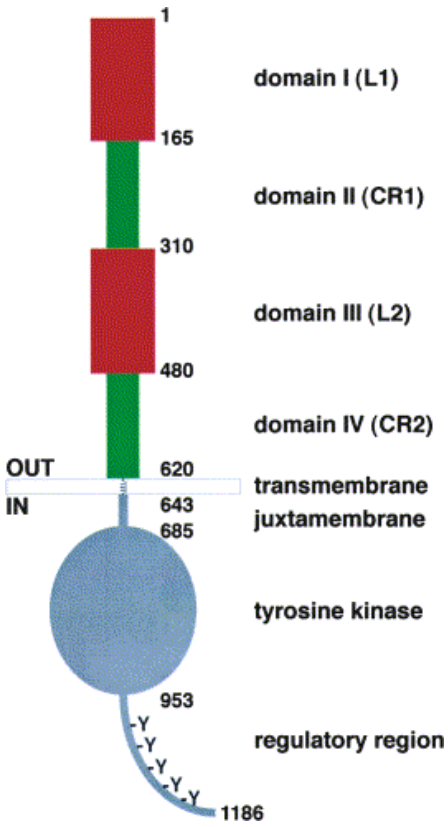

Figure 1.2 Domain organisation of HER receptors. The domains are referred to using the I, II, III, IV nomenclature [80]. An alternative nomenclature using domain names L1, CR1, L2, CR2 [76] is also used in the literature. Residue numbers for domain boundaries are for EGFR [72].

The EGFR transmembrane domain consists of 23 amino acids. It acts to anchor the receptor to the membrane, and also has a role in receptor dimerisation [81], and is involved in aligning the intracellular kinase domains following dimerisation, by rotational twisting [82].

The EGFR intracellular domain includes the tyrosine kinase domain, a juxtamembrane region, and a carboxy-terminal regulatory domain [83]. Ligand binding induces the formation of receptor homo- or hetero-dimers and subsequent activation of the intrinsic tyrosine kinase domain [84]. Receptor activation leads to phosphorylation of specific tyrosine residues within the cytoplasmic tail. These phosphorylated residues serve as docking sites for proteins such as those containing Src homology 2 (SH2) and phosphotyrosine binding (PTB) domains [74]. In addition to dimerisation, EGFR tyrosine phosphorylation may also occur by transactivation. For example, Src phosphorylates various residues on EGFR, leading to enhanced receptor signalling [85]. Other examples include cytokines such as growth hormone and prolactin which may indirectly activate EGFR or HER-2 through Janus tyrosine kinase 2 (Jak2). Jak2 phosphorylates specific tyrosine residues in the cytoplasmic domains of EGFR [86] and HER-2 [87].

A summary of signalling proteins that directly associate with EGFR are given in Table 1.2. The recruitment of these signalling proteins leads to activation of intracellular signalling pathways, including the key pathways Ras/Raf/mitogen-activated protein kinase (MAPK) and phosphatidylinositol 3-kinase (PI3K)/Akt (Figure 1.3).

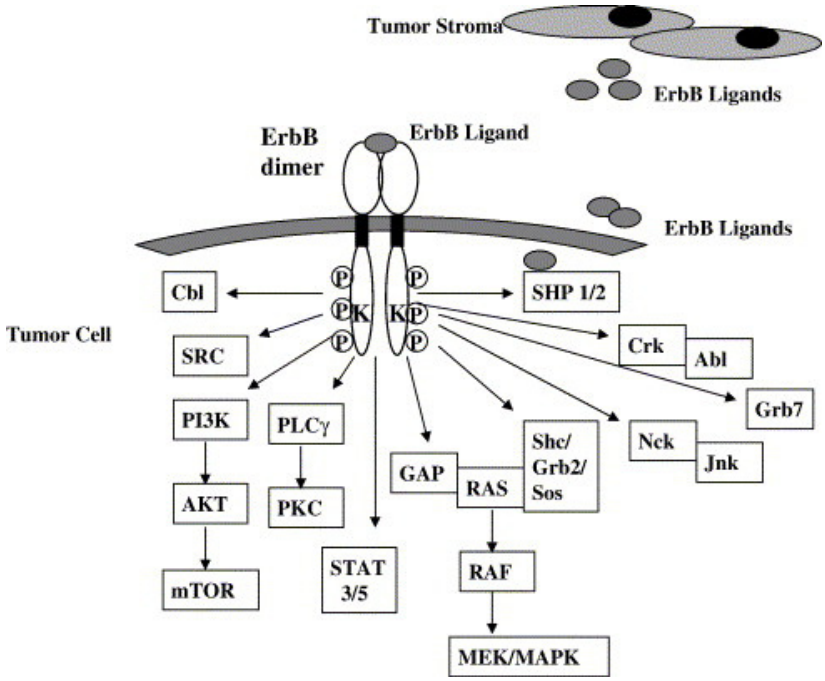

Figure 1.3 Mechanisms of action of ErbB receptors in tumour cells, such as EGFR. Binding of ligands to the extracellular domain of EGFR results in receptor dimerisation, tyrosine kinase activation and *trans*-phosphorylation (P). The activated receptors are able to interact with different signalling molecules that transmit the signal in the cell [74].

Table 1.2 Signalling proteins that associate directly with EGFR, and their function. Adapted from Jorissen *et al.* [76]

Protein	**Function**
GRB-2	Adaptor
Nck	Adaptor
Crk	Adaptor
Shc	Adaptor
Dok-R	Adaptor
PLC-γ	Phospholipase
P120RasGap	Ras attenuator
PTB-1B	Phosphatase
SHP-1	Phosphatase
Src	Tyrosine kinase
Abl	Tyrosine kinase

1.6.1.2 EGFR IN TRIPLE NEGATIVE BREAST CANCER

Expression of EGFR in cancer has been correlated with disease progression, poor survival, poor response to therapy [88], and the development of resistance to cytotoxic agents [89]. High levels of EGFR have been observed in a variety of cancer types, including prostate, gastric, colorectal, and ovarian [90]. A review of 5232 breast cancer patients from 40 different studies reported that on average 45 % of breast cancers were positive for EGFR (range 14 – 91 %) [91]. Another review of 370 patients found a 47 % positive rate [92]. Therefore, a wide range of EGFR positivity in breast cancer has been reported. However, as noted by Chan at al, several different techniques have been used in these various studies [93].

There is no consensus on EGFR as a prognostic marker for breast cancer (as there is for HER-2). However, a number of studies have reported that EGFR is over-expressed in triple negative breast cancers. In a series of 930 breast tumours, Nielsen *et al.* [15] reported 13 % positive immunostaining for EGFR (82/614 interpretable cores). However, EGFR expression was present in 44.1 % (41/93) of cases that were positive for basal cytokeratins. Also, EGFR expression was significantly less common among basal cytokeratin-negative cases (41/521 = 7.9 %, $p < 0.001$), and was present in only 2.0 % (5/254) of ER-positive cases. There was a significant correlation between EGFR positivity and poor survival (5.7 *versus* 13.4 years, $p < 0.01$). In multivariate analysis, EGFR expression was an independent negative prognostic factor (relative risk (RR) 1.54, $p = 0.017$), independent of tumour size (RR 1.12) or nodal status (RR 2.10), suggesting a potentially important prognostic role for EGFR.

Livasy *et al.* [94] assessed 56 breast tumours by immunohistochemistry and found that EGFR was detected in 72.2 % (13/18) of the basal-like tumours. All of the basal-like tumours were negative for ER and HER-2 expression. While the number of basal-like tumours in this study is small (n=18), the frequency of EGFR expression is notably high.

Kreike *et al.* [12] performed immunohistochemistry (CK5/6, p53, EGFR, c-kit) and generated gene expression profiles on 97 triple negative tumours. All tumours were

classified as basal-like on the basis of gene expression profiling. Twenty seven percent (26/93) of the tumours were positive for EGFR staining. Gene expression profiling of the basal-like tumours subdivided them into 5 sub-branches, and correlations with immunohistochemical characteristics were performed. EGFR expression was variable between each subgroup (I: 1 (3 %), II: 5 (28 %), III: 11 (50 %), IV: 6 (50 %), V: 3 21 %). The authors concluded that triple-negative tumours were synonymous with basal-like tumours. However, there were different subgroups within basal-like breast cancer, and no strong overall prognostic gene expression profile, including EGFR, was identified. Therefore EGFR-directed therapy may be appropriate in some basal-like breast tumours but not necessarily all.

Rakha *et al.* [95] examined a series of 1944 invasive breast carcinomas using tissue microarrays. Immunohistochemical analysis of markers including ER, PR, HER-2, androgen receptor, EGFR, P-cadherin, E-cadherin, CK5/6, CK14, and p53, was performed. EGFR was detected in 16.5 % (286/1726) of the tumours. Of the triple negative tumours, 32.6 % (92/282) expressed EGFR, compared to 13.4 % (194/1444) of non-triple-negative tumours ($p < 0.0001$). Of note, in this study, triple-negative tumours were associated with increased size, risk of recurrence and metastasis, poorer overall survival and disease-free survival. The frequency of EGFR expression in triple-negative breast cancers makes it an attractive target for treatment in patients with this disease.

Stratford *et al.* [96] studied the role of Y-box bind protein (YB-1) in EGFR regulation in basal-like breast cancer. YB-1 has been found to be commonly expressed in ER negative tumours [97]. YB-1 was originally isolated as a transcription factor that bound to enhancer sites on EGFR [98]. Over-expression of YB-1 in the ER positive MCF7 cell line leads to an increase in EGFR mRNA and protein [97]. Using breast tumour microarray analysis, the authors found frequent expression of both YB-1 (73 %) and EGFR (57.1 %) in basal-like tumours. YB-1 was found to regulate EGFR in basal-like breast cancer in SUM149 and HCC1937 cell lines. Gain of activity was observed by transfection with a hYB-1 plasmid, and significant loss of function was observed by siRNA knockdown. The combination of the EGFR inhibitor gefitinib and the LY294002, which has been shown to inhibit YB-1 phosphorylation as well as PI3K [99], led to enhanced sensitivity in HCC1937 compared to gefitinib alone. In

contrast, SUM149 was more sensitive to gefitinib alone. These findings suggest an important regulatory function for YB-1 in relation to EGFR, in basal-like breast cancer.

As discussed in section 1.6.1, EGFR effector proteins include the GTPase Ras family of proteins. Oncogenic mutations have been described in the KRAS gene, which results in constitutive activation, dysregulated proliferation, and decreased apoptosis (reviewed by Malumbres and Barbacid [100]). The functional differences between the normal and oncogenic alleles have been related to point mutations [100]. Somatic KRAS mutations are described in various cancers, including pancreatic (60 %), colon (32 %), lung (17 %), and less frequently in leukemias and breast cancer (5 %) [101, 102]. The efficacy of anti-EGFR inhibitors depend on wild type KRAS as mutant KRAS sends proliferative and anti-apoptotic signals independent of EGFR phosphorylation [100]. Consequently KRAS mutation is routinely assessed prior to administration of EGFR inhibitors such as cetuximab in colorectal cancer [103].

Sanchez-Munoz *et al.* examined 35 triple negative breast cancer tumours for KRAS mutations (including 27 tumours which were characterised as basal-like (77.1 %), by real-time PCR [102]. Interestingly, no KRAS mutation was found in any of the analysed tumours. In the context of over-expression of EGFR in triple negative breast cancers, the low rate of KRAS mutation suggests a possible therapeutic role for EGFR inhibitors in triple negative breast cancer.

1.6.2 THE MITOGEN-ACTIVATED PROTEIN KINASE (MAPK) SIGNALLING CASCADE AND ITS ROLE IN EGFR SIGNALLING

The key protein in EGFR-dependent Ras activation is Grb2 (Growth factor Receptor Bound 2) [104]. The Grb family of proteins are adaptor proteins that also contain SH2 domains. Grb2 can associate directly with EGFR or indirectly, by binding to EGFR-associated tyrosine-phosphorylated Shc [105]. Grb2 is bound in the cytosol to the guanine nucleotide exchange factor Sos [106], and recruitment of the Grb2-Sos complex to the plasma membrane stimulates the activation of GTP-binding protein Ras by exchanging its GDP for GTP. Activated Ras then activates the serine/threonine kinase Raf-1 [107].Through a series of intermediary kinases (including MEK1), activated Raf-1 leads to the phosphorylation, activation and nuclear translocation of Erk-1 and Erk-2 (p42/44 MAPK) which catalyse the phosphorylation of nuclear transcription factors [108]. These proteins in turn mediate numerous cell functions such as proliferation, differentiation, cell survival and transcription [109].

Constitutive activation of MAPK has been identified in the triple-negative/basal-like breast cancer cell line MDA-MB-468 [110]. Interestingly, treatment of MDA-MB-468 with cetuximab, a monoclonal antibody against EGFR, lead to hyperphosphorylation of EGFR with simultaneous decreased phosphorylation of p42/44 MAPK. It has also been reported that transfection of MDA-MB-468 cells with Insulin like growth factor binding protein-7 (IGFBP7) leads to decreased phosphorylation of MAPK, and decreased proliferation in comparison to parental MDA-MB-468 cells [111].

Heat shock protein 90 (Hsp90) is a molecular chaperone protein that is widely expressed in breast cancer [112], and has demonstrated activity in HER-2 positive breast cancer [113]. Treatment of the triple negative breast cancer cell lines MDA-MB-231 and HCC1806 with the Hsp90 inhibitor PU-H71 inhibited proliferation and induced decreased phosphorylation in ERK1/2 in a dose –dependent manner as well as down-regulation of proteins including EGFR, HER3, IGF-IR, Akt [114].

Metformin, a medication used to control blood sugar levels in non-insulin dependent diabetes mellitus, has recently shown preferential activity in triple negative breast

cancer [115]. Metformin was shown to decreased phosphorylation of MAPK *in vitro*, as well as decreased activity of EGFR, Src, cyclin D1 and cyclin E. This activity was associated with decreased proliferation, and induction of apoptosis. Metformin also demonstrated inhibition of proliferation and tumour growth in MDA-MB-231 xenograph murine models [115]

MAPK expression in triple negative breast cancer tumours have been studied by Eralp *et al.* in a series of 109 patient samples [116]. Thirty-eight of the tumours had positive immunohistochemical staining for MAPK (38/109, 34.9 %). MAPK expression was significantly associated with drug resistance to anthracyclines ($p = 0.008$), and reduced disease-free survival ($p = 0.029$).

In a cohort of 52 breast cancer patients, neoadjuvant treatment with the EGFR inhibitor erlotinib for 6 to 14 days inhibited proliferation, as measured by Ki67, as well as phosphorylation of EGFR and HER-2 [117]. Decreased proliferation was statistically significant for ER-positive tumours in comparison to ER-negative and triple negative subtypes ($p = 0.004$). Erlotinib treatment was significantly associated with decreased phosphorylation of MAPK ($p = 0.007$) and Akt ($p = 0.0002$) in pre- and post- treatment samples. When analysed by tumour subtype, these changes were only statistically significant in ER-positive tumours (P-MAPK, $p = 0.05$; P-Akt, $p = 0.001$), but not in triple negative tumours. Of note, only 5 of the tumours overall expressed EGFR. These data suggest that phosphorylation of MAPK and Akt may be important biomarkers of response to erlotinib, independent of EGFR status. While the number of patients included in this single arm study was small, these data suggest that treatment of triple negative tumours with EGFR inhibition alone may not be effective.

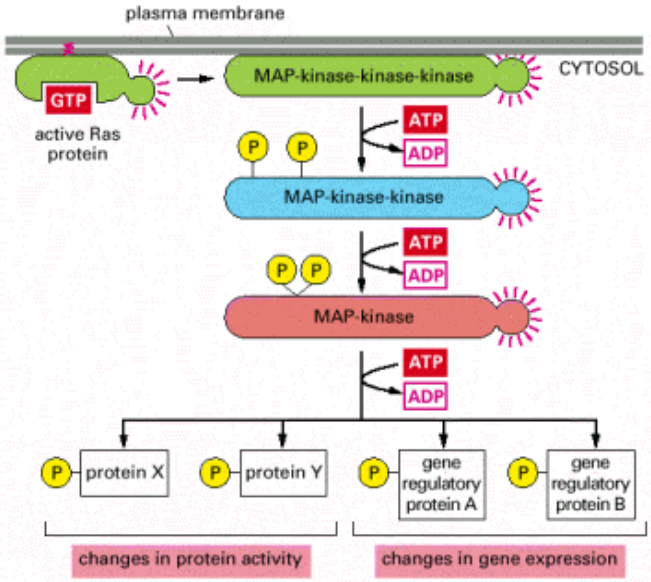

Figure 1.4 The Mitogen-activated protein kinase (MAPK) serine/threonine phosphorylation pathway activated by Ras. A MAP-kinase-kinase-kinase (Raf) activates the MAP-kinase-kinase (Mek), which then activates the MAP-kinase called *Erk*. Erk in turn phosphorylates a variety of downstream proteins, including other kinases, as well as gene regulatory proteins in the nucleus. The resulting changes in gene expression and protein activity cause complex changes in cell behaviour [from Molecular Biology of the Cell, 4th edition, Alberts *et al.*, 2002].

1.6.3 THE PI3-K/AKT SIGNALLING CASCADE AND ITS ROLE IN EGFR SIGNALLING

EGF stimulation of a cell has important effects on phospholipid metabolism, including phosphatidylinositol turnover and production of phosphatidic acid and arachidonic acid [76]. One of the enzymes in this pathway that can be activated directly by EGFR is phosphatidylinositol-3-kinase (PI3K). Downstream effectors of PI3K are activated by second messenger phosphatidylinositol derivatives, and are involved in cell proliferation, survival, metabolism, cytoskeletal reorganisation, and membrane trafficking [118, 119].

PI3K consists of a p110 catalytic subunit and a p85 adapter/regulatory subunit [120]. The p110 subunit of activated PI3K catalyses phosphorylation of the 3 position of the inositol ring of PI(4,5)P2 to generate PI(3,4,5)P3, a potent second messenger (Figure 1.5). The effects of PI(3,4,5)P3 are mediated through specific binding at protein-lipid binding domains, including the plekstrin homology (PH) domain [121]. Two such PH-containing-proteins are 3'-phosphoinositide-dependent kinase 1 (PDK1) and Akt.

Akt is a 57 kDa serine/threonine kinase [120] and is an important target of PI(3,4,5)P3. Akt binds to the lipid and is translocated to the plasma membrane where it is phosphorylated by PI(3,4,5)P3 and PDK-1 (Figure 1.5) [76, 120]. The tumour suppressor gene PTEN (phosphatase and tensin homolog deleted on chromosome 10) is known to regulate Akt signalling by dephosphorylating PI(4,5)P2 and PI(3,4,5)P3, preventing Akt recruitment [122]. One of the downstream substrates of Akt is BAD, a member of the Bcl-2 family of pro-apoptotic proteins [123]. Upon serine phosphorylation by Akt, BAD can no longer bind Bcl-$2X_L$ and is inactivated. Bcl-$2X_L$ is then able to exert its anti-apoptotic effects. Akt signalling through BAD therefore protects cells from apoptosis [124].

PIK3CA is the gene which encodes the 110 kDa subunit of PI3K, and is mutated in a variety of human cancers, including ovarian, cervical, colon, brain, gastric, and lung, in varying frequencies [125-127]. The frequency of PIK3CA somatic mutations in breast cancer has been reported as approximately 20 % [128, 129] in primary breast

tumours, and 8.7 % of breast tumours (8/92) had a gain in PIK3CA gene number [128]. Wu at al. reported 33.3 % frequency of PIK3CA mutations in a panel of breast cancer cell lines (5/15), including 2 mutations in the triple negative BT20 cell line [128]. In this study, BT20 showed the strongest level of Akt phosphorylation. The triple negative MDA-MB-231 cell line did not harbour a PIK3CA mutation, and had no appreciable phosphorylation of Akt.

Wu *et al.* [128] reported that somatic mutations of PIK3CA, rather than gain of copy number, was the main mutation found in breast cancer. In particular, the triple-negative breast cancer cell line BT20 contained two PIK3CA mutations. In another triple-negative cell line, MDA-MB-231, PI3K inhibition lead to a significant inhibition of basal ($P < 0.01$) and EGF-induced ($p < 0.01$) migration [130]. PIK3/Akt signalling has been implicated in BRCA1 activity, including the basal-like HCC1937 cell line, which harbours BRCA1 mutation and has constitutively active Akt [131]. Of note in the triple negative cell line MDA-MB-231, which expresses Akt, there is no appreciable phosphorylation of Akt in the basal state [132].

As discussed in Chapter 1.6.2, Hsp90 inhibition of triple negative breast cancer cell lines with PU-H71 inhibits proliferation and decreases phosphorylation of Akt in a dose-dependent manner [114]. This suggests that P-Akt may be an important biomarker of response to Hsp90 inhibitors.

The effects of hexadecylphosphocholine (HePC, miltefosine), an alkophosphocholine which has been used to treat cutaneous breast cancer metastases, have been tested in triple negative breast cancer cell lines [133]. A time-dependent decrease in phosphorylation of Akt in the triple negative cell lines MDA-MB-231 and MDA-MB-435 was associated with increased cell death. Recently, treatment of triple negative breast cancer cell lines with the fibroblast growth factor receptor 3 (FGFR3) inhibitor PD173074 has been shown to induce apoptosis via inhibition of the PI3K/Akt pathway [134]. Another treatment which has shown efficacy in MDA-MB-231 is the combination of cyclophosphamide and the mTOR inhibitor rapamycin, which appears to inhibit phosphorylation of Akt via HIF-1alpha expression [135].

In a study of 109 triple breast tumours, Eralp *et al.* reported 30.3% (33/109) had positive staining for PI3K [116]. Lerma *et al.* examined 64 triple negative breast cancer tumours [136]. They did not report Akt expression, but they reported that 28 % of the tumours had positive staining for P-Akt. Umemure *et al.* examined a panel of 44 breast cancer tumours, including 8 triple negative tumours [137]. The triple negative tumours had significantly increased Akt and P-Akt in comparison to the non-triple negative tumours by immunohistochemistry ($p = 0.0023$). These studies suggest that Akt is an important signalling pathway in triple negative breast cancers.

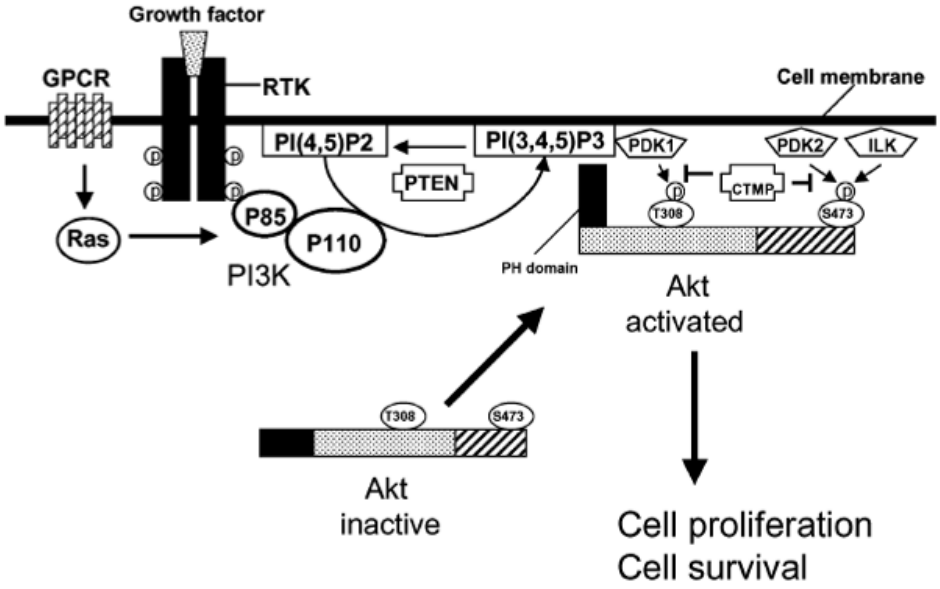

Figure 1.5 Model for the regulation of the PI3K-Akt signalling pathway. Binding of growth factors to their receptors e.g. EGFR, stimulates phosphorylation of phosphatidylinositol 3-kinase (PI3K), comprised of P85 and P110 subunits. PI3K converts phosphatidylinositole-4,5 bisphosphonate (PI(4,5)P2) to PI(3,4,5)P3, whereas PTEN reverses this reaction. Akt is phosphorylated by PI(3,4,5)P3 and PDK-1, and in turn phosphorylates downstream targets and mediates important cellular effects, including on proliferation and survival [120].

1.6.7 SRC IN TRIPLE NEGATIVE BREAST CANCER

Src was one of first identified oncogenes, and was initially described by Peyton Rous in 1911 as the transforming agent in chicken sarcomas [138]. Cellular Src (c-Src) is a non-receptor cytoplasmic membrane-associated tyrosine kinase. Src may be activated by cytoplasmic proteins e.g. focal adhesion kinase (FAK) or its molecular partner Crk-associated substrate (CAS), which are important in integrin signalling, and by ligand activation of cell surface receptors, including EGFR. These interactions disrupt intramolecular interactions within Src, leading to an open confirmation that enables the protein to interact with potential substrates and downstream signalling molecules. Src can also be activated by dephosphorylation of tyrosine residue Y530. Full Src activation requires the autophosphorylation of another tyrosine residue (Y419 in the human protein) present within the catalytic domain (Figure 1.6) [139].

Elevated Src activity may be caused by increased transcription or by deregulation due to over-expression of upstream growth factor receptors such as EGFR, HER-2, platelet-derived growth factor (PDGFR), vascular endothelial growth factor (VEGF), integrins, or focal adhesion kinase (FAK) [140].

Src may act as a signal transducer downstream of EGFR or may play a role in EGFR phosphorylation [76]. c-Src has been implicated in mitogenic signalling through multiple growth factor receptors, including EGFR [141-143]. Biscardi *et al.* found a physical and functional interaction between c-Src and EGFR [85]. Over-expression of Src proteins enhances EGF-mediated proliferation and transformation in fibroblasts and epithelial cells [144, 145]. In addition, Src inhibition can block EGF-dependent DNA synthesis [143]. DHER14 cells are EGFR-over-expressing variant of the murine fibroblast cell line NIH 3T3 [146]. Src inhibition has been shown to reverse the transformed phenotype of DHER14 cells, at least partially through decreased expression of the pro-apoptotic Bcl-X protein [147].

c-Src activity or expression has been shown to be increased in many human cancers, including breast, gastric, ovary, colon, and prostate [148-151]. c-Src has been shown to physically associate with EGFR and HER-2 in some human and mouse breast cancer

cells [152-154]. Elevated c-Src protein levels have been found in about 70 % of primary breast tumours, often in association with EGFR [155, 156].

Biscardi *et al.* observed increased levels of c-Src in 10 of 14 breast cancer cell lines, compared to normal human breast epithelial cells [85]. These included three triple-negative breast cancer cell lines (MDA-MB-468, MDA-MB-231, BT20), which also had increased EGFR levels, and displayed an EGF-dependent association between c-Src and EGFR. Increased Shc and MAPK activation was found in the cell lines which over-expressed c-Src and EGFR, including the triple-negative breast cancer cell lines MDA-MB-468 and MDA-MB-231. These cell lines also displayed increased tumorigenicity in nude mice. Potential effectors for c-Src mitogenesis via EGFR include PLC-γ and MAPK (Figure 1.7) [85].

Dimri *et al.* used non-tumorigenic human mammary epithelial cells (HMEC) and established a model of c-Src and EGFR co-over-expression [157]. They determined that co-overexpression c-Src and EGFR was required in order to initiate oncogenic transformation in their *in vitro* model. However, xenotransplants into nude mice did not result in tumour growth, suggesting that other factors are important for oncogenesis of EGFR and c-Src co-over-expressing cancers *in vivo*.

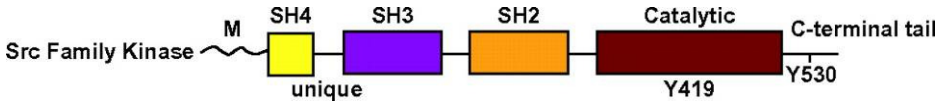

Figure 1.6 Structure of Src and Src family kinases (SFKs). Src is a 60-kDa non-receptor kinase consisting of a myristylation site (M), Src homology (SH) domains, a catalytic domain, a unique domain, and a negative regulatory tyrosine residue (Y530 in human Src). The unique domain varies the greatest between Src family kinases [158].

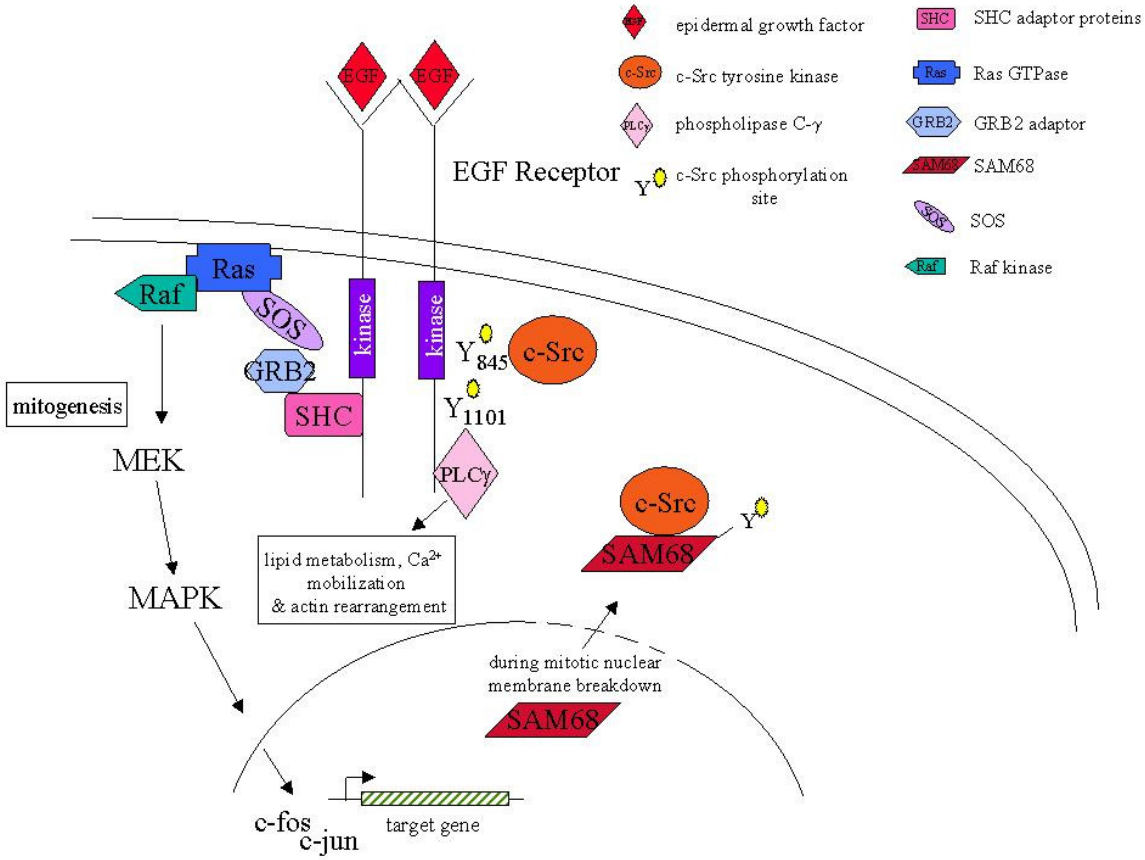

Figure 1.7 Postulated effect of c-Src on EGF mitogenic pathways. Two signalling pathways of the EGF receptor are depicted, namely, those involving PLC-γ and MAPK. Tyrosine residues 845 and 1101 of the EGF receptor are phosphorylated by c-Src, and phosphorylation of Y845 is believed to augment receptor tyrosine kinase activity, as manifested by increased phosphorylation of the receptor targets, PLC-γ and SHC [85].

Dasatinib is a novel orally active small molecule multi-target kinase inhibitor, with targets including Src, Abl, PDGFR and ephrin receptor kinases [159]. Using a panel of 39 breast cancer cell lines, Finn *et al.* [138], reported that the most sensitive cell lines to this agent were basal-like (6/9 basal-like cell lines tested) and post-epithelial-to-mesenchymal transition (6/7 post EMT tested) ($p = 0.008$). Of the resistant basal-like breast cancer cell lines, MDA-MB-468 has low levels of activated Abl [160]. Tryfonopoulos *et al.* reported sensitivity to dasatinib of the triple-negative breast cell lines MDA-MB-231, HCC1937, and BT20 [161]. These cells were more sensitive to dasatinib, and relatively resistant to imatinib, which has overlapping targets including Abl, c-KIT and PDGFR. This suggests that Src or ephrin A receptors are more likely targets for sensitivity to dasatinib in triple-negative breast cancer cell lines.

A recent study by Elsberger et al. assessed Src kinase expression in breast tissue samples, by immunohistochemistry [162]. They reported higher levels of c-Src in breast cancer tissue compared to other Src family members. Cytoplasmic expression of Src was associated with tumour proliferation, as measured by Ki67, and decreased survival.

The high frequency of c-Src over-expression, in breast cancer and in triple negative breast cancer cell models, makes this an important potential target for therapy in triple negative disease.

1.6.8 OTHER TYROSINE KINASES IN TNBC

1.6.8.1 c-KIT

The c-kit gene encodes for a protein that is a member of the RTK family. c-KIT (CD117) is expressed in various cell types during development, namely, endothelial, epithelial and endocrine cells and it has been linked to the promotion of cellular migration, proliferation and/or survival of melanoblasts, hematopoietic progenitors and primordial germ cells [163]. It has been noted that there is a general loss of c-KIT in breast cancer [164, 165], which leads to a tumour-promoting loss of mast cells [165]. However, as reported by Nielsen *et al.* [15], Krieke *et al.* [12], and others [166-168], c-KIT expression is a hallmark of the basal-like breast cancer phenotype. However, as discussed above, data in relation to imatinib in triple negative breast cancer cell lines by Tryfonopoulos *et al.* [161] suggest that targeting of c-KIT may not be effective in triple negative disease.

1.6.8.2 FAK

Focal adhesion kinase (FAK) was originally isolated as a tyrosine-phosphorylated 125-kDa protein in v-Src-transformed chicken embryo fibroblasts [169, 170]. FAK activity is regulated by extracellular matrix receptors and integrins and is involved in cellular processes such as migration, motility, proliferation, and survival [171, 172]. FAK is over-expressed in many human cancers, including breast [173-176]. FAK has been associated with EGFR [177, 178]. Golubovskaya *et al.* [179] found that EGFR over-expression the HER-2 positive BT474 cell line overcame apoptosis induced by FAK downregulation. Dual EGFR and FAK inhibition resulted in downregulation of both the MAPK and Akt survival pathways. Importantly, in the basal-like breast cancer cell line BT20, which has much higher endogenous levels of EGFR, dual EGFR/FAK inhibition also increased apoptosis and downregulated MAPK and Akt.

1.6.8.3 MET

In an analysis of 31 breast cancer cell lines to determine molecular subtype, Charafe-Jauffret *et al.* [28] used DNA microarrays to perform gene expression profiling, and immunohistochemistry on cell microarrays. The expression of 10 proteins (including MET, EGFR, CAV1, CD44, ETS1, GATA3, CK19 (luminal), CK5/6 (basal), CD10 and ERM protein moesin) was accurately able to discriminate between basal (8 cell lines), mesenchymal-like (4 cell lines) and luminal (15 cell lines) subtypes. MET was reported as a newly identified basal marker.

The MET family of tyrosine kinases can function as oncogenes, similar to other tyrosine kinases [180]. The MET gene (located on the same chromosomal region as CAV1 and CAV2, 7q31) encodes the tyrosine kinase receptor for hepatocyte growth factor involved in various cell processes and in cancer [181]. MET ligand binding results in cell dissociation, migration and invasion [182-184]. MET amplification has been implicated in resistance to HER inhibitors such as gefitinib [185].

Lee *et al.* [186] assessed MET and RON (another MET family tyrosine kinase) expression in a panel of breast cancer cell lines. Of the cell lines studied, only HCC1937 and MDA-MB-231 co-over-expressed RON and MET. These are both triple-negative breast cancer cell lines and have mutant p53 (consistent with the basal-like phenotype). In addition, the authors analysed a heterogeneous group of 103 node negative breast cancer patients, and correlated MET and RON tumour expression with prognostic factors. MET expression was an independent predictor of distant disease metastasis (odds ratio 4.7, $p = 0.009$). The lowest 10-year disease-free survival was in the group which co-expressed both tyrosine kinases (11.8 %) compared to patients with tumours negative for both (79.3 %). This suggests a prognostic significance for co-expression of these tyrosine kinases in breast cancer. While the authors did not stratify the patient samples into basal-like or luminal, the prognostic significance of co-expression of MET and RON, which was associated with p53 mutations suggests a potential role for these receptors in triple-negative breast cancer.

1.7 TARGETED THERAPIES FOR TRIPLE NEGATIVE BREAST CANCER

Given the multiplicity of potential molecular targets in basal-like/triple-negative breast cancer, and the large number of emerging targeted pharmacological agents, there are many potential therapies which may be beneficial in this subgroup of breast cancer patients.

1.7.1 EGFR TARGETED THERAPIES

EGFR inhibitors currently in clinical use include the small molecule tyrosine kinase inhibitors gefitinib and erlotinib, and the monoclonal antibody cetuximab.

Gefitinib (Iressa^{TM}, AstraZeneca) is an oral, selective inhibitor of EGFR which binds reversibly to the ATP binding site of EGFR [187]. Gefitinib is approved for treatment of non-small cell lung cancer (NSCLC). Phase II clinical trials in unselected refractory metastatic breast cancer patients have yielded poor results. Von Minckwitz *et al.* reported a 1.7 % (1/58) objective partial response rate in heavily pre-treated patients given 500 mg gefitinib daily [188]. Albain *et al.* reported a clinical benefit rate of 4.8 % (1 partial response and 2 with stable disease of 58 patients treated) in another trial in a heavily pre-treated population [189]. Baselga *et al.* reported no objective tumour responses, and 3/31 (9.7 %) patients with stable disease greater than 6 months in a phase II monotherapy trial [190]. Immunohistochemical analysis of patient samples in this trial showed inhibition of phosphorylated EGFR and MAPK, but not phosphorylated Akt, suggesting that the patient tumours were not addicted to EGFR signalling alone.

A phase II combination study of gefitinib and docetaxel as first-line treatment in metastatic breast cancer yielded a 54 % response rate [191]. The combination was well tolerated. Of note, significantly more patients with ER positive compared to ER negative tumours responded (70 % (19/27), *versus* 21 % (3/14), $p = 0.01$). It was suggested that this may reflect a switch to EGFR-dependency from estrogen-dependent mechanisms in the patients with prior adjuvant anti-estrogen therapy. In

contrast, another phase II randomised double-blind study of gefitinib and docetaxel as first-line treatment in metastatic breast cancer reported no added benefit from gefitinib [192]. A phase II study of first-line combined gefitinib and docetaxel in advanced breast cancer had a overall response rate of 39.4 % (95% CI: 22.9 – 57.9 %) [193]. Factors such as visceral disease on initiation of treatment, and withdrawals due to emerging poor results of EGFR inhibitor trials were suggested as possible reasons for a less than expected benefit. Toxicities of the combination were similar to gefitinib alone.

There are currently no trials with gefitinib in triple negative breast cancer reported in the literature. The evidence for *in vitro* sensitivity to gefitinib is mixed. Gefitinib has been tested in a number of EGFR over-expressing triple-negative/basal-like breast cancer cell lines. Stratford *et al.* [96] reported sensitivity of the triple-negative/basal-like SUM149 cells but resistance of HCC1937 cells when treated with gefitinib alone. Sensitivity to gefitinib of SUM149 cells has been confirmed elsewhere [194], as well as sensitivity in another basal-like breast cancer cell line, SUM102. Takabatake *et al.* [132] tested gefitinib and docetaxel in the triple negative MDA-MB-231 cell line. The combination was additive/antagonistic *in vitro* and gefitinib did not significantly enhanced response to docetaxel n a xenograft model.

The MEK/MAPK pathway has been implicated in resistance to the EGFR tyrosine kinase inhibitor gefitinib in breast cancer cell lines. Normanno *et al.* [195] have shown that growth of the gefitinib-sensitive MDA-MB-468 cells was significantly inhibited by both the PI3K-inhibitor LY294002 and the MEK-inhibitor PD98059. The combination of gefitinib and PD98059 was synergistic, and lead to significant increases in apoptosis compared to the single agents. Treatment with these agents resulted in decreased activation of MAPK, the pro-apoptotic protein BAD, and a paradoxical increase in Akt phosphorylation. The same group has also shown persistent activation of the MAPK pathway in gefitinib resistant clones of SKBR3, MDA-MB-175, and MDA-MB-361 breast cancer cell lines [196]. This was associated with significantly decreased activity of EGFR, HER-2, HER-3, and Akt. These data suggest that EGFR inhibition may be overcome by activation of MAPK through mechanisms other than activation of EGFR.

Erlotinib (Tarceva™, OSI Pharmaceuticals) is also a small molecule inhibitor of EGFR and binds reversibly to the ATP binding site of EGFR. Erlotinib is an EGFR-specific quinazoline derivative [197], and is approved for treatment of NSCLC and pancreatic cancer. Similarly to gefitinib, preliminary phase II trials of erlotinib in combination with chemotherapy in breast cancer showed disappointing response rates. In a phase II study of erlotinib combined with docetaxel in metastatic breast cancer, the partial response rate was 55 %, similar to response rates which have previously been reported for docetaxel alone [198]. Ongoing trials with erlotinib in triple negative breast cancer are listed in Table 1.3.

Table 1.3 Current trials with erlotinib in triple negative breast cancer (from www.clinicaltrials.gov)

Regimen	Setting	Phase	NCI Identifier
Erlotinib monotherapy	Metastatic EGFR-positive TNBC	II	NCT00739063
Erlotinib + Bendamustine	Metastatic/Locally advanced TNBC	II	NCT00834678
Erlotinib + neoadjuvant chemotherapy	Primary TNBC	II	NCT00491816
Nab-Paclitaxel + Bevacizumab → Bevacizumab + Erlotinib	Advanced TNBC	II	NCT00733408

Cetuximab (Erbitux™, ImClone Systems Incorporated) is a monoclonal antibody against EGFR. It binds with high affinity to the receptor and prevents ligand-binding and activation. Cetuximab may also exert its effects by recruitment of cytotoxic cells, such as monocytes and macrophages, and induction of antibody-dependent cellular cytotoxicity (ADCC) [199]. Current approved clinical applications of cetuximab include the treatment of head and neck cancer and metastatic colorectal carcinoma [200].

A phase I trial of cetuximab in combination with paclitaxel in advanced breast cancer has been reported [201]. Two of the 12 patients evaluated had stable disease. However, based on dose-limiting dermatological toxicities and disappointing preliminary efficacy, the combination of paclitaxel and cetuximab was not considered promising in this population. The addition of cetuximab to carboplatin in metastatic TNBC is currently being tested in a randomised phase II trial (TBCRC 001) [202]. Preliminary analysis showed a 10 % clinical benefit for cetuximab alone *versus* 27 % for cetuximab combined with carboplatin. While cetuximab was well tolerated, it appears to have low clinical activity in metastatic triple negative breast cancer. A number of studies of cetuximab in triple negative breast cancer are currently ongoing (Table 1.4).

Table 1.4 Current trials with cetuximab in TNBC (from **www.clinicaltrials.gov**)

Regimen	Setting	Phase	NCI Identifier
Cetuximab + carboplatin	Metastatic TNBC	II	NCT00420329
Cetuximab + carboplatin	Metastatic TNBC	II	NCT00492375
Cetuximab + cisplatin (BALI-1)	Metastatic TNBC	II	NCT00463788
Cetuximab + Ixabepilone	Advanced/ Metastatic TNBC	II	NCT00633464
Cetuximab + Docetaxel	neoadjuvant TNBC	II	NCT00600249

1.7.2 SRC TARGETED THERAPIES

Small molecule Src inhibitors are in early phases of clinical development in comparison to EGFR inhibitors (Table 1.5). Two important Src inhibitors in clinical trials in breast cancer are dasatinib and AZD-0530.

Dasatinib (Sprycel™, Bristol-Myers-Squibb) is an oral, small molecule multi-kinase inhibitor of several Src family kinases, as well as c-kit, PDGFR, Bcr-Abl, and ephrin receptor kinases [203]. Preclinical evaluation has shown that dasatinib can inhibit metastasis and proliferation, cause cell cycle arrest, and induce apoptosis [138].

Finn *et al.* tested dasatinib in a panel of breast cancer cell lines, and demonstrated significant sensitivity in basal-like and post-EMT breast cancer cell lines ($p = 0.008$) [138]. Sensitivity was defined as greater than 60 % inhibition at 1 μM dasatinib. Cells were moderately sensitive if growth inhibition was 40 – 59 % at 1 μM, and resistant if inhibition was less than 40 % at 1 μM dasatinib.

Huang *et al.* [204] used a panel of 23 breast cancer cell lines with known gene expression profiling, and correlated these data with *in vitro* sensitivity to dasatinib. A six-gene model derived from this method correctly predicted dasatinib sensitivity in a further 11/12 (92 %) breast cancer cell lines. This 6 gene model was then applied to a gene expression set for 134 primary breast cancers. Strikingly, a higher percentage of the tumours predicted to respond to dasatinib were of the triple negative phenotype, and expressed basal CK5/17. This difference in expression was significant for HER-2 ($p = 0.035$), ER ($p = 0.014$), and CK5/17 ($p = 0.010$), and approaching significance for PR ($p = 0.078$).

Given this significant sensitivity to dasatinib in triple-negative breast cancer, these data identify a subgroup of breast cancers which may be more sensitive to Src inhibition. A number of clinical trials with dasatinib in breast cancer are ongoing (Table 1.6).

Table 1.5 Src inhibitors in clinical development (adapted from Finn [138])

Compound	Molecular targets	Stage of development in breast cancer
Dasatinib	SFKs, Bcr-Abl, Kit, Eph, PDGFR receptors	Phase II
SKI-606 (bosutinib)	SFKs, Bcr-Abl	Phase II
AZD0530	Src, Bcr-Abl	Phase II
XL999	Src, FGFR1, Kit, PDGFR, VEGFR2	Phase II[a]
AP22161	Src	Preclinical
AP22408, AP23451, AP23588	Src (in bone)	Preclinical
CGP76030	SFKs, Abl, EGFR, VEGFR	Preclinical
CGP77675	SFKs, EGFR, FAK, VEGFR	Preclinical
PD173955	Src, Abl, Kit, Yes	Preclinical
UC15A	Src	Preclinical

[a] Clinical development of XL999 was suspended in all tumour types following concerns over cardiovascular toxicity; approval was recently granted by the Food and Drug Administration to resume development in NSCLC. SFK, Src family kinases; PDGFR, platelet-derived growth factor receptor; fibroblast growth factor receptor-1; VEGFR, vascular endothelial growth factor receptor; EGFR, epidermal growth factor receptor; FAK, focal adhesion kinase.

Table 1.6 Current trials with dasatinib in TNBC (from www.clinicaltrials.gov)

Regimen	Setting	Phase	NCI Identifier
Dasatinib + Capecitabine	Advanced breast cancer	I	NCT00452673
Dasatinib	Advanced breast cancer	II	NCT00546104
Dasatinib	ER+/PR+ or HER-2+ breast cancer	II	NCT00371345
Dasatinib	Advanced TNBC	II	NCT00371254
Dasatinib	Breast cancer metastatic to bone	II	NCT00410813

AZD-0530 (AstraZeneca) is an oral, potent selective inhibitor of Src and Abl kinases [205]. In a tamoxifen resistant MCF7 variant breast cancer cell line, AZD-0530 significantly decreased activation of FAK and paxillin, and inhibited invasion. Also, the combination of AZD-0530 and gefitinib was additive in inhibiting motility and invasion [206]. Treatment with AZD-0530 following suppression of FAK with siRNA reduced the effects of cell adhesion and migration [206], suggesting that AZD-0530 affects Src activity in these cells.

Current clinical trials with AZD-0530 in breast cancer include a safety and tolerability study in solid tumours (NCT00475956); a safety and efficacy study in patients with metastatic bone disease (NCT00558272) and a single agent phase II study in hormone receptor negative metastatic or inoperable breast cancer (NCT00559507).

1.7.3 OTHER/NOVEL TARGETED THERAPIES IN TNBC

A number of novel agents, as well as agents which have proved beneficial in other cancer types, are under investigation as potential therapeutic agents in TNBC. Targeted therapies which are currently in clinical trials are briefly mentioned below.

1.7.3.1 VASCULAR ENDOTHELIAL GROWTH FACTOR (VEGF) RECEPTOR

VEGF has been shown to have an important role in vascular formation and development in mouse models, and is a vital angiogenic factor in human cancer biology, including breast cancer [207, 208]. There are three VEGF tyrosine kinase receptors (VEGFR-1, -2, -3). Similar to other tyrosine kinase receptors such as EGFR, receptor activation is ligand-dependent. Ligand binding leads to receptor hetero- or homo-dimerisation. Receptor dimerisation and activation leads to phosphorylation of tyrosine residues and the initiation of intracellular signalling cascades (Figure 1.8) [207]. A recent retrospective analysis of VEGF levels in breast cancer patients, including 87 TNBC patients, found significantly higher VEGF levels in TNBC compared to other subtypes (8.2 pg/μL *vs.* 2.7 pg/μL; $p < 0.001$) [209]. TNBC status was also associated with earlier relapse (18.8 *vs.* 30.7 months) and shorter survival following relapse ($p = 0.087$). This is the first study to assess VEGF levels in a TNBC subtype.

A number of clinical trials with VEGF/VEGFR inhibitors in TNBC are ongoing. These include studies with bevacizumab (a monoclonal antibody against VEGF), and sunitinib (a multi-target tyrosine kinase inhibitor of VEGFR-1,-2, -3, which also targets PDGFR, RET, KIT, and FLT-3). A summary of these trials is shown in Table 1.7. Of note, Ebos *et al.* reported that sunitinib was associated with increased metastatic tumour proliferation and decreased overall survival in murine models of metastatic tumours, following short-term treatment [210]. This effect was also observed with other VEGFR tyrosine kinase inhibitors, and suggests that this may be a drug class effect. This pre-clinical data is clearly of concern in relation to the use of this agent in the clinical setting, and underscores the importance of monitoring follow-up data in clinical trials with these agents.

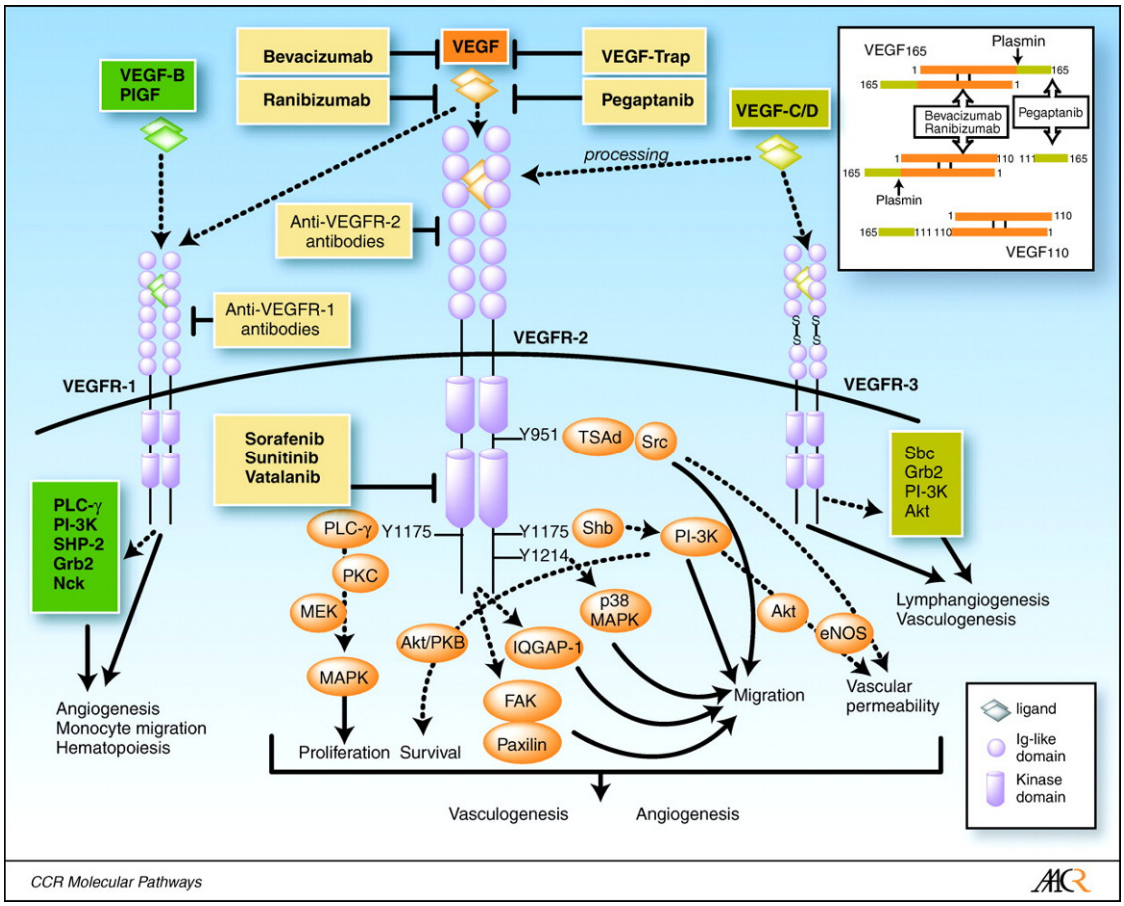

Figure 1.8 Signal transduction and biological processes mediated by VEGFRs and various therapeutic strategies to inhibit VEGF signalling. Inhibition of VEGF signalling can be achieved by monoclonal antibodies targeting VEGF (bevacizumab and ranibizumab), aptamers that bind the heparin-binding domain of $VEGF_{165}$ (pegaptanib), chimeric soluble receptors, such as VEGF-Trap, monoclonal antibodies targeting VEGFRs, and various small-molecule tyrosine kinase inhibitors (sorafenib, sunitinib, and vatalanib). *Top right inset,* because pegaptanib binds to VEGF within heparin-binding domain (*yellow*), it inactivates only $VEGF_{165}$. In contrast, bevacizumab and ranibizumab inactivate all biologically active forms of VEGF, such as $VEGF_{110}$. *eNOS,* endothelial nitric oxide synthase; *FAK,* focal adhesion kinase; *Grb2,* growth factor receptor-bound protein 2; *MAPK,* mitogen-activated protein kinase; *MEK,* mitogen-activated protein kinase/extracellular signal-regulated kinase kinase; *PI-3K,* phosphatidylinositol 3′-kinase; *PKB,* protein kinase B; *PKC,* protein kinase C; *PLC-γ,* phospholipase C-γ; *Shb,* Src homology 2 and β cells; *SHP-2,* Src homology phosphatase-2; *TSAd,* T-cell-specific adapter; *PlGF,* placental growth factor (from [207]).

Table 1.7 Current trials with VEGF-targeted therapy in TNBC (from www.clinicaltrials.gov); T: paclitaxel; C: carboplatin; A: doxorubicin; Cyc: cyclophosphamide

Regimen	Setting	Phase	NCI Identifier
T, C, **Sunitinib**	Dose-finding/efficacy	I	NCT00887575
T, **Bevacizumab**, Vorinostat	Metastatic/Recurrent	I	NCT00368875
Bevacizumab, T	Metastatic	II	NCT00472693
C, T, **Bevacizumab**	Metastatic	II	NCT00479674
A, C, **Bevacizumab**	Metastatic	II	NCT00608972
C, T, **Bevacizumab**	Metastatic	II	NCT00691379
T, **Bevacizumab** or Erlotinib	Metastatic	II	NCT00733408
Standard of Care *vs.* **Sunitinib**	Advanced	II	NCT00246571
T / Cyc **/Bevacizumab** → A / Cyc **/ Bevacizumab**	Neoadjuvant Operable	II	NCT00777673
T / dd AC **/Bevacizumab /** C (2x2)	Neoadjuvant Operable	II	NCT00861705
Chemotherapy (anthracycline ± taxane or taxane only) ± **Bevacizumab**	Adjuvant	III	NCT00528567 (BEATRICE)

1.7.3.2 POLY (ADP-RIBOSE) POLYMERASE (PARP) INHIBITION

The role of BRCA1 mutations, familial breast cancer, and the triple negative phenotype is discussed in section 1.4.3. One of the major causes of the genetic instability associated with BRCA1 deficiency is that BRCA1 mutant cells have an impaired ability to undergo homologous recombination (HR) [211], and therefore cannot effectively repair HR-mediated DNA damage, such as DNA double strand breaks (DSBs) (Figure 1.9). In the absence of BRCA1, DSBs can be gradually accumulated, which may result in the activation of oncogenes and inactivation of tumour suppressor genes, eventually leading to tumour formation.

Poly (ADP-Ribose) polymerase-1 (PARP-1) PARP-1 is essential for the repair of single strand DNA breaks during base excision repair (BER) of small DNA adducts induced by alkylating agents or ionizing radiation [212, 213]. PARP-1 inhibition leads to persistent single strand breaks in DNA [214], which result in formation of double strand breaks when they meet at replication forks (Figure 1.9A). In the presence of wild type BRCA1 and BRCA2, double strand breaks can be efficiently repaired by RAD51 mediated homologous recombination (Figure 1.9B). BRCA1 and BRCA2 interact with RAD51, and play essential role in homologous recombination [215]. Thus, in the event of DNA damage associated with PARP inhibition, BRCA1 or BRCA2 mutant cells cannot repair DNA double strand breaks properly, leading to the collapse of replication forks, and illegitimated DNA ends joining, consequently leading to growth arrest and apoptosis (Figure. 1.9C). This has been referred to as synthetic lethality [216]. This model provides a molecular basis for the reason that why BRCA1- and BRCA2-deficient cells are extremely sensitive to PARP-1 inhibition.

A list of current trials with PARP-1 inhibitors is shown in table 1.8. Recent data from a randomised phase II trial of BSI-201 in metastatic triple negative breast cancer, in combination with gemcitabine/carboplatin (NCT00540358), reported improved clinical benefit rate (62% *vs.* 21%, $p = 0.0002$), objective response rate (48% *vs.* 16%, $p = 0.002$), median progression-free survival (6.9 months *vs.* 3.3 months, HR = 0.342, $p < 0.0001$), and median overall survival (9.2 months *vs.* 5.7 months, HR = 0.348, $p = 0.0005$) compared with gemcitabine/carboplatin alone [217]. These data suggest a

promising role for PARP inhibitors in the treatment of BRCA1-mutated triple negative breast cancers.

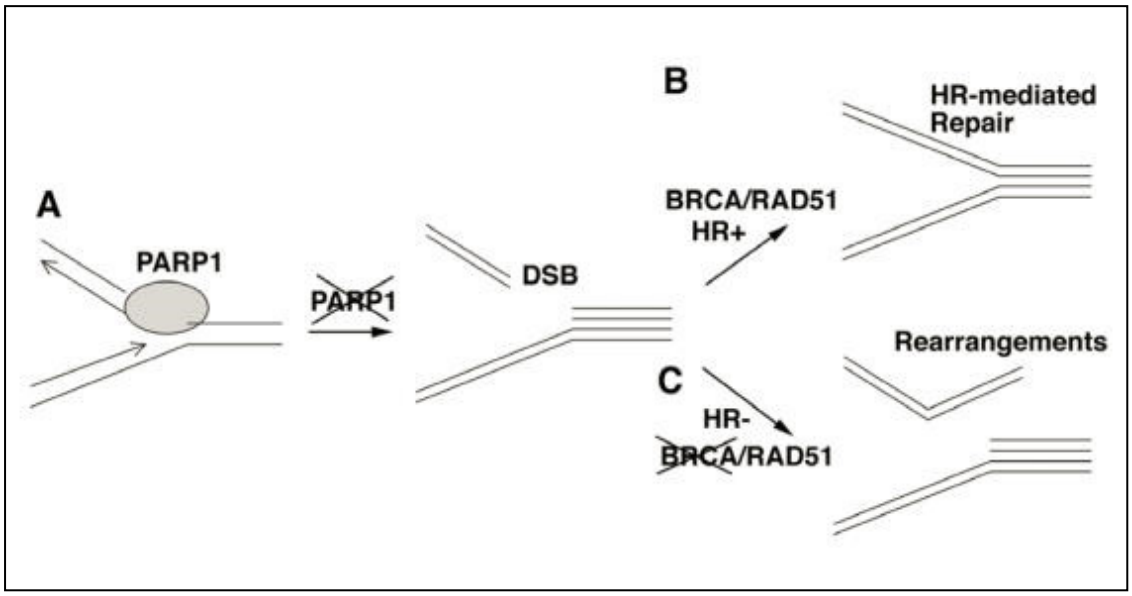

Figure 1.9 A model showing double strand breaks (DSB) formation and DNA rearrangement in the absence of BRCA and PARP1. **A.** PARP-1 binds and repairs single strand breaks (SSBs) in DNA. These SSBs result in formation of double strand breaks (DSBs) when they meet replication forks. **B.** In the presence of wild type BRCA1 and BRCA2, DSBs can be efficiently repaired by RAD51 mediated homologous recombination (HR). **C.** BRCA1 or BRCA2 mutant cells cannot repair DNA DSBs properly upon the inhibition of PARP, leading to DNA replication arrest and illegitimated DNA ends joining (from [33]).

Table 1.8 Current trials with PARP-1 inhibitor therapy in TNBC (from www.clinicaltrials.gov)

Regimen	Setting	Phase	NCI Identifier
Carboplatin, **AZD2281**	BRCA+ Metastatic Breast & Ovarian	I	NCT00647062
Gemcitabine, Carboplatin, **BSI-201**	Metastatic	II	NCT00540358
AZD2281	Recurrent BRCA+ Breast	II	NCT00679783
Gemcitabine, Carboplatin, **BSI-201**	Neoadjuvant	II	NCT00813956
Gemcitabine, Carboplatin, **BSI-201**	Metastatic/Recurrent	III	NCT00938652

1.7.3.2 mTOR

mTOR (mammalian Target Of Rapamycin) is a protein encoded by the FRAP1 gene [218]. It is a serine/threonine kinase that regulates cell growth, proliferation, motility, protein synthesis and survival [219]. mTOR is downstream of Akt in the PI3K/Akt pathway, and Akt is an important regulator of mTOR phosphorylation [219]. Interestingly, inhibition of mTOR by the inhibitor RAD001 results in increased Akt activation both in cancer cell lines and patient tumours [220]. Given the importance of the Akt pathway in breast cancer, this suggests that combination therapy with mTOR inhibition and another inhibitor of this pathway would be necessary to yield enhanced efficacy. Recent *in vitro* data, showing enhanced inhibition of growth in triple negative breast cancer cell lines using RAD001 and the dual EGFR/HER-2 tyrosine kinase inhibitor lapatinib support this hypothesis [221]. Current clinical studies examining the potential therapeutic role for mTOR inhibition are listed in Table 1.9

Table 1.9 Current trials with mTOR inhibitor therapy in TNBC (from **www.clinicaltrials.gov**)

Regimen	Setting	Phase	NCI Identifier
RAD001 (evirolimus)	Metastatic	II	NCT00827567
Paclitaxel ± FEC, **RAD001**	Neoadjuvant	II	NCT00499603
Cisplatin + Paclitaxel **± RAD001**	Neoadjuvant	II	NCT00930930

1.8 SUMMARY AND CONCLUSION

The traditional classification of breast cancer, based on phenotypic and histopathological characteristics, has provided the basis for clinical treatment decision-making for a number of decades. The revolution in genomics over the last decade has provided a molecular reclassification of breast cancer subtypes which reproducibly correlates with clinico-pathological characteristics, and has increased our understanding of breast carcinogenesis. Breast cancer is increasingly being recognised as being a heterogeneous disease. Among these subgroups, triple negative/basal-like breast cancers generally express CK5/6 and 17, and EGFR, and lack expression of ER, PR, and HER-2 amplification. Other important tyrosine kinases in triple negative breast cancer include Src and c-kit. Important signalling pathways in breast cancer include the Akt and MAPK pathways.

Many, but not all, basal-like breast cancers are of the triple negative phenotype. In the clinical setting at present however, the triple negative phenotype is a useful surrogate for identifying these tumours.

The triple-negative/basal-like breast cancer subgroup is associated with younger age of diagnosis and poorer prognosis compared to other subtypes. This group currently lacks approved therapeutic targets. There is urgent need for the development and understanding of new targeted therapy options for triple negative breast cancer. Clinical trials assessing the potential role of therapies targeted at EGFR, PARP, VEGFR, and mTOR are ongoing.

Our research focuses on evaluating EGFR targeted therapies and dasatinib as novel therapies for triple negative breast cancer.

1.9 STUDY AIMS

The aims of this thesis are as follows:

- To investigate the role of epidermal growth factor receptor (EGFR) in triple negative breast cancer (TNBC)

- To examine EGFR and P-EGFR in breast tumours

- To develop and characterise a model of acquired resistance to dasatinib in TNBC

- To perform proteomic analysis of TNBC model of acquired resistance to dasatinib

Chapter 2

MATERIALS AND METHODS

2.1 CELL LINES, CELL CULTURE AND REAGENTS

Five TNBC cell lines (BT20, HCC1937, MDA-MB-231, HCC1143, MDA-MB-468) and two HER-2 over-expressing cell lines (BT474, SKBR3) were obtained from the American Type Culture Collection (ATCC). Cell lines were maintained in RPMI-1640 medium supplemented with 10 % fetal bovine serum (BioWhittaker), at 37 ^{o}C with 5 % CO_2. In addition, HCC1937 medium was supplemented with 1 % sodium pyruvate (Sigma). Regular screening for mycoplasma infection was performed on all cell lines used.

Gefitinib (IRESSA™, AstraZeneca), cetuximab (ERBITUX™, Bristol-Myers Squibb/MERCK), docetaxel (TAXOTERE™, sanofi aventis), carboplatin (PARAPLATIN™, Bristol-Meyers Squibb), and doxorubicin (ADRIAMYCIN PFS™, Pharmacia and Upjohn) were purchased from the Pharmacy Department, St. Vincent's University Hospital, Dublin. Erlotinib and dasatinib were purchased from Sequoia Research Products. All agents were reconstituted in dimethyl sulfoxide (DMSO), and stored at either ambient temperature (gefitinib, docetaxel, carboplatin, erlotinib, dasatinib) or at 4 ºC (cetuximab, doxorubicin).

2.2 PROLIFERATION ASSAYS

96-well plates were seeded with $3x10^3$ cells (in 100 µL) per well for all cell lines. Following overnight incubation, drug was added at the appropriate concentrations (100 µL per well) and incubated for 5 days. Media was removed and cells washed once with PBS**.** 100 µl of acid-phosphatase substrate (7.25 mM para-nitrophenyl-phosphate (Sigma) in sodium acetate buffer (0.1 M sodium acetate pH 5.5 + 1.0 % Triton-X-100)) was added to each well and incubated at 37 ^{o}C for 1 hour. 50 µL of 1 M NaOH was added to stop the reaction, and the absorbance was read at 405 nM with 620 nM as the reference wavelength. Cell proliferation was measured relative to control cells (treated with serum-containing medium only), included in each experiment. All assays were performed in triplicate.

2.2.1 COMBINATION ASSAYS

Two types of combination assays were used. Fixed combination assays combined a single concentration of one agent with a range of concentrations of the second agent. Cells were seeded in 96-well plates as described in section 2.2. After 24 hours, cells were treated with each agent singly, and in combination. The cells were incubated for a further 120 hours. The effects of the treatments on proliferation were measured using the acid phosphatise assay as described in section 2.2. Results represent triplicate independent experiments.

Fixed ratio proliferation assays tested the effects on cell proliferation of three agents over a range of concentrations which were constant relative to each other. The effects on proliferation were measured for each agent alone, for each pair of agents, and for the three agents together. Conditions were otherwise as those used for the fixed ratio assays.

2.2.2 SCHEDULING ASSAYS

Alternate scheduling of agents was tested using a fixed concentration combination assay. Cells were seeded in 96-well plates as described in section 2.2. After 24 hours, the first agent was added at the appropriate concentrations (in 50 µL per well). After a further 24 hours, the second agent was added at the appropriate concentrations (in 50 µL per well). The cells were incubated for a further 72 hours. Cell proliferation was measured using the acid phosphatase assay as described in section 2.2.

2.3 PROTEIN EXTRACTION/PREPARATION OF CELL LYSATES

Cells were grown in 100 mm petri dishes until approximately 80 % confluency was achieved. After drug treatment for the specified time, cells were washed with ice-cold PBS and lysed in 250-500 µL RIPA buffer (Sigma) containing protease inhibitors, 1 mM PMSF and 1 mM sodium orthovanadate (Sigma). After 20 minutes incubation on ice, the lysate was passed through a 21-gauge needle and centrifuged at 13,200 rpm for five minutes at 4 ^{o}C. Protein quantification was performed using the bicinchoninic acid (BCA) assay (Pierce).

2.4 IMMUNOPRECIPITATION (IP)

500 µg of protein lysate was diluted in 900 µl RIPA buffer and incubated with 3 µg antibody (anti-EGFR (Labvision); anti-EphA2 (Santa Cruz)) at 4 ^{o}C, shaking, for 30 minutes. 50 µl of packed Protein-G agarose beads (Santa Cruz Biotechnology) were added and the samples incubated overnight, shaking, at 4 ^{o}C. The samples were centrifuged at 13,200 rpm for 25 seconds, the supernatants removed and the pellets washed with IP wash buffer (Mild Lysis Buffer (Cell Signalling Technology) with protease inhibitors). The wash was repeated twice and the samples were centrifuged for 35 seconds. The supernatants were removed and the pellets resuspended in 50 µl denaturing buffer and denatured at 95 ^{o}C for five minutes. Denatured samples were then centrifuged at 14,000 rpm for 3 minutes and the supernatants collected and stored at -20 ^{o}C.

2.5 WESTERN BLOTTING

20 - 30 µg of protein in sample buffer was heated to 95 ^{o}C for five minutes and proteins were separated using 7.5 % or 10 % polyacrylamide gels (Lonza). Protein was transferred to Hybond-ECL nitrocellulose membrane (Amersham Biosciences) and the membrane was blocked with blocking solution (milk powder or bovine serum albumen (BSA)/PBS-Tween) at room temperature for 1 hour. After overnight incubation at 4 ^{o}C with primary antibody in blocking solution, three washes with PBS-Tween were performed, followed by incubation at room temperature with secondary antibody in blocking solution for 1 hour. Following three washes with PBS-Tween and one PBS wash, protein bands were detected using Luminol (Santa Cruz Biotechnology Inc.) or ECL-Advance (Amersham Biosciences). Specific conditions for each antibody used are detailed in Table 2.1. For detection of P-EGFR: following immunoprecipitation (Chapter 2.4) P-EGFR was detected using anti-phospho-tyrosine antibody (Cell Signalling).

Table 2.1 Details of antibodies and experimental conditions used for detection of protein by immunoblotting.

Primary antibody	Source	Company	Dilution used	Blocking Solution	Washes
EGFR Ab-15 (Clone 15), cytoplasmic domain	Mouse	Labvision	1 µg/ml	3 % non fat milk powder/ PBS-0.1 % Tween	PBS-0.1 % Tween
α-tubulin	Mouse	Sigma Aldrich	2 µg/ml in 5 % non fat milk powder in PBS-0.1 % Tween	5 % milk/ PBS-0.1 % Tween	PBS-0.1 % Tween
Phospho-tyrosine (mouse monoclonal $IgG_{2b\kappa}$)	Mouse	Medical Supply Company	0.75 µg/ml (1:666.67 dilution) in 3 % BSA in PBS-0.1% Tween	3 % BSA/ PBS-0.1 %	PBS-0.1 % Tween
P-MAPK p42/44	Rabbit	Cell Signalling	1 µg/ml in 5 % non fat milk powder in PBS-0.1 % Tween	5 % milk/ PBS-0.1 % Tween	PBS-0.5 % Tween
MAPK p42/44	Rabbit	Cell Signalling	1 µg/ml in 5 % non fat milk powder in PBS-0.1 % Tween	5 % milk/ PBS-0.1 % Tween	PBS-0.5 % Tween
P-Akt (Ser 473)	Rabbit	Cell Signalling	1 µg/ml in 5 % non fat milk powder in PBS-0.1 % Tween	5 % milk/ PBS-0.1 % Tween	PBS-0.5 % Tween

Table 2.1 continued

Primary antibody	Source	Company	Dilution used	Blocking Solution	Washes
Akt	Rabbit	Cell Signalling	1 µg/ml (1:1000) in 5 % non fat milk powder in PBS-0.1 % Tween	5 % milk/ PBS-0.1 % Tween	PBS-0.5 % Tween
P-Src [pY^{418}]	Rabbit	Invitrogen	2 µg/ml (1:5000) in 5 % non fat milk powder in PBS-0.1 % Tween	5 % milk/ PBS-0.1 % Tween	PBS-0.5 % Tween
Src (pp60^{Src} Kinase)	Mouse	Upstate Biotechnology	1 µg/ml (1:1000) in 5 % non fat milk powder in PBS-0.1 % Tween	5 % milk/ PBS-0.1 % Tween	PBS-0.5 % Tween
ERα (F-10)	Mouse	Santa Cruz	1 µg/ml (1:200) in 3 % non fat milk powder in PBS-0.1 % Tween	3 % milk/ PBS-0.1 % Tween	PBS-0.1 % Tween
P-EphA2 (Tyr594)	Rabbit	Cell Signalling	1 µg/ml (1:1000) in 5 % non fat milk powder in PBS-0.1 % Tween	5 % milk/ PBS-0.1 % Tween	PBS-0.5 % Tween

Table 2.1 continued

Primary antibody	Source	Company	Dilution used	Blocking Solution	Washes
EphA2	Mouse	Millipore	1 µg/ml (1:1000) in 5 % non fat milk powder in PBS-0.1 % Tween	5 % milk/ PBS-0.1 % Tween	PBS-0.5 % Tween
HER-2 (3B5)	Mouse	Calbiochem	1:1000 in 5 % non fat milk powder in PBS-0.1 % Tween	5 % milk/ PBS-0.1 % Tween	PBS-0.5 % Tween
ANXA1	Mouse	Abcam	1 µg/ml in 5 % non fat milk powder in PBS-0.1 % Tween	5 % milk/ PBS-0.1 % Tween	PBS-0.5 % Tween
CCT3	Mouse	ProteinTech Group	1:12000 in 3 % non fat milk powder in PBS-0.1 % Tween	3 % milk/ PBS-0.1 % Tween	PBS-0.1 % Tween
ENO1	Mouse	Abcam	1:1000	3 % milk/ PBS-0.1 % Tween	PBS-0.1 % Tween
Anti-mouse (secondary)	-	Sigma	1:1000	3 % milk/ PBS-0.1 % Tween	PBS-0.1 % Tween
Anti-rabbit (secondary)	-	Sigma	1:3000	5 % milk/ PBS-0.1 % Tween	PBS-0.5 % Tween

2.6 ENZYME-LINKED IMMUNOSORBENT ASSAY (ELISA)

EGFR and phosphorylated EGFR (P-EGFR) were measured by ELISA. 1 µg protein (TNBC cell lines) or 5 µg protein (HER-2 positive cell lines) was used for the EGFR ELISA (R&D Systems). EGFR protein concentrations were estimated from a standard curve and expressed as pg EGFR per µg of total protein. For P-EGFR, TNBC cells were serum starved for 24 hours and treated with serum-free medium (control), 10 ng/ml EGF (Sigma) for 10 minutes, or 1 µM gefitinib for 15 minutes followed by 10 ng/ml EGF for 10 minutes. 1 µg (BT20) or 5 µg (HCC1937, MDA-MB-231) protein was tested in the P-EGFR ELISA (R&D Systems). P-EGFR levels were expressed relative to control untreated cells.

2.7 CELL CYCLE ASSAYS

24-well plates were seeded with $1x10^5$ cells per well. Following overnight incubation, cells were treated with drug(s) for 24 or 48 hours. An untreated control and a DMSO control were also tested. Non-adherent cells were collected and combined with adherent cells after trypsinisation, then centrifuged at 2300 rpm for 5 minutes. Cells were washed in PBS, then resuspended in 20 µL PBS and fixed in 200 µL ice-cold 70 % ethanol at 4 ^oC overnight in a 96-well round bottom plate. The plate was centrifuged at 2300 rpm for 5 minutes with the brake on low at ambient temperature. The supernatant was carefully removed. The remaining cell pellet in each well was resuspened in 200 µL PBS, and the suspension mixed by pipette The plate was allowed to stand for one minute at ambient temperature, then centrifuged as before. The supernatant was carefully removed. 200 µL Cell Cycle Reagent (Guava Technologies) was added to each well, and the suspension mixed by pipette. The plate was incubated shielded away from light for 30 minutes. Assays were analysed on the Guava EasyCyte. Data analysis was performed using ModFit LT ™ software (Verity).

2.8 GUAVA VIACOUNT

Medium was removed from each well in a 96-well plate. The well was washed with 50 µL dilute trypsin (50 % trypsin in PBS). 30 µL dilute trypsin was added to each well, and following incubation for 5 – 10 minutes, 70 µL of medium was added. Depending upon concentration of cells present, a 1:1 to 1:3 mixture of the cell suspension and the Viacount Flex reagent (Guava Technologies) was made. Cell counting was analysed on the Guava EasyCyte.

2.9 DOUBLING TIME ASSAYS

24-well plates were seeded with $2x10^3$ cells in 1 ml of serum-containing medium (day -1). On day 0, fresh medium (control) or drug-containing medium was added to the cells. Duplicate wells per cell line for each condition (control and drug treatments) were seeded for each time point: day 0, day 4, and day 7. Cell counts for each time point were measured by the Guava Viacount method (described in section 2.8). Doubling times were calculated between days 4 and 7 using the formula

$$\text{Doubling time (hours)} = 24 \times \left(\frac{\log 2 \times (Tt - T0)}{(\log Nt - \log N0)} \right)$$

where Tt is the end time point and T0 is the beginning time point (days), which in this case were 7 and 4, respectively, and N is the average cell count on each day. Each assay was performed in triplicate.

2.10 MOTILITY AND INVASION ASSAYS

Motility and invasion assays were performed using the method previously described [222]. 24-well invasion inserts (Falcon) were coated with 100 µL Matrigel (BD Biosciences, diluted to 1 µg/µL in Dulbecco's Modified Eagle's Medium) and left

overnight at 4 °C. The following day, the plates were placed at 37 °C for one hour. Excess Matrigel was removed. $5x10^4$ cells in 100 µL 5 % fetal calf serum (FCS) medium were added to Matrigel-coated inserts for invasion assays, and uncoated inserts for motility assays. 500 µL of 10 % FCS-medium were added to each well beneath the insert. Cells were incubated for 6 hours at 37 °C before treatment, to allow cells to attach. Following treatment (100 µL 5 % FCS-medium or dasatinib-containing 5 % FCS-medium), cells were further incubated for 18 hours. Cells were stained with 0.25 % crystal violet and the number of invading or migrating cells was estimated by counting 10 fields of view at 200 X magnification. The average count was multiplied by the conversion factor 140 (growth area of membrane divided by field of view area, viewed at 200 X magnification) to determine the total number of migrating or invading cells. All assays were performed in triplicate.

2.11 DASATINIB ACCUMULATION ASSAYS

Cells were seeded at the specified numbers in T25cm^2 cell culture flasks (Costar). Triplicate flasks per cell line per condition were used. After 24 hours, the cell culture medium was removed and cells were treated with 5 mls of fresh medium (control) or 5 mls of 2 µM dasatinib for two hours. . Non-adherent cells were collected and combined with adherent cells after trypsinisation, then centrifuged at 900 rpm for 3 minutes. The supernatant was removed, and the cells were resuspended in 1 ml of ice-cold PBS. 50 µl of the cell suspension was removed for cell counting using the Guava Viacount method (described in section 2.8). The cell suspension was centrifuged as before, and the supernatant was removed. The cell pellet was stored at -20 ^oC.

Quantification of the mass of dasatinib present in the cells collected was performed using liquid chromatography tandem mass spectrometry (LC-MS). This technique was performed by Sandra Roche and Dr. Robert O'Connor, using the method described by Roche *et al.* [223]. Briefly, the method used was as follows. The drug was extracted from the cells using a liquid-liquid extraction procedure. 100 µL of 500 ng/ml lapatinib was added to an extraction tube (internal standard), along with 200 µL of 1 M Ammonium Formate pH 3.5 buffer and 1.6 mL of extraction solvent *tert*-Butyl Methyl Ether (*t*BME)/ acetonitrile (ACN) (3:1). The extraction tubes were vortexed and

mixed on a blood tube mixer for 15mins. The samples were centrifuged at 4000 rpm for 5 minutes; the organic layer was removed with a glass pasteur pipette and 1.1 mL of solvent was transferred to conical bottomed glass LC autosampler vials (Chromacol). The vials were evaporated to dryness using a Genevac EZ-2 (Ipswich, UK) evaporator at ambient temperature, without light. The samples were reconstituted in 40 µL of acetonitrile with 20 µL injected automatically by the autosampler.

The LC-MS was run in with isocractic mobile phase (54 % ACN:10 mM ammounium formate pH 4) on a Hyperclone BDS C18 column, in multi reaction monitoring (MRM) positive ion mode.

Analysis was performed using MRM mode with the following transitions: m/z 581→m/z 365 for lapatinib, and m/z 488→m/z (231 and 401) for dasatinib, with a dwell time of 200 ms. Quantification was based on the integrated peak area as determined by the Masshunter Quantification Analysis software which quantititates the peak areas of the MRM transitions of each analyte.

All results are reported as mean and standard deviation (SD) of the mass per million cells in triplicate flasks. Mass per million cells was calculated as the mass of drug measured divided by the counted number of cells and multiplied by a million.

2.12 PROTEOMIC ANALYSIS

All proteomic analyses detailed in this thesis were performed under the supervision of Dr. Paul Dowling.

2.12.1 PROTEIN PREPARATION

Cells were grown to approximately 80 % confluence in 225 cm^2 flasks, and treated for 6 hours with control growth media (RPMI 1640 + 10 % FCS), or media containing 50 nM dasatinib. Triplicate samples of each treatment were prepared. Total protein was extracted using the Pierce™ Phosphoprotein Enrichment Kit (Pierce Biotechnology). Using this kit, cells were washed twice with cold HEPES buffer (50 mM, pH 7), and

lysed using the Lysis/Binding/Wash buffer provided, supplemented with CHAPS (0.25%), 1X Halt Protease Inhibitor EDTA-free and 1X Halt Phosphatase Inhibitor Cocktail (Pierce Biotechnology). Cells were scraped into microcentrifuge tubes, and placed on ice for 45 minutes, vortexing periodically. The lysed cells were centrifuged at 10,400 rpm for 20 minutes at 4 ^{o}C and the supernatant collected and stored at -80 ^{o}C. Protein quantification was performed using a bicinchoninic acid (BCA) assay (Pierce Biotechnology). Enrichment for phosphoproteins was not performed due to insufficient protein obtained, Samples were then stored at -80^{o}C. To make the samples suitable for isoelectric focusing (IEF) and 2D gel electrophoresis, the samples were purified using the ReadyPrep ™ 2-D cleanup kin (Bio-Rad). Following the clean-up step, protein was quantified using the Bradford Assay (Bio-Rad).

2.12.2 PROTEIN LABELLING AND TWO-DIMENSIONAL DIFFERENTIAL GEL ELECTROPHORESIS (DIGE)

DIGE was performed using three CyDye DIGE Fluor Minimal dyes Cy3, Cy5 and Cy2 (GE Healthcare) [224]. In this technique, 50 µg of each protein sample was added to microcentrifuge tubes and labelled with Cy3 or Cy5 dye (200 pico mole (pmol) in 1 µl anhydrous dimethylformamide (DMF)). Each tube was mixed by vortexing, and placed on ice for 30 minutes in the dark. Under these conditions approximately 1% of the lysine residues of the protein are covalently conjugated to the CyDyes. The reaction was quenched by the addition of a 50-fold molar excess of free lysine to the dye for 10 minutes on ice in the dark. The labelled samples were stored at –80 ^{o}C.

Each gel compared two samples, one labelled with Cy3 and the other with Cy5 (Table 2.2). Triplicate gels were run for each comparison. A Cy2-labelled pool was prepared containing 25 µg of protein from each of the 12 samples. This pool was used on all gels as an internal standard to allow for accurate quantification [224]. A mix of each sample was also prepared to run on a preparative gel to facilitate protein identification after electrophoresis. An equal volume of 2X sample buffer (2.5 ml rehydration buffer stock solution (7 M urea, 2 M thiourea, 4 % CHAPS), pharmalyte broad range pH 4-7 (2%) (GE Healthcare), DTT (2%)) (Sigma) was added to the labelled protein samples. The mixture was left on ice for 10 minutes before the next step.

The protein samples were then passively rehydrated into immobiline 24-cm linear pH gradient strips (IPG, pH 3-11) (GE Healthcare) using rehydration buffer solution (7 M urea, 2 M thiourea, 4 % CHAPS, 0.5% IPG buffer, 50 mM DTT). Each strip was overlaid with 3 ml IPG Cover Fluid (GE Healthcare) and allowed to rehydrate overnight at RT. Isoelectric focussing (IEF) was then performed using the IPGphor apparatus (40 kv/hr @ 20 ^{o}C with resistance set at 50mA) (GE Healthcare).

Table 2.2. DIGE experimental design, showing gel number and the Cy dye used for each sample comparing the parental MDA-MB-231 cell line and dasatinib-resistant variant MDA-MB-231-Das (triplicate samples were run for each comparison). C: Control sample (untreated), D: Dasatinib 100 nM.

Gel no.	Cy2 (50 µg)	Cy3 (50 µg)	Cy5 (50 µg)
1	Cy2 pool	MDA-MB-231 (C1)	MDA-MB-231 (D1)
2	Cy2 pool	MDA-MB-231 (C2)	MDA-MB-231 (D2)
3	Cy2 pool	MDA-MB-231 (C3)	MDA-MB-231 (D3)
4	Cy2 pool	MDA-MB-231-Das (C1)	MDA-MB-231-Das (D1)
5	Cy2 pool	MDA-MB-231-Das (C2)	MDA-MB-231-Das (D2)
6	Cy2 pool	MDA-MB-231-Das (C3)	MDA-MB-231-Das (D3)

For second dimension separation, the strips were equilibrated by incubating in equilibrium solution (50 mM Tris-HCL, pH 8.8, 6 M urea, 30% glycerol, 1% SDS) containing 65 mM DTT for 20 minutes, followed by 20 minutes incubation in the

same buffer containing 240 mM iodoacetamide (both at RT). 12.5 % acrylamide gel solutions (acrylamide/bis 40 %, 1.5 M Tris pH 8.8, 10 % SDS) were prepared, and prior to pouring, 10 % ammonium persulfate and 100 µL neat TEMED were added. The gels were overlaid with 1 ml saturated butanol, and left to set for at least three hours at RT. Equilibrated IPG strips were transferred onto 24 cm 12.5% uniform polyacrylamide gels poured between low fluorescence glass plates. Strips were overlaid with 0.5% low melting point agarose in running buffer containing bromophenol blue. Gels were run at 2.5 W/gel for 30 min and then 100 W total at 10 ^{o}C until the dye front had run off the bottom of the gels.

2.12.2.1 2D DIGE GEL IMAGING

All of the gels were scanned using the Typhoon 9400 Variable Mode Imager (GE Healthcare) to generate gel images at the appropriate excitation and emission wavelengths from the Cy2-, Cy3- and Cy5-labelled samples. The resultant gel images were cropped using the ImageQuant software tool and imported into Decyder 6.5 software. The biological variation analysis (BVA) module of Decyder 6.5 was used to compare the control *versus* test samples to generate lists of differentially expressed proteins.

2.12.3 PHOSPHOPROTEIN ANALYSIS

The Pro-Q® Diamond phosphoprotein gel stain was used to detect phosphorylated proteins in the total cell lysate obtained from the procedure described in section 2.12.1. Briefly, the method used is as follows. 300 µg of each protein sample was used. Duplicate samples were used for each condition. The protein was separated in two dimensions using polyacrylamide electrophoresis, similar to that described in section 2.12.2. For optimal staining, un-backed gels were used. The gel was immersed in 500 mL of fix solution (50 % methanol, 10 % acetic acid) and incubated at room temperature with gentle agitation for 60 minutes. The gel was then incubated in 500 mL of dH_20 with gentle agitation for 15 minutes. This wash step was repeated twice more. The gel was incubated in the dark in 500 mL of Pro-Q® Diamond

phosphoprotein gel stain with gentle agitation of 135 minutes. The incubation time was identical for all gels, to minimise variation. To destain the gel, it was incubated in 500 ml of destain solution (20 % acetonitrile, 50 mM sodium acetate pH 4) for 60 minutes, protected from the light. This step was repeated twice more for 30 minutes each, followed by three 15 minute wash steps, as before.

2.12.3.1 PHOSPHOPROTEIN GEL IMAGING

All of the gels were scanned using the Typhoon 9400 Variable Mode Imager (GE Healthcare) to generate gel images at the appropriate excitation and emission wavelengths for the Pro-Q® Diamond phosphoprotein stain (532 nm laser and 560 nm emission filter, respectively). The resultant gel images were cropped using the ImageQuant software tool and imported into Progenesis Samespots software (nonlinear dynamics). The software analysis was used to compare the control *versus* treated samples to generate lists of differentially abundant phosphoproteins.

2.12.4 SPOT DIGESTION

Preparative gels containing 300 mg of protein were fixed and then post-stained with colloidal CBB stain (Sigma). The subsequent gels were scanned using the Typhoon 9400 Variable Mode Imager (GE Healthcare) to generate gel images at the appropriate excitation and emission wavelengths for the colloidal CBB stain. Preparative gel images were then matched to the Master gel image generated from the DIGE experiment. Spots of interest were selected and a pick list was generated and imported into the software of the Ettan Spot Picker robot (GE Healthcare). Gel plugs were placed into pre-siliconised microtitre plate and stored at 47^{o}C until digestion. Tryptic digestions were performed using the Ettan Digestor robot (GE Healthcare). Excess liquid was removed from each plug, and washed for three cycles of 20 min using 50 mM NH4HCO3 in 50% methanol solution. The plugs were then washed for two cycles of 15 min using 70% ACN and left to air dry for 1 h. Lyophilised sequencing grade trypsin (Promega) was reconstituted with 50 mM acetic acid as a stock solution and then diluted to a working solution with 40 mM NH4HCO3 in 10% ACN solution, to a concentration of 12.5 ng trypsin per mL. Samples were digested at 37ºC overnight and

were then extracted twice with 50% ACN and 0.1% TFA solution for 20 minutes each. All extracts were pooled and concentrated by SpeedVac (Thermo Scientific) for 40 minutes.

2.12.5 MALDI TOF/TOF MASS SPECTROMETRY AND PROTEIN IDENTIFICATION

One fifth of the peptide extract solution from the digest was added to a 384 spot MALDI sample plate (Applied Biosystems) and supplemented with 0.5 µl of a 5 mg/ml solution of recrystalised α-cyano-4-hydroxy-trans-cinnamic acid matrix (Laser Biolabs) plus 10mM $NH_4H_2PO_4$ in 50% acetonitrile/water containing 0.1% TFA and allowed to air dry prior to analysis. MALDI mass spectra were generated using a 4800 TOF/TOF Proteomics Analyzer instrument (Applied Biosystems). An internal sample mix, Pep4 (Laser Biolabs) was also spotted onto target slides and used as an internal calibrant. All MS and MS/MS experiments were carried out in positive reflectron mode. Ten precursor ions for MS/MS were selected automatically on the basis of intensity from the MS spectra. The MS and MS/MS data were combined and searched against a number of databases using GPS Explorer software (Applied Biosystems) and a local MASCOT (Matrix Science) search engine for protein identification. A mass window of 75 ppm was set for database searching on all precursors.

2.13 IMMUNOHISTOCHEMISTRY (IHC)

Automated immunohistochemistry was performed using the DAKO Autostainer system. Antibodies against EGFR (EGFR PharmDx kit, DAKO), and phospho-EGFR (Tyr1173)(53A5) (Cell Signalling) were used. The EGFR PharmDx kit was supplied with positive control slides consisting of fixed cells from cell lines with different intensities of EGFR staining. Head & neck tumour sections which were optimised for P-EGFR staining, were used as positive controls for the P-EGFR IHC experiments. Tissue microarray slides containing the same tumour sections being tested were included as negative controls, using the DAKO antibody diluent only for the antibody step (Table 2.3).

For EGFR staining, paraffin-embedded tissue samples were de-waxed in xylenes (2 x 5 minutes), then re-hydrated in grading alcohols 100 %, 90 %, and 70 % (2 x 3 minutes each). For P-EGFR staining, paraffin-embedded tissue samples were de-waxed, rehydrated, and antigen retrieval performed using DAKO target retrieval solution pH 9. After de-paraffinisation, the tissue slides were placed in the DAKO Autostainer, which performed the programmed application of reagents in order as listed in Table 2.3. Washes were performed, with DAKO wash buffer, before and after the application of the each reagent, except in the case of the Real HP Block, where a blow step was performed. Slides were subsequently dehydrated in grading alcohols 70 %, 90 %, and 100 % (2 x 3 minutes each). Samples were then cleared in xylenes (2 x 5 minutes) and mounted in DPX (BDH). Negative controls in which the antibody was replaced by either the supplied EGFR PharmDx negative control or antibody diluent were included for all experiments.

Table 2.3 Programmed steps for immunostaining procedure for EGFR and P-EGFR using DAKO Autostainer system

Reagent	**EGFR**	**P-EGFR**
Real HP Block (DAKO)	5 minutes	10 minutes
Antibody (30 minutes)	EGFR PharmDx (ready-to-use)	1:60 dilution
Real EnVision (DAKO)	30 minutes	30 minutes
Real DAB (DAKO)	5 minutes	5 minutes
Real DAB (DAKO)	5 minutes	5 minutes
Hematoxylin S3302 (DAKO)	5 minutes	5 minutes

Staining was scored by two independent observers using the following guidelines. EGFR levels were evaluated semi-quantitatively using the DakoCytomation EGFR PharmDx™ scoring guidelines, which were created for the kit used in this experiment. These guidelines state that EGFR negative is recorded in the absence of specific *membrane* staining within the tumour, and given a score of 0 (no staining). EGFR positive staining is defined as any IHC staining of tumour cell membranes above background level, whether complete or incomplete circumferential staining, and is scored as 1+ (weak intensity), 2+ (moderate intensity), or 3+ (strong intensity). P-EGFR levels were scored using similar guidelines.

2.12 SMALL-INTERFERING RNA (siRNA) TRANSFECTION

A pool of four siRNA molecules targeting the ANXA1 gene was obtained from Thermo Scientific/Dharmacon [Table 2.4]. A siRNA molecule targeting kinesin (KIF11 siRNA, Ambion) was used as the positive control. A scrambled sequence siRNA molecule (Negative Control siRNA, Ambion) was used as the negative control.

Table 2.4. Target sequences of four anti-ANXA1 siRNA molecules, (with Thermo Scientific/Dharmacon siRNA ID number), which are part of the ON-TARGETplus SMARTpool Human ANXA1 used in this study.

ID	Target Sequence	Mol. Weight (g/mol)
J-011161-07, ANXA1	CAAAGGUGGUCCCGGAUCA	13,459.9
J-011161-08, ANXA1	GAAGUGCGCCACAAGCAAA	13,444.8
J-011161-09, ANXA1	UGACCGAUCUGAGGACUUU	13,429.8
J-011161-10, ANXA1	UAACUAAGCGAAACAAUGC	13,399.8

Experimental conditions for 96-well and 6-well plates are outlined in Table 2.5. Each siRNA molecule was transfected at a final concentration of 30 nM. Cells were resuspended in 10% RPMI 1640. Each siRNA and NeoFX™ transfection agent was diluted in Gibco™ Opti-MEM reduced serum medium (Invitrogen), and incubated at room temperature (RT) for 10 minutes. Diluted NeoFX™ was then added to each diluted siRNA and incubated for a further 10 minutes at RT. The transfection mix was then added to the wells followed by the addition of the cell suspension. After 24 hours, the transfection media was replaced with 10 % RPMI with or without 100 nM dasatinib. 6-well plates were used to prepare lysates after 72 hours. Cells in 96-well plates were harvested after three days dasatinib treatment and counted using the Guava EasyCyte (section 2.8).

Table 2.5. Experimental conditions for ANXA1 siRNA transfection in MDA-MB-231 cells, in 96-well and 6-well plates.

Reagent	**96-well plate**	**6-well plate**
Cell suspension	7000 cells /well (70 µL/well)	1.5 x 10^5 cells/well (1000 µL/well)
NeoFX ™	0.36 µL/well	6 µL/well
SiRNA	30 nM	30 nM
Transfection mixture	30 µL/well	100 µL/well

2.13 CALCULATIONS AND STATISTICAL ANALYSIS

Where indicated in the text, p values for statistical significance were calculated using a t-test unless otherwise stated, and were calculated based on triplicate results.

2.13.1 CALCULATION OF COMBINATION INDEX (CI) VALUES TO ASSESS POTENTIAL SYNERGY IN A FIXED-RATIO DRUG COMBINATION ASSAY

For fixed-ratio assays, combination indices (CI) at the ED_{50} (effective dose of combination that inhibits 50% of growth) were determined using the Chou and Talalay equation [225], on CalcuSyn software (Biosoft). The combination index equation is based on the multiple drug-effect equation of Chou-Talalay derived from enzyme kinetic models [226, 227]. The equation determines only the additive effect rather than synergism or antagonism. Synergism is defined as a more than expected additive effect, and antagonism as a less than expected additive effect [228]. Determination of synergy/antagonism used in our work was based on the recommended descriptions as shown in Table 2.6. As recommended by Chou *et al.*, the prerequisites for CI calculations included a dose-effect curve, at least three data points for each single drug, but any number of points for a combination, and a constant combination ratio design [228]. Additionally, the ratio for two drug combinations should correspond to three drug combinations. Where there is a three drug combination, synergism or antagonism can be calculated using their method with or without component dissections [228]. Where more than two drugs are involved in combination, mutual exclusivity can be assumed for the calculations [225, 228].

Table 2.6 Range of combinations index values which determine synergism or antagonism in drug combination studies analysed with the Combination Index Method[a]

Range of Combination Index (CI)	Symbol	Description
< 0.10	+ + + + +	Very strong synergism
0.10 – 0.30	+ + + +	Strong synergism
0.30 – 0.70	+ + +	Synergism
0.70 – 0.85	+ +	Moderate synergism
0.85 – 0.90	+	Slight synergism
0.90 – 1.10	±	Nearly additive
1.10 – 1.20	–	Slight antagonism
1.20 – 1.45	– –	Moderate antagonism
1.45 – 3.30	– – –	Antagonism
3.30 – 10.00	– – – –	Strong antagonism
> 10.00	– – – – –	Very strong antagonism

[a]The combination index method is based on that described by Chou and Talalay ([225, 229]) and the computer software of Chou and Chou [230, 231] and CalcuSyn. (***from 'CalcuSyn Manual' by Chou and Hayball, © Biosoft 1996 - 2005***) [228].

2.13.2 STATISTICAL CALCULATIONS OF PARAMETRIC AND NON-PARAMETRIC DATA

To assess for statistical significance in the immunohistochemistry analysis, Mann-Whitney U test was used to calculate p values for non-parametric data. Fisher's exact test was used to calculate p values for 2x2 table parametric data, as the overall number of tumours in the study was low. Chi-square test was used to calculate p values for parametric data greater than 2x2. The Bonferroni test was used to adjust p values for

multiple testing. The Bonferroni test was determined as the product of the p value and the number of tests performed on the data set [232].

Chapter 3

EGFR INHIBITION IN TRIPLE NEGATIVE BREAST CANCER

Sections of the work presented in this chapter were published in the paper "Epidermal growth factor receptor as a potential therapeutic target in triple-negative breast cancer," Annals of Oncology 2009 May;20(5):862-7.

3.1 INTRODUCTION

EGFR mRNA is detected more frequently and at higher levels in triple-negative/basal-like breast cancers [6]. In a tissue microarray study, EGFR expression was observed in 54 % of cases positive for basal cytokeratins. EGFR expression was also associated with poor survival, independent of nodal status and size [15].

EGFR inhibitors currently in clinical use include the small molecule tyrosine kinase inhibitors gefitinib and erlotinib and the monoclonal antibody cetuximab, which are approved for treatment of a number of other solid tumours [187, 200]. In this study we have investigated EGFR inhibition as a therapeutic option in the treatment of TNBC.

3.2 EGFR EXPRESSION IN TRIPLE NEGATIVE BREAST CANCER CELLS

EGFR expression was measured by ELISA in the TNBC cell lines BT20, HCC1937, and MDA-MB-231, and the HER-2 positive cell lines BT474 and SKBR3 (Figure 3.1, Table 3.1). Significantly higher levels of EGFR were detected in each of the TNBC cell lines compared to the HER-2 positive cell lines, which over-express HER-2 but have low levels of EGFR [233].

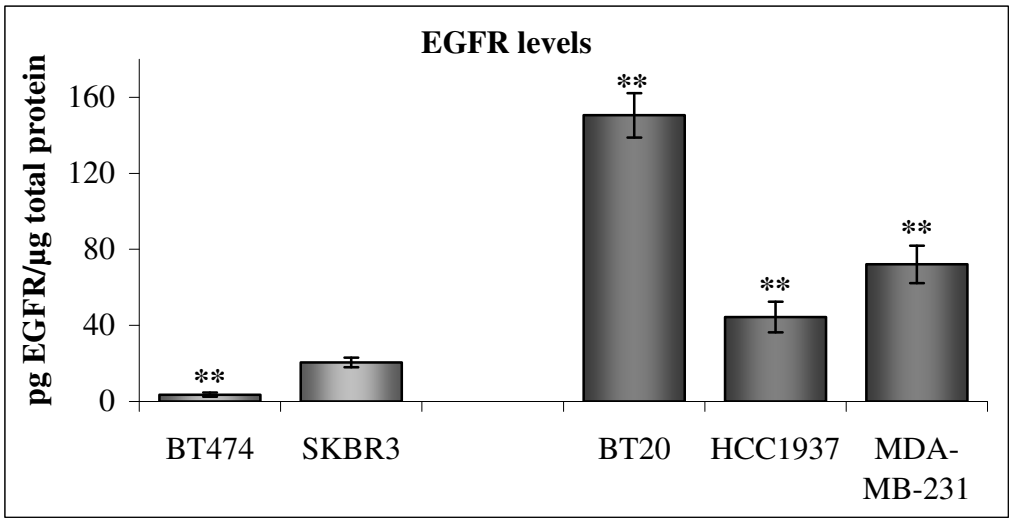

Figure 3.1 Levels of epidermal growth factor receptor in triple negative breast cancer cell lines and HER-2 positive cell lines, measured by ELISA. Error bars represent the standard deviation of three independent experiments. p values are calculated relative to SKBR3; * implies $p < 0.05$; ** implies $p < 0.005$

Table 3.1 Levels of EGFR (± standard deviation of three independent experiments), measured by ELISA, in HER-2 positive and triple negative breast cancer cell lines.

Cell line	***pg EGFR/µg total protein***
SKBR3	20.5 ± 2.5
BT474	3.6 ± 1.1
BT20	150.5 ± 11.7
HCC1937	44.4 ± 8.1
MDA-MB-231	72.1 ± 9.8

3.3 EGFR INHIBITION

Sensitivity to a panel of EGFR inhibitors was assessed using proliferation assays (section 2.2). The TNBC cell lines were less sensitive to gefitinib and erlotinib than the HER-2 positive cell lines (Table 3.2). Gefitinib was the most effective EGFR inhibitor tested, with HCC1937 the most sensitive of the TNBC cell lines (IC_{50}: 8.4 ± 1.5 µM). An IC_{50} concentration was not achieved with cetuximab for any of the cell lines tested. Maximum inhibition of growth was achieved in HCC1937 cells (approximately 20 %), when treated with 100 µg/ml cetuximab.

Table 3.2 Sensitivity of the breast cancer cell lines to EGFR inhibitors. IC_{50}: Drug concentration required to inhibit 50 % of cell growth ± standard deviation of three independent experiments.

Cell line	Gefitinib	Erlotinib	Cetuximab
	IC_{50} (μM)	*IC_{50} (μM)*	*(% inhibition at 100 μg/ml)*
SKBR3	0.88 ± 0.31	3.6 ± 0.4	no inhibition
BT474	0.25 ± 0.05	3.1 ± 0.4	no inhibition
BT20	15.5 ± 1.4	20.1 ± 2.7	17.0 % ± 2.0
HCC1937	8.4 ± 1.5	26.2 ± 9.3	19.7 % ± 5.0
MDA-MB-231	20.7 ± 1.1	42.6 ± 3.1	no inhibition

3.3 EFFECTS OF EGFR INHIBITION ON EGFR SIGNALLING

Gefitinib was the most effective EGFR inhibitor in the TNBC cell lines tested, and was used to assess the effects of EGFR inhibition on EGFR signalling. Higher levels of phosphorylated EGFR (P-EGFR) were detected in the BT20 cell line, by western blot, and phosphorylation was reduced in response to gefitinib treatment. Lower levels of P-EGFR were observed in MDA-MB-231 and HCC1937 cells (Figure 3.2). Gefitinib also reduced phosphorylation of EGFR in HCC1937 cells but a significant reduction was not detected in MDA-MB-231 cells.

Although low levels of P-EGFR were detected, EGF treatment significantly increased phosphorylation of EGFR in all three TNBC cell lines and gefitinib treatment efficiently blocked EGF-induced phosphorylation of EGFR (Figure 3.3).

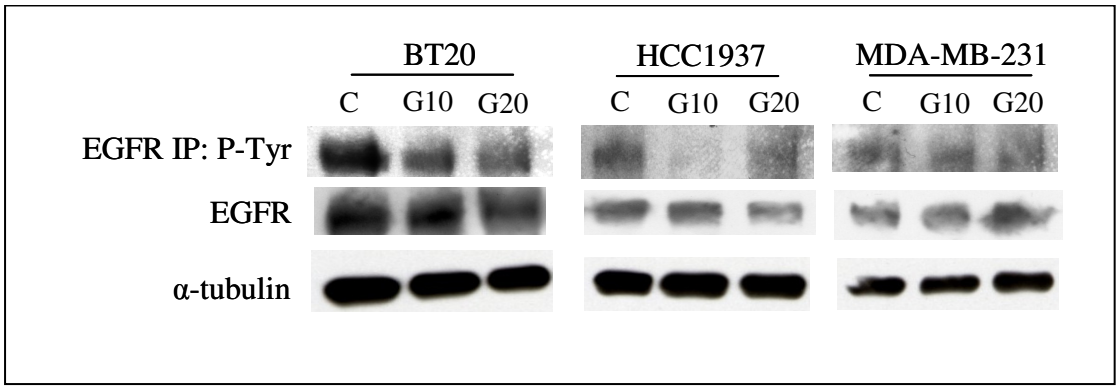

Figure 3.2 Detection of EGFR and P-EGFR in TNBC cell lines treated with gefitinib for 48 hours. (EGFR IP P-tyr: EGFR immunoprecipitation, followed by immunoblotting with a phospho-tyrosine antibody; C: control (untreated); G10: gefitinib 10 μM; G20: gefitinib 20 μM). Images represent results of a single experiment.

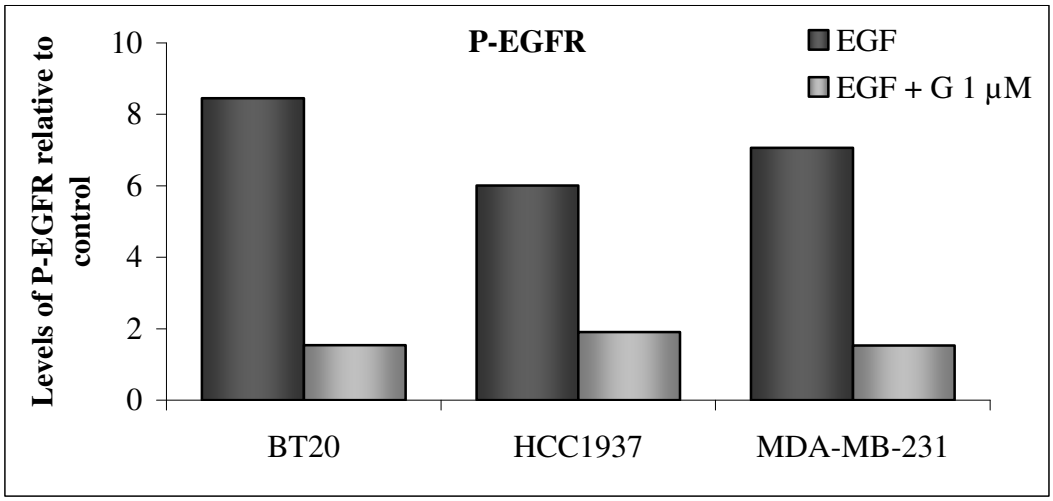

Figure 3.3 Levels of P-EGFR in EGF-stimulated TNBC cells (10 ng/ml EGF) with and without gefitinib (G) pre-treatment, compared to untreated (control) cells. Cells were cultured for 24 hours in serum-free medium before treatment. P-EGFR levels were measured by ELISA. Values represent the average of duplicate assays.

Gefitinib decreased both phospho-MAPK (P-MAPK) and phospho-Akt (P-Akt) levels in the sensitive HER-2 positive cell lines, BT474 and SKBR3 (Figure 3.4). A similar response to gefitinib was also observed in the most sensitive TNBC cell line HCC1937 (Figure 3.4). In contrast, this pattern of response was not observed in the more resistant TNBC cell lines BT20 and MDA-MB-231. Gefitinib decreased P-MAPK levels in BT20 cells but no change in Akt phosphorylation was observed. Gefitinib did not significantly alter P-MAPK in MDA-MB-231 cells. P-Akt was not detected in MDA-MB-231 cells by western blot, which has been reported previously [128, 132].

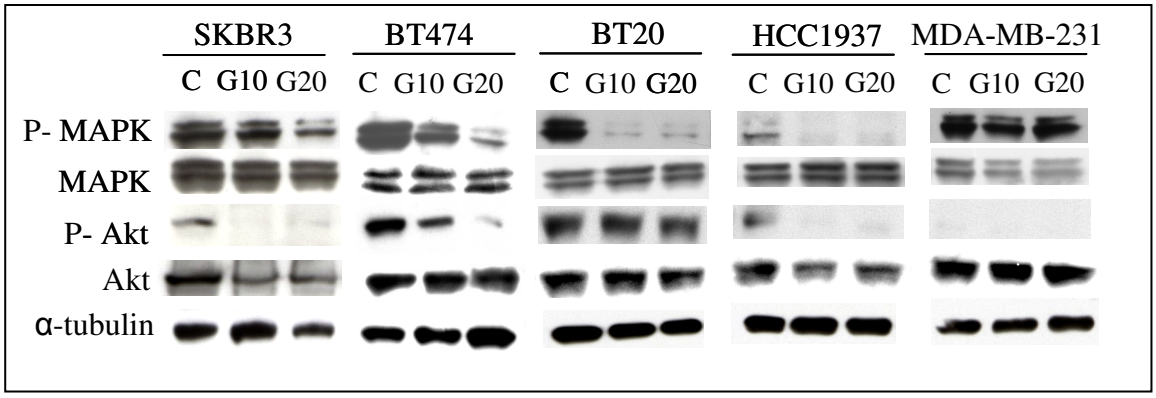

Figure 3.4 Detection of MAPK, P-MAPK, Akt and P-Akt in TNBC and HER-2 positive breast cancer cell lines treated with gefitinib for 48 hours. (P-: phospho-; C: control (untreated); G10: gefitinib 10 μM; G20: gefitinib 20 μM). Images represent single experiments.

3.4 EFFECTS OF EGFR INHIBITION ON CELL CYCLE PROGRESSION

Response to EGFR inhibition is associated with induction of G1 cell cycle arrest [234, 235]. An increase in G1 was observed in the sensitive HER-2 positive SKBR3 cells treated with 5 μM and 10 μM gefitinib for 24 or 48 hours, reflecting G1 phase arrest (Figure 3.5A). This was associated with reductions in S and G2/M phases. Gefitinib also induced similar changes in the HER-2 positive cell line BT474 after 48 hours of treatment (Figure 3.5B). An increase in G1 and reductions in S and G2/M phases were observed.

Although the TNBC cell lines over-express EGFR, gefitinib did not consistently induce G1 arrest. In BT20 cells, which have the highest levels of EGFR of the cell lines tested, no marked increase in G1 phase was observed with 10 μM gefitinib after 24 or 48 hours (Figure 3.6). However, an increase in G1 phase in response to 20 μM gefitinib was observed after 24 hours and 48 hours of treatment, with an associated decrease in G2/M, compared to the DMSO control. A slight increase in the G2/M phase was observed for the DMSO control after 48 hours.

In the most sensitive TNBC cell lines tested, HCC1937, increased G1 arrest was observed with 20 μM gefitinib after 48 hours, with associated decreases in S and G2/M phases (Figure 3.7). Of note, there was in increase in G1 phase in the DMSO control after 48 hours with an associated decrease in the S phase. However, there was an increase in G1 with 20 μM gefitinib compared to both the control and the DMSO control cells.

In the MDA-MB-231 cell line, 20 μM gefitinib caused a small increase in G1 phase after 24 and 48 hours, compared to the control (Figure 3.8).

A

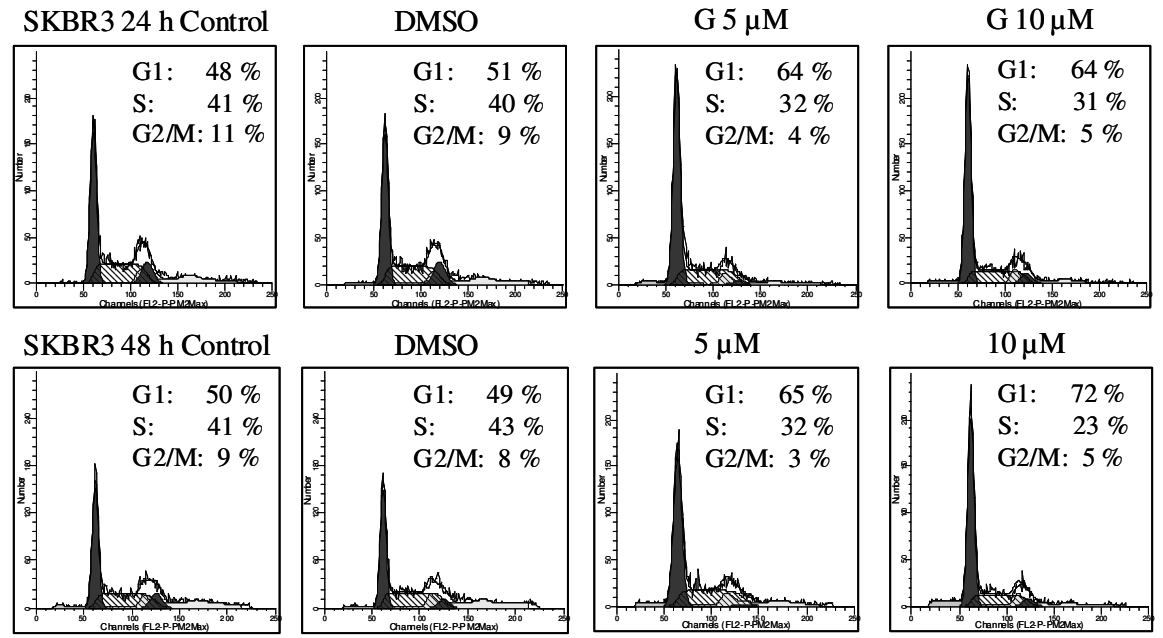

B

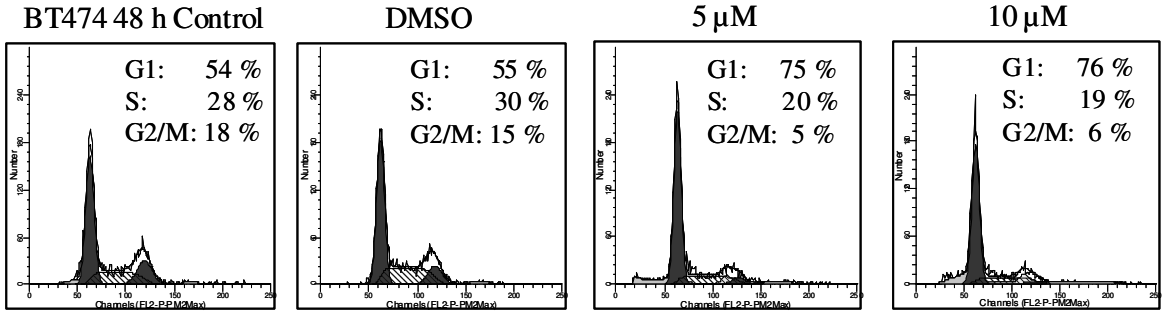

Figure 3.5 A Flow cytometric analysis of the effects of 24 and 48 hours of treatment with gefitinib, on cell cycle progression in SKBR3.. **B** Analysis of the effects of 48 hours of treatment with gefitinib, on cell cycle progression in BT474. The DNA histograms were generated by flow cytometry and the percentage of cells in each phase of the cell cycle was determined using ModFit (the average of duplicate independent experiments). The y-axis represents the number of cells.

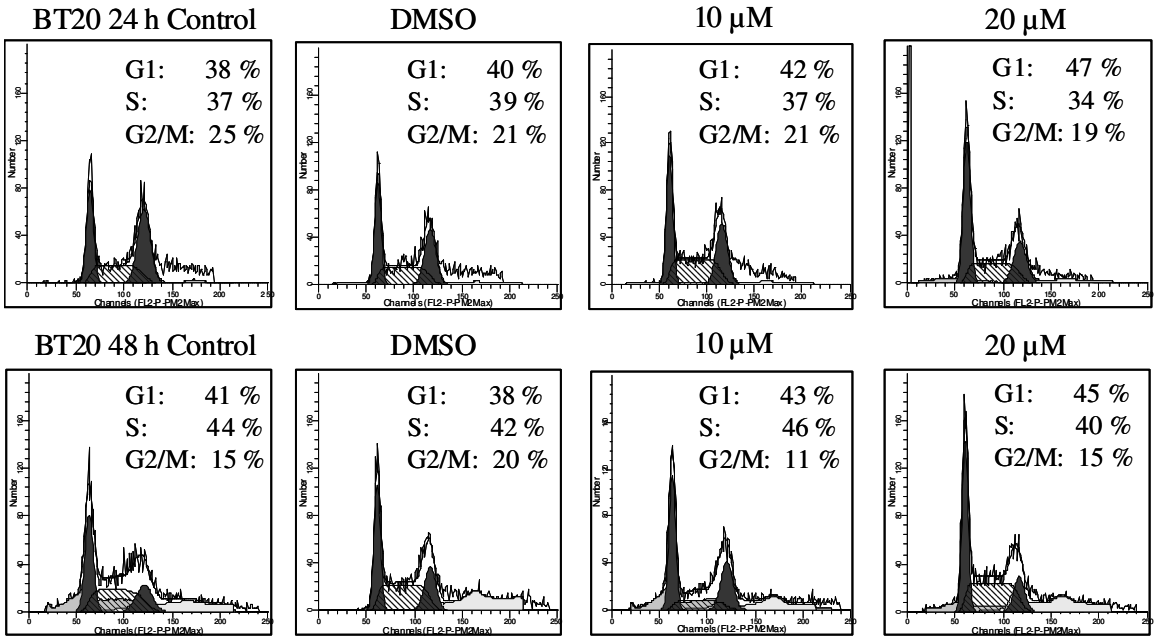

Figure 3.6 Flow cytometric analysis of the effects of 24 and 48 hours of treatment with gefitinib, on cell cycle progression in BT20. The percentage of cells in each phase of the cell cycle was determined using ModFit (the average of duplicate independent experiments). The y-axis represents the number of cells.

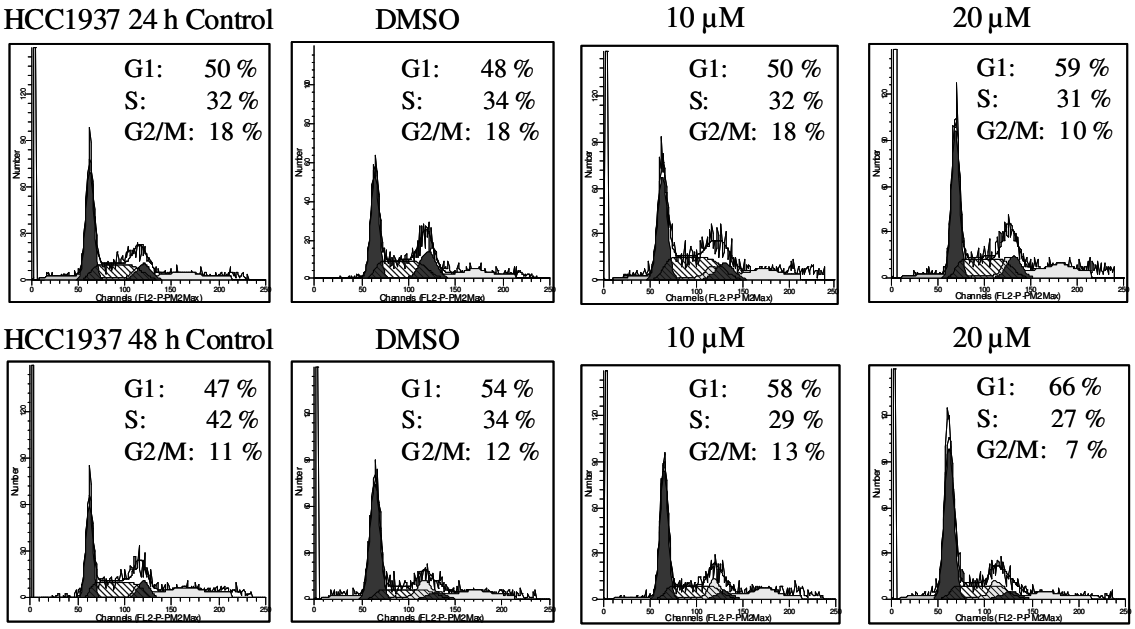

Figure 3.7 Flow cytometric analysis of the effects of 24 hours and 48 hours of treatment with gefitinib, on cell cycle progression in HCC1937. The percentage of cells in each phase of the cell cycle was determined using ModFit (the average of duplicate independent experiments). The y-axis represents the number of cells.

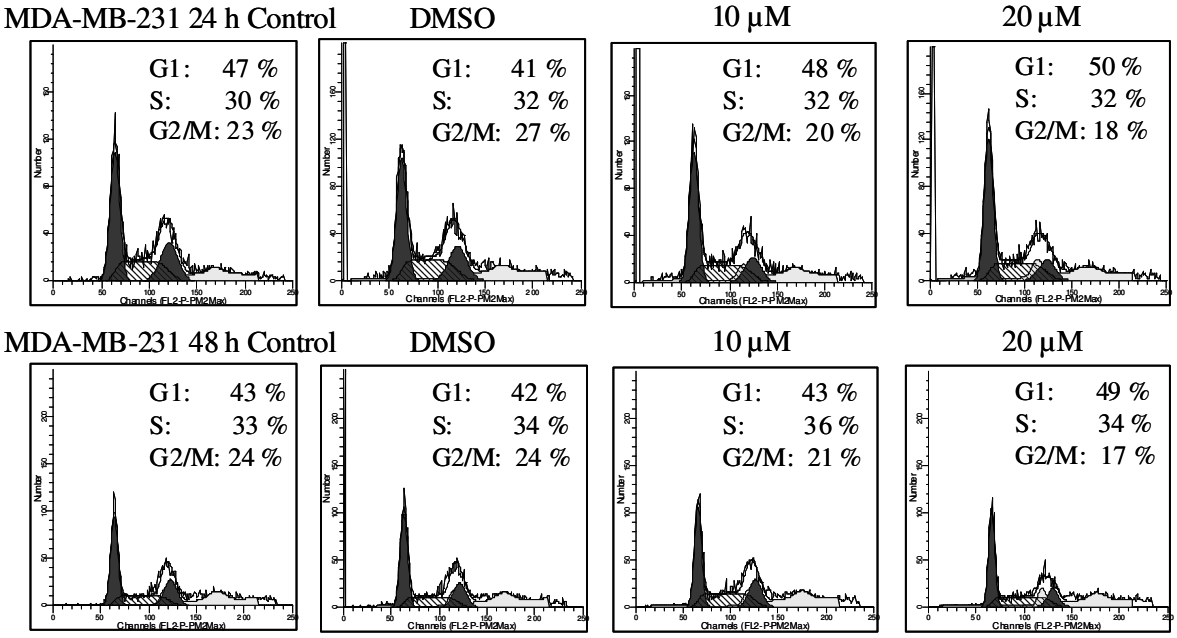

Figure 3.8 Flow cytometric analysis of the effects of 24 and 48 hours with gefitinib, on cell cycle progression in MDA-MB-231. The percentage of cells in each phase of the cell cycle was determined using ModFit (the average of duplicate independent experiments). The y-axis represents the number of cells.

3.5 CHEMO-SENSITIVITY IN BREAST CANCER CELLS

Sensitivity to chemotherapy drug was examined in a panel of TNBC and HER-2 positive cell lines (Table 3.3). No significant difference in chemo-sensitivity was observed between the TNBC and the HER-2 positive cell lines.

Table 3.3 IC_{50} concentrations (± standard deviation for 3 independent experiments) for gefitinib and chemotherapy drugs in HER2 positive and TNBC cell lines

	Gefitinib	**Carboplatin**	**Docetaxel**	**Doxorubicin**
Cell line	*IC_{50} (μM)*	*IC_{50} (μM)*	*IC_{50} (nM)*	*IC_{50} (nM)*
SKBR3	0.9 ± 0.3	9.7 ± 5.3	1.2 ± 0.6	27.0 ± 9.0
BT474	0.3 ± 0.1	>20	2.8 ± 0.3	117.0 ± 40.0
BT20	15.5 ± 1.4	8.6 ± 4.8	2.4 ± 1.4	34.7 ± 9.5
HCC1937	8.4 ± 1.5	11.6 ± 2.8	7.2 ± 2.5	38.6 ± 1.6
MDA-MB-231	20.7 ± 1.1	15.4 ± 3.3	3.0 ± 0.5	59.6 ± 9.8
HCC1143	>20	13.7 ± 1.3	1.3 ± 0.1	NT
MDA-MB-468	1.2 ± 0.8	0.8 ± 0.2	1.0 ± 0.1	NT

NT: not tested

3.6 EGFR INHIBITION AND CHEMOTHERAPY COMBINATIONS

Gefitinib was the most effective EGFR inhibitor tested in the TNBC cell lines (Table 3.2). A fixed dose of gefitinib (approximately an IC_{30} concentration) was combined with a range of doses of chemotherapy drugs in the TNBC cell lines BT20, HCC1937 and MDA-MB-231.

Gefitinib combined with carboplatin in HCC1937 and MDA-MB-231 cells displayed greater activity than either gefitinib or carboplatin alone (Figure 3.9, Table 3.4, Table 3.5). Gefitinib also enhanced response to carboplatin in BT20 cells up to 10 μM carboplatin but appeared to be antagonistic with 20 μM carboplatin (Figure 3.9A, Table 3.3).

Similar results were observed with the combinations of gefitinib and docetaxel (Figure 3.10, Table 3.3) or doxorubicin (Figure 3.11, Table 3.4) in BT20 and HCC1937 cells, Similar responses were observed in MDA-MB-231 cells except at the highest concentrations of the chemotherapy drugs (Figures 3.10C, 3.11C, Table 3.5).

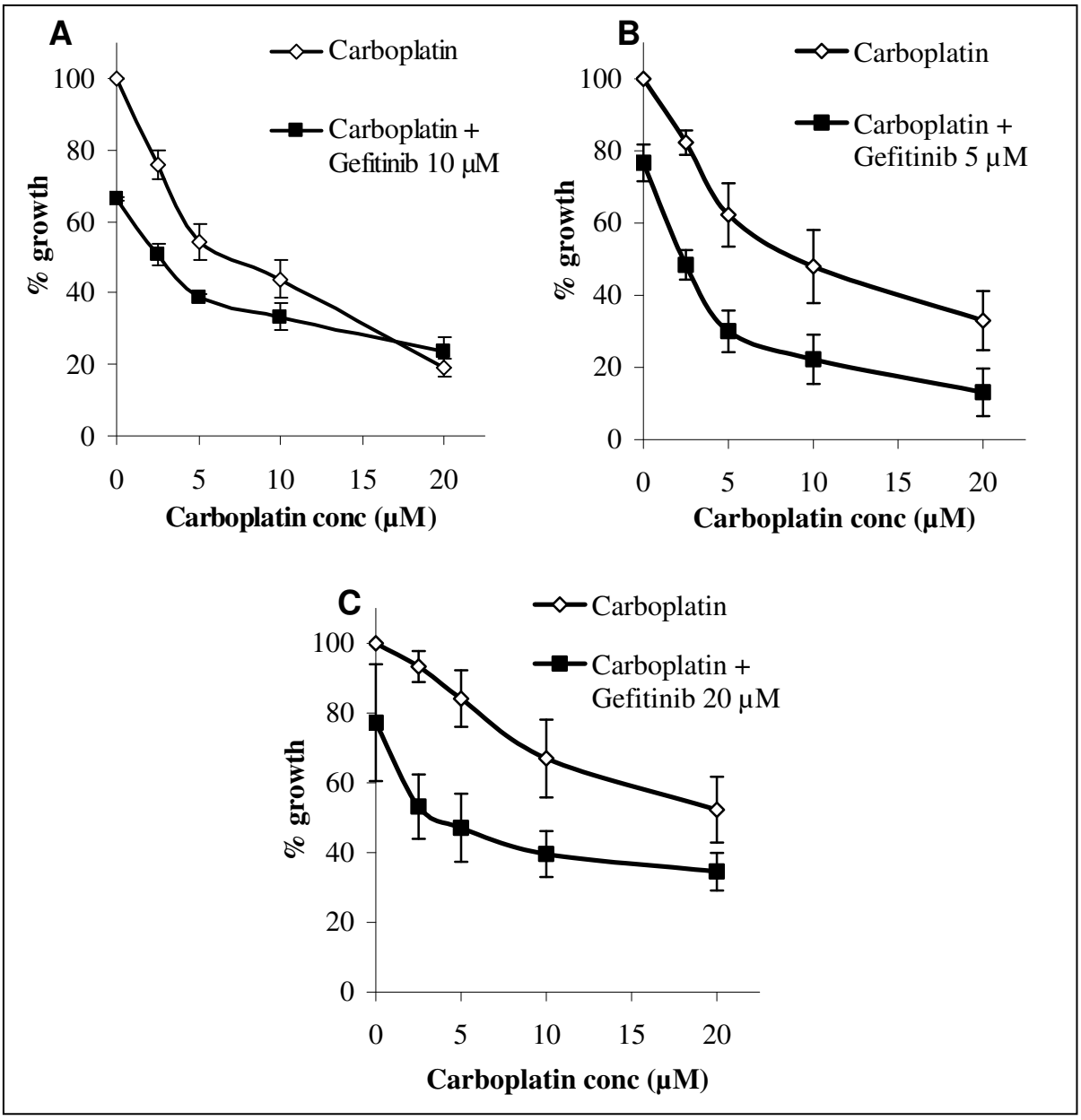

Figure 3.9 Proliferation assays of TNBC cells treated with carboplatin combined with a fixed dose of gefitinib (20 µM) in (A) BT20; (B) HCC1937; and (C) MDA-MB-231. Error bars represent the standard deviation of triplicate independent experiments.

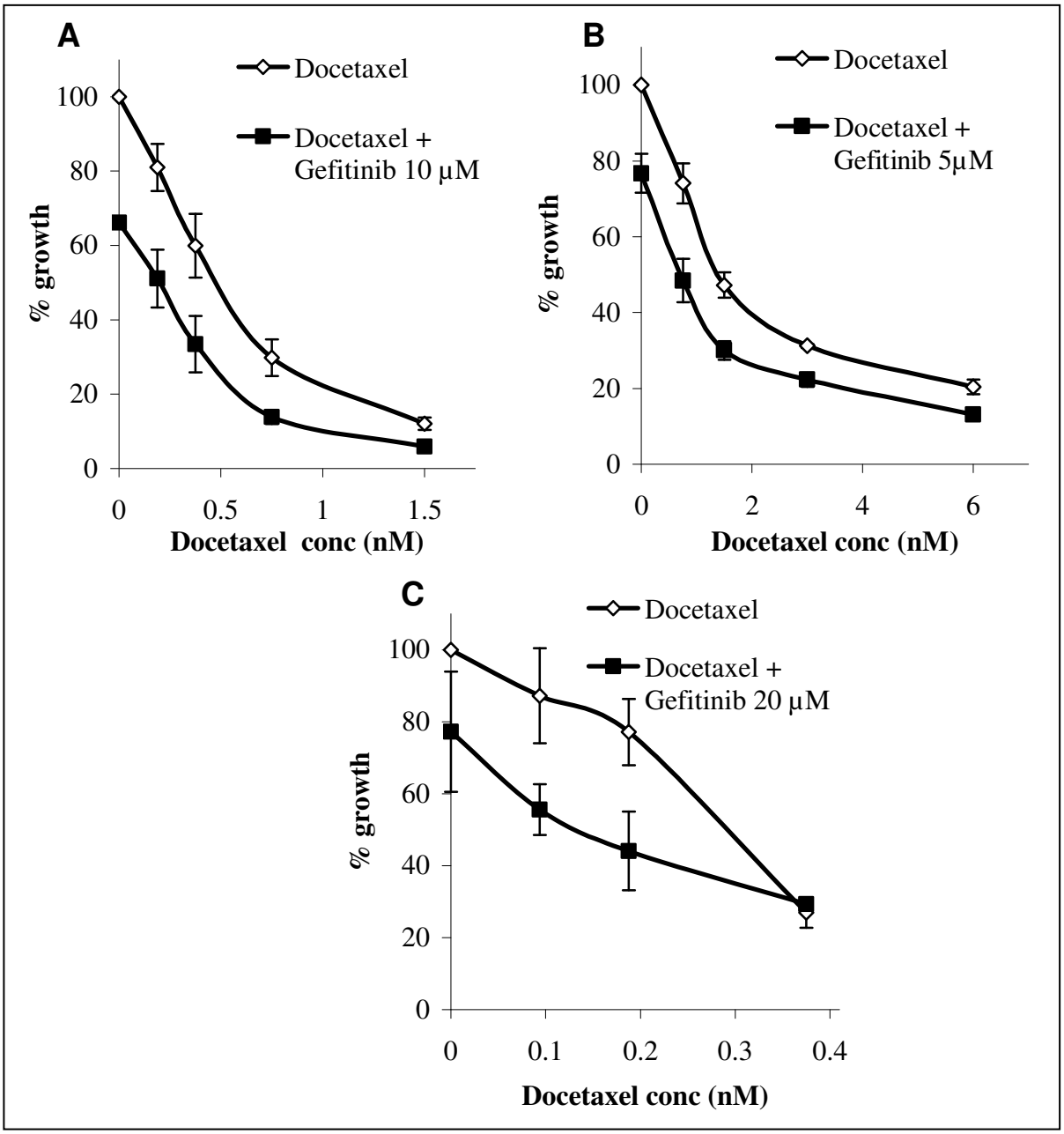

Figure 3.10 Proliferation assays of TNBC cells treated with docetaxel combined with a fixed dose of gefitinib (20 µM) in (A) BT20; (B) HCC1937; and (C) MDA-MB-231 Error bars represent the standard deviation of triplicate independent experiments.

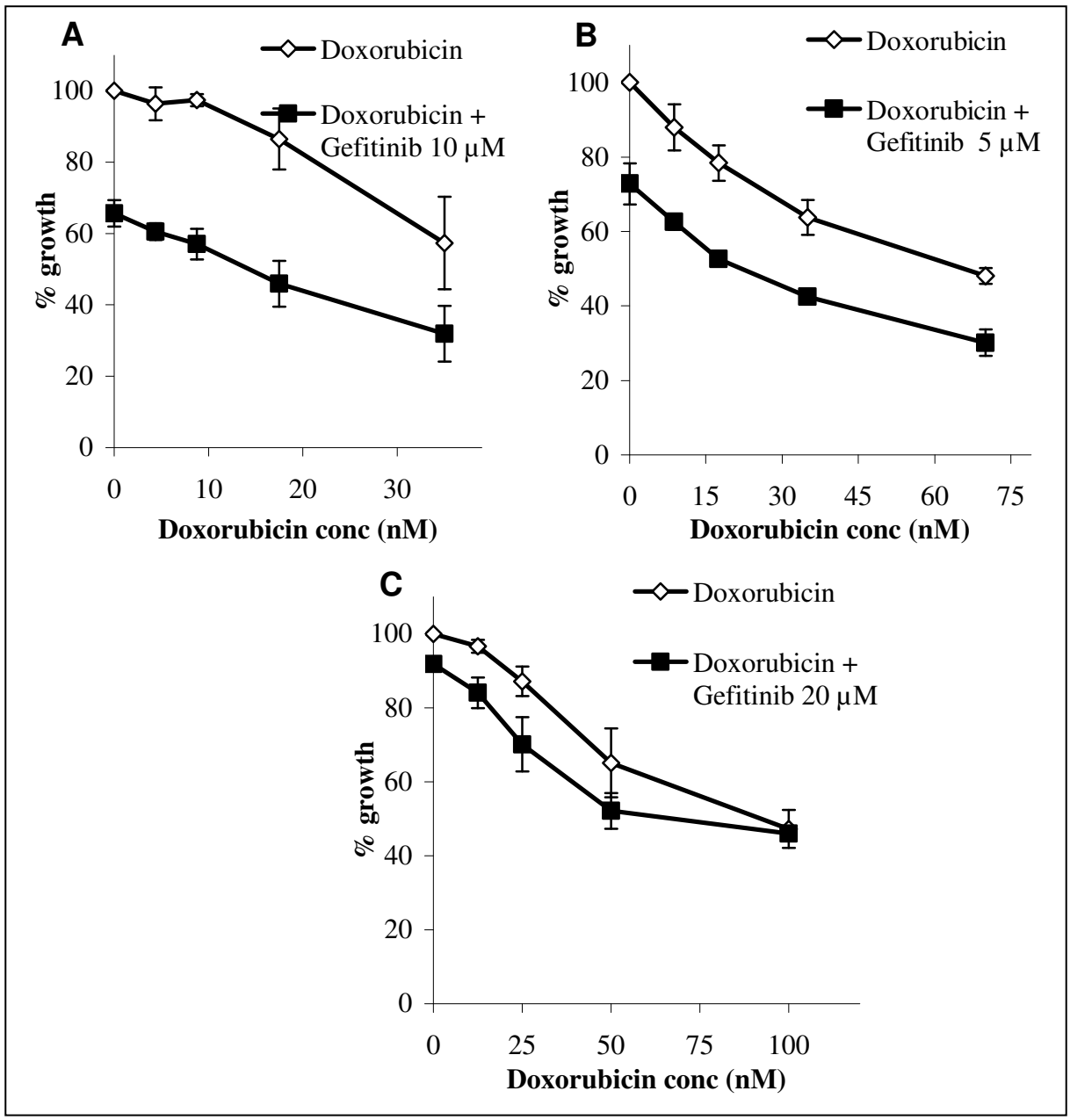

Figure 3.11 Proliferation assays of TNBC cells treated with doxorubicin combined with a fixed dose of gefitinib (20 µM) in (A) BT20; (B) HCC1937; and (C) MDA-MB-231. Error bars represent the standard deviation of triplicate independent experiments.

Table 3.3 Percentage growth of BT20 cells treated with gefitinib alone or in combination with chemotherapy drugs (± standard deviation of triplicate experiments).

BT20		**Proliferation (%)**	
	Concentration	**Single agent**	**Combination**
Gefitinib (µM)	10.0	66.2 ± 0.5	-
Carboplatin (µM)	2.5	75.9 ± 3.9	50.7 ± 2.8
	5.0	54.1 ± 5.1	38.9 ± 0.9
	10.0	43.9 ± 5.3	33.4 ± 3.6
	20.0	19.1 ± 2.6	23.5 ± 4.2
Docetaxel (nM)	0.2	81.0 ± 6.3	51.1 ± 7.8
	0.4	59.9 ± 8.6	33.5 ± 7.6
	0.7	29.8 ± 4.9	13.9 ± 1.9
	1.5	12.1 ± 1.7	5.9 ± 1.2
Doxorubicin (nM)	4.4	96.4 ± 4.6	60.5 ± 2.4
	8.7	97.4 ± 1.7	57.0 ± 4.3
	17.5	86.5 ± 8.5	45.9 ± 6.4
	35.0	57.3 ± 12.9	31.9 ± 7.8

Table 3.4 Percentage growth of HCC1937 cells treated with gefitinib alone or in combination with chemotherapy drugs (± standard deviation of triplicate experiments).

HCC1937		**Proliferation (%)**	
	Concentration	**Single agent**	**Combination**
Gefitinib (µM)	5.0	76.7 ± 5.1	-
Carboplatin (µM)	2.5	82.3 ± 3.4	60.7 ± 4.1
	5.0	62.3 ± 8.8	47.6 ± 5.8
	10.0	48.0 ± 10.2	37.5 ± 6.9
	20.0	33.0 ± 8.2	27.0 ± 6.6
Docetaxel (nM)	0.7	74.1 ± 5.3	48.4 ± 5.7
	1.5	47.2 ± 3.4	30.0 ± 2.5
	3.0	31.2 ± 0.6	22.3 ± 1.8
	6.0	20.4 ± 2.0	13.1 ± 1.2
Doxorubicin (nM)	8.7	88.0 ± 6.2	62.5 ± 2.1
	17.5	78.4 ± 4.8	52.5 ± 1.3
	35.0	63.8 ± 4.7	42.4 ± 1.4
	70.0	48.1 ± 2.1	30.1 ± 3.6

Table 3.5 Percentage growth of MDA-MB-231 cells treated with gefitinib alone or in combination with chemotherapy drugs (± standard deviation of triplicate experiments).

MDA-MB-231		**Proliferation (%)**	
	Concentration	**Single agent**	**Combination**
Gefitinib (µM)	20.0	80.8 ± 16.3	-
Carboplatin (µM)	2.5	93.3 ± 4.5	53.1 ± 9.2
	5.0	84.1 ± 8.1	47.1 ± 9.8
	10.0	66.9 ± 11.2	39.6 ± 6.6
	20.0	52.3 ± 9.4	34.5 ± 5.4
Docetaxel (nM)	0.09375	87.2 ± 13.2	55.6 ± 7.0
	0.1875	77.1 ± 9.2	44.1 ± 11.1
	0.375	27.0 ± 4.2	29.3 ± 1.2
Doxorubicin (nM)	12.5	96.6 ± 1.7	84.1 ± 4.2
	25.0	87.2 ± 4.0	70.1 ± 7.3
	50.0	65.1 ± 9.3	52.1 ± 4.8
	100.0	47.2 ± 5.2	46.0 ± 1.7

3.8 ALTERNATIVE SCHEDULING OF GEFITINIB AND CHEMOTHERAPY

To determine if alternative scheduling of the drugs impacted on the response, pre-treatment with either gefitinib or the chemotherapy drug (carboplatin or docetaxel) was tested in HCC1937. Enhanced response to carboplatin (Figure 3.12, Table 3.6) and docetaxel (Figure 3.13, Table 3.7) was observed whether cells were treated with either gefitinib or the chemotherapy drug first. The response observed for gefitinib or carboplatin/docetaxel pre-treatment was similar to concomitant treatment with gefitinib and carboplatin (Figure 3.9B) or docetaxel (Figure 3.10B) (Table 3.4).

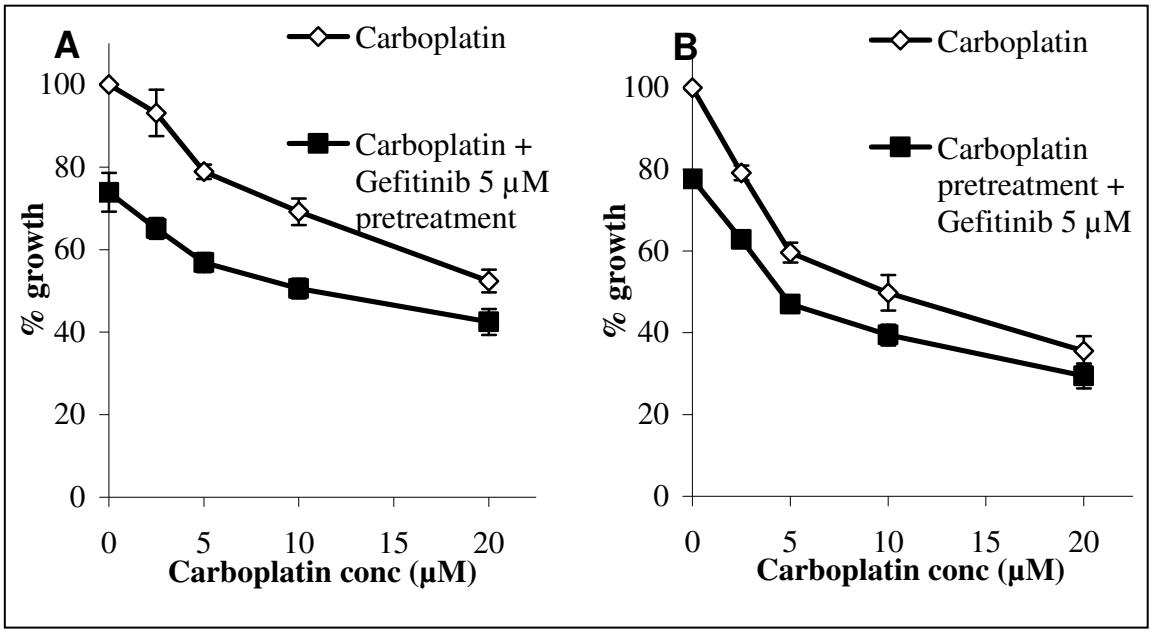

Figure 3.12 Percentage growth of HCC1937 cells treated with carboplatin combined with a fixed dose of gefitinib (**±** standard deviation of triplicate experiments). **A:** 5 µM gefitinib for 24 hours followed by addition of carboplatin for a further 96 hours; **B:** carboplatin for 24 hours followed by addition of 5 µM gefitinib for a further 96 hours.

Table 3.6 Percentage growth of HCC1937 cells treated with gefitinib alone or in combination with carboplatin (± standard deviation of triplicate experiments), as concomitant treatment or with pre-treatment with either drug for 24 hours. The second drug was added for a further 96 hours.

HCC1937			**Proliferation (%)**	
		Carboplatin (µM)	**Single agent**	**Combination**
Gefitinib (µM)[a]	5.0	-	77.1 ± 6.0	-
Concomitant		2.5	82.3 ± 3.4	60.7 ± 4.1
		5.0	62.3 ± 8.8	47.6 ± 5.8
		10.0	48.0 ± 10.2	37.5 ± 6.9
		20.0	33.0 ± 8.2	27.0 ± 6.6
Gefitinib pre-treatment		2.5	93.1 ± 5.6	65.1 ± 2.5
		5.0	78.9 ± 1.7	56.8 ± 2.3
		10.0	69.2 ± 3.2	50.6 ± 2.4
		20.0	52.4 ± 2.8	42.5 ± 3.1
Gefitinib (µM)[b]	5.0	-	77.7 ± 1.7	-
Carboplatin pre-treatment		2.5	79.2 ± 1.8	62.8 ± 2.1
		5.0	59.6 ± 2.4	47.0 ± 2.1
		10.0	49.8 ± 4.3	39.5 ± 2.6
		20.0	35.6 ± 3.6	29.5 ± 3.0

[a] 120 hours; [b] 96 hours.

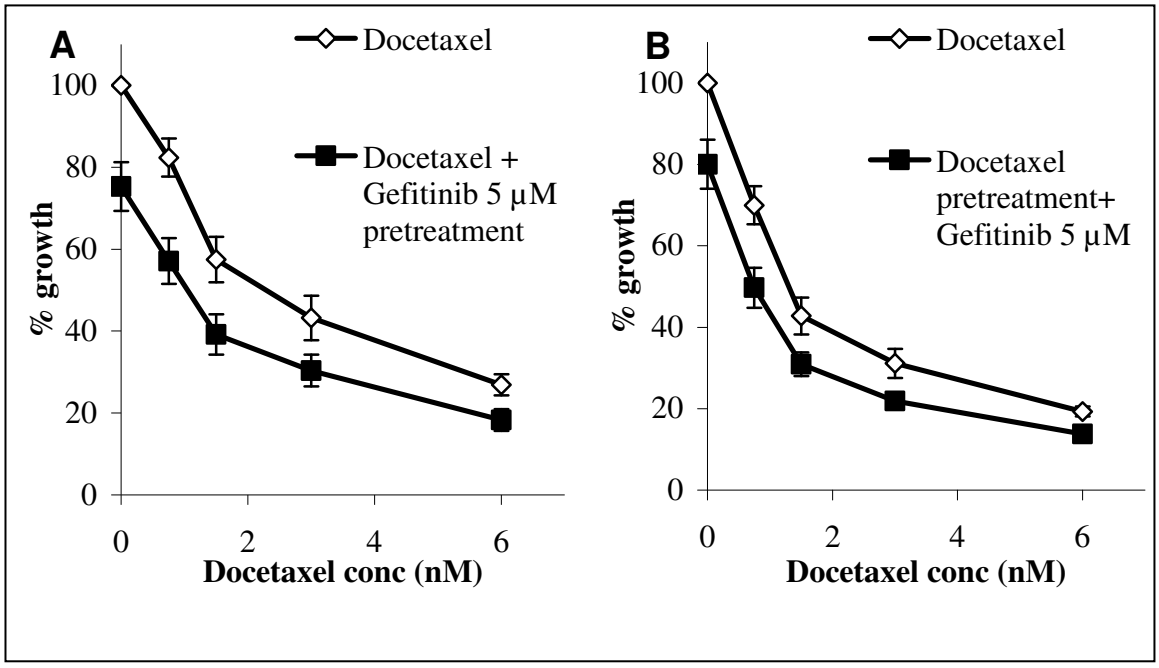

Figure 3.13 HCC1937 cells treated with docetaxel combined with a fixed dose of gefitinib. A: 5 µM gefitinib for 24 hours followed by the addition of docetaxel for a further 96 hours; B: docetaxel for 24 hours followed by the addition of 5 µM gefitinib for a further 96 hours. Error bars represent the standard deviation of triplicate independent experiments.

Table 3.7 Percentage growth of HCC1937 cells treated with gefitinib alone or in combination with docetaxel (± standard deviation of triplicate experiments), as concomitant treatment or with pre-treatment with either drug for 24 hours. The second drug was added for a further 96 hours.

HCC1937			**Proliferation (%)**	
		Docetaxel (nM)	**Single agent**	**Combination**
Gefitinib (μM)[a]	5.0	-	75.1 ± 3.9	-
Concomitant		0.75	74.1 ± 5.3	48.4 ± 5.7
		1.5	47.2 ± 3.4	30.0 ± 2.5
		3	31.2 ± 0.6	22.3 ± 1.8
		6	20.4 ± 2.0	13.1 ± 1.2
Gefitinib pre-treatment		0.75	82.4 ± 4.7	57.1 ± 5.6
		1.5	57.5 ± 5.5	39.2 ± 4.9
		3	43.2 ± 5.4	30.4 ± 3.9
		6	26.9 ± 2.6	18.3 ± 2.7
Gefitinib (μM)[b]	5.0	-	80.1 ± 6.0	-
Docetaxel pre-treatment		0.75	70.0 ± 4.7	49.7 ± 4.9
		1.5	42.8 ± 4.5	30.9 ± 2.9
		3	31.1 ± 3.6	21.9 ± 1.7
		6	19.3 ± 1.2	13.8 ± 1.5

[a] 120 hours; [b] 96 hours.

3.9 GEFITINIB, PLATINUM, AND DOCETAXEL TRIPLE COMBINATIONS

The triple combination of gefitinib, carboplatin, and docetaxel was tested in 4 TNBC cell lines (BT20, HCC1937, HCC1143, and MDA-MB-468) using a fixed ratio assay (gefitinib:carboplatin:docetaxel: - 10 000:10 000:1). Combination index (CI) values were calculated at ED_{25} (the effective dose required to inhibit 25 % of cell growth), ED_{50} and ED_{75}. It was noted that the CI values varied for different concentrations of drugs in each cell line. Therefore, the CI values should be interpreted with caution in relation to determining overall synergy or antagonism in these drug interactions. For descriptive purposes, the CI values at the ED_{50} are used.

In BT20, the effect of the triple combination of gefitinib, carboplatin, and docetaxel was greater than each drug alone, or the chemotherapy doublet (Figure 3.14, Table 3.7). The triple combination was synergistic at the ED_{50} concentration (CI = 0.6 ± 0.1), while the chemotherapy doublet was moderately antagonistic (CI = 1.2 ± 0.2) (Table 3.8).

Similarly, the triple combination produced an increased response in HCC1937 cells compared to each drug alone. The triple combination suggested additivity/slight synergy (CI = 0.8 ± 0.4) while the combination of the chemotherapy drugs suggested slight antagonism (CI = 1.2 ± 0.1), at the ED_{50}.

A similar range of drug concentrations were tested in the TNBC cell lines HCC1143 and MDA-MB-468 (Figure 3.14, Table 3.7). In both cases the effect of the triple combinations was greater than each drug alone. However, docetaxel had little effect at the concentrations tested, and the effect of chemotherapy in the double and triple combinations was likely to be largely due to carboplatin in these two cell lines. For the HCC1143 cell line, both the chemotherapy doublet and the triple combination were antagonistic (Table 3.8). In the case of MDA-MB-468, both the doublet and the triple combination were synergistic at the ED_{50}.

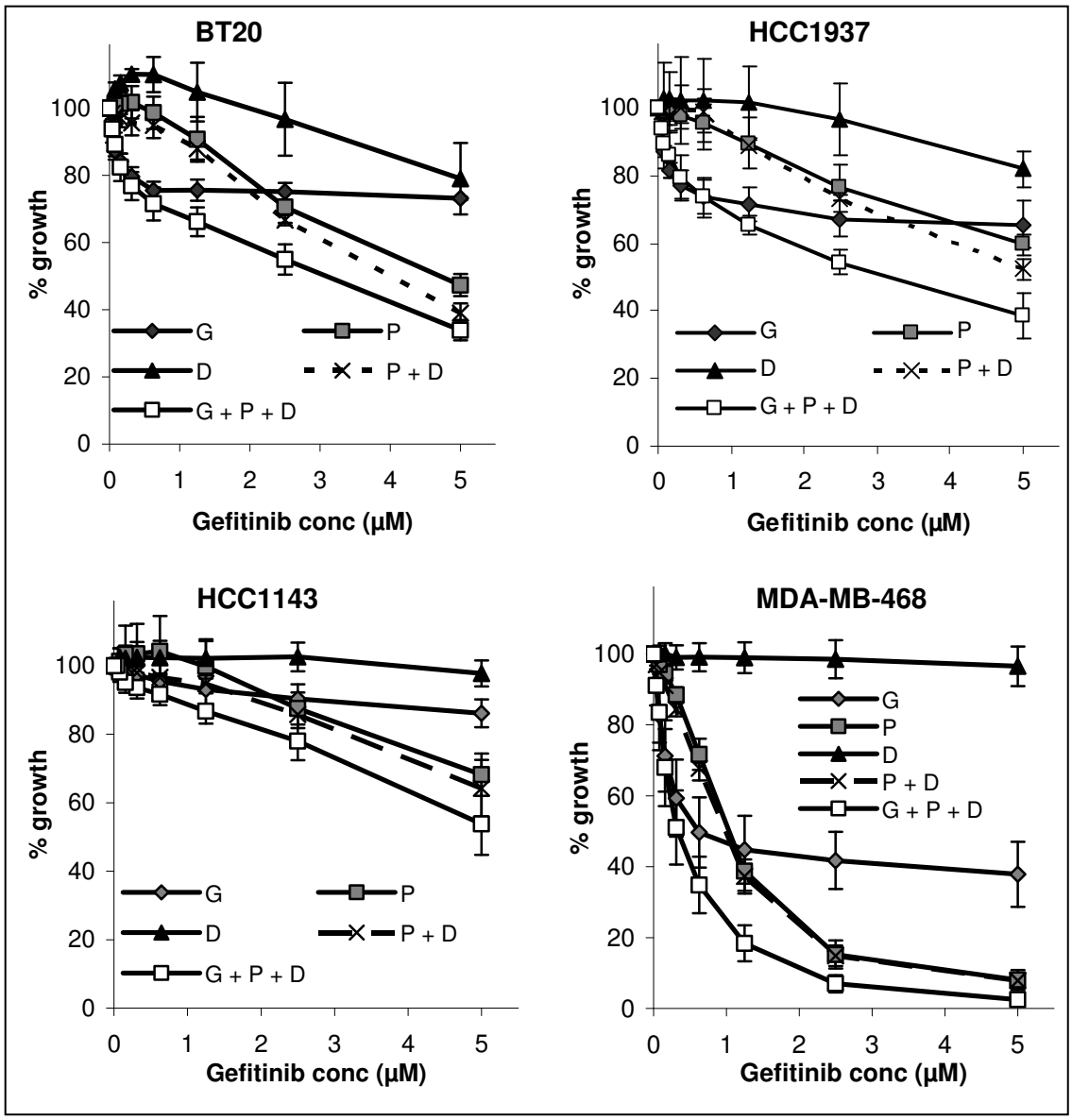

Figure 3.14 Proliferation assays with gefitinib (G), carboplatin (P), and docetaxel (D), alone and in combination, in BT20, HCC1937, HCC1143 and MDA-MB-468 cells (drug ratios: G:P:D – 10000:10000:1).

Table 3.7 Percentage growth (± standard deviation of triplicate independent experiments) in cells treated with gefitinib (G), carboplatin (P), and docetaxel (D), individually and combined.

Cell Line (% growth)	***G*** ***5 μM***	***P*** ***5μM***	***D*** ***0.5 nM***	***P+D***	***G+P+D***
BT20	73.1 ± *0.5*	47.3 ± *3.3*	96.9 ± *5.5*	39.0 ± *2.8*	33.9 ± *3.0*
HCC1937	62.0 ± *1.0*	55.8 ± *3.9*	81.7 ± *5.5*	54.0 ± *0.8*	37.8 ± *7.7*
HCC1143[a]	86.1± *4.1*	68.2 ± *6.2*	97.8 ± *3.8*	64.3 ± 8.3	53.8 ± *9.0*
MDA-MB-468	37.9 ± *9.2*	8.0 ± *2.8*	96.6 ± *5.6*	7.9 ± *2.0*	2.5 ± *1.3*

[a] maximum inhibition achieved with 20 μM gefitinib was 50 %

Table 3.8 Combination index values (± standard deviation of triplicate independent experiments) for carboplatin (P), docetaxel (D)**,** and gefitinib (G) in triple negative breast cancer cell lines. Definitions of synergy/antagonism are based on Table 2.2.

	CI (P+D)			***CI (G+P+D)***		
Cell Line	ED_{25}	ED_{50}	ED_{75}	ED_{25}	ED_{50}	ED_{75}
BT20	0.8 ± 0.1	1.2 ± 0.2	2.0 ± 0.8	0.5 ± 0.1	0.6 ± 0.1	1.4 ± 0.3
Synergy/antagonism	++	--	---	+++	+++	--
HCC1937	1.3 ± 0.3	1.2 ± 0.1	1.2 ± 0.4	1.4 ± 1.2	0.8 ± 0.4	1.1 ± 0.2
Synergy/antagonism	--	--	--	--	++	-
HCC1143	1.2 ± 0.3	1.4 ± 0.3	1.9 ± 0.6	0.9 ± 0.2	1.2 ± 0.4	2.0 ± 1.1
Synergy/antagonism	--	--	---	±	--	---
MDA-MB-468	0.8 ± 0.0	0.9 ± 0.0	1.0 ± 0.1	1.5 ± 0.6	0.7 ± 0.2	0.6 ± 0.1
Synergy/antagonism	++	+	±	---	++	+++

The triple combination of gefitinib, cisplatin, and docetaxel was tested in BT20 and HCC1143 (Figure 3.15). Consistent with the triple combination with carboplatin in BT20, the chemotherapy doublet was slightly antagonistic (CI = 1.3 ± 0.1) while the triple combination was moderately synergistic (CI = 0.7 ± 0.2) (Table 3.10). In HCC1143, the chemotherapy combination of cisplatin and docetaxel was antagonistic (CI = 1.2 ± 0.3), as was the triple combination (CI = 1.2 ± 0.4) (Table 3.10).

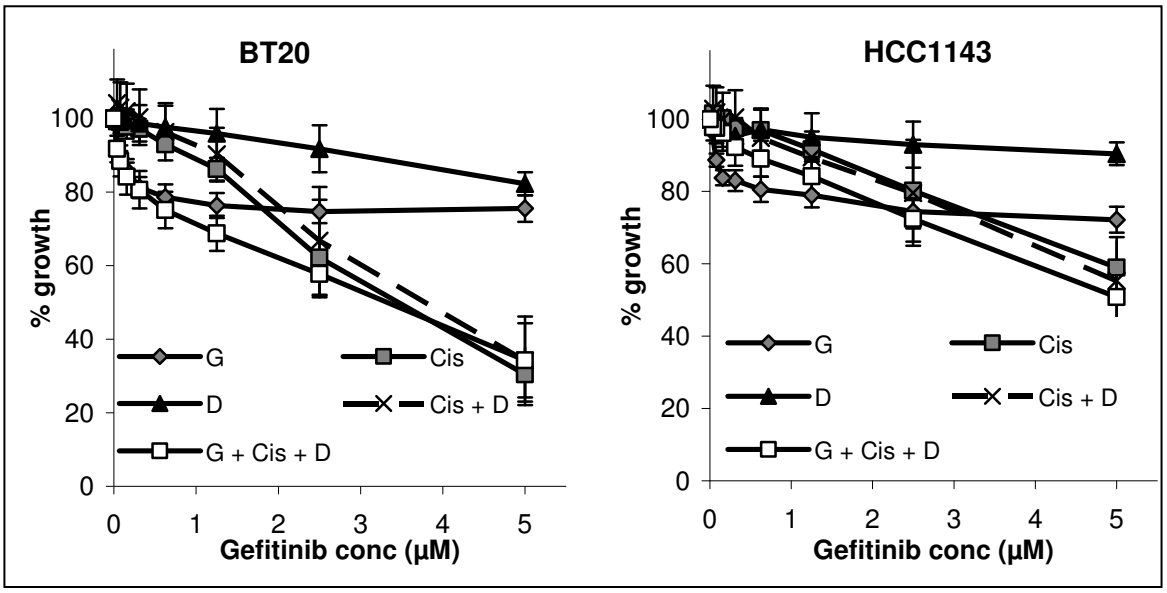

Figure 3.15 Proliferation assays with gefitinib (G), cisplatin (Cis), and docetaxel (D), alone and in combination, in BT20 and HCC1143 cells (drug ratios: G:Cis:D – 10000:10000:1).

Table 3.9 Percentage growth (± standard deviation of triplicate independent experiments) in cells treated with gefitinib (G), cisplatin (Cis), and docetaxel (D), individually and combined.

Cell Line (% growth ± *std dev*)	***G*** ***2.5 µM***	***Cis*** ***2.5 µM***	***D*** ***0.25 nM***	***Cis+D***	***G+Cis+D***
BT20	74.8 ± *3.2*	62.2 ± *10.4*	91.7 ± *6.4*	66.8± *14.6*	57.8 ± *6.3*
HCC1143	74.5 ± *9.6*	80.2 ± *7.1*	93.0 ± *2.4*	79.6 ± *3.8*	72.4 ± *1.0*

Table 3.10 Combination index values (± standard deviation of triplicate independent experiments) for the cisplatin (Cis), docetaxel (D)**,** and gefitinib (G) in triple negative breast cancer cell lines. Definitions of synergy/antagonism are based on Table 2.2.

	CI (Cis+D)			***CI (G+Cis+D)***		
Cell Line	ED_{25}	ED_{50}	ED_{75}	ED_{25}	ED_{50}	ED_{75}
BT20	1.7 ± 1.1	1.3 ± 0.1	1.4 ± 0.9	0.5 ± 0.3	0.7 ± 0.2	2.0 ± 1.2
Synergy/antagonism	---	--	--	+++	++	---
HCC1143	1.4 ± 0.1	1.2 ± 0.3	1.3 ± 0.8	2.7 ± 2.3	1.2 ± 0.4	1.5 ± 1.5
Synergy/antagonism	--	--	--	---	--	--

3.10 EFFECTS OF GEFITINIB AND CHEMOTHERAPY ON CELL CYCLE PROGRESSION

The effect of the triple combination of gefitinib, carboplatin and docetaxel on cell cycle progression was assessed in BT20 and HCC1937 cells (Figure 3.16, 3.17). In both cell lines, treatment with carboplatin and docetaxel caused an increase in G2, with an associated decrease in G1, in comparison to untreated control cells. The combination of gefitinib with carboplatin and docetaxel induced similar G2 arrest and an increase in G1 compared to the chemotherapy drugs alone. The sub-G0/G1 fraction (which is an indirect measure of cell apoptosis) was increased in HCC1937 cells treated with the chemotherapy doublet and the triple combination, compared to untreated cells (Figure 3.17). A similar, but smaller trend, was also observed in the BT20 cells (Figure 3.16).

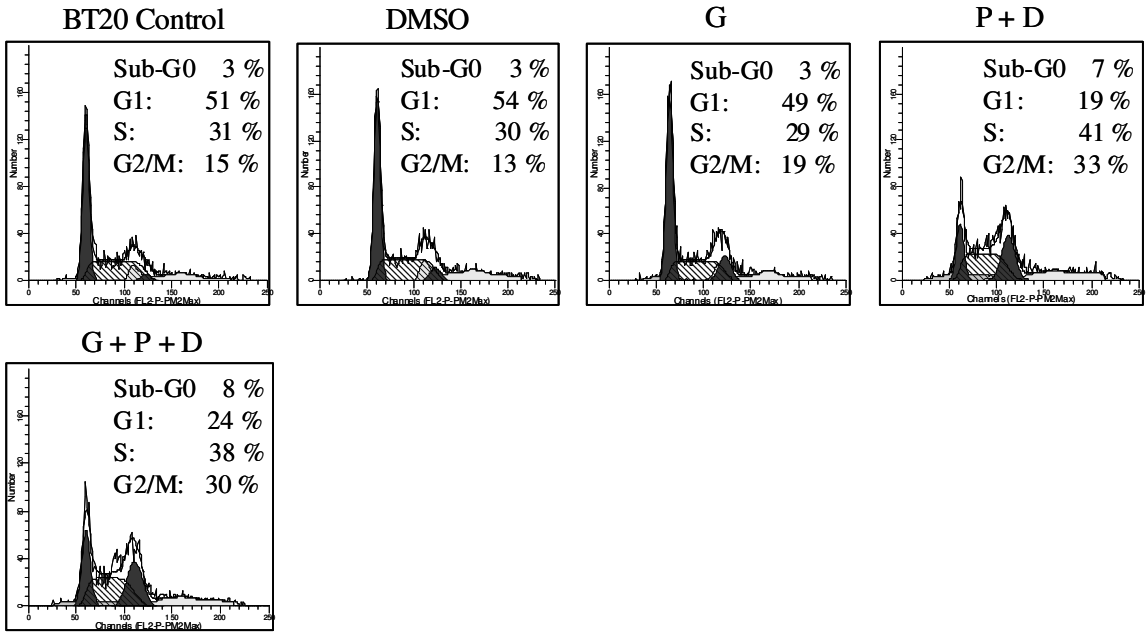

Figure 3.16 Flow cytometric analysis of the effects of 48 hours with 10 μM gefitinib, 10 μM carboplatin (P) and 1 nM docetaxel (D), on cell cycle progression in BT20. The percentage of cells in each phase of the cell cycle was determined using ModFit (the average of duplicate independent experiments). The y-axis represents the number of cells.

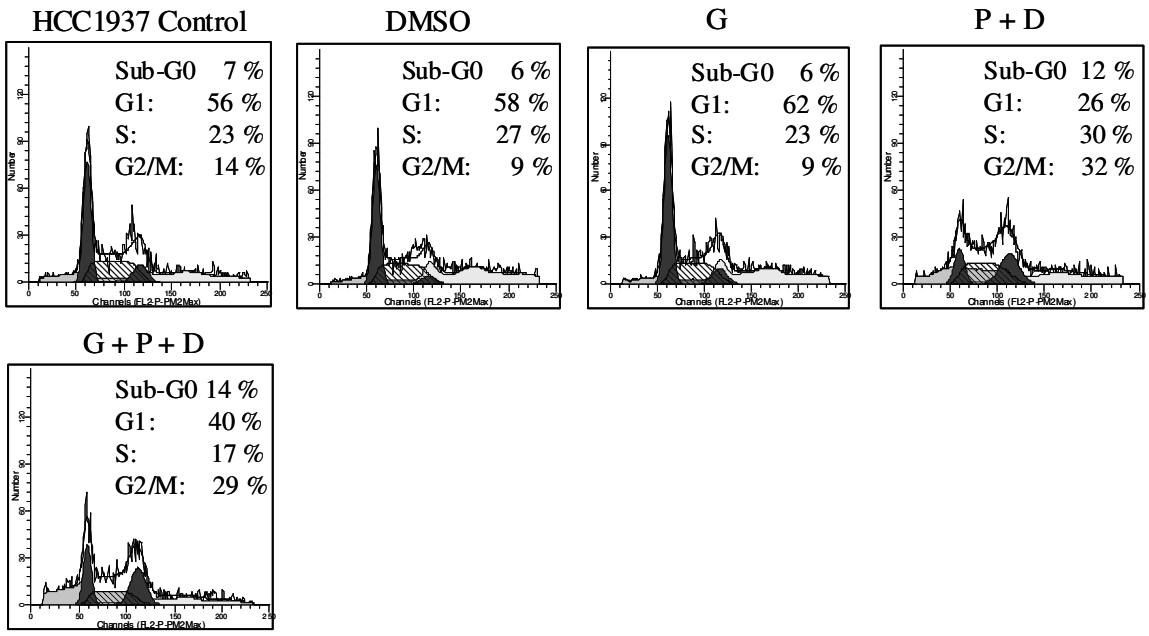

Figure 3.17 Flow cytometric analysis of the effects of 48 hours with 10 μM gefitinib, 10 μM carboplatin (P) and 1 nM docetaxel (D), on cell cycle progression in HCC1937. The percentage of cells in each phase of the cell cycle was determined using ModFit (the average of duplicate independent experiments). The y-axis represents the number of cells.

3.11 SUMMARY/CONCLUSIONS

Our data confirm the observation that EGFR is over-expressed in TNBC [11, 12, 14, 15]. While our data confirm the activity of the EGFR inhibitor gefitinib in TNBC cell lines, we found higher activity for this agent in HER-2 positive breast cancer cell lines, despite the fact that these cells had lower levels of EGFR. In the TNBC cell lines studied, significant levels of phosphorylated EGFR were only detected in BT20 cells. Very low levels of phosphorylated EGFR were detected in MDA-MB-231 and HCC1937 cells, by immunoblotting. Although basal levels of phosphorylated EGFR in TNBC cells were low, EGF treatment induces significant phosphorylation of EGFR and gefitinib efficiently blocks the phosphorylation of EGFR in EGF-treated TNBC cells.

Phosphorylation of both MAPK and Akt were reduced in the gefitinib-sensitive, HER-2 over-expressing BT474 and SKBR3 cell lines in response to gefitinib. HCC1937 cells, which show the greatest sensitivity to gefitinib, also showed reduced phosphorylation of both MAPK and Akt. In BT20 cells a decrease in phosphorylation of MAPK was observed with no change in phosphorylated Akt. No changes in either MAPK or Akt phosphorylation were observed in MDA-MB-231 cells. This suggests that response to EGFR inhibition requires efficient blockade of both MAPK and Akt signalling. Furthermore, these observations suggest that combined assessment of P-MAPK and P-Akt levels may potentially represent useful biomarkers for assessing response to EGFR inhibition with gefitinib,

Although the TNBC cells are not inherently sensitive to EGFR inhibition, combined treatment with gefitinib and chemotherapy has a greater effect on proliferation than either gefitinib or the chemotherapy alone. G1 phase cell cycle arrest was observed in sensitive cells following treatment with gefitinib. Treatment with chemotherapy resulted in G2/M phase arrest. Combined induction of G2/M and G1 arrest observed with treatment with gefitinib, and chemotherapy may, at least in part, explained the additional benefit observed with the triple combination in the TNBC cell lines.

Chapter 4

EGFR AND P-EGFR IN BREAST TUMOURS

4.1 INTRODUCTION

EGFR expression has been associated with poorer outcomes and response to therapy in different cancer types, including lung [88] and breast [236]. The reported rate of EGFR expression in breast cancer varies widely in the literature. A review in 1992 by Klijn *et al.* of 5232 breast cancer patients from 40 different studies reported that on average 45 % of breast cancers were positive for EGFR (range 14 – 91 %) [91]. Fox *et al.* reported a 47 % positive rate in a cohort of 370 primary breast carcinomas [92]. In a recent review of 2567 breast tumours, Rimawi et al reported 475 (18 %) were positive for EGFR [236]. However, as noted by Chan at al, several different techniques have been used in these various studies [93].

The data are similarly unclear regarding levels of P-EGFR in breast carcinomas. Magkou *et al.* reported EGFR and P-EGFR expression in a cohort of 154 invasive breast cancers (11.3 % and 35.7 % respectively) [237]. Nieto *et al.* examined EGFR and P-EGFR expression in 225 locoregionally advanced breast cancers (43 % and 54 %) [238]. Again, it is likely that variations in patient populations and techniques used contribute to the disparities between studies. There are no published data regarding EGFR and P-EGFR levels in breast carcinomas in an Irish population.

We examined a cohort of 101 breast carcinomas selected at random from patients attending St. Vincent's University Hospital, Dublin. We assessed these tumours for EGFR expression and phosphorylation by immunohistochemistry (IHC). IHC was performed using the DAKO Autostainer™. The staining method used, and the scoring guidelines are described in section 2.13. The same guidelines were applied to scoring EGFR and P-EGFR. Briefly, a negative score was recorded in the absence of specific staining within the tumour, and given a score of 0 (no staining). EGFR positive staining was scored as 1+ (weak intensity), 2+ (moderate intensity), or 3+ (strong intensity). Examples of the staining obtained are shown for EGFR (Figure 4.1) and P-EGFR (Figure 4.2). The guidelines for total EGFR staining provided with the DAKO kit used state that any level of EGFR staining (i.e. 1+, 2+, or 3+) is regarded as positive. This is in contrast to the DAKO guidelines for scoring of immunohistochemical scoring of HER-2 (2+ and 3+ are taken as positive, reflecting

HER-2 amplification (www.dako.com). No guidelines were available for scoring the intensity of P-EGFR staining. In this study, we focused on levels of EGFR expression and phosphorylation, and the results are summarised and analysed as either negative (0) or positive (1+, 2+, 3+), and also by each intensity of staining (0, 1+, 2+ 3+).

4.2 PATIENT CHARACTERISTICS

The patient characteristics are outlined in Table 4.1. These were predominantly older patients (68.3 % ≥ 50 years) with tumours ≥ 2 cm (69.3 %). The majority of the tumours were ductal (83.2 %), hormone receptor positive (estrogen receptor (ER) positive 63.7 %), and positive for lymph node spread (55.5 %). 17.8 % were HER-2 positive. 16 (15.8 %) of the tumours are triple negative.

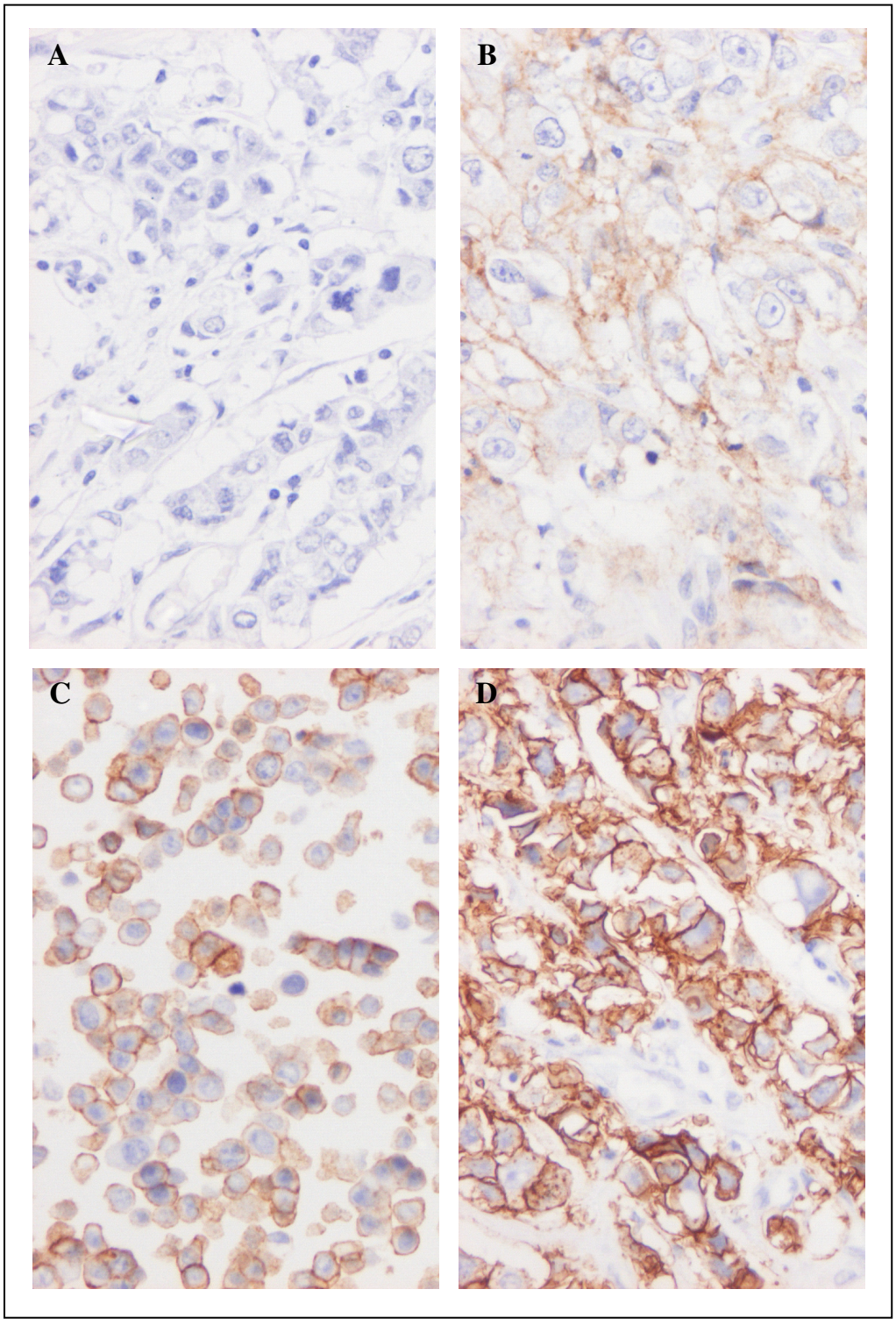

Figure 4.1 Representative pictures of EGFR staining with different scores: **A.** EGFR negative; **B.** EGFR 1+; **C.** EGFR 2+; and **D.** EGFR 3+.

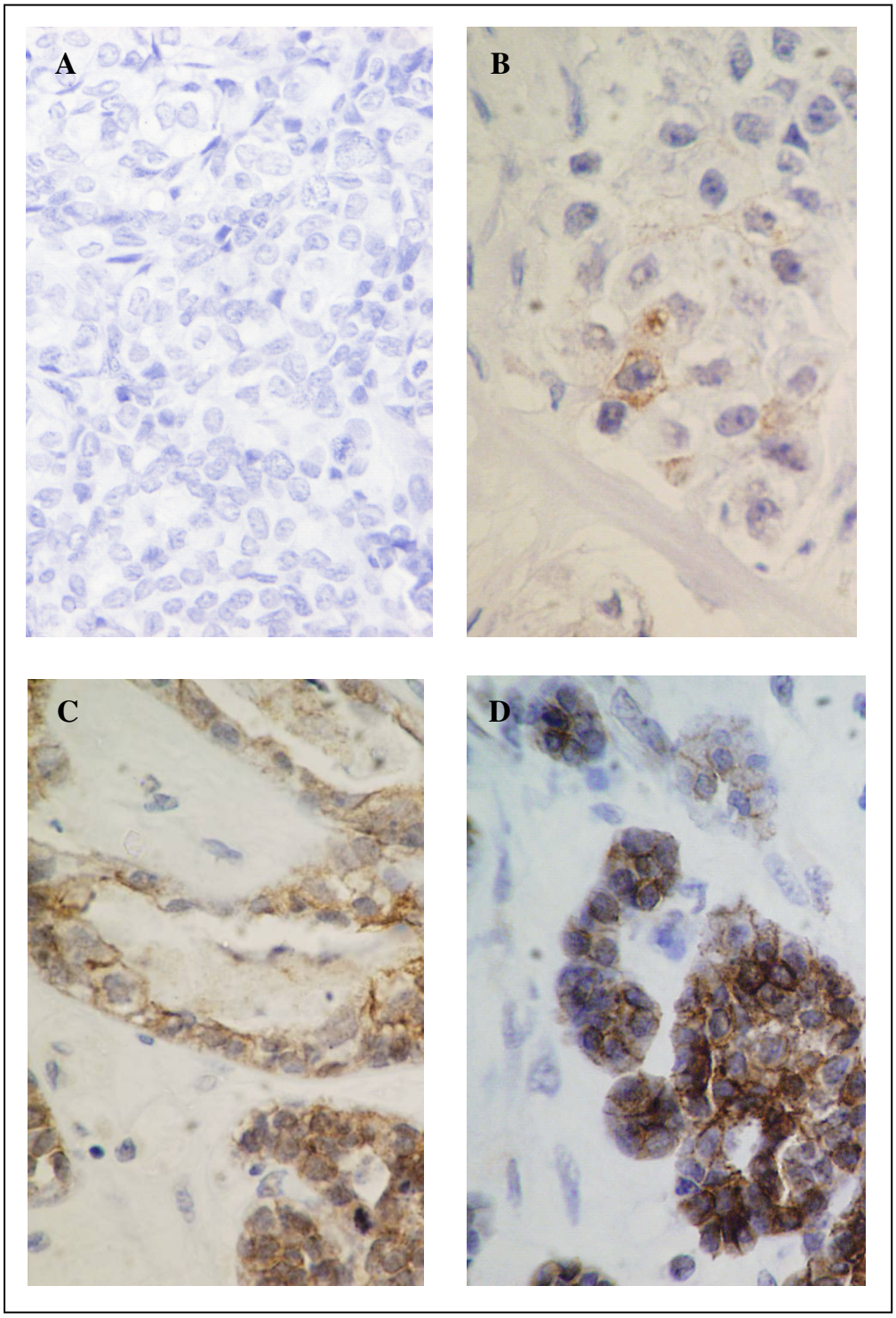

Figure 4.2 Representative pictures of P-EGFR staining with different scores: **A.** P- EGFR negative; **B.** P-EGFR 1+; **C.** P-EGFR 2+; and **D.** P-EGFR 3+.

Table 4.1 Characteristics of the breast cancer patients analysed (n = 101).

(n = 101)		**N**	**%**
Age at diagnosis	< 50	28	27.7
	≥ 50	69	68.3
	Unknown	4	4.0
Tumour size	≤ 2 cm	28	27.7
	> 2 cm	70	69.3
	Unknown	3	3.0
Nodal status	Negative	39	38.6
	Positive	56	55.5
	Unknown	3	3.0
Grade	1	6	5.9
	2	50	49.5
	3	40	39.6
	Unknown	5	5.0
Histology	Ductal	84	83.2
	Lobular	12	11.9
	Mucinous	2	2.0
	Unknown	3	3.0
ER status	Negative	28	27.7
	Positive	64	63.7
	Unknown	9	8.9
PR status	Negative	42	41.6
	Positive	50	50.0
	Unknown	9	8.9
HER-2 status	Negative	82	81.2
	Positive (2+/3+)	18	17.8
	1+/Unknown	1	1.0
Triple negative		16	15.8

4.3 EGFR AND P-EGFR EXPRESSION IN UNSELECTED BREAST CANCER PATIENTS

Tissue microarrays (TMAs) containing 101 breast tumour samples were obtained and were stained for EGFR and P-EGFR expression (Table 4.2). Hematoxylin and eosin (H&E)-stained TMAs were assessed by a consultant pathologist to confirm tumour presence on the tissue section tested. EGFR was detected in 11/101 (11 .0 %) of the breast tumours. P-EGFR was detected in 9/101 (8.9 %) of the tumours, with 1+ staining detected in 6 tumours and 2+ staining detected in 3 tumours. No tumours had 3+ staining for P-EGFR.

Sixteen of the breast tumours tested were triple negative (Table 4.3). 5 (31.5 %) of the triple negative tumours were positive for EGFR staining. P-EGFR was detected in only 1 (6.2 %) of the triple negative tumours (1+ intensity).

Table 4.2 EGFR and P-EGFR scores in 101 patient samples, as measured by IHC.

(n = 101)	**N**	%
EGFR status		
0	90	89.9
1+	5	5.0
2+	4	4.0
3+	2	2.0
Total positive	**11**	**11.0**
P-EGFR status		
0	92	91.0
1+	6	5.9
2+	3	3.0
3+	0	0.0
Total positive	**9**	**8.9**

Table 4.3 EGFR and P-EGFR status, as measured by IHC, in triple negative breast cancer patients

(n = 16)	**N**	*%*
EGFR status		
0	11	69.0
1+	0	0.0
2+	3	19.0
3+	2	12.5
Total positive	**5**	**31.5**
P-EGFR status		
0	15	93.8
1+	1	6.2
2+	0	0.0
3+	0	0.0
Total positive	**1**	**6.2**

4.4 EGFR & P-EGFR: RELATIONSHIP WITH PROGNOSTIC INDICATORS

Analysis of the relationship between EGFR positivity (1+, 2+, 3+) and prognostic factors are shown in Table 4.4. No significant relationship between EGFR positivity and patient age, HER-2 positivity, tumour grade, or histological subtype was observed. There was a statistically significant correlation between EGFR positivity and the triple negative phenotype ($p = 0.0181$), as well as nodal status ($p = 0.0066$), although these correlations were not statistically significant when the p values were adjusted for multiple testing using the Bonferroni test.

The relationship between intensity of EGFR staining and the same prognostic factors are show in Table 4.5. In this analysis, there was a significant correlation between different intensities of staining (0, 1+, 2+, 3+) and ER status ($p = 0.0309$), PR status ($p = 0.0341$), the triple negative phenotype ($p < 0.0001$), and nodal negativity ($p = 0.016$). The p values adjusted for multiple testing were statistically significant for the triple negative phenotype and node negativity, but not for ER and PR status (Table 4.5).

There was no significant relationship between EGFR positivity and tumour size ($p = 0.7356$). There was a significant association between EGFR and the number of involved lymph nodes ($p = 0.0166$).

The comparison of P-EGFR positivity and prognostic factors did not show any significant correlations (Table 4.6), including hormone receptor status, HER2 positivity, nodal status or the triple negative phenotype. Similarly, there were no significant correlations between P-EGFR staining intensities and prognostic factors (Table 4.7). Analyses of P-EGFR positivity and tumour size and the number of involved lymph nodes were non-significant ($p = 0.4794$ and $p = 0.5210$ respectively).

Table 4.4 EGFR positivity and patient prognostic indicators. P values were calculated using Fisher's exact test or Chi square test (marked †). Statistically significant p values were adjusted for multiple testing using the Bonferroni test

		EGFR			p
	n	**Positive**	**Negative**	**p**	**(adjusted)**
Age (years)					
< 50	28	2	26	0.5025	
≥ 50	69	9	60		
Size (cm)					
≤ 2	28	4	24	0.5046	
> 2	70	7	63		
Nodal status					
Neg	39	9	30	**0.0066**	0.0594
Pos	56	2	54		
ER status					
Neg	28	6	22	0.0620	
Pos	64	4	60		
PR status					
Neg	42	7	35	0.2019	
Pos	50	4	46		
HER2 status					
Neg	83	10	73	0.6836	
Pos	18	1	17		
Triple negative	16	5	11	**0.0181**	0.1629
Non-triple negative	79	6	73		
Grade					
1	6	1	5		
2	50	5	45	0.8573†	
3	40	5	35		
Histology					
Ductal	84	11	73	0.3488	
Lobular	12	0	12		

Table 4.5 EGFR level and patient prognostic indicators. P values were calculated using Chi square test. Statistically significant p values were adjusted for multiple testing using the Bonferroni test

		EGFR					p
	n	**0**	**1+**	**2+**	**3+**	**p**	**(adjusted)**
Age (years)							
< 50	28	26	1	1	0	0.7746	
≥ 50	69	60	4	3	2		
Size (cm)							
≤ 2	28	24	2	2	0	0.5598	
> 2	70	63	3	2	2		
Nodal status							
Neg	39	30	5	4	0	**0.0016**	**0.0144**
Pos	56	54	0	0	2		
ER status							
Neg	28	22	1	3	2	**0.0309**	0.2781
Pos	64	60	3	1	0		
PR status							
Neg	42	35	1	4	2	**0.0341**	0.3069
Pos	50	46	4	0	0		
HER2 status							
Neg	83	73	5	3	2	0.6306	
Pos	18	17	0	1	0		
Triple negative	16	11	0	3	2	**<0.0001**	**<0.0010**
Non-triple negative	79	73	5	1	0		
Grade							
1	6	5	0	1	0		
2	50	45	3	1	1	0.7504	
3	40	35	2	2	1		
Histology							
Ductal	84	73	5	4	2	0.6204	
Lobular	12	12	0	0	0		

Table 4.6 P-EGFR positivity and patient prognostic indicators. P values were calculated using Fisher's exact test or Chi square test (marked †).

		P-EGFR		
	n	**Positive**	**Negative**	**p**
Age (years)				
< 50	28	2	26	>0.9999
≥ 50	69	7	62	
Size (cm)				
≤ 2	28	3	25	0.7120
> 2	70	6	64	
Nodal status				
Neg	39	3	35	0.7326
Pos	56	6	50	
ER status				
Neg	28	1	27	0.4272
Pos	64	7	57	
PR status				
Neg	42	6	36	0.2915
Pos	50	3	47	
HER2 status				
Neg	83	7	76	0.6600
Pos	18	2	16	
Triple negative	16	1	15	>0.9999
Non-triple negative	79	8	71	
Grade				
1	6	0	6	
2	50	5	45	0.7182†
3	40	4	36	
Histology				
Ductal	84	9	75	0.5965
Lobular	12	0	12	

Table 4.7 P-EGFR level and patient prognostic indicators. P values were calculated using Chi square test.

		P-EGFR				
	n	**0**	**1+**	**2+**	**3+**	**p**
Age (years)						
< 50	28	26	2	4	0	0.5232
≥ 50	69	62	4	3	0	
Size (cm)						
≤ 2	28	25	1	2	0	0.2780
> 2	70	64	5	1	0	
Nodal status						
Neg	39	36	1	2	0	0.3149
Pos	56	50	5	1	0	
ER status						
Neg	28	27	1	0	0	0.4658
Pos	64	57	5	2	0	
PR status						
Neg	42	36	4	2	0	0.4116
Pos	50	47	2	1	0	
HER2 status						
Neg	83	76	4	3	0	0.4387
Pos	18	16	2	0	0	
Triple negative	16	15	1	0	0	0.7299
Non-triple negative	79	71	5	3	0	
Grade						
1	6	6	0	0	0	
2	50	45	3	2	0	0.9243
3	40	36	3	1	0	
Histology						
Ductal	84	75	6	3	0	0.4920
Lobular	12	12	0	0	0	

4.5 SUMMARY/CONCLUSIONS

The reported expression of EGFR and P-EGFR in breast carcinomas varies widely in the literature. Differences in techniques and populations studied likely contribute to this variation. There are no published data regarding EGFR expression and phosphorylation in an Irish population.

We examined EGFR expression and phosphorylation by immunohistochemistry in a cohort of 101 unselected breast carcinomas from St. Vincent's University Hospital. This was a cohort of predominantly older, high grade, node positive tumours. Overall the rate of EGFR and P-EGFR levels (2+/3+ intensity) is 6.0 % and 3.0 % respectively. In the triple negative subgroup, EGFR expression was 31.5 %. Only 1 triple negative tumour (6.2 %) had any degree of staining for P-EGFR.

Although the numbers of EGFR and P-EGFR positive tumours identified in the this study were low, there was a statistically significant relationship between EGFR positivity and the triple negative phenotype. The correlation with hormone receptor status was not statistically significant following adjustment for multiple testing using the Bonferroni test. There was a statistically significant correlation between the intensity of EGFR staining and lymph node status. No significant correlations between P-EGFR and prognostic factors were identified.

Chapter 5

DASATINIB IN TRIPLE NEGATIVE BREAST CANCER

5.1 INTRODUCTION

Dasatinib is a multi-target tyrosine kinase inhibitor, whose targets include Bcr/Abl and Src kinases. Finn *et al.* tested dasatinib in a panel of 39 molecularly-characterised breast cancer cell lines, including luminal, basal-like, and post-EMT subtypes. Using a dasatinib concentration of 1 μM, cells were classified as highly sensitive (> 60 % growth inhibition), moderately sensitive (40 – 59 % growth inhibition), or resistant. Interestingly, response to dasatinib varied significantly by cell line subtype ($p = 0.008$). Specifically, the basal-like and post-EMT subtypes were the most sensitive [138]. These data strongly suggested a rationale for testing of dasatinib in triple negative breast cancer. We tested this observation in our panel of triple negative breast cancer cell lines. Furthermore, our aim was to assess potential mechanisms of response and resistance to dasatinib in triple negative breast cancer. To achieve this, we developed a novel *in vitro* model of acquired resistance to dasatinib in a triple negative breast cancer cell line.

5.2 DASATINIB SENSITIVITY IN TRIPLE NEGATIVE BREAST CANCER CELL LINES

BT20 was the least sensitive and MDA-MB-231 was the most sensitive of the three triple negative breast cancer cell lines tested for response to dasatinib (Table 5.1).

Table 5.1 Sensitivities of a panel of TNBC cell lines to dasatinib. IC_{50} values are shown ± standard deviation of triplicate experiments.

Cell line	**Dasatinib** *IC_{50} (nM)*
BT20	2265 ± 241
HCC1937	95 ± 19
MDA-MB-231	36 ± 2

5.3 DEVELOPMENT OF A MODEL OF ACQUIRED DASATINIB RESISTANCE

Of the three TNBC cell lines tested, MDA-MB-231 was the most sensitive to dasatinib (IC_{50} = 39.3 ± 14.2, Table 5.1). In order to develop a model of acquired resistance to dasatinib, MDA-MB-231 cells were continuously exposed to dasatinib. An initial concentration of 200 nM dasatinib was used, which resulted in approximately 60 % growth inhibition (Figure 5.1).

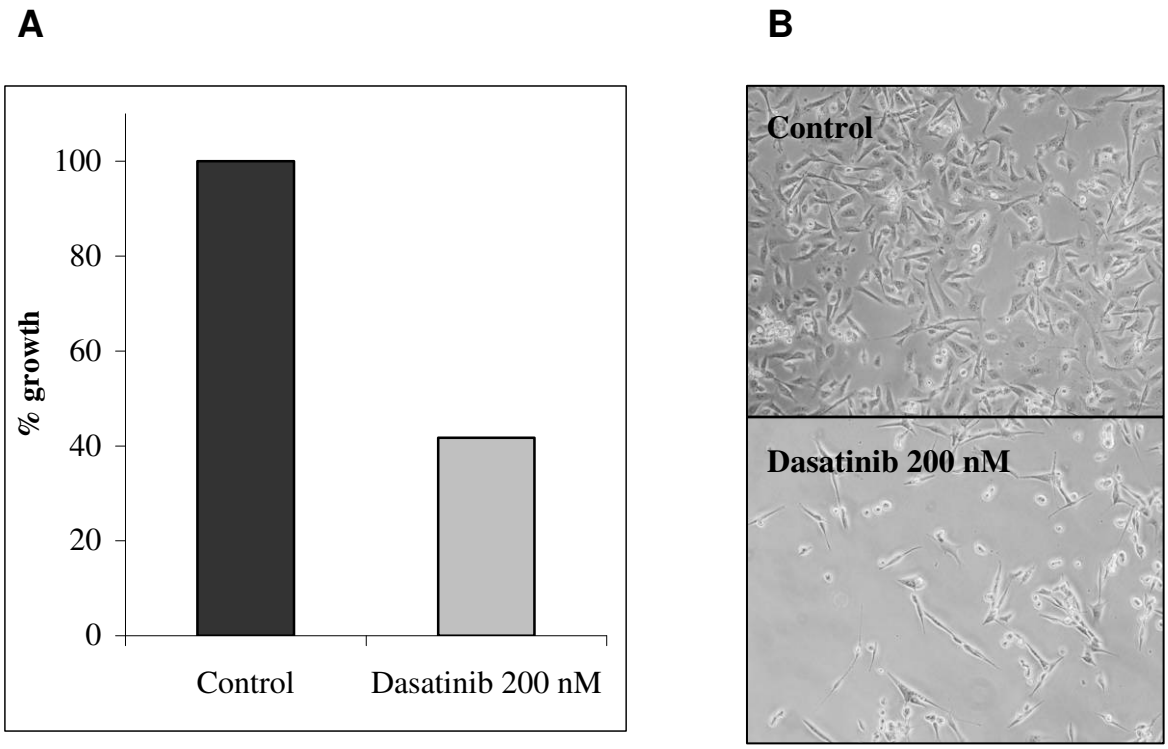

Figure 5.1 A. Growth inhibition of MDA-MB-231 cells, measured by cell number. The cells were cultured in medium with 200 nM dasatinib, compared to cells grown in the absence of drug (control). Cell count was performed when the control flask was confluent, using the Guava Viacount assay. Data represents a single assay. Percentage growth is expressed relative to the cell numbers for the control flask. **B**. Morphology of control cells and cells treated with continuous 200 nM dasatinib.

The concentration of dasatinib was increased incrementally to a maximum of 500 nM dasatinib over a period of 13 weeks. Untreated (parental) cells were cultured in tandem. The experiment was performed in duplicate with two sets of parental and dasatinib-treated cells (designated A and B).

Proliferation assays were performed on the dasatinib-conditioned cell lines, cultured in the absence of dasatinib (for a maximum period up to 8 weeks). The IC_{50} for dasatinib was increased to greater than 5 µM and confirmed resistance to dasatinib (IC_{50} > 1 µM [138]) compared to parental cells (Figure 5.2 A, Table 5.2). Resistance was maintained in the variant cells following a freeze-thaw cycle (Figure 5.2 B, Table 5.2). Interestingly, the parental cells had a small but significant increase in sensitivity to dasatinib following the freeze-thaw cycle (Table 5.2). MDA-MB-231-Das-B was more resistant to dasatinib than MDA-MB-231-Das-A, both before and after the freeze-thaw cycle.

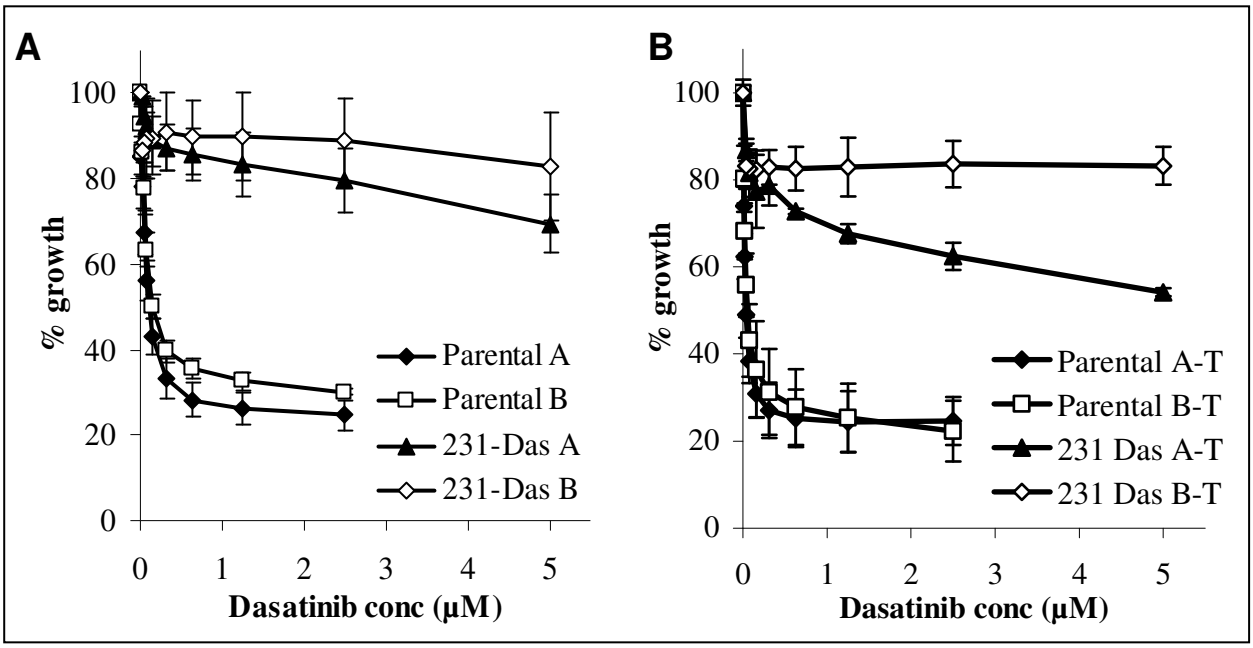

Figure 5.2 Proliferation assays comparing MDA-MB-231-Das-A and MDA-MB-231-Das-B to parental MDA-MB-231 cells. **A.** Proliferation assays on cell lines after development of resistant variant. **B.** Proliferation assays on cell lines following a freeze-thaw cycle (-T). Error bars represent standard deviations of three independent experiments.

Table 5.2 Sensitivity of MDA-MB-231 parental and variant cell lines to dasatinib, from the cells originally cultured during the development of the variant cell line, and after these cells underwent a freeze-thaw cycle.

		Original	Post freeze-thaw cycle	*p*
Parental A	***IC_{50} (nM)***	164 ± 67	64 ± 27	*0.027*
Parental B		300 ± 78	94 ± 80	*0.024*
231-Das A	***Inhibition at 10 µM***	59 ± 9 %	59 ± 17 %	*0.955*
231-Das B		27 ± 9 %	29 ± 14 %	*0.881*

5.4 CHARACTERISATION OF DRUG SENSITIVITY OF MDA-MB-231-DAS CELLS

As the MDA-MB-231-Das-B (231-DasB) variant was more resistant to dasatinib than the A variant, it was selected for further characterisation of acquired dasatinib resistance. Sensitivity to chemotherapy and the EGFR inhibitor gefitinib were assessed in the parental and resistant variant (Table 5.3). There is no significant difference in sensitivity to the EGFR inhibitor gefitinib, or to carboplatin. There is a small, but significant increase in sensitivity to docetaxel and doxorubicin in the variant cell line. The dasatinib resistant variant was significantly less sensitive to the Src inhibitor PD 180970 ($p = 0.003$).

Table 5.3 Sensitivities of the MDA-MB-231 parental cell line and dasatinib-resistant variant to gefitinib, various chemotherapy drugs, and the Src inhibitor PD 180970.

Drug	Parental	Variant	*p*[a]
Gefitinib *IC_{50} (μM)*	23.1 ± 2.2	20.9 ± 2.1	*0.289*
Carboplatin *IC_{50} (μM)*	13.2 ± 0.8	11.5 ± 1.3	*0.147*
Docetaxel *IC_{50} (nM)*	1.9 ± 0.1	1.2 ± 0.1	*0.003*
Doxorubicin *IC_{50} (nM)*	138.3 ± 1.0	97.2 ± 6.6	*0.007*
PD 180970 *IC_{50} (nM)*	400.2 ± 35.6	876.1 ± 74.4	*0.003*

[a] *p* values were calculated using a two-tailed t-test assuming unequal variance.

5.4.1 DASATINIB ACCUMULATION IN MDA-MB-231 PARENTAL AND DASATINIB RESISTANT VARIANT CELLS

It has been reported that dasatinib is a substrate for the drug efflux pumps BCRP and MDR-1 [239]. Therefore, in order to determine if drug efflux pumps were involved in resistance to dasatinib in these cells, we assessed the uptake of dasatinib in the parental MDA-MB-231 cells and the resistant variant. Drug accumulation assays to measure the concentration of dasatinib in the cells were performed in collaboration with Sandra Roche and Dr. Robert O'Connor, as previously described [223].

Initially, dasatinib accumulation was measured in MDA-MB-231 parental and variant cells, using 2 μM dasatinib, across a range of cell seeding numbers. Results were calculated as ng mass dasatinib per million cells. While the relative mass of drug measured increased with decreasing cell density, no significant difference in accumulation between parental and variant cells was observed (Figure 5.3).

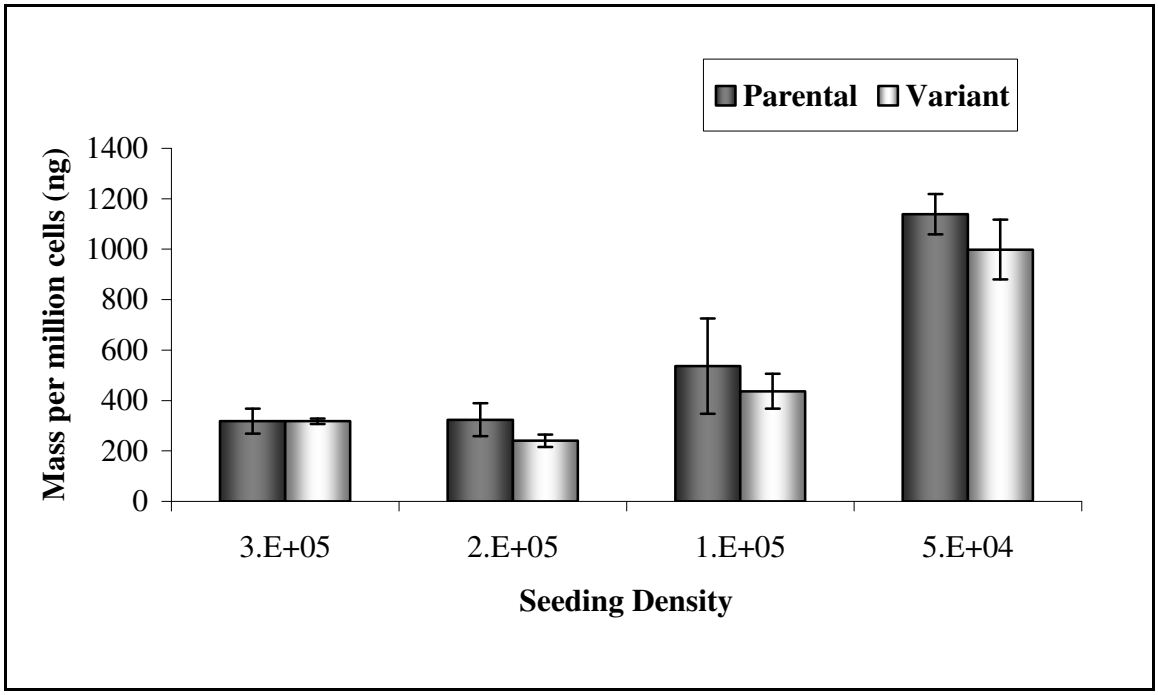

Figure 5.3 Dasatinib accumulation assays in MDA-MB-231 parental and resistant variant cells. Cells seeded at different densities were treated with 2 μM dasatinib for two hours. Cells were then counted using the Guava EasyCyte flow cytometry. The mass of dasatinib per sample was measured by mass spectrometry and expressed as ng per million cells. Error bars represent standard deviations of three replicate flasks for each seeding density.

This observation suggests that drug efflux mechanisms do not play a significant role in dasatinib resistance in this model. To confirm this, we tested growth inhibition with dasatinib combined with the potent BCRP and MDR-1 inhibitor elacridar [240]. Proliferation was measured in the parental and variant cell lines treated with dasatinib alone or in combination with a concentration of elacridar sufficient to inhibit BCRP [241] and MDR-1 [242] (Figure 5.4). A small but non-significant increase in growth inhibition was observed in the parental cell line treated with the combination. No difference in inhibition was observed in the variant cell line, although the effect of dasatinib alone on growth was predictably small.

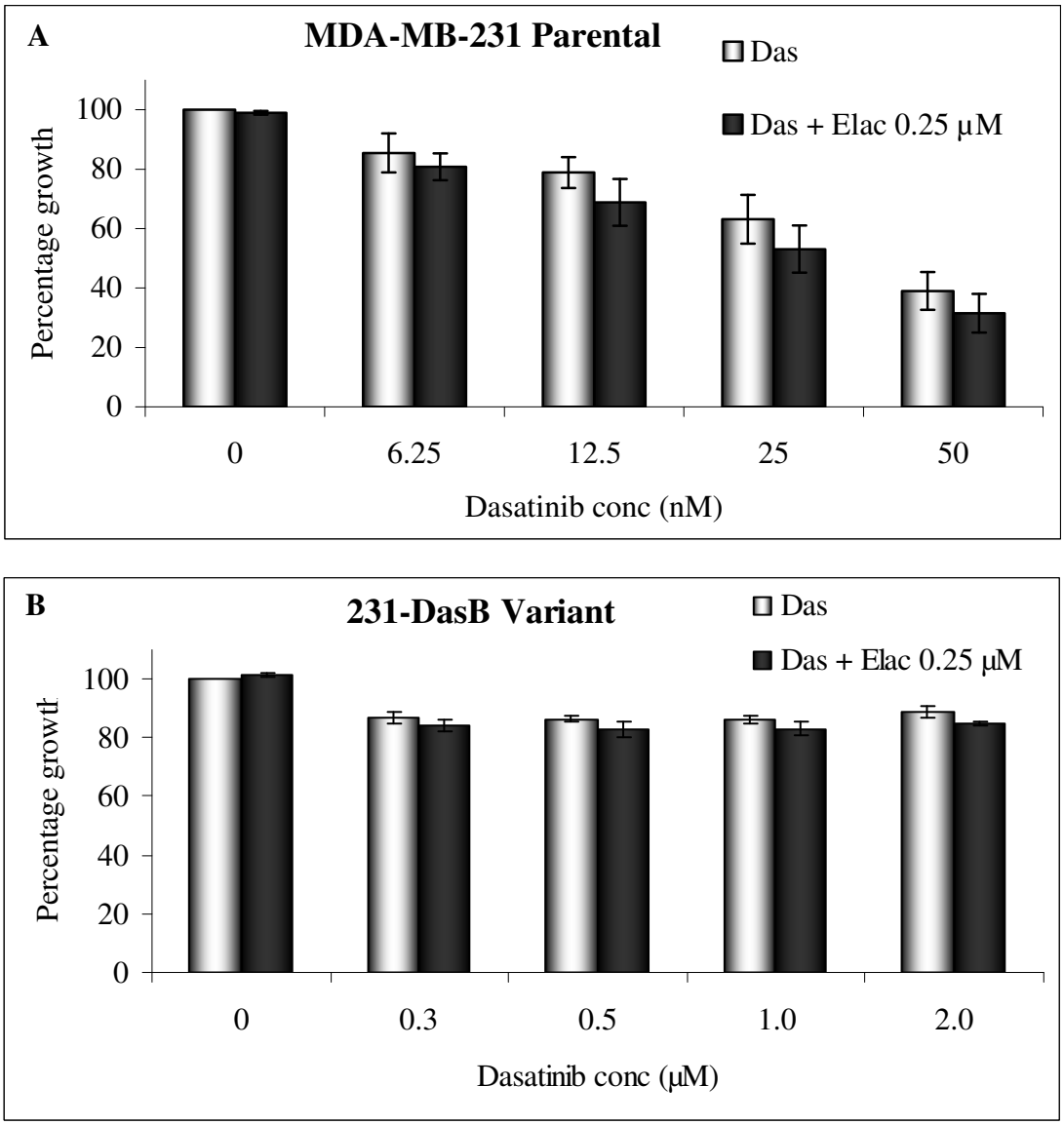

Figure 5.4 Proliferation assays in MDA-MB-231 parental (A) and 231-DasB variant (B) cells treated with dasatinib (Das) alone and combined with a fixed concentration of elacridar (Elac). Error bars represent the standard deviations of triplicate experiments.

5.4.2 EFFECTS OF DASATINIB ON KEY SIGNALLING TARGETS IN MDA-MB-231 PARENTAL AND DASATINIB RESISTANT VARIANT CELLS

We examined the effects of dasatinib treatment on key signalling proteins in the MDA-MB-231 parental and variant cells (Figures 5.5 – 5.7). In both cell lines, there was no appreciable change in Akt levels in response to dasatinib. P-Akt levels were not reproducibly detected, consistent with previous examination of this protein (Chapter 3). In the dasatinib-sensitive parental cell line, there was a slight increase in MAPK levels in response to dasatinib, but no alteration in MAPK phosphorylation (Figure 5.5). In contrast, in the dasatinib-resistant variant, MAPK levels decreased slightly at the highest concentration of dasatinib used, and there was a slight decrease in P-MAPK in response to dasatinib.

No alteration in EphA2 levels was observed in either cell line. P-EphA2 levels were not detected in either cell line, using both a phospho-specific antibody and immunoprecipitation for total EphA2 and immunoblotting for phospho-tyrosine. Src kinase levels and phosphorylation were examined in the parental and resistant variant cell lines in response to increasing concentrations of dasatinib (Figure 5.6). There was no change in Src levels in either cell line. However, Src phosphorylation decreased in a dose-dependent manner in response to dasatinib in the sensitive parental cell line. In contrast, no change in P-Src was observed in response to dasatinib in the resistant cell line.

A potential mechanism of altered Src phosphorylation status in the resistant cell line is constitutive activation of Src. This was examined by serum starvation of both parental and variant cells, followed by the re-addition of serum (Figure 5.7). No difference in Src phosphorylation was observed in either cell line in this experiment.

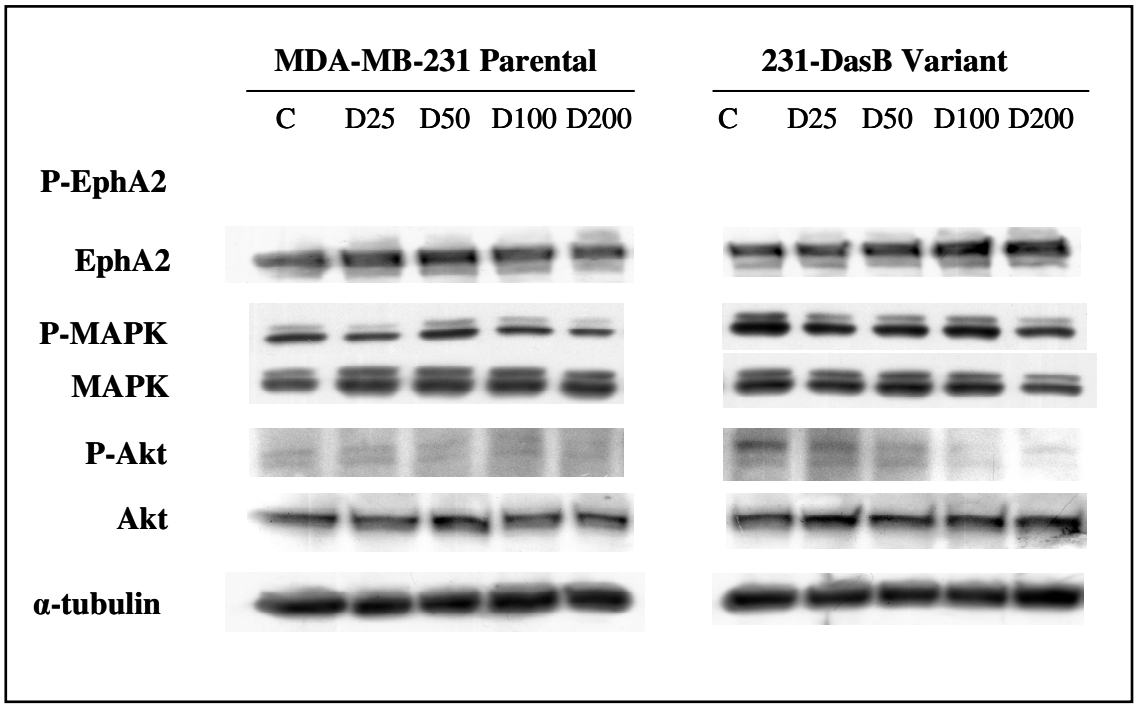

Figure 5.5. Detection of total and phosphorylated EphA2, MAPK, and Akt in MDA-MB-231 breast cancer cell lines (parental and dasatinib-resistant variant) treated with dasatinib for 6 hours. (P-: phospho-; C: Control (untreated); D: Dasatinib (nM)). The blots shown are representative of triplicate experiments.

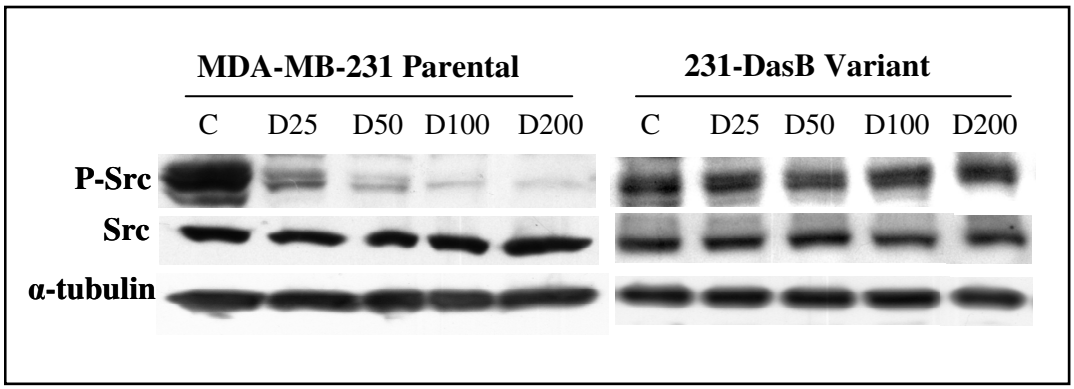

Figure 5.6. Detection of Src and phosphorylated Src [pY^{418}] in MDA-MB-231 breast cancer cell lines (parental and dasatinib-resistant variant) treated with dasatinib for 6 hours. (P-: phospho-; C: Control (untreated); D: Dasatinib (nM)). The images represent results of a single experiment.

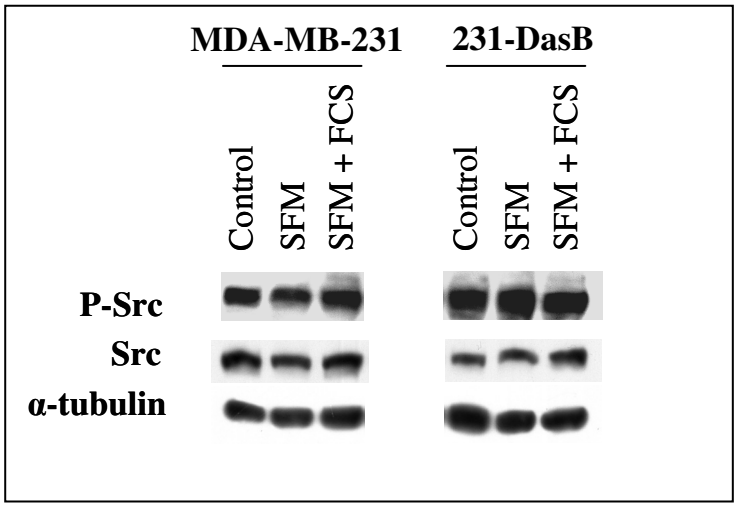

Figure 5.7 Detection of Src and phospho-Src in the MDA-MB-231 breast cancer cell line (parental and dasatinib-resistant variant) with untreated control cells, serum-starvation for 24 hours (SFM), and serum-starvation followed by serum-containing medium for 2 further hours (SFM +FCS) (P-: phospho-). The images represent results of a single experiment.

An inverse correlation between Src and estrogen receptor α (ERα) expression in breast cancer cell lines has been reported [243]. Src has been shown to interact with estrogen to initiate estrogen receptor α (ERα) proteolysis [243]. To determine if Src inhibition altered ERα expression in the dasatinib resistant cell line we examined ERα protein by immunoblotting. No ERα expression was detected in either cell line (Figure 5.9).

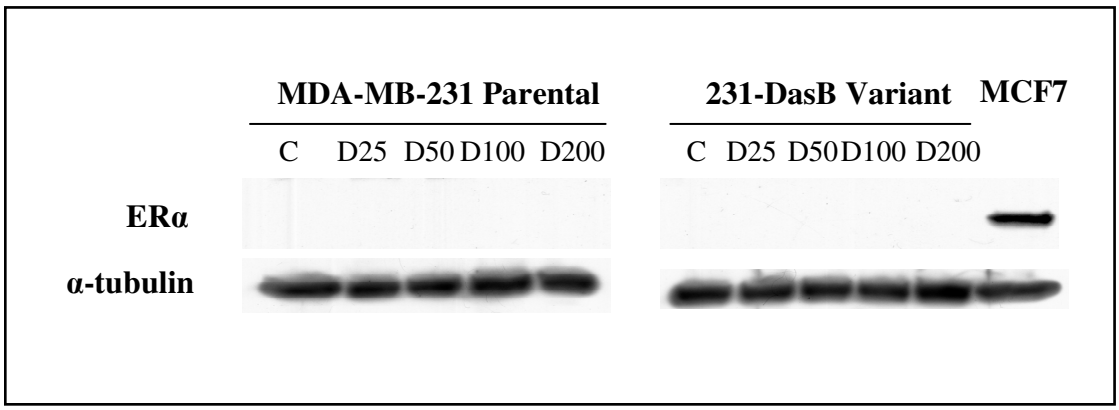

Figure 5.8 Detection of estrogen receptor (ERα) in MDA-MB-231 breast cancer cell lines (parental and dasatinib-resistant variant) treated with dasatinib for 6 hours. (P-: phospho-; C: Control (untreated); D: Dasatinib (nM)).). The MCF7 breast cancer cell line is used as a positive control. The images represent results of a single experiment.

5.4.3 EFFECTS OF DASATINIB ON INVASION AND MOTILITY IN MDA-MB-231 PARENTAL AND DASATINIB RESISTANT VARIANT CELLS

Src is know to play a key role in invasion and metastasis in cancer [206]. Consequently, to further characterise the novel model of dasatinib resistance, we examined the invasion and motility status of the parental and variant cell lines, alone and in response to dasatinib.

In the parental MDA-MB-231 cell line, a significant decrease in invasion was observed in response to dasatinib (Figure 5.9 and 5.10, $p = 0.0216$). In contrast, in the MDA-MB-231-Das resistant variant, no significant change in invasion was observed in response to dasatinib ($p = 0.7721$). The variant cell line displayed increased invasion compared to the parental cell line, although this was not statistically significant ($p = 0.1622$)

Similar results for motility as for invasion were observed (Figure 5.11 and 5.12). Motility was significantly decreased in the parental cell line in response to dasatinib ($p = 0.0018$), but not in the variant cell line ($p = 0.3401$). There was a significant increase in motility in the variant compared to the parental cell line ($p = 0.0090$).

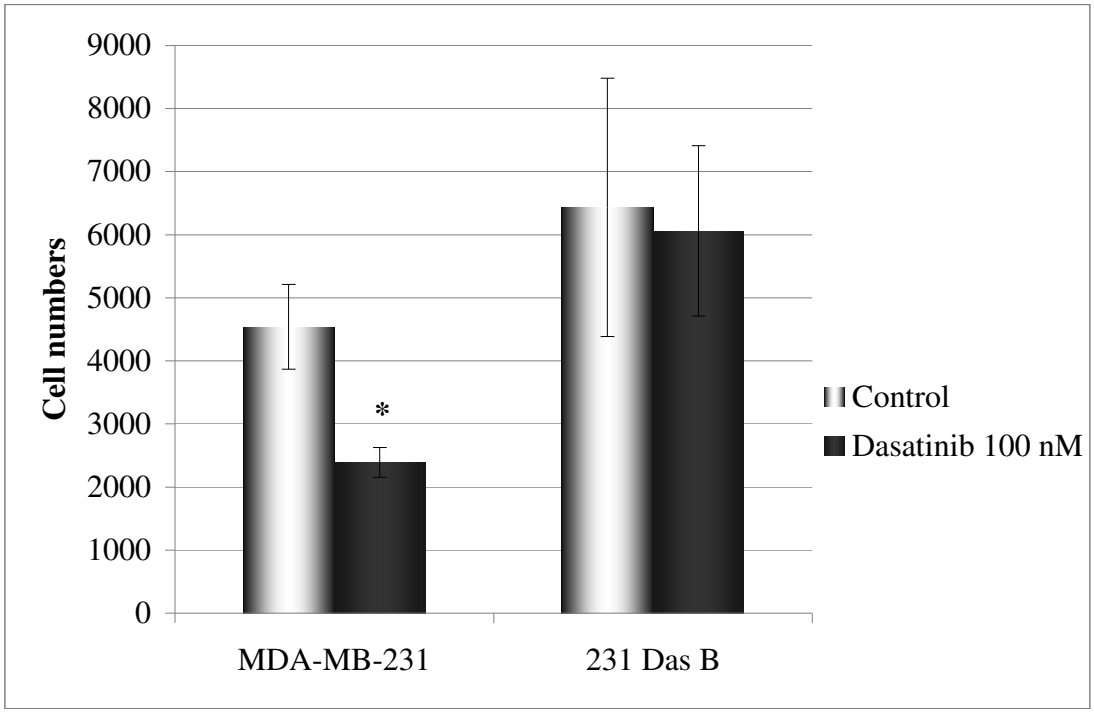

Figure 5.9 Invasion assays comparing the triple negative breast cancer cell line MDA-MB-231 and resistant variant (231-Das B). Cells were seeded in reduced serum medium (5 % FCS in RPMI 1640) and treated with either 5 % FCS (Control) or 100 nM dasatinib after 6 hours. The number of invasive cells was counted after 18 hours further incubation. Error bars represent standard deviation of three independent experiments.

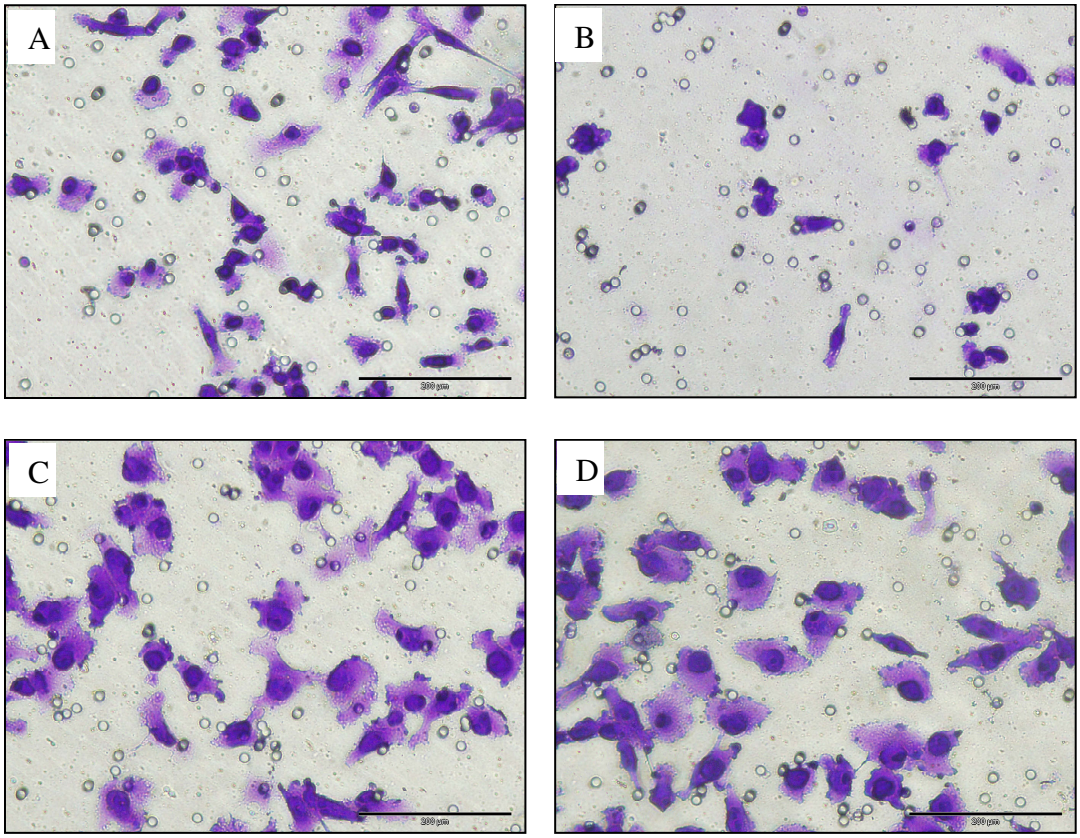

Figure 5.10 Representative images of invasion assays in MDA-MB-231 and 231-DasB cell line at 200X magnification. **A**. MDA-MB-231 Control; **B**. MDA-MB-231 100 nM dasatinib; **C**. 231 DasB Control; **D**. 231 DasB 100 nM dasatinib.

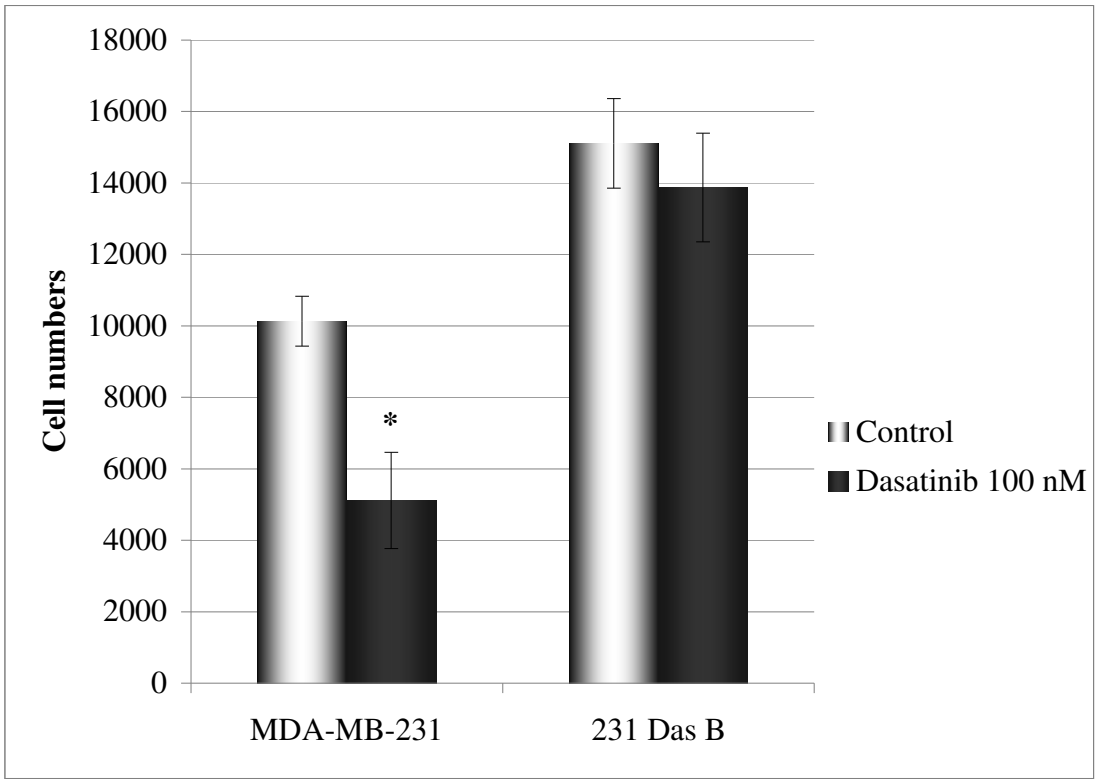

Figure 5.11 Migration assays comparing the triple negative breast cancer cell line MDA-MB-231 and resistant variant (231-Das B). Cells were seeded in reduced serum medium (5 % FCS in RPMI 1640) and treated with either 5 % FCS (Control) or 100 nM dasatinib after 6 hours. The number of migratory cells was counted after 18 hours further incubation. Error bars represent standard deviation of three independent experiments.

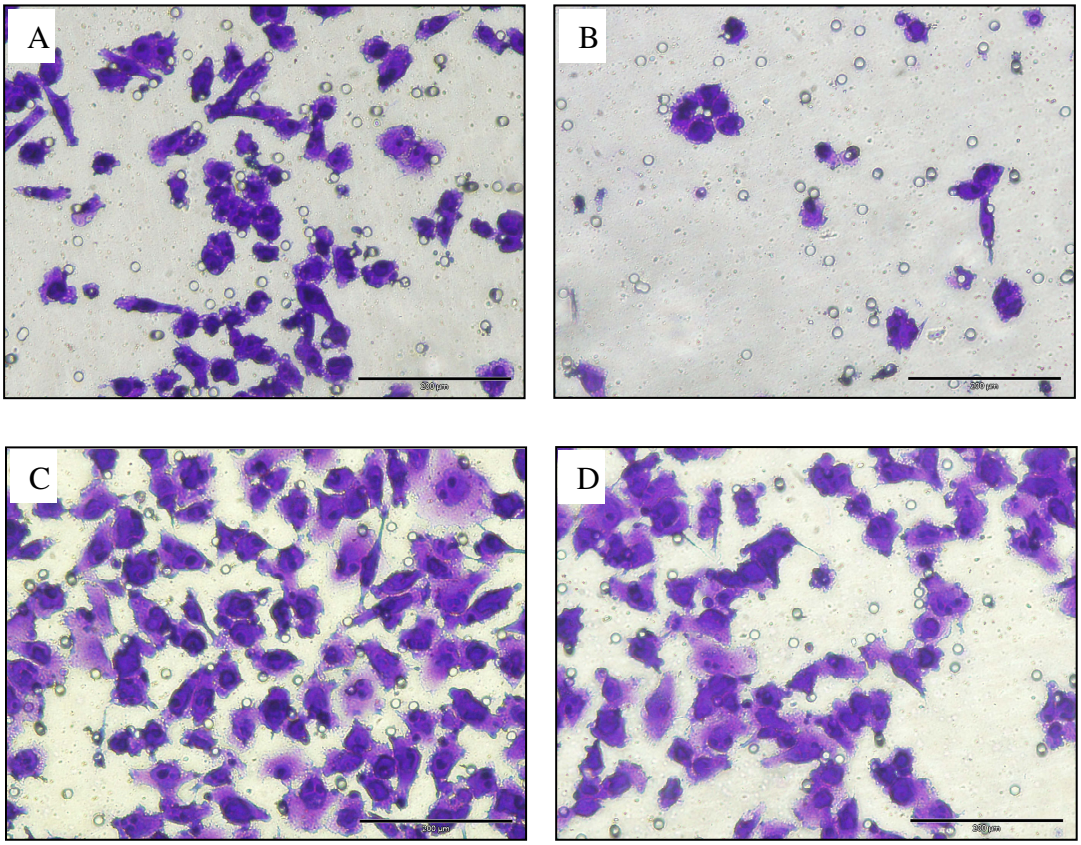

Figure 5.12 Representative images of migration assays in MDA-MB-231 and 231-DasB cell line at 200X magnification. **A**. MDA-MB-231 Control; **B**. MDA-MB-231 100 nM dasatinib; **C**. 231 DasB Control; **D**. 231 DasB 100 nM dasatinib.

5.4.4 EFFECTS OF DASATINIB ON DOUBLIN TIME IN MDA-MB-231 PARENTAL AND DASATINIB RESISTANT VARIANT CELLS

To further characterise the novel dasatinib-resistant variant, we compared the doubling time of the parental and variant cells, untreated and in response to dasatinib. The doubling time of the resistant cell line was similar to the parental cell line (Table 4.4). However, in response to dasatinib, there was a significant dose-dependent decrease in growth rate in the sensitive parental cell line (dasatinib 50 nM, p = 0.0098; 100 nM, p = 0.0073). In contrast, the doubling time of the variant cell line was not significantly altered by dasatinib treatment (50 nM, p = 0.2976; 100 nM, p = 0.3915).

Table 5.4 Doubling time in hours (**±** standard deviation) and growth rate of MDA-MB-231 and MDA-MB-231-Das cells with and without dasatinib treatment.

(hours)	**Control**	**D 50 nM**	*p*[a]	**D 100 nM**	*p*
MDA-MB-231	**17.6** ± 1.2	**32.2** ± 3.3	0.0098	**46.8** ± 5.1	0.0073
Growth rate (%)	100.0	54.7		37.6	
231 DasB	**19.1** ± 2.4	**21.0** ± 0.2	0.2976	**21.2** ± 3.1	0.3915
Growth rate (%)	100.0	91.0		90.1	
p	0.4134				

[a] p values were calculated using a two-tailed t-test.

5.5 SUMMARY

Dasatinib has been shown to preferentially inhibit growth in triple negative breast cancer cell lines in comparison to other breast cancer subtypes [138, 204]. We developed a novel model of acquired resistance to dasatinib, using the sensitive triple negative MDA-MB-231 cell line. This was achieved by continuous exposure to incrementally increasing concentrations of dasatinib. The resistance achieved in the variant cell line was stable following a freeze-thaw cycle.

Dasatinib is reported to be a substrate for BCRP and MDR-1. Therefore, we assessed the possibility that these drug efflux pumps play a role in the dasatinib resistance in these cells. No significant differences in dasatinib accumulation were observed. Furthermore, combining dasatinib with the BCRP/MDR-1 inhibitor elacridar did not enhance growth inhibition. These observations suggest that these drug efflux pumps do not play a significant role in acquired resistance to dasatinib in this model.

Examination of key cancer signalling pathways suggests that phosphorylation of Src kinase plays an important role in resistance to dasatinib in this model. Consistent with the role of Src kinase in invasion, we also observed alterations in invasion and motility between the parental and variant cell lines in response to dasatinib.

Chapter 6

PROTEOMIC ANALYSIS OF DASATINIB RESISTANCE

6.1 INTRODUCTION

Two-dimensional (2D) gel electrophoresis is a well established and powerful technique that enables simultaneous visualisation of relatively large portions of the proteome [244, 245]. The principle of 2D electrophoresis is based on separation of the proteins according to their charge in the first dimension by isoelectric focusing (IEF), and size in the second dimension by SDS-PAGE. Traditionally, this is a time- and labour-intensive technique, requiring multiple gels to be run, analysed and compared, which is associated with issues of excessive variability and reproducibility. The development of 2D difference gel electrophoresis (DIGE), first described by Unlu *et al.* [246], allowed more than one sample to be run on a single 2D polyacrylamide gel, using prelabeling of two protein extracts with fluorescent cyanine dyes (Cy3 and Cy5). Visualisation of the samples using fluorescence imaging enables detection of differences in protein abundance between the two samples.

Dasatinib, a multi-target tyrosine kinase inhibitor, whose targets include Bcr/Abl and Src kinases, has shown increased activity in TNBC compared to other breast caner subtypes [138]. We have developed and characterised a novel model of acquired resistance to dasatinib in TNBC (Chapter 5). Identifying and understanding proteins which may be involved in sensitivity or resistance to this agent has important therapeutic implications. 2D DIGE analysis of total protein and Pro-Q® Diamond gel staining for phospho-proteins were used to analyse potential differences between the parental and variant cell lines.

6.1 2D DIFFERENCE GEL ELECTROPHORESIS (DIGE) ANALYSIS

Protein lysates were prepared from parental MDA-MB-231 and dasatinib-resistant variant MDA-MB-231-Das cells untreated and treated with 100 nM dasatinib. Proteomic analysis was performed on total protein (as described in section 2.12). 2500 spots were detected on the DIGE gels, and each was assigned a unique ID number (Figure 6.1). The results of each set of replicate gels were analysed using the DeCyder differential in-gel analysis (DIA) module, and the difference in protein expression between two samples is expressed as fold-change. The DeCyder software produces 3-

D images of protein abundance, and constructs graphs of relative protein abundance of each of the samples analysed (Figure. 6.2).

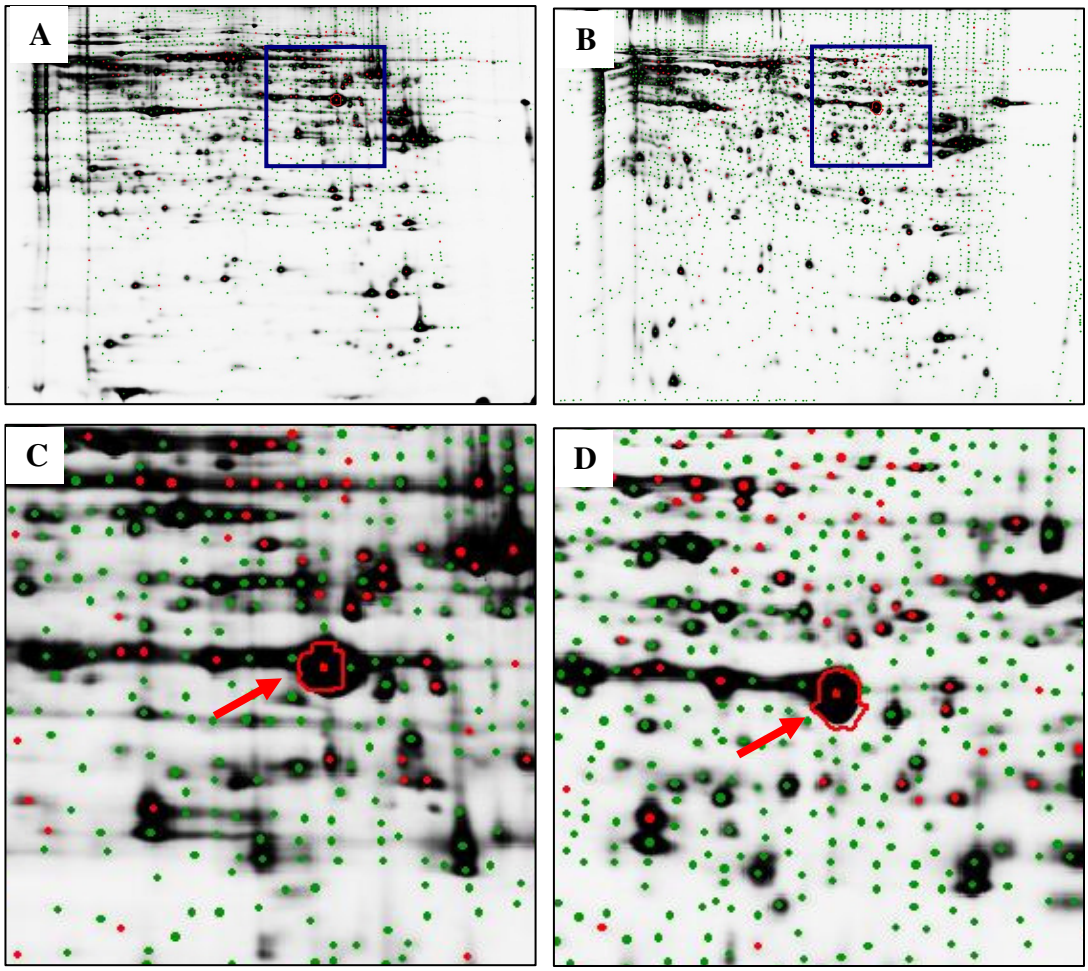

Figure 6.1 Example of DIGE gel pictures using different Cy dyes scanned at different wavelengths to reveal spots from **A.** Gel 1 Cy3-labelled parental MDA-MB-231 cells, **B.** Gel 4 Cy5-labelled MDA-MB-231-Das cells. The spots detected by the DeCyder software are marked with red and green dots. **C.** and **D.** are cropped pictures of A and B, respectively, focusing on the upper region of the gel, with the location of spot ID 1095 (ENO1 protein, arrow).

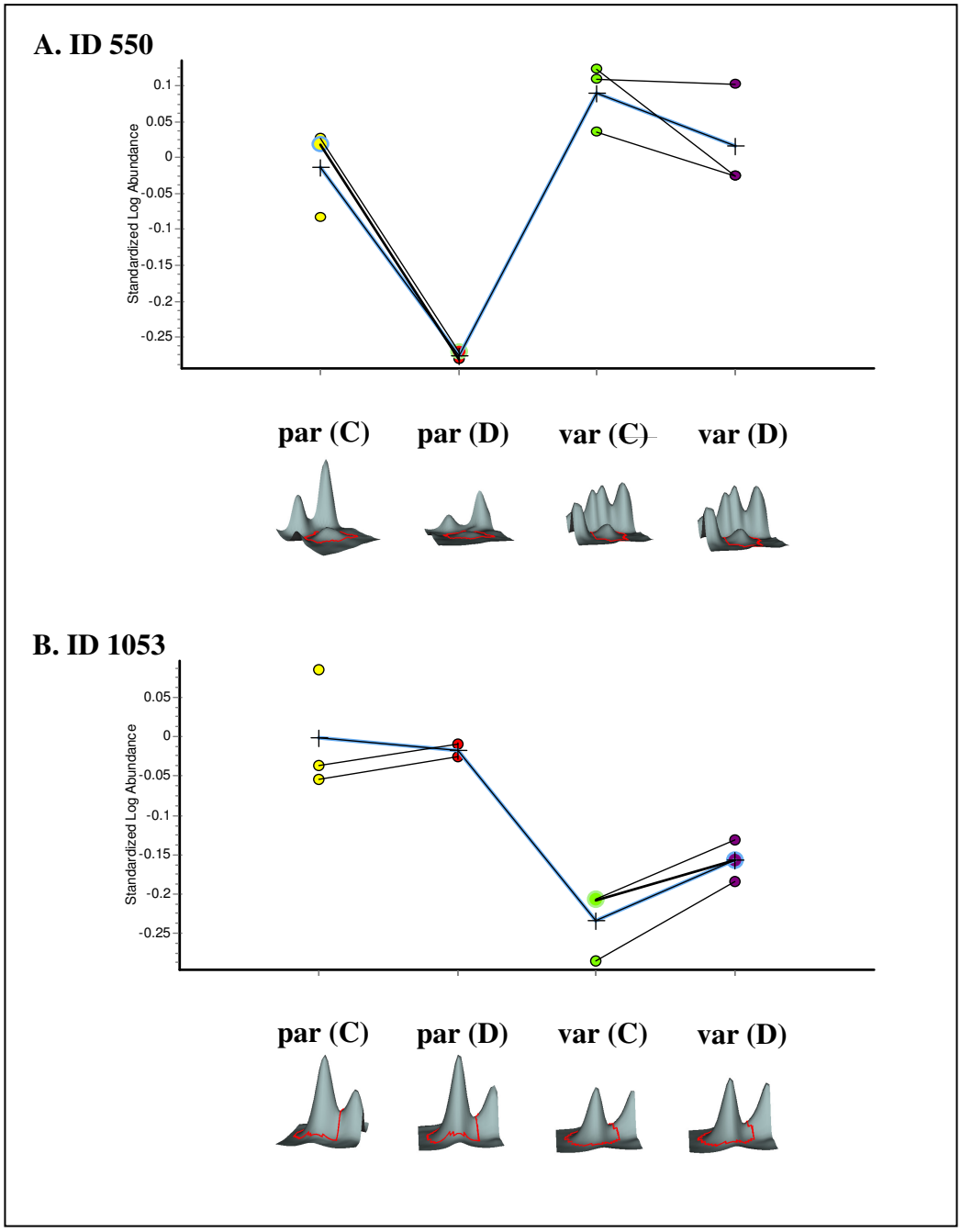

Figure 6.2 Examples of 3-D view of protein abundance in untreated and treated MDA-MB-231 (par) and 231-DasB (var) cells, and graphs of protein abundance in untreated (C), and dasatinib treated (D), analysed by the DeCyder software. The solid blue line in the graph is the average of replicate measurements (dotted lines) of protein abundance. **A.** ID no. 550 chaperonin containing TCP1; subunit 3 (gamma) (CCT3); **B.** ID no. 1053 Enolase 1 (ENO1).

Gel spots for identification were selected. Gel spots which were increased or decreased by ≥ 1.2-fold and had significant ANOVA p values of less than 0.05 were selected for protein identification. Spots appearing on the majority of the images generated by the DeCyder software using the different Cy dyes were selected and picked as described in section 2.12.4. Maldi TOF/TOF mass spectrometry and protein identification was performed (section 2.12.5), using the analysis setting displayed in Figure 6.3

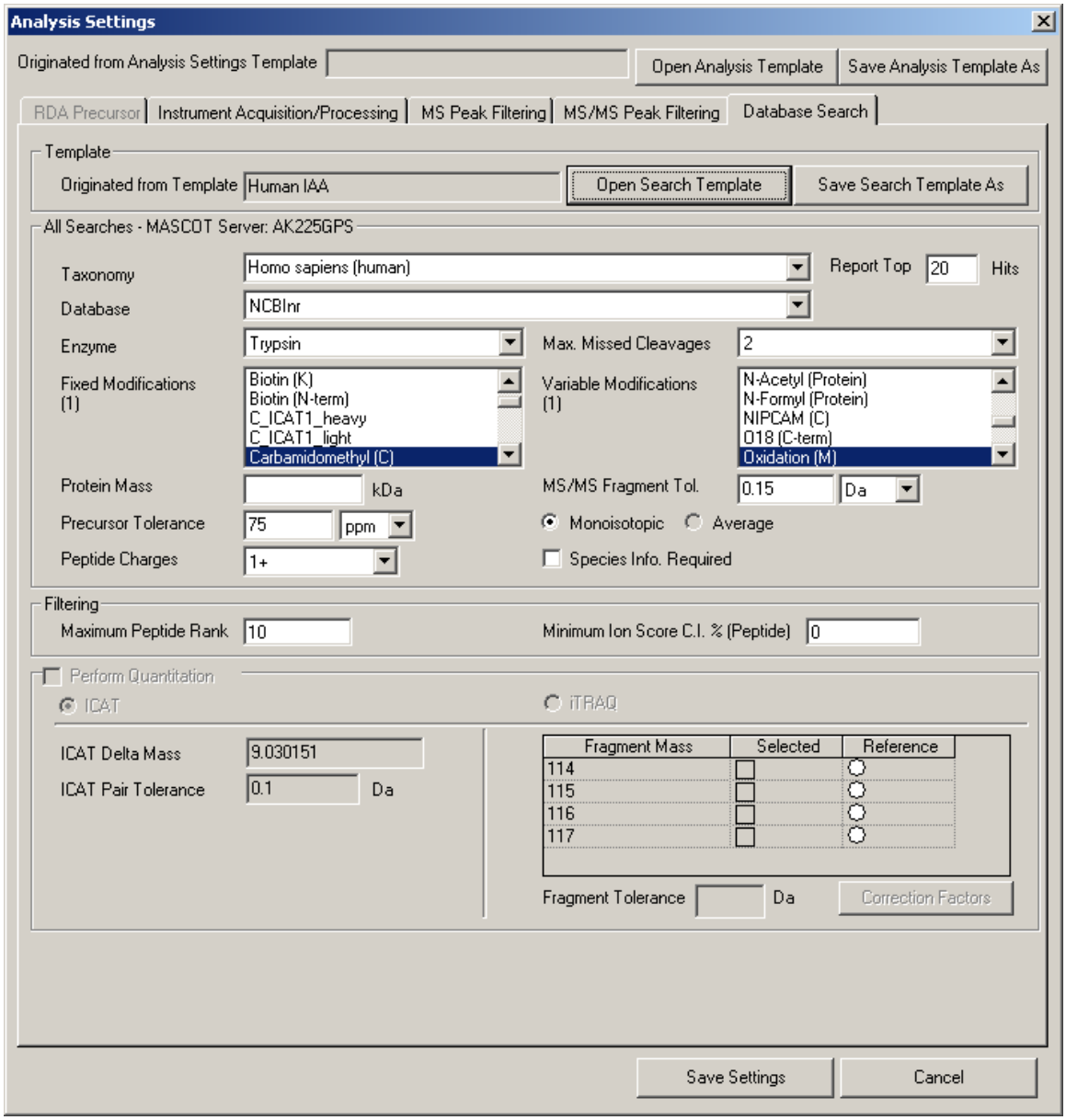

Figure 6.3 The settings used for protein identification. The MS/MS data were searched against the NCBI database using GPS Explorer software (Applied Biosystems) and a local MASCOT (Matrix Science) search engine for protein identification. A mass window of 75 ppm was set for database searching on all precursors.

Examples of the analyses performed to achieve confident protein identification are shown (Figure 6.4 – Figure 6.6). Figure 6.4 lists all the peptides identified for protein ID no. 1345 (annexin A1), and the corresponding peptide scores. The high scores reflect high confidence in identification. An example of a matched peptide with a high ion score, and a high level of homology, and the coverage achieved to identify the protein are shown in Figure 6.5. The fragmented y ions which were used to identify this peptide are shown in Figure 6.6.

gi|54696696	Mass: 38918		Score: 961	Expect: 1E-91		Queries matched: 31			
annexin A1		[Homo sapiens]						Peptide	
Observed	Mr(expt)	Mr(calc)	Delta	Start	End	Miss	Ions	Score	
763.4123	762.405	762.4024	0.0026	229	-	234	0	**28**	R.SYPQLR.R
829.5078	828.5005	828.4956	0.0049	251	-	257	0	**---**	K.VLDLELK.G
908.4485	907.4412	907.4399	0.0013	205	-	212	0	**22**	R.ALYEAGER.R
908.4485	907.4412	907.4399	0.0013	205	-	212	0	**---**	R.ALYEAGER.R
1064.4965	1063.4892	1063.4856	0.0037	304	-	312	0	**---**	R.SEIDMNDIK.A
1080.4846	1079.4773	1079.4805	-0.0031	304	-	312	0	**---**	R.SEIDMNDIK.A
1213.5352	1212.5279	1212.5258	0.0021	167	-	177	0	**---**	K.DITSDTSGDFR.N
1262.6018	1261.5945	1261.5939	0.0007	114	-	124	0	**80**	K.TPAQFDADELR.A
1262.6018	1261.5945	1261.5939	0.0007	114	-	124	0	**---**	K.TPAQFDADELR.A
1387.7626	1386.7553	1386.7606	-0.0053	59	-	71	0	**---**	K.GVDEATIIDILTK.R
1543.874	1542.8667	1542.8617	0.005	59	-	72	1	**---**	K.GVDEATIIDILTKR.N
1550.8198	1549.8125	1549.81	0.0025	215	-	228	0	**51**	K.GTDVNVFNTILTTR.S
1550.8198	1549.8125	1549.81	0.0025	215	-	228	0	**---**	K.GTDVNVFNTILTTR.S
1605.9524	1604.9451	1604.9501	-0.0049	99	-	113	0	**104**	K.ALTGHLEEVVLALLK.T
1605.9524	1604.9451	1604.9501	-0.0049	99	-	113	0	**---**	K.ALTGHLEEVVLALLK.T
1678.918	1677.9107	1677.9049	0.0058	214	-	228	1	**108**	R.KGTDVNVFNTILTTR.S
1678.918	1677.9107	1677.9049	0.0058	214	-	228	1	**---**	R.KGTDVNVFNTILTTR.S
1702.8904	1701.8831	1701.8784	0.0047	129	-	144	0	**124**	K.GLGTDEDTLIEILASR.T
1702.8904	1701.8831	1701.8784	0.0047	129	-	144	0	**---**	K.GLGTDEDTLIEILASR.T
1739.7377	1738.7304	1738.7281	0.0023	189	-	204	0	**122**	R.SEDFGVNEDLADSDAR.A
1739.7377	1738.7304	1738.7281	0.0023	189	-	204	0	**---**	R.SEDFGVNEDLADSDAR.A
1757.8317	1756.8244	1756.8375	-0.0131	318	-	332	0	**---**	K.MYGISLCQAILDETK.G
1776.9341	1775.9268	1775.9305	-0.0037	82	-	97	0	**---**	K.AAYLQETGKPLDETLK.K
1905.0291	1904.0218	1904.0254	-0.0036	82	-	98	1	**82**	K.AAYLQETGKPLDETLKK.A
1905.0291	1904.0218	1904.0254	-0.0036	82	-	98	1	**---**	K.AAYLQETGKPLDETLKK.A
2141.0146	2140.0073	2140.0112	-0.0039	10	-	26	0	**---**	K.QAWFIENEEQEYVQTVK.S
2157.002	2155.9947	2156.2126	-0.2178	251	-	269	2	**---**	K.VLDLELKGDIEKCLTAIVK.C
2334.0957	2333.0884	2333.0919	-0.0034	318	-	337	1	**---**	K.MYGISLCQAILDETKGDYEK.I
2350.0811	2349.0738	2349.0868	-0.013	318	-	337	1	**---**	K.MYGISLCQAILDETKGDYEK.I
2356.1567	2355.1494	2355.1494	0	30	-	53	0	**115**	K.GGPGSAVSPYPTFNPSSDVAALHK.A

Figure 6.4 Detailed MS analysis for protein ID no. 1345 (annexin A1) including all peptides associated with this protein, with corresponding peptide scores which indicate high confidence in protein identification. Peptide scores > 50 reflect high percentage sequence coverage.

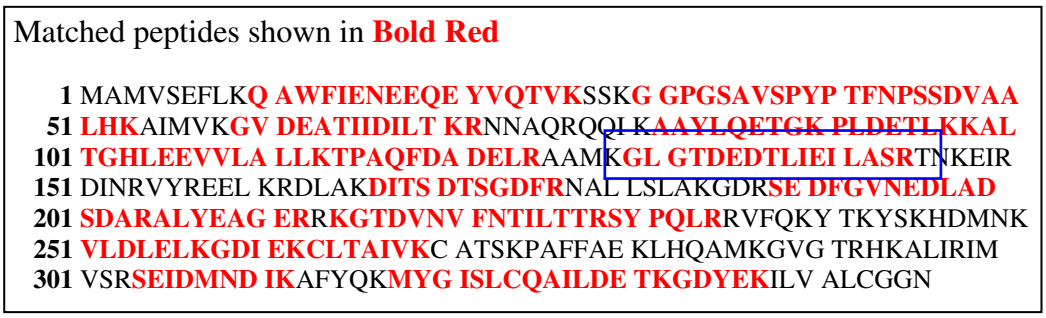

Figure 6.5 Protein sequence of protein ID no. 1345 (annexin A1), which had 63 % protein coverage. The matched peptide sequences are in red. The outlined peptide sequence corresponds to amino acids 129 – 144, and this peptide fragment had a high ion score of 124, indicating a high level of homology.

A MS/MS Fragmentation of **GLGTDEDTLIEILASR**

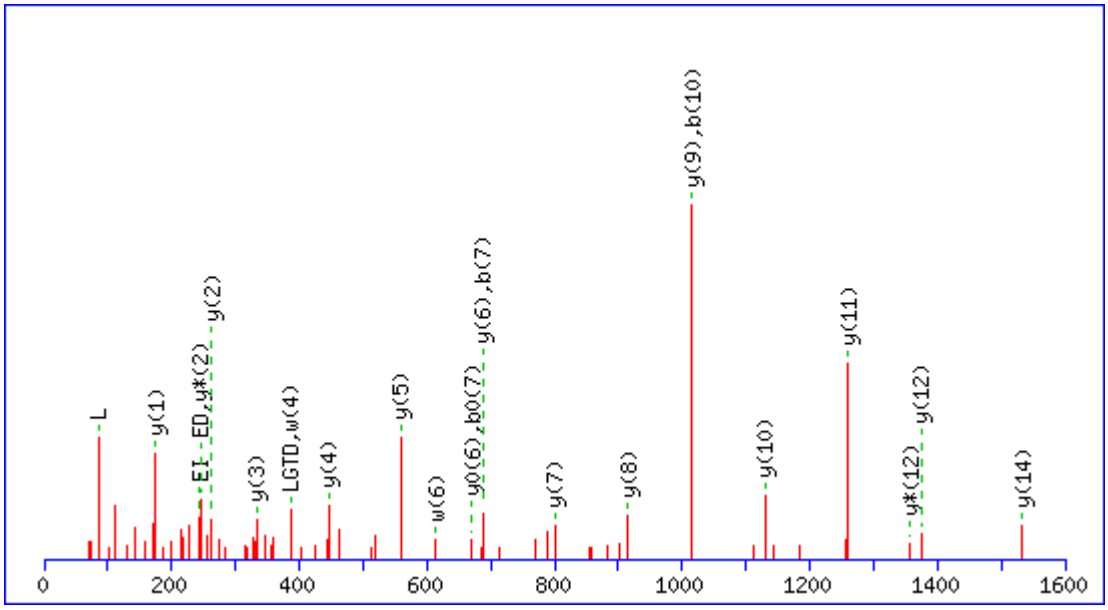

B

#	Immon.	a	a^0	b	b^0	Seq.	v	w	w'	y	y*	y^0	#
1	30.0338	30.0338		58.0287		G							16
2	86.0964	143.1179		171.1128		L	1587.7860	1586.7908		1645.8643	1628.8377	1627.8537	15
3	30.0338	200.1393		228.1343		G				1532.7802	1515.7537	1514.7696	14
4	74.0600	301.1870	283.1765	329.1819	311.1714	T	1429.7169	1442.7373	1444.7166	1475.7588	1458.7322	1457.7482	13
5	88.0393	416.2140	398.2034	444.2089	426.1983	D	1314.6899	1313.6947		1374.7111	1357.6845	1356.7005	12
6	102.0550	545.2566	527.2460	573.2515	555.2409	E	1185.6474	1184.6521		1259.6841	1242.6576	1241.6736	11
7	88.0393	660.2835	642.2729	688.2784	670.2678	D	1070.6204	1069.6252		1130.6415	1113.6150	1112.6310	10
8	74.0600	761.3312	743.3206	789.3261	771.3155	T	969.5727	982.5931	984.5724	1015.6146	998.5881	997.6040	9
9	86.0964	874.4152	856.4047	902.4101	884.3996	L	856.4887	855.4934		914.5669	897.5404	896.5564	8
10	86.0964	987.4993	969.4887	1015.4942	997.4836	I	743.4046	756.4250	770.4407	801.4829	784.4563	783.4723	7
11	102.0550	1116.5419	1098.5313	1144.5368	1126.5262	E	614.3620	613.3668		688.3988	671.3723	670.3882	6
12	86.0964	1229.6259	1211.6154	1257.6209	1239.6103	I	501.2780	514.2984	528.3140	559.3562	542.3297	541.3456	5
13	86.0964	1342.7100	1324.6994	1370.7049	1352.6944	L	388.1939	387.1987		446.2722	429.2456	428.2616	4
14	44.0495	1413.7471	1395.7365	1441.7420	1423.7315	A	317.1568			333.1881	316.1615	315.1775	3
15	60.0444	1500.7791	1482.7686	1528.7741	1510.7635	S	230.1248	229.1295		262.1510	245.1244	244.1404	2
16	129.1135					R	74.0237	73.0284		175.1190	158.0924		1

Figure 6.6 Interpretation of a Tandem Mass Spectrum corresponding to a peptide from protein ID no. 1345 (annexin A1). The precursor (or parent) ions are fragmented by collision induced dissociation (CID). The fragment ion mass spectra (MS/MS) can be used to determine the peptide sequence (**GLGTDEDTLIEILASR**). The figure (A) and table (B) show how to determine sequence from y ions (red) produced by cleavage of the amide bond with C-terminal charge retention. The blue letters indicate the amino acids that can be determined by ladder sequencing.

Comparisons of altered proteins were performed using DeCyder software. The comparisons were between the parental (MDA-MB-231) and variant (231-DasB) cell lines, control (untreated) and dasatinib-treated (Table 6.1). The numbers of spots identified by the software for each comparison are listed at the bottom of each table which lists identified proteins (Table 6.2 – 6.7). Proteins unique to each comparison displaying an increase or decrease ≥ 1.2-fold and significant ANOVA p values less than 0.05 are included in the tables.

Table 6.3 List of tables detailing comparisons of proteins used in proteomic analysis of MDA-MB-231 (parental) and 231-DasB (dasatinib-resistant variant) cell lines, in untreated (U) and dasatinib-treated (D).

Comparison	Table	Number of spots showing significant change	Number of proteins identified by MS
MDA-MB-231 – D *vs.* U	**6.2**	71	9
231-DasB – D *vs.* U	**6.3**	46	12
231-DasB U *vs.* MDA-MB-231 U	**6.4**	134	30
231-DasB D *vs.* MDA-MB-231 D	**6.5**	148	29
Uniquely differentially regulated proteins in MDA-MB-231 D	**6.6**	-	6
Uniquely differentially regulated proteins in 231-DasB D	**6.7**	-	9

Three proteins were found to be significantly upregulated in the parental MDA-MB-231 cell line, treated with dasatinib compared to untreated (Table 6.2): Tryptophanyl-tRNA synthetase (WARS, IPF53), which is involved in regulation of angiogenesis [247, 248], and negative regulation of the cell cycle [249]; villin 2, a cytoskeletal protein [250]; and transaldolase 1 (TALDO1), a metabolic protein [251]. Seven proteins with decreased expression were identified in this comparison. These included Cofilin 2, which is involved in protein binding [252]; basic transcription factor 3 (Btf3), a transcription factor [253]; guanine monophosphate synthetase, which plays a role in biosynthesis [254]; and chaperonin containing TCP1, subunit 3 (gamma) (CCT3), a cytoskeletal protein involved in protein binding [255].

Nine proteins which were increased in the 231-DasB variant cell line in response to dasatinib treatment were identified (Table 6.3) These included adenylyl cylase-associated protein, annexin A1, a tumour suppressor gene involved in proliferation in breast cancer [256]; migration-inducing gene 10 protein, an ATP-generating glycolytic enzyme that forms part of the glycolytic pathway, which is associated with prostate tumour cell proliferation *in vitro* [257]); enolase 1 (ENO1), which has been reported by Ray *et al.* to suppress colony formation in MCF7 breast cancer cells [258]; and GSS, which is a metabolic protein [259]. Proteins which were decreased in response to dasatinib in the variant cell line included guanine monophosphate synthetase and cofilin 2.

Proteins which were altered in the 231-DasB variant cell line compared to MDA-MB-231 parental cell line in the absence (Table 6.4) and/or presence of dasatinib (Table 6.5) were identified. Uniquely altered proteins following dasatinib treatment in the parental cell line included significantly increased expression of IPF53, villin 2, and TALDO2, and decreased Btf3 and CCT3 (Table 6.6). Uniquely altered proteins following dasatinib treatment in the variant cell line included significantly increased expression of adenylyl cyclise-associated protein, annexin A1, migration-inducing gene 10 protein, ENO1, and glutaredoxin 3 (GLXR3) (Table 6.7).

Table 6.2 Differentially regulated proteins in MDA-MB-231 parental cell line – dasatinib treated *vs.* untreated, including MS data (right hand side). A protein score > 40 reflects high confidence of identification. Proteins are listed in order of decreasing fold change observed.

Gel ID	Identified protein	Ratio	ANOVA	Accession no. in NCBI	MW (Da)	p*I*	Protein Score	No. of matched peptides	% Sequence coverage
779	**IFP53**	1.65	0.031	gi|32709	53558	5.93	78	16	31
255	**Villin 2**	1.25	0.013	gi|46249758	69312	5.94	71	13	15
1312	**TALDO1**	1.22	0.0012	gi|16307182	35534	9.07	97	10	25
2259	**Chain F; Cypa Complexed With Hvgpia**	-1.2	0.008	gi|2981764	18097	7.82	273	15	49
2184	**Cofilin 2**	-1.27	0.034	gi|15030332	18839	7.66	80	7	36
2142	**Btf3**	-1.44	0.0066	gi|51593629	17688	6.85	120	7	48

`**Table 6.2** continued

Gel ID	Identified protein	Ratio	ANOVA	Accession no. in NCBI	MW (Da)	p*I*	Protein Score	No. of matched peptides	% Sequence coverage
509	**guanine monophosphate synthetase**	-1.75	0.0031	gi|4504035	77408	6.42	140	20	27
550	**chaperonin containing TCP1; subunit 3 (gamma)**	-1.84	0.0012	gi|31542292	60934	6.1	103	24	38
515	**guanine monophosphate synthetase**	-2.0	0.0026	gi|4504035	77408	6.42	362	35	46

Note: Number of spots increased ≥ 1.2-fold, ANOVA $p < 0.05$: 12; Number of spots decreased ≥ 1.2-fold, ANOVA $p < 0.05$: 59

Table 6.3 Differentially regulated proteins in 231-DasB variant cell line – dasatinib-treated *vs.* untreated, including MS data (right hand side). A protein score > 40 reflects high confidence of identification. Proteins are listed in order of decreasing fold change observed.

Gel ID	Identified protein	Ratio	ANOVA	Accession no. in NCBI	MW (Da)	p*I*	Protein Score	No. of matched peptides	% Sequence covered
869	**adenylyl cyclase-associated protein**	1.29	0.032	gil30583143	51925	8.07	286	18	40
1357	**annexin A1**	1.26	0.007	gil54696696	38918	6.57	510	22	54
1205	**migration-inducing gene 10 protein**	1.24	0.00081	gil41350401	44985	8.3	231	22	55
1082	**ACTB**	1.24	0.021	gil15277503	40536	5.55	329	17	41
1044	**ENO1**	1.23	0.00035	gil29792061	47481	7.01	539	33	63
882	**GSS**	1.22	0.021	gil8248826	52523	5.67	543	29	51
1229	**TXNL2**	1.22	0.0049	gil48257132	32822	5.36	236	17	55

Table 6.3 continued

Gel ID	Identified protein	Ratio	ANOVA	Accession no. in NCBI	MW (Da)	p*I*	Protein Score	No. of matched peptides	% Sequence covered
1670	**chloride intracellular channel 4**	1.22	0.0052	gil55665384	28981	5.45	139	16	70
1303	**phosphoserine aminotransferase**	1.2	0.049	gil25140375	40795	7.56	342	26	55
515	**guanine monophosphate synthetase**	-1.23	0.0026	gil4504035	77408	6.42	362	35	46
509	**guanine monophosphate synthetase**	-1.25	0.0031	gil4504035	77408	6.42	140	20	27
2184	**Cofilin 2**	-1.63	0.034	gil15030332	18839	7.66	80	7	36

Note: Number of spots increased ≥ 1.2-fold, ANOVA $p < 0.05$: 25 Number of spots decreased ≥ 1.2-fold, ANOVA $p < 0.05$: 21

Table 6.4 Differentially regulated proteins in untreated 231-DasB variant relative to the MDA-MB-231 parental cell line, including MS data (right hand side). A protein score > 40 reflects high confidence of identification. Proteins are listed in order of decreasing fold change observed.

Gel ID	Identified protein	Ratio	ANOVA	Accession no. in NCBI	MW (Da)	p*I*	Protein Score	No. of matched peptides	% Sequence covered
941	**RuvB-like protein 1**	1.61	0.0000018	gi|57100857	50538	6.02	163	17	41
509	**guanine monophosphate synthetase**	1.3	0.0031	gi|4504035	77408	6.42	140	20	27
550	**chaperonin containing TCP1; subunit 3 (gamma)**	1.26	0.0012	gi|31542292	60934	6.1	103	24	38
515	**guanine monophosphate synthetase**	1.22	0.0026	gi|4504035	77408	6.42	362	35	46
1099	**ACTB**	-1.21	0.00047	gi|15277503	40536	5.55	264	15	33

Table 6.4 continued

Gel ID	Identified protein	Ratio	ANOVA	Accession no. in NCBI	MW (Da)	p*I*	Protein Score	No. of matched peptides	% Sequence covered
1951	**Proteasome subunit beta type 1**	-1.21	0.013	gil55666609	26700	8.27	357	25	62
805	**pyruvate kinase M2**	-1.21	0.038	gil5702302	6086	5.69	198	4	69
796	**Catalase**	-1.23	0.0028	gil4557014	59946	6.9	212	18	36
1101	**fumarate hydratase**	-1.23	0.0014	gil32880021	54773	8.85	420	21	38
1266	**aspartate transaminase (EC 2.6.1.1)**	-1.24	0.015	gil105387	46334	6.81	169	20	38
1424	**glyceraldehyde-3-phosphate dehydrogenase**	-1.25	0.026	gil32891805	36201	8.57	511	26	51

Table 6.4 continued

Gel ID	Identified protein	Ratio	ANOVA	Accession no. in NCBI	MW (Da)	p*I*	Protein Score	No. of matched peptides	% Sequence covered
1013	**ENO1**	-1.27	0.01	gil29792061	47481	7.01	362	24	47
1541	**capping protein (actin filament)**	-1.28	0.028	gil55586343	31615	5.36	332	22	57
1797	**Phosphoglycerate mutase 1**	-1.29	0.00017	gil56081766	28899	6.67	399	23	70
835	**aldehyde dehydrogenase 1 family; member B1**	-1.3	0.0033	gil30583675	57658	6.36	170	22	37
869	**adenylyl cyclase-associated protein**	-1.32	0.032	gil30583143	51925	8.07	286	18	40
255	**Villin 2**	-1.34	0.013	gil32709	69312	5.94	71	13	15

Table 6.4 continued

Gel ID	Identified protein	Ratio	ANOVA	Accession no. in NCBI	MW (Da)	p*I*	Protein Score	No. of matched peptides	% Sequence covered
1312	**TALDO1**	-1.37	0.0012	gil16307182	35534	9.07	97	10	25
1303	**phosphoserine aminotransferase**	-1.43	0.049	gil25140375	40795	7.56	342	26	55
1095	**ENO1**	-1.47	0.000001	gil29792061	47481	7.01	612	33	70
784	**Chain A; Catalytic Fragment Of Human Tryptophanyl-Trna Synt**	-1.49	0.0088	gil50513261	43586	7.12	191	23	55
1670	**chloride intracellular channel 4**	-1.49	0.0052	gil55665384	28981	5.45	139	16	70

Table 6.4 continued

Gel ID	Identified protein	Ratio	ANOVA	Accession no. in NCBI	MW (Da)	p*I*	Protein Score	No. of matched peptides	% Sequence covered
762	**tyrosyl-tRNA synthetase**	-1.5	0.0076	gil4507947	59448	6.61	85	16	29
945	**Chain F; Structure Of Human Glutamate Dehydrogenase**	-1.57	0.0016	gil20151194	56315	6.71	487	36	50
1096	**C14orf3**	-1.57	0.0000017	gil5262359	38421	5.41	125	11	32
1044	**ENO1**	-1.58	0.00035	gil29792061	47481	7.01	539	33	63
1219	**migration-inducing gene 10 protein**	-1.59	0.0003	gil41350401	44985	8.3	755	36	67

Table 6.4 continued

Gel ID	Identified protein	Ratio	ANOVA	Accession no. in NCBI	MW (Da)	p*I*	Protein Score	No. of matched peptides	% Sequence covered
1205	**migration-inducing gene 10 protein**	-1.62	0.00081	gil41350401	44985	8.3	231	22	55
1053	**ENO1**	-1.71	0.0022	gil29792061	47481	7.01	124	18	41
1357	**annexin A1**	-1.77	0.007	gil54696696	38918	6.57	510	22	54

Note: Number of spots increased ≥ 1.2-fold, ANOVA $p < 0.05$: 48; Number of spots decreased ≥ 1.2-fold, ANOVA $p < 0.05$: 86

Table 6.5 Differentially regulated proteins in dasatinib-treated 231-DasB variant relative to the untreated MDA-MB-231 parental cell line, including MS data (right hand side). A protein score > 40 reflects high confidence of identification. Proteins are listed in order of decreasing fold change observed.

Gel ID	Identified protein	Ratio	ANOVA	Accession no. in NCBI	MW (Da)	p*I*	Protein Score	No. of matched peptides	% Sequence covered
515	**guanine monophosphate synthetase**	1.98	0.0026	gil4504035	77408	6.42	362	35	46
550	**chaperonin containing TCP1; subunit 3 (gamma)**	1.98	0.0012	gil31542292	60934	6.1	103	24	38
941	**RuvB-like protein 1**	1.88	0.0000018	gil57100857	50538	6.02	163	17	41
509	**guanine monophosphate synthetase**	1.81	0.0031	gil4504035	77408	6.42	140	20	27

Table 6.5 continued

Gel ID	Identified protein	Ratio	ANOVA	Accession no. in NCBI	MW (Da)	p*I*	Protein Score	No. of matched peptides	% Sequence covered
962	**GDP dissociation inhibitor 2**	1.38	0.00042	gil30582575	51087	6.11	249	29	57
1229	**GLRX3**	1.33	0.0049	gil48257132	32822	5.36	236	17	55
1280	**ALDOA**	1.25	0.027	gil49456715	39879	8.49	190	17	44
2259	**Chain F; Cypa Complexed With Hvgpia**	1.23	0.008	gil2981764	18097	7.82	273	15	49
1295	**aldolase A**	1.22	0.0066	gil34577112	39851	8.3	728	31	77
2142	**Btf3**	1.21	0.0066	gil51593629	17688	6.85	120	7	48
2017	**prostatic binding protein**	1.2	0.036	gil4505621	21157	7.01	344	15	80

Table 6.5 continued

Gel ID	Identified protein	Ratio	ANOVA	Accession no. in NCBI	MW (Da)	p*I*	Protein Score	No. of matched peptides	% Sequence covered
835	**aldehyde dehydrogenase 1 family; member B1**	-1.23	0.0033	gil30583675	57658	6.36	170	22	37
796	**catalase**	-1.24	0.0011	gil4557014	59946	6.9	212	18	36
1205	**migration-inducing gene 10 protein**	-1.24	0.00081	gil41350401	44985	8.3	231	22	55
762	**tyrosyl-tRNA synthetase**	-1.25	0.0076	gil4507947	59448	6.61	85	16	29
1670	**chloride intracellular channel 4**	-1.29	0.0052	gil55665384	28981	5.45	139	16	70
1044	**ENO1**	-1.32	0.00035	gil29792061	47481	7.01	539	33	63

Table 6.5 continued

Gel ID	Identified protein	Ratio	ANOVA	Accession no. in NCBI	MW (Da)	p*I*	Protein Score	No. of matched peptides	% Sequence covered
1303	**phosphoserine aminotransferase**	-1.33	0.049	gil25140375	40795	7.56	342	26	55
1095	**ENO1**	-1.34	0.000001	gil29792061	47481	7.01	612	33	70
1357	**annexin A1**	-1.36	0.007	gil54696696	38918	6.57	510	22	54
784	**Chain A; Catalytic Fragment Of Human Tryptophanyl-Trna Synt**	-1.37	0.0088	gil50513261	43586	7.12	191	23	55
1053	**ENO1**	-1.38	0.0022	gil29792061	47481	7.01	124	18	41
1312	**TALDO1**	-1.43	0.0012	gil16307182	35534	9.07	97	10	25

Table 6.5 continued

Gel ID	Identified protein	Ratio	ANOVA	Accession no. in NCBI	MW (Da)	p*I*	Protein Score	No. of matched peptides	% Sequence covered
1219	**migration-inducing gene 10 protein**	-1.46	0.0003	gi|41350401	44985	8.3	755	36	67
779	**IFP53**	-1.49	0.031	gi|32709	53558	5.93	78	16	31
2184	**Cofilin 2**	-1.51	0.034	gi|15030332	18839	7.66	80	7	36
945	**Chain F; Structure Of Human Glutamate Dehydrogenase-Apo Form**	-1.52	0.0016	gi|20151194	56315	6.71	487	36	50
255	**Villin 2**	-1.53	0.013	gi|46249758	69312	5.94	71	13	15
1096	**C14orf3**	-1.58	0.0000017	gi|5262359	38421	5.41	125	11	32

Note: Number of spots increased ≥ 1.2-fold, ANOVA $p < 0.05$: 87; Number of spots decreased ≥ 1.2-fold, ANOVA $p < 0.05$: 61

Table 6.6 Uniquely differentially regulated proteins in dasatinib-treated MDA-MB-231 parental cell line, including MS data (right hand side). A protein score > 40 reflects high confidence of identification. Proteins are listed in order of decreasing fold change observed.

Gel ID	Identified protein	Ratio	ANOVA	Accession no. in NCBI	MW (Da)	p*I*	Protein Score	No. of matched peptides	% Sequence covered
779	**IFP53**	1.65	0.031	gi|32709	53558	5.93	78	16	31
255	**Villin 2**	1.25	0.013	gi|46249758	69312	5.94	71	13	15
1312	**TALDO1**	1.22	0.0012	gi|16307182	35534	9.07	97	10	25
2259	**Chain F; Cypa Complexed With Hvgpia**	-1.2	0.008	gi|2981764	18097	7.82	273	15	49
2142	**Btf3**	-1.44	0.0066	gi|51593629	17688	6.85	120	7	48
550	**chaperonin containing TCP1; subunit 3 (gamma)**	-1.84	0.0012	gi|31542292	60934	6.1	103	24	38

Table 6.7 Uniquely differentially regulated proteins in dasatinib-treated 231-DasB variant cell line, including MS data (right hand side). A protein score > 40 reflects high confidence of identification. Proteins are listed in order of decreasing fold change observed.

Gel ID	Identified protein	Ratio	ANOVA	Accession no. in NCBI	MW (Da)	p*I*	Protein Score	No. of matched peptides	% Sequence covered
869	**adenylyl cyclase-associated protein**	1.29	0.032	gil30583143	51925	8.07	286	18	40
1357	**annexin A1**	1.26	0.007	gil54696696	38918	6.57	510	22	54
1205	**migration-inducing gene 10 protein**	1.24	0.00081	gil41350401	44985	8.3	231	22	55
1082	**ACTB**	1.24	0.021	gil15277503	40536	5.55	329	17	41
1044	**ENO1**	1.23	0.00035	gil29792061	47481	7.01	539	33	63
882	**GSS**	1.22	0.021	gil8248826	52523	5.67	543	29	51
1229	**TXNL2**	1.22	0.0049	gil48257132	32822	5.36	236	17	55

Table 6.7 continued

Gel ID	Identified protein	Ratio	ANOVA	Accession no. in NCBI	MW (Da)	p*I*	Protein Score	No. of matched peptides	% Sequence covered
1670	**chloride intracellular channel 4**	1.22	0.0052	gil55665384	28981	5.45	139	16	70
1303	**phosphoserine aminotransferase**	1.2	0.049	gil25140375	40795	5.45	139	16	70

6.3 PHOSPHOPROTEIN ANALYSIS

For further analysis of the MDA-MB-231 and 231-DasB cell lines, analysis of alterations in phosphorylation of proteins was performed using the ProQ Diamond stain technique (Chapter 2.12.3) (Table 6.8). Of note, only a limited number of significantly altered proteins were identified, which may be partly due to using total protein rather than enriched phosphoproteins for the analysis . In addition, this may be due to limitations identified in the ProQ Diamond staining technique. The gels used were non-backed (free-floating gels) which were fragile and prone to breaking. The ProQ Diamond staining itself was variable from gel to gel, which led to difficulties with reproducibility, and reduced the number of significantly altered proteins which were identified. The spots identified were picked manually, so only spots which could be confidently picked were selected.

Table 6.8 List of tables detailing comparisons of proteins used in phosphoproteomic analysis of MDA-MB-231 (parental) and 231-Das (dasatinib-resistant variant) cell lines, in untreated (U) and dasatinib-treated (D).

Comparison	Table	Number of proteins identified by MS
MDA-MB-231 – D *vs.* U	**6.9**	4
231-DasB – D *vs.* U	**6.10**	2
231-DasB U *vs.* MDA-MB-231 U	**6.11**	2

Levels of phosphorylation of four proteins were significantly altered in the parental MDA-MB-231 cell line in response to dasatinib treatment, compared to untreated control cells (Table 6.9). Phosphorylation of HSPA8, a cytosolic member of the Hsp70 chaperone family [260], was decreased 1.6-fold in response to dasatinib. HSPA8 secretion has been associated with cancer cell proliferation [261]. Decreases in phosphorylation of stathmin-1 and ER-60 were also observed. Stathmin is a microtubule regulator protein that has been shown to be involved in cell cycle regulation and apoptosis, and is over-expressed in p53 mutant breast cancer cell lines [262]. ER-60 is a chaperone protein involved in modulation of folding of newly formed glycoproteins [263], and has been shown to be involved in chemoresistance by modulation of microtubules after taxane treatment in ovarian cancer cell lines [264].

Phosphorylation of cofilin 2 was significantly increased by 1.4-fold in response to dasatinib in the parental cell line (Table 6.9). Cofilin proteins have an important role in the regulation of actin filament turnover, although the detailed function of cofilin 2 is unclear [265].

Proteins with significantly increased phosphorylation in the variant-treated compared to the parental-treated MDA-MB-231 cell lines included NM23-H1 and ENO-1 (table 6.10). NM23-H1 has been identified as a tumour metastasis suppressor gene, and has been shown to interact with the MAPK pathway in breast cancer cells [266].

No significantly altered phosphoproteins were identified in variant cell line in response to dasatinib treatment .

IMPDH2 (inosine monophosphate dehydrogenase 2) phosphorylation was significantly decreased in the untreated variant cell line in comparison to the untreated parental cell line (Table 6.11). IMPDH2 codes for IMP dehydrogenase, the rate-limiting enzyme of *de novo* GTP biosynthesis [267]. IMPDH2 expression has been shown to be significantly increased in colorectal tumour tissue compared to normal tissue [268].

Table 6.9 Phosphorylated proteins identified in parental MDA-MB-231 dasatinib-treated relative to untreated control cells, including MS data (right hand side). A protein score > 40 reflects high confidence of identification. Proteins are listed in order of decreasing fold change observed.

Gel spot	Identified protein	ANOVA	Fold difference	Accession no. in NCBI	MW (Da)	p*I*	Protein Score	No. of matched peptides	% Sequence covered
1	**Cofilin 2**	0.0309	1.4	gi|15030332	18839	7.66	92	2	6
4	**ER-60**	0.0331	-1.2	gi|2245365	57147	5.88	319	20	28
3	**Stathmin-1**	0.0431	-1.5	gi|57528035	17292	5.76	174	6	18
17	**Heat shock 70 kDa protein 8 isoform 2**	0.000893	-1.6	gi|24234686	53598	5.62	297	20	33

Table 6.10 Phosphorylated proteins identified in 231-DasB dasatinib-treated compared to MDA-MB-231 dasatinib-treated, including MS data (right hand side). A protein score > 40 reflects high confidence of identification. Proteins are listed in order of decreasing fold change observed.

Gel spot	Identified protein	ANOVA	Fold difference	Accession no. in NCBI	MW (Da)	p*I*	Protein Score	No. of matched peptides	% Sequence covered
2	**NM23-H1**	0.0392	1.8	gi|29468184	19869	5.42	175	8	27
8	**ENO-1**	0.0463	1.6	gi|29792061	47481	7.01	340	24	47

Table 6.11 Phosphorylated proteins identified in variant 231-DasB untreated cells compared to parental MDA-MB-231 untreated cells, including MS data (right hand side). A protein score > 40 reflects high confidence of identification. Proteins are listed in order of decreasing fold change observed.

Gel spot	Rank	Identified protein	ANOVA	Fold difference	Accession no. in NCBI	MW (Da)	p*I*	Protein Score	No. of matched peptides	% Sequence covered
15	110	**tubulin, alpha-1 chain**	0.0149	1.4	gil2119266	50804	4.94	372	21	34
28	82	**IMP (inosine monophosphate) dehydrogenase 2**	0.044	-1.6	gil13543973	56226	6.44	587	26	35

6.3 PRELIMINARY VALIDATION OF TARGETS IDENTIFIED BY PROTEOMIC ANALYSIS OF DASATINIB RESISTANT CELLS

6.3.1 ANNEXIN A1 (ANXA1)

ANXA1 is a member of the Ca2(+)-dependent phospholipid binding proteins, and has a molecular weight 40 kDa [269]. ANXA1 expression has been shown to increase cell proliferation, decrease apoptosis, and alter the cell cycle in transfected pancreatic cells [270]. In breast cancer, a microarray study by Cao *et al.* suggested most tumours which express ANXA1 are triple negative [271]. In a series of 21 breast carcinomas from the same study, where single tumour sections contained benign, *in situ*, and invasive tissue, the loss of ANXA1 expression was found to be an early event. This suggests a role for ANXA1 in early malignant transformation. Ang *et al.* reported an antiproliferative role for ANXA1 in MCF7 breast cancer cell lines [256]. These data suggest a potentially important role for ANXA1 in breast carcinogenesis and progression. Interestingly, Konecny *et al.* have reported that increased dasatinib sensitivity in ovarian cancer cell lines was associated with increased ANXA1 levels [272]. ANXA1 was selected as a target of interest for validation and further assessment from the proteomic analysis.

Based on the proteomic analysis, ANXA1 expression was decreased 1.77-fold in the 231-Das variant cell line in comparison to the MDA-MB-231 parental cell line (Figure 6.7, Table 6.5). No significant change in ANXA1 expression was observed in the parental cell line in response to dasatinib treatment. However ANXA1 was increased 1.26-fold in the variant cell line in response to dasatinib (Figure 6.7, Table 6.3). These trends were partly validated by semi-quantitative western blot analysis and densitometry (Figure 6.8). There was a significant 2.31-fold decrease in ANXA1 expression in the variant compared to the parental cell line ($p = 0.001$). ANXA1 expression was not significantly increased (1.12-fold, $p = 0.5919$) in the parental cells treated with dasatinib. No significant change was observed in the dasatinib-treated variant cells in comparison to untreated variant cells.

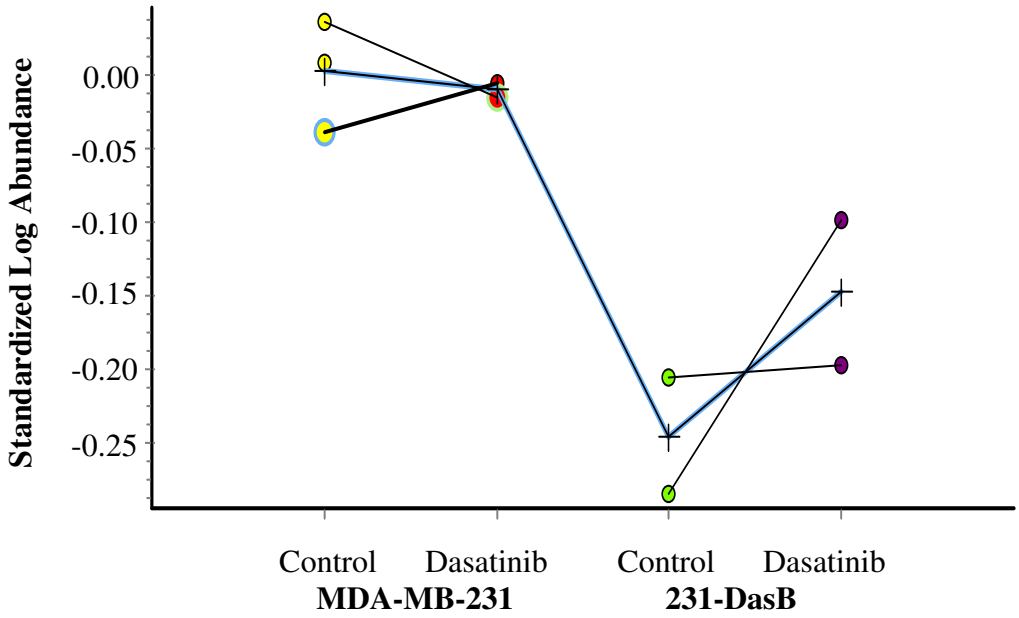

Figure 6.7 Relative protein expression of ANXA1 in proteomic analysis (ID 1357). Expression was detected in triplicate samples, using 2D-DIGE. Black lines indicate the trend for individual pairs of samples, and the averages are represented by the blue lines.

A

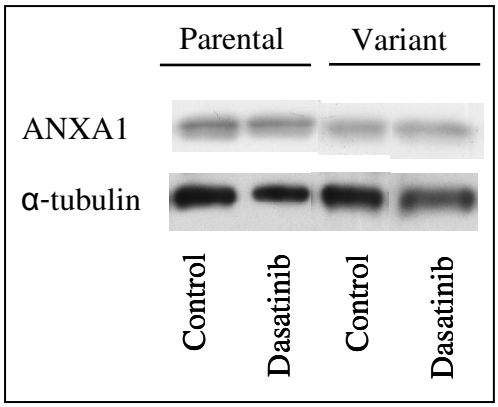

B

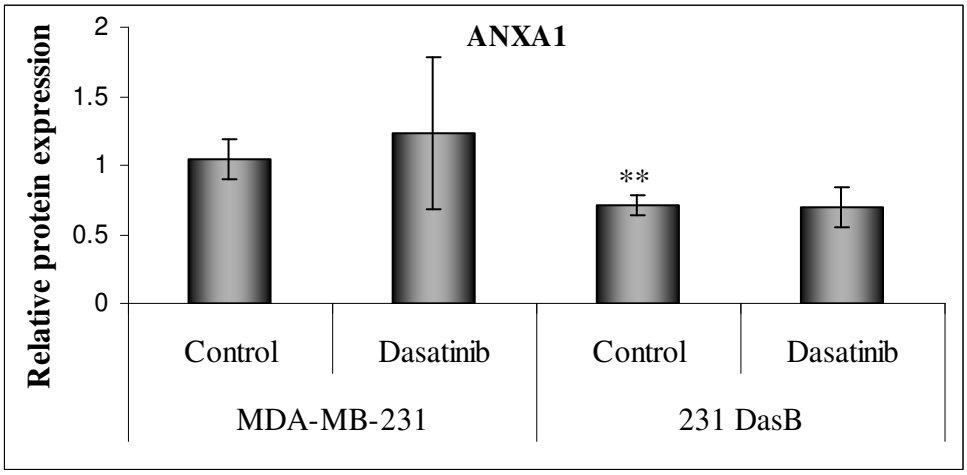

Figure 6.8 Relative protein expression of ANXA1 by western blot, comparing untreated (control) and dasatinib treated MDA-MB-231 parental and dasatinib-resistant variant cells (231 DasB). **A.** ANXA1 and α-tubulin, detected by immunoblot. This image is representative of triplicate blots. **B.** ANXA1 densitometry readings, measured relative to α-tubulin for each sample (± the standard deviation of triplicate samples).

The aim of the proteomic analysis of the MDA-MB-231 parental and dasatinib-resistant cell lines was to identify potential markers of response or resistance to dasatinib. Our proteomic data suggest that decreased ANXA1 expression may contribute to dasatinib resistance.

We examined the effects of decreased ANXA1 expression in MDA-MB-231 using pooled ANXA1 siRNA (described in Chapter 2.12). Scrambled siRNA was used as a negative control. Kinesin siRNA was used as a positive control. The average decrease in ANXA1 expression by ANXA siRNA, as measured semi-quantitatively by western blot was 21.5 ± 12.5 % compared to untreated control cells (Figure 6.9A). ANXA1 siRNA significantly decreased proliferation in comparison to the NeoFX control ($p = 0.0098$). There was also a significant decrease in proliferation with ANXA1 siRNA combined with dasatinib in comparison to ANXA1 knockdown alone ($p = 0.0129$; Figure 6.9B). However, ANXA1 siRNA combined with dasatinib did not decrease proliferation more than dasatinib with scrambled siRNA ($p = 0.1000$). The siRNA experiments suggest that ANXA1 increases response to dasatinib, although not significantly compared to the combination of dasatinib with scrambled siRNA. These results suggest that decreasing ANXA1 levels alone is not sufficient to induce resistance to dasatinib.

A

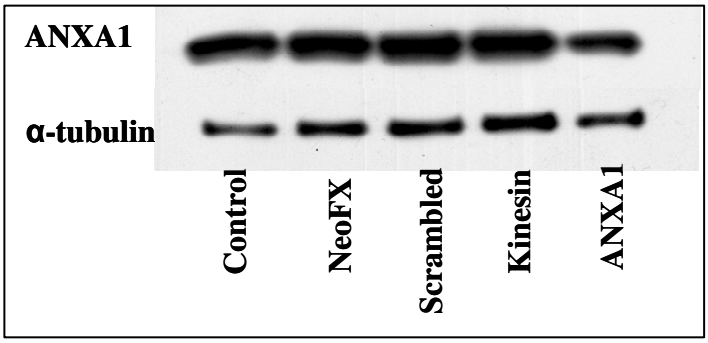

B

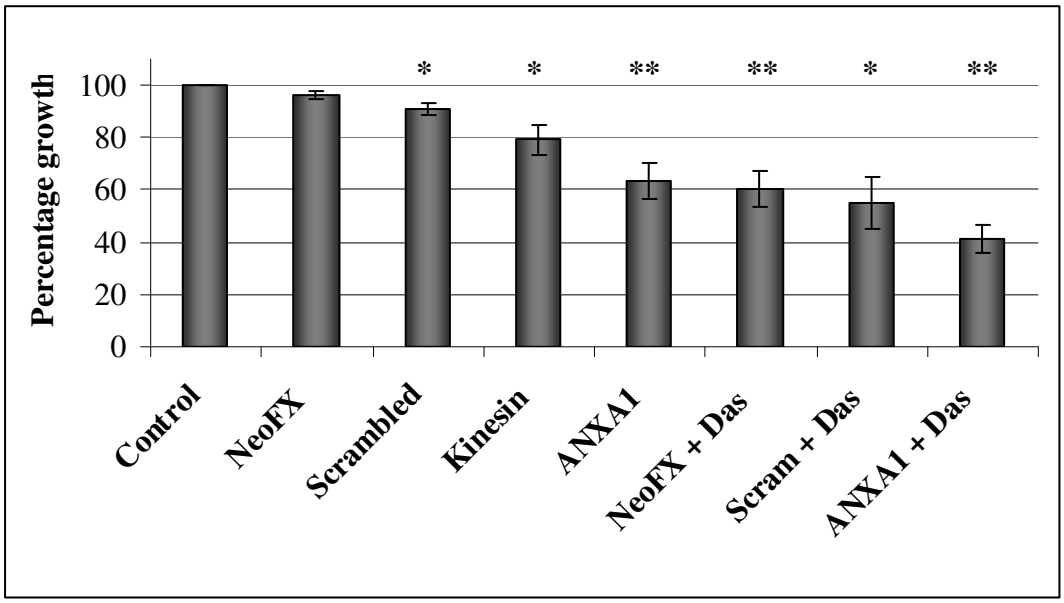

Figure 6.9 Examination of effect of ANXA1 knockdown by siRNA on proliferation in MDA-MB-231 breast cancer cell line. **A.** Representative western blot of ANXA1 protein levels in experiment in Figure 6.9B, to confirm decreased ANXA1 expression in cells treated with ANXA1 siRNA. This blot is representative of triplicate blots. **B**. Proliferation (± the standard deviation of triplicate samples) in MDA-MB-231 cells, including control (untreated), NeoFX (transfection agent), scrambled siRNA (Scram, negative control), kinesin (positive control), ANXA1 siRNA, and dasatinib (Das) combinations. Significant values in comparison to NeoFX are marked.

6.3.2 CHAPERONIN CONTAINING TCP1, SUBUNIT 3 GAMMA (CCT3)

CCT3 is part of the molecular chaperone hetero-oligomeric ring complex TCP1, that plays an important role in folding of actin and tubulin [273], and is inducible by heat shock [274]. CCT3 plays a role in dedifferentiation in hepatocellular carcinomas [275], and is upregulated in this disease [276]. Elevated CCT3 gene expression has also been demonstrated in ovarian carcinoma [277], and late stage colorectal carcinoma [278], although its role in these diseases is unclear. There is no reported involvement of CCT3 in breast carcinogenesis.

The proteomic analysis of CCT3 (ID 550) in the parental and variant cell lines, untreated and dasatinib-treated is shown in Figure 6.10. CCT3 expression was significantly decreased 1.84-fold following dasatinib treatment in the parental MDA-MB-231 cell line (Table 6.2). The level of CCT3 expression was also significantly higher in the dasatinib-resistant variant compared to the parental cell line (untreated: 1.26-fold, Table 6.4; dasatinib treated: 1.98-fold, Table 6.5). CCT3 was one of the proteins which was identified as uniquely altered in the parental cell line in response to dasatinib, in comparison to the variant cell line (Table 6.6).

Semi-quantitative measurement of CCT3 protein expression in the parental and variant cell lines was performed by immunoblot (Figure 6.11). In contrast to the proteomic analysis, no significant difference in CCT3 levels were observed in the parental cell line response to dasatinib (1.3 ± 0.9-fold increase, $p = 0.613$). No significant differences in CCT3 expression were observed between the parental and variant cell lines.

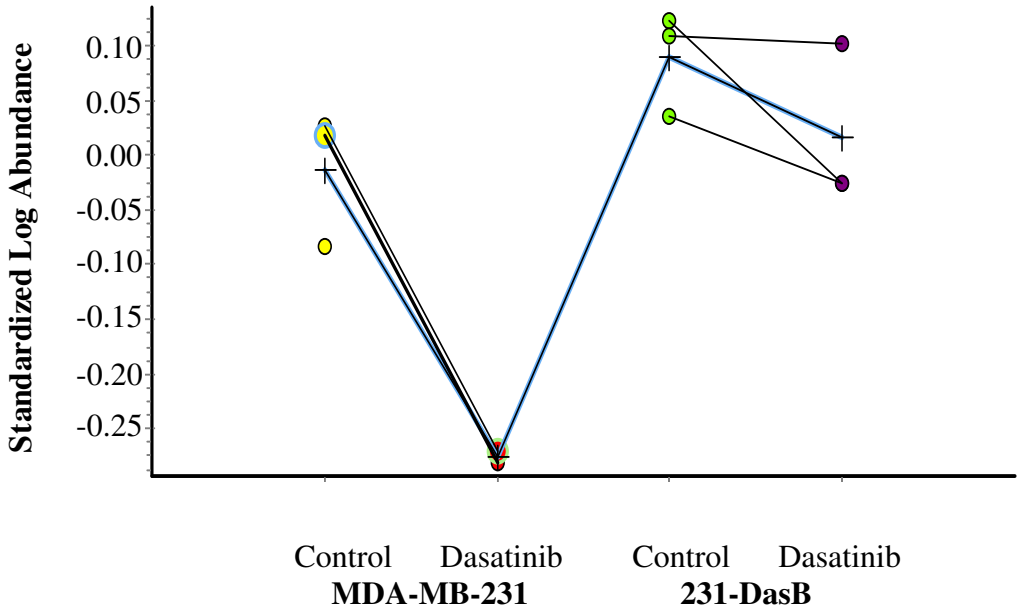

Figure 6.10 Relative protein expression of CCT3 in proteomic analysis (ID 550). Expression was detected in triplicate samples, using 2D-DIGE. Black lines indicate the trend for individual pairs of samples, and the averages are represented by the blue lines.

A

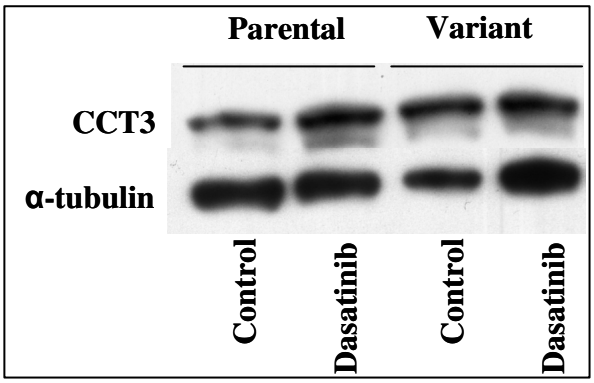

B

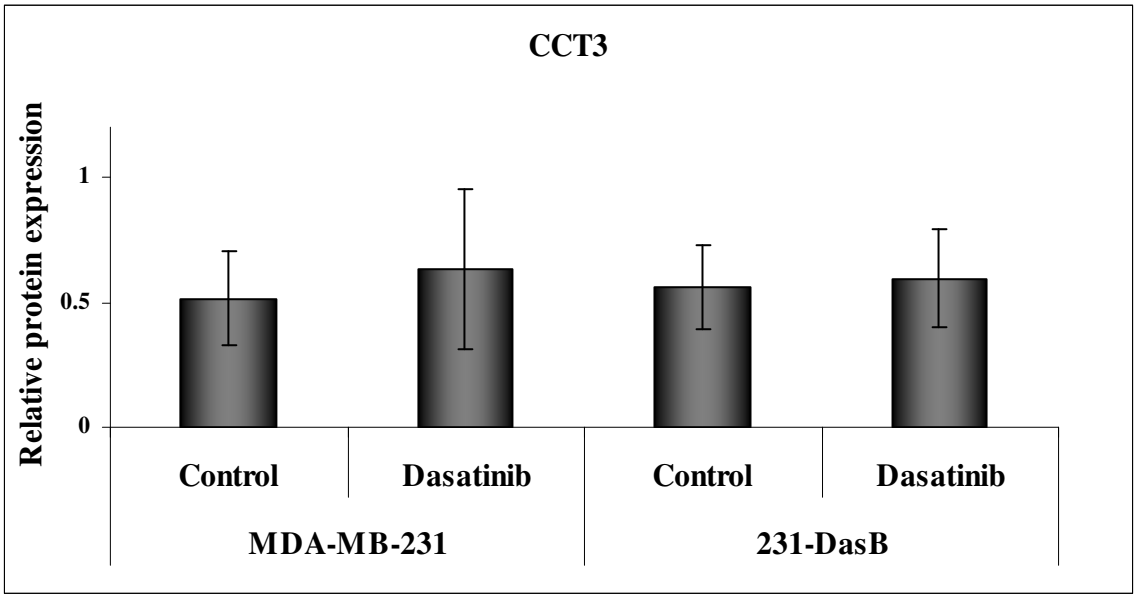

Figure 6.11 Relative protein expression of CCT3 by western blot, comparing untreated (control) and dasatinib treated MDA-MB-231 parental and dasatinib-resistant variant cells (231 DasB). **A.** Representative images of CCT3 and α-tubulin, detected by immunoblot. This image is representative of triplicate blots. **B.** CCT3 densitometry readings, measured relative to α-tubulin for each sample (± the standard deviation of triplicate experiments).

6.3.3 ENOLASE 1 (ENO1)

ENO1 is a negative regulator of the c-myc oncogene [279]. ENO1 reduces invasiveness in transfected breast cancer *in vitro*, and has been reported to suppresses tumour formation in murine models [279]. ENO1 transfection induces cell death in neuroblastoma cells [280]. ENO1 has also been proposed as one of the central gene 'hubs' involved in colon carcinogenesis [281].

The proteomic analysis of ENO1 (ID 1053) in the parental and variant cell lines, untreated and dasatinib-treated is shown in Figure 6.12. A significant 1.71-fold decrease in ENO1 expression was observed in the untreated variant cell line in comparison to the untreated parental cell line (Table 6.4). A significant 1.38-fold decrease was observed in the dasatinib-treated variant cell line in comparison to the untreated parental cell line (Table 6.5). A number of isoforms of ENO1 with altered expression were identified by proteomic analysis (gel ID 1013, 1044, 1053, and 1095). The isoform at gel ID 1044 was found to uniquely and significantly increased 1.23-fold in the dasatinib treated variant cells (Table 6.7). Based on the Pro Q-Diamond phosphorylation analysis, a significant increase in phosphorylation of ENO1 was observed in the dasatinib-treated variant cell line in comparison to the dasatinib treated parental cell line (1.6-fold, Table 6.10).

Semi-quantitative measurement of ENO1 protein expression in the parental and variant cell lines was performed by immunoblot (Figure 6.13). In contrast to the proteomic analysis, similar levels of ENO1 expression were measured in the untreated parental and variant cell lines. There was no significant altered expression of ENO1 either parental or variant cell line in response to dasatinib (parental: 1.5 ± 0.6-fold increase, $p = 0.1660$; variant: 1.2 ± 0.17-fold increase, $p = 0.115$).

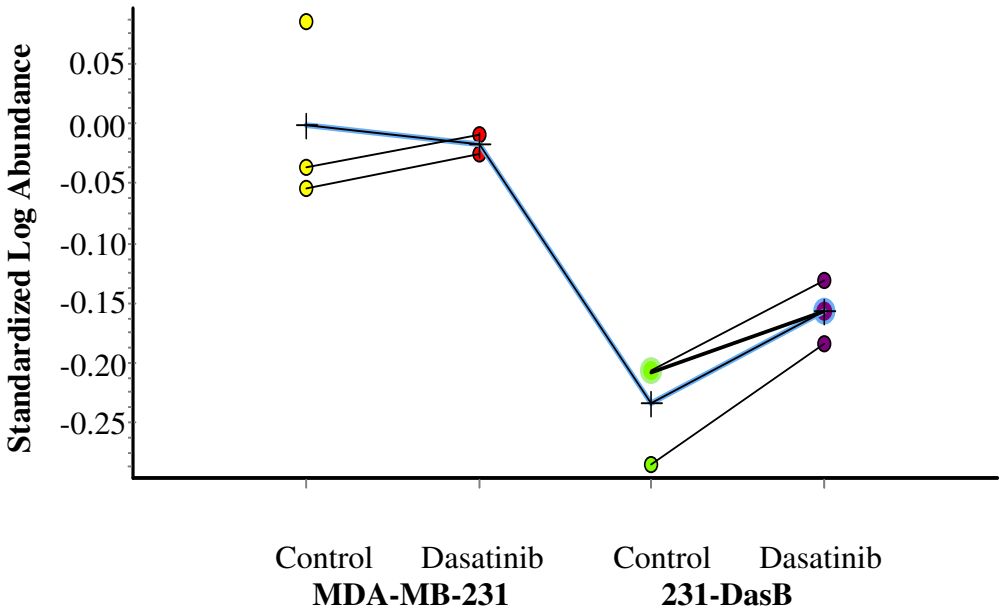

Figure 6.12 Relative protein expression of ENO1 in proteomic analysis (ID 1053). Expression was detected in triplicate samples, using 2D-DIGE. Black lines indicate the trend for individual pairs of samples, and the averages are represented by the blue lines.

A

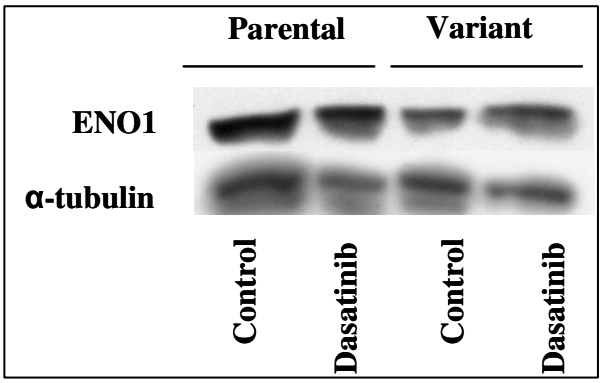

B

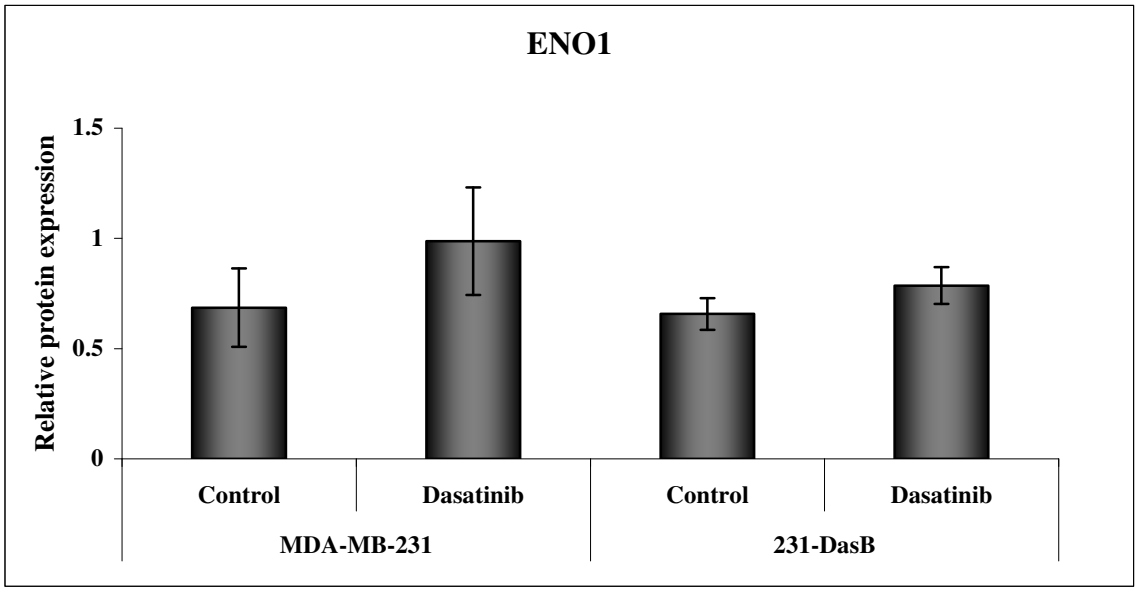

Figure 6.13 Relative protein expression of ENO1 by western blot, comparing untreated (control) and dasatinib treated MDA-MB-231 parental and dasatinib-resistant variant cells (231 DasB). **A.** Representative images of ENO1 and α-tubulin, detected by immunoblot. This image is representative of triplicate blots. **B.** ENO1 densitometry readings, measured relative to α-tubulin for each sample (± the standard deviation of triplicate experiments).

6.4 SUMMARY

Proteomic and phosphoproteomic analyses were performed on a dasatinib-sensitive triple negative breast cancer cell lines, MDA-MB-231, and a dasatinib resistant variant of this cell line, 231-DasB. We studied alterations in protein levels in both untreated and dasatinib-treated conditions to identify potential protein involved in dasatinib response and resistance.

Using 2D DIGE, 78 significantly altered proteins were identified. Nine proteins were altered in MDA-MB-231 in response to dasatinib, and 12 proteins were significantly altered in response to dasatinib in 231-DasB. We identified 6 proteins which were uniquely altered in MDA-MB-231 in response to dasatinib, and 9 proteins which were uniquely altered in 231-DasB in response to dasatinib.

Phosphoprotein staining of total protein was also performed using ProQ Diamond stain. There were a number of technical limitations with this technique, and the experiment yielded a limited number of significantly altered proteins.

ANXA1 was identified as a protein uniquely altered in 231-DasB in response to dasatinib (1.26-fold increase). It has previously been associated with breast cancer carcinogenesis and proliferation [256, 271], and has been associated with dasatinib sensitivity in ovarian cancer cell lines [272]. ANXA1 siRNA significantly decreased proliferation in comparison to the NeoFX control ($p = 0.0098$). siRNA knockdown of ANXA1 combined with dasatinib resulted in a significant decrease in proliferation in MDA-MB-231 compared to siRNA alone ($p = 0.0129$). However this decrease was not significant when compared to scrambled siRNA combined with dasatinib ($p = 0.1000$). The siRNA experiments suggest that ANXA1 increases response to dasatinib, although not significantly compared to the combination of dasatinib with scrambled siRNA. These results suggest that decreasing ANXA1 alone does not induce resistance to dasatinib.

Preliminary analysis of other significantly altered proteins in this model, CCT3 and ENO1, was performed. A number of isoforms of ENO1 were identified by proteomic

analysis. Semi-quantitative examination of expression of CCT3 and ENO1 did not show any significant alterations by immunoblot, which was not consistent with the results obtained from the proteomic analysis.

Chapter 7

DISCUSSION AND CONCLUSIONS

7.1 EGFR AS A THERAPEUTIC TARGET IN TRIPLE NEGATIVE BREAST CANCER

The results of our studies in triple negative breast cancer cell lines confirm the observation that EGFR is over-expressed in TNBC [11, 12, 14, 15]. The lack of a proven targeted therapy for TNBC, together with the availability of a number of approved EGFR inhibitors, provides a powerful rationale for the study of these agents, alone and in combination with chemotherapy, in TNBC. While these data confirm the activity of the EGFR inhibitor gefitinib in TNBC cell lines, we found higher activity for this agent in HER-2 positive breast cancer cell lines, despite the fact that these cells had lower levels of EGFR. Cetuximab showed no inhibition of growth of the TNBC cell lines tested in this study. Lack of efficacy of cetuximab in breast cancer cells *in vitro* has been reported previously [194]. However, Hoadley *et al.* [194] identified a basal-like breast cancer cell line (SUM102) which displayed sensitivity to both cetuximab and gefitinib *in vitro*. The SUM102 cell line has previously been shown to be dependent on EGFR for growth [282]. This suggests that cells which are addicted to the EGFR pathway are more likely to be sensitive to EGFR inhibitors such as gefitinib. As such, activation of EGFR may be an important predictor of response to EGFR inhibitors, including gefitinib.

In the TNBC cell lines studied, significant levels of phosphorylated EGFR were only detected in BT20 cells. Very low levels of phosphorylated EGFR were detected in MDA-MB-231 and HCC1937 cells, by immuno-blotting. This suggests that despite high levels of EGFR protein in TNBC cells, they may not be dependent on EGFR signalling for growth and this may explain their relative resistance to EGFR inhibition, compared to the HER-2 positive cell lines, at least *in vitro*. Although basal levels of phosphorylated EGFR in TNBC cells were low, EGF treatment induces significant phosphorylation of EGFR and gefitinib efficiently blocks the phosphorylation of EGFR in EGF-treated TNBC cells. Therefore, EGFR is capable of activation in these TNBC cell lines, and gefitinib can inhibit this activation. Measurement of the phosphorylation status of EGFR in triple negative tumours may help to clarify if triple negative breast cancers are dependent on EGFR signalling, and potentially sensitive to EGFR inhibitors.

Phosphorylation of both MAPK and Akt were reduced in the gefitinib-sensitive, HER-2 over-expressing BT474 and SKBR3 cell lines in response to gefitinib. HCC1937 cells, which show the greatest sensitivity to gefitinib, also showed reduced phosphorylation of both MAPK and Akt. In BT20 cells a decrease in phosphorylation of MAPK was observed with no change in phosphorylated Akt. No changes in either MAPK or Akt phosphorylation were observed in MDA-MB-231 cells. Moasser *et al.* found that gefitinib did not decrease levels of Akt phosphorylation in the TNBC MDA-MB-468 cell line [283]. Piechocki *et al.* [284] developed a breast cancer cell line (Bam1a) which over-expressed HER-2 and HER-3, and demonstrated sensitivity to gefitinib. The authors showed that gefitinib decreased phosphorylation of HER-3, EGFR and HER-2 in these cells. Gefitinib decreased MAPK and Akt phosphorylation *in vitro* and *in vivo* in a mouse model. This suggests that response to EGFR inhibition requires efficient blockade of both MAPK and Akt signalling. Consequently, combined analysis of P-MAPK and P-Akt may provide biomarkers of response to gefitinib.

Triple negative breast cancer cell lines can also be divided into basal-like and post-epithelial mesenchymal transition (EMT), or into basal-A and basal-B [28, 138, 285]. The BT-20 and HCC1937 cells are classified as basal-like or basal-A while the MDA-MB-231 cells which show greatest resistance to gefitinib are classified as post-EMT or basal-B. EMT has been implicated in resistance to EGFR inhibition in lung cancer [286, 287] and may contribute to the gefitinib resistance observed in the MDA-MB-231 cells.

Gefitinib induces G1 phase cell cycle arrest in the HER-2 positive cell lines BT474 and SKBR3. Gefitinib has been shown previously to induce cell cycle arrest in HER-2 over-expressing lung cancer [288] and breast cancer cell lines [284, 289]. In contrast, gefitinib does not consistently cause G1 cell cycle arrest in the TNBC cell lines.

Krol *et al.* [289] reported that gefitinib targets the transcription factor FOXO3a to mediate cell cycle arrest and cell death in sensitive cell lines (including SKBR3 and BT474), and is associated with de-phosphorylation of FOXO3a at Akt sites and nuclear translocation. In contrast, in resistant breast cancer cell lines, including MDA-

MB-231, FOXO3a remained phosphorylated and in the cytoplasm. This suggests that FOXO3a is an important target in determining sensitivity to gefitinib. Interestingly, FOXO3a has been implicated in sensitivity to the tyrosine kinase inhibitor lapatinib, which inhibits EGFR and HER-2. Lapatinib treatment increased gene expression of FOXO3a in two sensitive breast cancer cell lines BT474 and SKBR3 [290]. In addition, gene expression analysis of a phase III trial with lapatinib and capecitabine suggested that elevated baseline mRNA FOXO3a levels correlated with response [291].

Although the TNBC cells are not inherently sensitive to EGFR inhibition, combined treatment with gefitinib and chemotherapy has a greater effect on proliferation than either gefitinib or the chemotherapy alone. A fixed concentration of gefitinib combined with single chemotherapy drugs showed significantly enhanced activity compared to each drug alone. Takabatake *et al.* [132] previously tested the combination of gefitinib and docetaxel in MDA-MB-231 cells, and observed an additive effect, although there was evidence of antagonism at the highest concentrations used (30 μM gefitinib and 90 nM docetaxel) which were higher than in our assays. As discussed below, tumour concentrations of gefitinib up to approximately 16 μM have been observed *in vivo* [292].

It has been hypothesised that the sequence of administration of EGFR inhibitors with chemotherapy may be important for optimising the cytotoxic effects of treatment. It has been suggested that cells may activate EGFR in response to cytotoxic or radiation-induced damage as a survival mechanism [191, 293]. Morelli *et al.* [191] observed that pre-treatment with EGFR inhibitors, including gefitinib, prior to taxane or platinum chemotherapy drugs in KYSE30 cells (an oesophageal epithelial cell line) resulted in an antagonistic interaction. In contrast, pre-treatment with the chemotherapy before the EGFR inhibitor lead to a synergistic inhibition of proliferation. This was associated with an increase in apoptosis and G2/M phase arrest. In the triple-negative MDA-MB-468 cell line, which is not BRCA1 mutated, treatment with either cetuximab or cisplatin has been shown to increase BRCA1 expression and increase apoptosis [110]. However co-administration of both cetuximab and cisplatin resulted in cetuximab antagonising the ability of cisplatin to upregulate BRCA1. However, alternate

scheduling of gefitinib with carboplatin or docetaxel did not alter response in the TNBC cells we tested.

Using combination indices we have shown that the triple combination of gefitinib with platinum drugs (carboplatin or cisplatin) and docetaxel may be synergistic in the TNBC cells. The assays achieved mildly synergistic combination index values at the ED_{50} drug concentrations, but these CI values were not observed throughout the assay, and may be antagonistic at lower concentrations. In order to determine whether there is true synergy with this combination, *in vivo* assessment would be beneficial. This potential positive interaction may be partly due to interaction between gefitinib and the individual chemotherapy drugs. However, the dual combination of carboplatin and docetaxel appears to be antagonistic in BT20 and HCC1937 cells while the addition of gefitinib results in synergy. Similarly, the combination of cisplatin and docetaxel in BT20 is antagonistic, while the addition of gefitinib is synergistic. Hoadley *et al.* also showed that combinations of cetuximab or gefitinib with chemotherapy were synergistic in the basal-like breast cancer cell line SUM102 [194].

Similar interactions between gefitinib and chemotherapy have been observed in the HER-2 positive SKBR3 and BT474 cells lines [294]. Pegram *et al.* [295] also showed that the triple combination of trastuzumab, carboplatin and docetaxel was highly synergistic in HER-2 positive breast cancer cells and this combination has shown efficacy in the treatment of early stage HER-2 positive breast cancer [296].

Combined induction of G2/M and G1 arrest observed for treatment with gefitinib, carboplatin and docetaxel may, at least in part, explain the synergy observed with the triple combination in the TNBC cell lines. An increase in the sub-G0/G1 fraction was also observed with the chemotherapy combination and the triple combination, suggesting an increase in apoptosis.

Despite their relative resistance to gefitinib, these data show that combination of gefitinib with platinum drugs and docetaxel improves response in the TNBC cell lines. Although the concentrations of gefitinib used in these *in vitro* assays are high, evidence from the BCIRG103 study suggests that a preferential distribution of gefitinib from blood into tumour tissue occurs *in vivo* [292]. Following treatment of

breast cancer patients with oral gefitinib (250 mg/d for at least 14 days, n=19) gefitinib concentrations in breast tumour tissue (mean = 16.7 μM) were 42 times higher than plasma concentrations.

Previous single agent clinical trials in breast cancer with EGFR inhibitors, in general, have been disappointing. However, these have often been in heavily pre-treated, and unselected patient populations [188, 297]. Our results showed cetuximab had little activity in the TNBC cell lines tested. However, one might expect additional activity for this agent *in vivo* through antibody-dependent cellular cytotoxicity which is a known mechanism of action of cetuximab [298]. In addition, there is emerging evidence for the use of platinum-based chemotherapy regimens in both early and advanced triple negative breast cancer [299, 300]. However, preliminary analysis of a Phase II randomised trial of cetuximab and carboplatin compared to cetuximab alone in metastatic TNBC has not shown a significant benefit for the addition of cetuximab. [301]. There was a 10 % clinical benefit for cetuximab alone *versus* 27 % for cetuximab combined with carboplatin. While cetuximab was well tolerated, it appears to have low clinical activity in metastatic triple negative breast cancer. Interestingly, the chemotherapy doublet of carboplatin and docetaxel has shown activity in neoadjuvant TNBC [300]. At present, there are no clinical trials with gefitinib in TNBC. Our data suggest that the triple combination of gefitinib with docetaxel and platinum drugs is a rational combination that may provide additional benefit in TNBC patients, and warrants further investigation.

7.2 EGFR AND P-EGFR IN BREAST TUMOURS

Analysis of EGFR expression and levels of phosphorylation was performed in a group of 101 unselected breast cancer patient tumours. These are the first data in relation to EGFR expression in an Irish breast cancer population. These patients form a group of predominantly older patients with high grade, lymph node positive tumours. The 15.8 % frequency of triple negative breast cancers correlates well with reported incidence of this phenotype of approximately 15 % [302, 303]. EGFR expression was detected in 11.0 % of the breast tumours and P-EGFR was detected in 9.0 % of the samples.

The frequency of EGFR expression in this study is low in the context of the wide variation in EGFR positivity reported in the literature (range 14 – 91 %) [91, 237] . Eralp *et al.* reported a 13.8 % (15/109) rate of expression of EGFR in a series of 109 triple negative breast cancers [116]. Magkou *et al.* reported 11.3 % positivity for EGFR expression in a series of 154 breast carcinomas [237]. We used a standardised automated kit (PharmDx, DAKO) for detection of EGFR. One potential explanation for the relatively low frequency of expression of EGFR in our cohort is the small number of patients included in the study. The frequency of EGFR expression in the triple-negative subgroup was higher (31.5 %), where levels of expression in TNBC ranging from 27 % to 72 % has been reported [12, 94]. The correlation between EGFR positivity and the triple negative phenotype was statistically significant ($p < 0.0010$) when adjusted for multiple testing), confirming the observation that EGFR over-expression is a characteristic feature of this subgroup [15, 94, 304, 305]. Levels of EGFR expression were inversely correlated with ER ($p = 0.0309$), and PR ($p = 0.0341$) status, but were not statistically significant when adjusted for multiple testing. EGFR expression was not significantly associated with HER-2 overexpression.

There was a statistically significant correlation between EGFR expression and axillary lymph node negativity of the breast tumours studied, when analysed by level of EGFR expression ($p = 0.0144$ adjusted for multiple testing). Our observation is in contrast to a study by Liu *et al.* of 200 primary breast tumours which reported increased levels of EGFR expression in primary breast cancer tumours with lymph node metastases [306]. The number of positive tumours identified in our study was relatively low, and an increased tumour cohort may clarify whether our observation is truly significant. Lymph node positivity in breast cancer is well recognised as an important prognostic factor [307], and there is a direct correlation between the number of involved axillary lymph nodes and the risk of distant recurrence [308]. Clarifying the relationship between EGFR expression and lymph node status would be important for determining its importance in relation to the aggressive of triple negative tumours.

Low levels of P-EGFR were detected in the breast tumours in our study (9.0 %). No significant correlations were clinicopathological characteristics were observed. In contrast to our study , Magkou *et al.* detected P-EGFR protein in 35.7 % (55/154) of their breast tumours tested [237]. Their patient cohort had similar clinicopathological

characteristics, and the same antibody was used for detecting the P-EGFR antigen. One potential difference is that our tumour sections were tested as tissue microarrays (TMAs) whereas Magkou *et al.* tested on whole tissue sections. It was noted during the optimisation of our conditions that P-EGFR staining on whole tissue sections which had high levels of EGFR, that immunostaining for P-EGFR was heterogeneous regardless of the antibody dilution tested. This suggests that the low rate of positivity for P-EGFR in our tumour sections may be related to sampling variations when the TMAs were constructed.

Focal expression of proteins in breast tumours has been identified as an important technical issue. For example, Van de Rijn *et al.* examined basal cytokeratin expression in 564 breast tumours [26]. By immunohistochemical analysis in paraffin-embedded tissue, where cytokeratins 5/6 and 17 were present, the expression was focal, with often less than 10% of tumour cells staining. Over 600 patient samples were available, and tissue microarrays were made using central and peripheral tumour areas to maximise the possibility of detecting focal cytokeratin expression. A number of microarray sections to be examined were either lost or had no convincing evidence of invasive tumour, resulting in different numbers of tumours available for each protein in the study. 532 breast tumours for CK17, 535 tumours for CK5/6, and 564 tumours for either CK5/6 or CK 17, were ultimately assessed. Consideration of the use of paraffin-embedded tissue samples or tissue microarrays is likely to be important for examination of protein expression in breast tumours.

The frequency of expression of EGFR in TNBC has potential implications for the use of EGFR inhibitors in TNBC, as patients with EGFR positive TNBC are most likely to benefit from gefitinib treatment. Our data suggest that EGFR is significantly over-expressed in the TNBC phenotype in an Irish population. EGFR assessment in the clinical setting is likely to be important in predicting response to EGFR inhibitors and in realising the full potential of EGFR targeted therapies for TNBC. P-EGFR may also be important in predicting response to EGFR targeted therapies, but further work, on full tumour sections, would be required to determine its potential as a predictive biomarker of response to EGFR inhibition,

7.3 DASATINIB IN TNBC

In addition to EGFR inhibition, other rational targets for therapy in TNBC are being sought. A number of these are in clinical trials in breast cancer or TNBC. One of the most advanced agents is dasatinib. Dasatinib is an orally active small molecule multi-target kinase inhibitor with targets including Src, Abl, c-kit, PDGFR and ephrin A receptor kinases [203] . Finn *et al.* showed that triple negative and post-EMT breast cancer cell lines were more sensitive to dasatinib than luminal or HER-2 positive breast cancer cell lines [138]. Using the criterion of greater than 60 % inhibition at 1 μM dasatinib as being a highly sensitive cell line (as concentrations greater than 1 μM are unlikely to be achieved *in vivo* [138]), the authors showed that triple negative and post-EMT breast cancer cell lines were most sensitive to dasatinib. Huang *et al.* developed a 6 gene model for predicting response to dasatinib, and found a significantly higher likelihood of response in triple negative breast cancer cell lines in comparison to other subtypes [204]. These data are encouraging for dasatinib as a potential therapeutic option in TNBC.

Of the TNBC cell lines tested, MDA-MB-231, which is a post-EMT or mesenchymal cell line, showed the greatest sensitivity to dasatinib. We developed a model of acquired resistance to dasatinib by continuous exposure to the drug. There are currently no models of acquired resistance to dasatinib in breast cancer reported in the literature.

It has been reported that dasatinib is a substrate for the drug efflux pumps BCRP and MDR-1 [239]. No significant differences in drug accumulation were observed in either parental or variant cell lines. Furthermore, no significant difference in proliferation was observed when each cell line was treated with dasatinib with or without the BCRP/MDR-1 inhibitor elacridar. These data suggest that BCRP and MDR-1 pump efflux mechanisms do not contribute significantly to dasatinib resistance in this model.

We examined key signalling proteins by immunoblot with dasatinib treatment in the parental and variant cell lines to determine potential markers of resistance to dasatinib. Src is one of the principal targets of dasatinib, which also targets bcr-abl, PDGFR, and ephrin kinases [138]. Src phosphorylation was decreased in the sensitive parental line,

but not the dasatinib-resistant variant. This suggests that Src is an important kinase which is altered in resistance to dasatinib in this model. While EphA2 was expressed in both parental and variant cells, P-EphA2 was not detected in these cells, which suggests that the phosphorylation status of EphA2 is unlikely to contribute to resistance to dasatinib in this model.

The dasatinib resistant variant (231-DasB) showed small but significant increased sensitivity to the chemotherapy drugs docetaxel and doxorubicin (Table 4.3). Src has been implicated in augmenting sensitivity to both of these agents. Src increases sensitivity to taxanes (docetaxel and paclitaxel) in Src-transfected gallbladder epithelial cells (HAG-1), possibly via apoptotic signal transduction pathways [309]. Src has been shown to inhibit doxorubicin-related senescence and G2 cell cycle arrest in HT1080 fibrosarcoma cells. [310]. Our results show that Src phosphorylation is unaffected by dasatinib in the variant cell line, suggesting that acquired alterations in Src in this cell line may contribute to the altered drug resistance observed.

Potential alterations in Src phosphorylation in this model include constitutive activation, or genetic mutation. Src is not over-expressed in comparison to the parental cell line, by immunoblotting. Constitutive activation was examined by serum starvation of both parental and variant cells, followed by the re-addition of serum. However no alteration in phosphorylation was observed. This suggests that Src is not constitutively activated in 231-DasB. Alternatively, the altered response of phospho-Src to dasatinib may be related to an acquired mutation in Src in the variant cell line. Future work will include sequencing the coding region of the kinase domain of Src in these cells to identify potential mutations.

Src mutations in cancer are rare. A truncating, activating carcinogenic mutation at codon 531 has been reported in a subset of advanced colon cancers [311], and endometrial cancers [312]. However, other studies have not identified this mutation in other populations of colorectal cancer patients [313-315]. The identification of an activating Src mutation in breast cancer cells would be a novel finding, with important implications for therapy with Src inhibitors such as dasatinib.

While mutations of Src in human cancers are rare, activation of Src is common (reviewed by Irby *et al.* [316]). Interestingly, murine experiments with breast cancer cell lines with increased Src and EGFR (MDA-MB-231 and MDA-MB-468, both triple negative), were compared to cell lines with increased Src only (MCF7 and ZR-75-1) [85]. Increased tumorigenicity was observed in the cell lines which expressed both kinases, suggesting that the interplay of Src and EGFR may contribute to enhanced aggressiveness of tumours with increased Src.

Src has been implicated in progression and metastases in many human cancers [316]. There was decreased growth rate in the parental cells in response to dasatinib, but not in the resistant variant. Dasatinib decreased the migration and invasive ability of the dasatinib-sensitive MDA-MB-231 cell line. In contrast, dasatinib did not affect motility or invasion in the variant cell line. Increased Src activation in the variant cell line is a potential mechanism for the resistance observed in these assays. Furthermore, we observed increased invasiveness (although not statistically significant) in the variant compared to the parental cell line. Increased Src enhances the metastatic potential of colon cancer cells, in combination with EGFR [317]. Our data suggests that there is increased Src activity in the variant cell lines, contributing to an enhanced metastatic phenotype.

Recently, a novel intracellular soluble isoform of the vascular endothelial growth factor receptor (sVEGFR-1) has been identified in MDA-MB-231 cells [318]. Overexpression of this receptor by transfection in these cells increased Src phosphorylation and invasiveness. Conversely, decrease of sVEGFR-1 by siRNA knockdown reduced Src phosphorylation and invasiveness. These data further support the hypothesis that Src phosphorylation is important in the mechanisms of response and resistance in the MDA-MB-231 cells and resistant variant.

We further characterised the model of acquired dasatinib resistance by proteomic profiling of the parental and variant cell lines, both untreated and in response to dasatinib. Significantly altered proteins involved in a variety of cellular functions were identified such as angiogenesis (IPF53), metabolism and biosynthesis (TALDO1, guanine monophosphate synthetase), structural proteins (Villin 2, CCT3), and suppression of proliferation (ANXA1, ENO1).

Phosphoproteomic profiling of these cells was also performed. These experiments yielded a limited number of significantly altered phosphoproteins. There are a number of potential reasons for these results. The phosphoproteomic staining was performed on total protein, rather than protein enriched for phosphoproteins. Insufficient protein was obtained during the experiment to perform enrichment. Also, we found that the technique used (ProQ Diamond) has practical limitations. In order to obtain usable images with the scanning equipment, free-floating (unbacked) gels were required. These were fragile, and several of these fragmented during the staining and de-staining washes required. Furthermore the stain itself was inconsistent between gels, which limited the ability of the software to identify subtle differences in altered proteins.

Of note, no significantly altered phosphoproteins were identified in the dasatinib-resistant variant cell line in response to dasatinib treatment . Src is one of important targets for dasatinib, and dasatinib does not inhibit phosphorylation of Src in the resistant variant. This suggests that dasatinib may not have any significant effects on phosphorylation signalling in proteins related to Src in the resistant cells.

Annexin A1 (ANXA1), a member of the annexin family which are calcium- and phospholipid binding proteins thought to be involved in several cellular processes, including motility, proliferation and differentiation [319], was downregulated in the resistant cells.

In breast cancer, ANXA1 expression occurs predominantly in the triple negative subgroup [271]. It has been reported that ANXA1 levels are decreased in DCIS and invasive ductal carcinomas compared to either normal or hyperplastic breast tissue [320] This observation may suggest that decreased ANXA1 expression is associated with breast tumorigenesis and progression [320]. In addition, it has been reported that there is decreased ANXA1 expression in high grade prostatic intraepithelial neoplasia and prostatic adenocarcinoma [321], and in bladder cancer [322]. In our analysis, there was decreased expression of ANXA1 in the resistant variant compared to the parental cell line, suggesting an increased aggressive phenotype for the variant. This is consistent with our data on motility and invasion in this model. Interestingly, Konecny *et al.* reported that increased ANXA1 levels were associated with inherent dasatinib

sensitivity in a panel of ovarian cancer cell lines (24/42, 71 %) [272]. This observation supports a potential role for ANXA1 in determining response to dasatinib.

ANXA1 has been implicated in multi-drug resistance in breast cancer cell lines, including MDA-MB-231, independently of MDR-1, BCRP, or MRP1 [323]. As previously mentioned, dasatinib is a substrate for MDR-1 and BCRP [223]. Based on our data regarding decreased ANXA1 in the dasatinib-resistant variant, we tested the hypothesis that decreased ANXA1 expression would result in increased resistance to dasatinib in the parental MDA-MB-231 cell line. The significant changes observed by proteomic analysis were partly validated by Western blot analysis. While ANXA1 knockdown decreased cell growth in the parental cell line, there was no significant increase in resistance, as measured by changes in proliferation.

There are no direct links between ANXA1 and Src reported in the literature. As phosphorylation of Src is resistant to dasatinib the variant cell line, it would be interesting to examine the potential relationship between P-Src and ANXA1 expression.

A number of the proteins identified by proteomic profiling represent rational targets for resistance to dasatinib and warrant further investigation. For example, migration-inducing gene 10 protein, an ATP-generating glycolytic enzyme that forms part of the glycolytic pathway, is associated with prostate tumour cell proliferation *in vitro* [257] and is increased in the variant cell line in response to dasatinib. Investigation of the role of this protein in proliferation in this model may yield an additional target to enhance response to dasatinib. Enolase 1 (ENO1), has been reported to suppress colony formation in MCF7 breast cancer cells [258]. Levels of ENO1 are increased in response to dasatinib. Our densitometry results were not consistent with the proteomics observations. However, a number of isoforms of ENO1 were significantly altered in this experiment, potentially making detection of fold-changes difficult. Further validation and functional assessment of the role of ENO1 in triple negative disease is warranted. Investigation of structural proteins, such as CCT3 and cofilin 2, which were decreased in response to dasatinib, may yield additional targets which can be exploited to enhance response to this inhibitor. We anticipate that validation and

functional analysis of identified proteins will lead to novel therapeutic targets and/or biomarkers for dasatinib resistance in triple negative breast cancer.

In summary, we have examined the role of EGFR in triple negative breast cancer cell lines and a cohort of Irish breast cancer patients. We have confirmed that EGFR is over-expressed in triple negative breast cancer. While triple negative breast cancer cell lines are relatively resistant to EGFR inhibition with gefitinib, the combination of gefitinib with chemotherapy enhanced the response of these cells to chemotherapy, and suggest that there is a rationale for a clinical trial with this combination. In addition, we have developed and characterised a novel model of acquired resistance to dasatinib, an agent with notable activity in triple negative breast cancer. Proteomic analysis has yielded a number of interesting proteins which represent rational targets for resistance to dasatinib.

7.4 SUMMARY/CONCLUSION AND FUTURE WORK

1. **The potential role of Epidermal Growth Factor (EGFR) as a therapeutic target in triple negative breast cancer (TNBC)**

- EGFR is over-expressed in TNBC cell lines compared to HER-2 positive cell lines.
- The TNBC cell lines tested are less sensitive to EGFR inhibition than HER-2 positive cell lines. Gefitinib, a small molecule, was the most effective EGFR inhibitor tested.
- Sensitivity to EGFR inhibition with gefitinib was associated with decreased phosphorylation of MAPK and Akt. Combined assessment of the phosphorylation of these proteins may represent biomarkers for response to gefitinib.
- Although the TNBCS cell lines have low levels of P-EGFR, levels can be increased by ligand stimulation. Gefitinib can inhibit ligand-stimulated phosphorylation.
- Gefitinib causes G1 phase cell cycle arrest in sensitive cell lines.

- Gefitinib combined with chemotherapy causes greater inhibition of proliferation than either gefitinib or chemotherapy alone.

2. EGFR and phospho-EGFR (P-EGFR) in breast tumours

- EGFR was detected in 11.0 % (11/101) of the breast tumours tested. EGFR was detected in 31.5 % (5/16) of the triple negative breast tumours.
- Phosphorylation of EGFR was detected in 8.9 % (9/101) of the tumours. 6.2 % (1/16) of the triple negative tumours had positive staining for P-EGFR.
- EGFR positivity was significantly associated with ER negativity ($p = 0.0314$), the triple negative phenotype ($p = 0.070$), and with lymph node positivity ($p = 0.0035$).
- No significant correlations with P-EGFR were identified.

3. Development and characterisation of a model of acquired resistance to dasatinib in TNBC

- Of the TNBC cell lines tested MDA-MB-231 displayed the greatest sensitivity to the multi-target tyrosine kinase inhibitor dasatinib.
- Continuous exposure of MDA-MB-231 cells to incrementally increasing concentrations of dasatinib resulted in induction of stable resistance to dasatinib (231-DasB).
- There was a significant decrease in cell doubling times in response to dasatinib treatment in the MDA-MB-231 cell line, but not in the 231-DasB cell line.
- Dasatinib caused a significant decrease in invasion in the sensitive MDA-MB-231 cell lines ($p = 0.0216$), but not in the 231-DasB cell line.
- Dasatinib caused a significant decrease in migration in the parental cell lines ($p = 0.0018$), but not in the resistant variant cell line, There was a significant increase in migration in the variant compared to the parental cell lines ($p = 0.0090$).
- No significant differences in dasatinib accumulation were observed between the parental and variant cell lines.

- The combination of dasatinib with the BCRP/MDR-1 inhibitor elacridar did not enhance growth inhibition.

4. Proteomic analysis of TNBC model of acquired resistance to dasatinib

- Proteomic and phospho-proteomic analysis was performed comparing MDA-MB-231 (parental) and 231-DasB (resistant variant) with and without dasatinib treatment. Seventy-eight significantly altered proteins were identified in comparisons between each cell line, and between treated and untreated cells.
- Annexin A1 (ANXA1) was significantly decreased in the MDA-MB-231-Das cells compared to the parental cell line.
- siRNA knockdown of ANXA1 combined with dasatinib resulted in a significant decrease in proliferation in MDA-MB-231 compared to siRNA alone ($p = 0.01$). The decreased proliferation was not significant when compared to scrambled siRNA combined with dasatinib ($p = 0.10$).

5. Future Work

- In the resistant variant cell line, dasatinib does not inhibit phosphorylation of Src kinase, so there may be an alteration in Src which makes it resistant to dasatinib Gene sequencing of Src may identify mutations contributing to dasatinib resistance in our model of acquired dasatinib resistance
- It is anticipated that further proteins identified by the proteomic analysis of the novel model of dasatinib resistance will provide potential markers of dasatinib sensitivity or resistance and/or potential novel therapeutic targets.
- Immunohistochemistry assessment of EGFR and P-EGFR levels in our cohort of breast cancer patients identified significant correlations between EGFR expression and lymph node negativity, as well as the triple negative phenotype. No significant correlations were P-EGFR positivity were identified. However, a relatively low number of positive tumours were identified. Further immunohistochemistry tested with an expanded cohort of patients would be

required to confirm these correlations and the frequency of EGFR expression and phosphorylation in triple negative breast tumours. Collection of triple negative tumour tissue samples pre- and post- treatment may identify further tyrosine kinase targets of interest.

REFERENCES

1. WHO, *The global burden of disease: 2004 update* 2008, World Health Organisation: Geneva.
2. *AJCC Cancer Staging Manual*. 6th edition ed, ed. A.J.C.o. Cancer. 2002, New York, NY: Springer. pp 171-180.
3. Slamon, D.J., et al., *Human breast cancer: correlation of relapse and survival with amplification of the HER-2/neu oncogene.* Science, 1987. **235**(4785): p. 177-82.
4. Slamon, D.J., et al., *Use of chemotherapy plus a monoclonal antibody against HER2 for metastatic breast cancer that overexpresses HER2.* N Engl J Med, 2001. **344**(11): p. 783-92.
5. *AJCC Cancer Stagin Manual*. 2002, New York: Springer.
6. Perou, C.M., et al., *Molecular portraits of human breast tumours.* Nature, 2000. **406**(6797): p. 747-52.
7. Rakha, E.A., J.S. Reis-Filho, and I.O. Ellis, *Basal-like breast cancer: a critical review.* J Clin Oncol, 2008. **26**(15): p. 2568-81.
8. Bertucci, F., et al., *Identification and validation of an ERBB2 gene expression signature in breast cancers.* Oncogene, 2004. **23**(14): p. 2564-75.
9. Biswas, D.K. and J.D. Iglehart, *Linkage between EGFR family receptors and nuclear factor kappaB (NF-kappaB) signaling in breast cancer.* J Cell Physiol, 2006. **209**(3): p. 645-52.
10. Sorlie, T., et al., *Gene expression patterns of breast carcinomas distinguish tumor subclasses with clinical implications.* Proc Natl Acad Sci U S A, 2001. **98**(19): p. 10869-74.
11. Tischkowitz, M., et al., *Use of immunohistochemical markers can refine prognosis in triple negative breast cancer.* BMC Cancer, 2007. **7**: p. 134.
12. Kreike, B., et al., *Gene expression profiling and histopathological characterization of triple-negative/basal-like breast carcinomas.* Breast Cancer Res, 2007. **9**(5): p. R65.
13. Abd El-Rehim, D.M., et al., *High-throughput protein expression analysis using tissue microarray technology of a large well-characterised series identifies biologically distinct classes of breast cancer confirming recent cDNA expression analyses.* Int J Cancer, 2005. **116**(3): p. 340-50.
14. Tan, D.S., et al., *Triple negative breast cancer: molecular profiling and prognostic impact in adjuvant anthracycline-treated patients.* Breast Cancer Res Treat, 2007.
15. Nielsen, T.O., et al., *Immunohistochemical and clinical characterization of the basal-like subtype of invasive breast carcinoma.* Clin Cancer Res, 2004. **10**(16): p. 5367-74.
16. Sorlie, T., et al., *Distinct molecular mechanisms underlying clinically relevant subtypes of breast cancer: gene expression analyses across three different platforms.* BMC Genomics, 2006. **7**: p. 127.
17. Herschkowitz, J.I., et al., *Identification of conserved gene expression features between murine mammary carcinoma models and human breast tumors.* Genome Biol, 2007. **8**(5): p. R76.
18. Furuse, M., et al., *Claudin-1 and -2: novel integral membrane proteins localizing at tight junctions with no sequence similarity to occludin.* J Cell Biol, 1998. **141**(7): p. 1539-50.
19. Hennessy, B.T., et al., *Characterization of a naturally occurring breast cancer subset enriched in epithelial-to-mesenchymal transition and stem cell characteristics.* Cancer Res, 2009. **69**(10): p. 4116-24.

20. Tusher, V.G., R. Tibshirani, and G. Chu, *Significance analysis of microarrays applied to the ionizing radiation response.* Proc Natl Acad Sci U S A, 2001. **98**(9): p. 5116-21.
21. Sorlie, T., et al., *Repeated observation of breast tumor subtypes in independent gene expression data sets.* Proc Natl Acad Sci U S A, 2003. **100**(14): p. 8418-23.
22. Geisler, S., et al., *TP53 gene mutations predict the response to neoadjuvant treatment with 5-fluorouracil and mitomycin in locally advanced breast cancer.* Clin Cancer Res, 2003. **9**(15): p. 5582-8.
23. Geisler, S., et al., *Influence of TP53 gene alterations and c-erbB-2 expression on the response to treatment with doxorubicin in locally advanced breast cancer.* Cancer Res, 2001. **61**(6): p. 2505-12.
24. van 't Veer, L.J., et al., *Gene expression profiling predicts clinical outcome of breast cancer.* Nature, 2002. **415**(6871): p. 530-6.
25. West, M., et al., *Predicting the clinical status of human breast cancer by using gene expression profiles.* Proc Natl Acad Sci U S A, 2001. **98**(20): p. 11462-7.
26. van de Rijn, M., et al., *Expression of cytokeratins 17 and 5 identifies a group of breast carcinomas with poor clinical outcome.* Am J Pathol, 2002. **161**(6): p. 1991-6.
27. Malzahn, K., et al., *Biological and prognostic significance of stratified epithelial cytokeratins in infiltrating ductal breast carcinomas.* Virchows Arch, 1998. **433**(2): p. 119-29.
28. Charafe-Jauffret, E., et al., *Gene expression profiling of breast cell lines identifies potential new basal markers.* Oncogene, 2006. **25**(15): p. 2273-84.
29. Ross, D.T. and C.M. Perou, *A comparison of gene expression signatures from breast tumors and breast tissue derived cell lines.* Dis Markers, 2001. **17**(2): p. 99-109.
30. Farmer, P., et al., *A stroma-related gene signature predicts resistance to neoadjuvant chemotherapy in breast cancer.* Nat Med, 2009. **15**(1): p. 68-74.
31. Finak, G., et al., *Stromal gene expression predicts clinical outcome in breast cancer.* Nat Med, 2008. **14**(5): p. 518-27.
32. Wennmalm, K., A. Ostman, and J. Bergh, *Stromal signature identifies basal breast cancers.* Nat Med, 2009. **15**(3): p. 237-8; author reply 238.
33. De Soto, J.A. and C.X. Deng, *PARP-1 inhibitors: are they the long-sought genetically specific drugs for BRCA1/2-associated breast cancers?* Int J Med Sci, 2006. **3**(4): p. 117-23.
34. Garber, J.E. and K. Offit, *Hereditary cancer predisposition syndromes.* J Clin Oncol, 2005. **23**(2): p. 276-92.
35. Wooster, R. and B.L. Weber, *Breast and ovarian cancer.* N Engl J Med, 2003. **348**(23): p. 2339-47.
36. Lakhani, S.R., et al., *The pathology of familial breast cancer: predictive value of immunohistochemical markers estrogen receptor, progesterone receptor, HER-2, and p53 in patients with mutations in BRCA1 and BRCA2.* J Clin Oncol, 2002. **20**(9): p. 2310-8.
37. Foulkes, W.D., et al., *Disruption of the expected positive correlation between breast tumor size and lymph node status in BRCA1-related breast carcinoma.* Cancer, 2003. **98**(8): p. 1569-77.
38. Chappuis, P.O., V. Nethercot, and W.D. Foulkes, *Clinico-pathological characteristics of BRCA1- and BRCA2-related breast cancer.* Semin Surg Oncol, 2000. **18**(4): p. 287-95.

39. Chappuis, P.O., et al., *Germline BRCA1/2 mutations and p27(Kip1) protein levels independently predict outcome after breast cancer.* J Clin Oncol, 2000. **18**(24): p. 4045-52.
40. Greenblatt, M.S., et al., *TP53 mutations in breast cancer associated with BRCA1 or BRCA2 germ-line mutations: distinctive spectrum and structural distribution.* Cancer Res, 2001. **61**(10): p. 4092-7.
41. Foulkes, W.D., et al., *Germline BRCA1 mutations and a basal epithelial phenotype in breast cancer.* J Natl Cancer Inst, 2003. **95**(19): p. 1482-5.
42. Hu, Z., et al., *The molecular portraits of breast tumors are conserved across microarray platforms.* BMC Genomics, 2006. **7**: p. 96.
43. Foulkes, W.D., et al., *The prognostic implication of the basal-like (cyclin E high/p27 low/p53+/glomeruloid-microvascular-proliferation+) phenotype of BRCA1-related breast cancer.* Cancer Res, 2004. **64**(3): p. 830-5.
44. Sjogren, S., et al., *The p53 gene in breast cancer: prognostic value of complementary DNA sequencing versus immunohistochemistry.* J Natl Cancer Inst, 1996. **88**(3-4): p. 173-82.
45. Carey, L.A., et al., *Race, breast cancer subtypes, and survival in the Carolina Breast Cancer Study.* Jama, 2006. **295**(21): p. 2492-502.
46. de Cremoux, P., et al., *p53 mutation as a genetic trait of typical medullary breast carcinoma.* J Natl Cancer Inst, 1999. **91**(7): p. 641-3.
47. Vincent-Salomon, A., et al., *Identification of typical medullary breast carcinoma as a genomic sub-group of basal-like carcinomas, a heterogeneous new molecular entity.* Breast Cancer Res, 2007. **9**(2): p. R24.
48. De Maeyer, L., et al., *Does estrogen receptor negative/progesterone receptor positive breast carcinoma exist?* J Clin Oncol, 2008. **26**(2): p. 335-6; author reply 336-8.
49. Rakha, E.A., et al., *Biologic and clinical characteristics of breast cancer with single hormone receptor positive phenotype.* J Clin Oncol, 2007. **25**(30): p. 4772-8.
50. Krieke, B. and M.J.v.d. Vijver, *Are triple-negative tumours and basal-like breast cancer synonymous? Authors' response.* Breast Cancer Res, 2007. **9**: p. 405.
51. Thike, A.A., et al., *Triple-negative breast cancer: clinicopathological characteristics and relationship with basal-like breast cancer.* Mod Pathol. **23**(1): p. 123-33.
52. Banerjee, S., et al., *Basal-like breast carcinomas: clinical outcome and response to chemotherapy.* J Clin Pathol, 2006. **59**(7): p. 729-35.
53. Osborne, C., et al. *Clinical and pathological characterisastion of basal-like breast cancer*. in *San Antonio Breast Conference*. 2005: Abstract No. 2098.
54. Rodriguez-Pinilla, S.M., et al., *Prognostic significance of basal-like phenotype and fascin expression in node-negative invasive breast carcinomas.* Clin Cancer Res, 2006. **12**(5): p. 1533-9.
55. Tsuda, H., et al., *Large, central acellular zones indicating myoepithelial tumor differentiation in high-grade invasive ductal carcinomas as markers of predisposition to lung and brain metastases.* Am J Surg Pathol, 2000. **24**(2): p. 197-202.
56. Dent, R., et al., *Pattern of metastatic spread in triple-negative breast cancer.* Breast Cancer Res Treat, 2008.

57. Kaplan, H.G., J.A. Malmgren, and M. Atwood, *T1N0 triple negative breast cancer: risk of recurrence and adjuvant chemotherapy.* Breast J, 2009. **15**(5): p. 454-60.
58. Kennecke, H., et al., *Metastatic Behavior of Breast Cancer Subtypes.* J Clin Oncol.
59. Huo, D., et al., *Population differences in breast cancer: survey in indigenous African women reveals over-representation of triple-negative breast cancer.* J Clin Oncol, 2009. **27**(27): p. 4515-21.
60. Bauer, K.R., et al., *Descriptive analysis of estrogen receptor (ER)-negative, progesterone receptor (PR)-negative, and HER2-negative invasive breast cancer, the so-called triple-negative phenotype: a population-based study from the California cancer Registry.* Cancer, 2007. **109**(9): p. 1721-8.
61. Millikan, R.C., et al., *Epidemiology of basal-like breast cancer.* Breast Cancer Res Treat, 2008. **109**(1): p. 123-39.
62. Olopade, O., I. F, and C.M. Perou. *Intrinsic Gene Expression subtypes correlated with grade and morphometric parameters reveal a high proportion of aggressive basal-like tumours among black women of African Ancestry*. in *ASCO Annual Meeting*. 2004. New Orleans, LA, USA.
63. Carey, L.A., et al., *The triple negative paradox: primary tumor chemosensitivity of breast cancer subtypes.* Clin Cancer Res, 2007. **13**(8): p. 2329-34.
64. Guarneri, V., et al., *Prognostic value of pathologic complete response after primary chemotherapy in relation to hormone receptor status and other factors.* J Clin Oncol, 2006. **24**(7): p. 1037-44.
65. Urruticoechea, A., I.E. Smith, and M. Dowsett, *Proliferation marker Ki-67 in early breast cancer.* J Clin Oncol, 2005. **23**(28): p. 7212-20.
66. Harris, L.N., et al., *Molecular subtypes of breast cancer in relation to paclitaxel response and outcomes in women with metastatic disease: results from CALGB 9342.* Breast Cancer Res, 2006. **8**(6): p. R66.
67. Reis-Filho, J.S. and A.N. Tutt, *Triple negative tumours: a critical review.* Histopathology, 2008. **52**(1): p. 108-18.
68. Carpenter, G., et al., *Characterization of the binding of 125-I-labeled epidermal growth factor to human fibroblasts.* J Biol Chem, 1975. **250**(11): p. 4297-304.
69. Cohen, S., G. Carpenter, and L. King, Jr., *Epidermal growth factor-receptor-protein kinase interactions. Co-purification of receptor and epidermal growth factor-enhanced phosphorylation activity.* J Biol Chem, 1980. **255**(10): p. 4834-42.
70. Cohen, S., et al., *A native 170,000 epidermal growth factor receptor-kinase complex from shed plasma membrane vesicles.* J Biol Chem, 1982. **257**(3): p. 1523-31.
71. Herbst, R.S., *Review of epidermal growth factor receptor biology.* Int J Radiat Oncol Biol Phys, 2004. **59**(2 Suppl): p. 21-6.
72. Burgess, A.W., et al., *An open-and-shut case? Recent insights into the activation of EGF/ErbB receptors.* Mol Cell, 2003. **12**(3): p. 541-52.
73. Yarden, Y. and M.X. Sliwkowski, *Untangling the ErbB signalling network.* Nat Rev Mol Cell Biol, 2001. **2**(2): p. 127-37.
74. Normanno, N., et al., *Epidermal growth factor receptor (EGFR) signaling in cancer.* Gene, 2006. **366**(1): p. 2-16.

75. Ferguson, K.M., et al., *EGF activates its receptor by removing interactions that autoinhibit ectodomain dimerization.* Mol Cell, 2003. **11**(2): p. 507-17.
76. Jorissen, R.N., et al., *Epidermal growth factor receptor: mechanisms of activation and signalling.* Exp Cell Res, 2003. **284**(1): p. 31-53.
77. Ogiso, H., et al., *Crystal structure of the complex of human epidermal growth factor and receptor extracellular domains.* Cell, 2002. **110**(6): p. 775-87.
78. King, A.C. and P. Cuatrecasas, *Resolution of high and low affinity epidermal growth factor receptors. Inhibition of high affinity component by low temperature, cycloheximide, and phorbol esters.* J Biol Chem, 1982. **257**(6): p. 3053-60.
79. Leahy, D.J., *Structure and function of the epidermal growth factor (EGF/ErbB) family of receptors.* Adv Protein Chem, 2004. **68**: p. 1-27.
80. Lax, I., et al., *Functional analysis of the ligand binding site of EGF-receptor utilizing chimeric chicken/human receptor molecules.* Embo J, 1989. **8**(2): p. 421-7.
81. Schlessinger, J., *Ligand-induced, receptor-mediated dimerization and activation of EGF receptor.* Cell, 2002. **110**(6): p. 669-72.
82. Moriki, T., H. Maruyama, and I.N. Maruyama, *Activation of preformed EGF receptor dimers by ligand-induced rotation of the transmembrane domain.* J Mol Biol, 2001. **311**(5): p. 1011-26.
83. Walton, G.M., et al., *Analysis of deletions of the carboxyl terminus of the epidermal growth factor receptor reveals self-phosphorylation at tyrosine 992 and enhanced in vivo tyrosine phosphorylation of cell substrates.* J Biol Chem, 1990. **265**(3): p. 1750-4.
84. Olayioye, M.A., et al., *The ErbB signaling network: receptor heterodimerization in development and cancer.* Embo J, 2000. **19**(13): p. 3159-67.
85. Biscardi, J.S., A.P. Belsches, and S.J. Parsons, *Characterization of human epidermal growth factor receptor and c-Src interactions in human breast tumor cells.* Mol Carcinog, 1998. **21**(4): p. 261-72.
86. Yamauchi, T., et al., *Tyrosine phosphorylation of the EGF receptor by the kinase Jak2 is induced by growth hormone.* Nature, 1997. **390**(6655): p. 91-6.
87. Yamauchi, T., et al., *Constitutive tyrosine phosphorylation of ErbB-2 via Jak2 by autocrine secretion of prolactin in human breast cancer.* J Biol Chem, 2000. **275**(43): p. 33937-44.
88. Brabender, J., et al., *Epidermal growth factor receptor and HER2-neu mRNA expression in non-small cell lung cancer Is correlated with survival.* Clin Cancer Res, 2001. **7**(7): p. 1850-5.
89. Meyers, M.B., et al., *Increased epidermal growth factor receptor in multidrug-resistant human neuroblastoma cells.* J Cell Biochem, 1988. **38**(2): p. 87-97.
90. Baselga, J., *Why the epidermal growth factor receptor? The rationale for cancer therapy.* Oncologist, 2002. **7 Suppl 4**: p. 2-8.
91. Klijn, J.G., et al., *The clinical significance of epidermal growth factor receptor (EGF-R) in human breast cancer: a review on 5232 patients.* Endocr Rev, 1992. **13**(1): p. 3-17.
92. Fox, S.B., et al., *The epidermal growth factor receptor as a prognostic marker: results of 370 patients and review of 3009 patients.* Breast Cancer Res Treat, 1994. **29**(1): p. 41-9.

93. Chan, S.K., M.E. Hill, and W.J. Gullick, *The role of the epidermal growth factor receptor in breast cancer.* J Mammary Gland Biol Neoplasia, 2006. **11**(1): p. 3-11.
94. Livasy, C.A., et al., *Phenotypic evaluation of the basal-like subtype of invasive breast carcinoma.* Mod Pathol, 2006. **19**(2): p. 264-71.
95. Rakha, E.A., et al., *Prognostic markers in triple-negative breast cancer.* Cancer, 2007. **109**(1): p. 25-32.
96. Stratford, A.L., et al., *Epidermal growth factor receptor (EGFR) is transcriptionally induced by the Y-box binding protein-1 (YB-1) and can be inhibited with Iressa in basal-like breast cancer, providing a potential target for therapy.* Breast Cancer Res, 2007. **9**(5): p. R61.
97. Wu, J., et al., *Disruption of the Y-box binding protein-1 results in suppression of the epidermal growth factor receptor and HER-2.* Cancer Res, 2006. **66**(9): p. 4872-9.
98. Sakura, H., et al., *Two human genes isolated by a novel method encode DNA-binding proteins containing a common region of homology.* Gene, 1988. **73**(2): p. 499-507.
99. Evdokimova, V., et al., *Akt-mediated YB-1 phosphorylation activates translation of silent mRNA species.* Mol Cell Biol, 2006. **26**(1): p. 277-92.
100. Malumbres, M. and M. Barbacid, *RAS oncogenes: the first 30 years.* Nat Rev Cancer, 2003. **3**(6): p. 459-65.
101. Karnoub, A.E. and R.A. Weinberg, *Ras oncogenes: split personalities.* Nat Rev Mol Cell Biol, 2008. **9**(7): p. 517-31.
102. Sanchez-Munoz, A., et al., *Lack of evidence for KRAS oncogenic mutations in triple-negative breast cancer.* BMC Cancer. **10**: p. 136.
103. Karapetis, C.S., et al., *K-ras mutations and benefit from cetuximab in advanced colorectal cancer.* N Engl J Med, 2008. **359**(17): p. 1757-65.
104. Lowenstein, E.J., et al., *The SH2 and SH3 domain-containing protein GRB2 links receptor tyrosine kinases to ras signaling.* Cell, 1992. **70**(3): p. 431-42.
105. Sasaoka, T., et al., *The signaling pathway coupling epidermal growth factor receptors to activation of p21ras.* J Biol Chem, 1994. **269**(51): p. 32621-5.
106. Craparo, A., T.J. O'Neill, and T.A. Gustafson, *Non-SH2 domains within insulin receptor substrate-1 and SHC mediate their phosphotyrosine-dependent interaction with the NPEY motif of the insulin-like growth factor I receptor.* J Biol Chem, 1995. **270**(26): p. 15639-43.
107. Hallberg, B., S.I. Rayter, and J. Downward, *Interaction of Ras and Raf in intact mammalian cells upon extracellular stimulation.* J Biol Chem, 1994. **269**(6): p. 3913-6.
108. Johnson, G.L. and R.R. Vaillancourt, *Sequential protein kinase reactions controlling cell growth and differentiation.* Curr Opin Cell Biol, 1994. **6**(2): p. 230-8.
109. Roberts, P.J. and C.J. Der, *Targeting the Raf-MEK-ERK mitogen-activated protein kinase cascade for the treatment of cancer.* Oncogene, 2007. **26**(22): p. 3291-310.
110. Oliveras-Ferraros, C., et al., *Growth and molecular interactions of the anti-EGFR antibody cetuximab and the DNA cross-linking agent cisplatin in gefitinib-resistant MDA-MB-468 cells: new prospects in the treatment of triple-negative/basal-like breast cancer.* Int J Oncol, 2008. **33**(6): p. 1165-76.

111. Amemiya, Y., et al., *Insulin like growth factor binding protein-7 reduces growth of human breast cancer cells and xenografted tumors.* Breast Cancer Res Treat.
112. Beliakoff, J. and L. Whitesell, *Hsp90: an emerging target for breast cancer therapy.* Anticancer Drugs, 2004. **15**(7): p. 651-62.
113. Workman, P., et al., *Drugging the cancer chaperone HSP90: combinatorial therapeutic exploitation of oncogene addiction and tumor stress.* Ann N Y Acad Sci, 2007. **1113**: p. 202-16.
114. Caldas-Lopes, E., et al., *Hsp90 inhibitor PU-H71, a multimodal inhibitor of malignancy, induces complete responses in triple-negative breast cancer models.* Proc Natl Acad Sci U S A, 2009. **106**(20): p. 8368-73.
115. Liu, B., et al., *Metformin induces unique biological and molecular responses in triple negative breast cancer cells.* Cell Cycle, 2009. **8**(13): p. 2031-40.
116. Eralp, Y., et al., *MAPK overexpression is associated with anthracycline resistance and increased risk for recurrence in patients with triple-negative breast cancer.* Ann Oncol, 2008. **19**(4): p. 669-74.
117. Guix, M., et al., *Short preoperative treatment with erlotinib inhibits tumor cell proliferation in hormone receptor-positive breast cancers.* J Clin Oncol, 2008. **26**(6): p. 897-906.
118. Leevers, S.J., B. Vanhaesebroeck, and M.D. Waterfield, *Signalling through phosphoinositide 3-kinases: the lipids take centre stage.* Curr Opin Cell Biol, 1999. **11**(2): p. 219-25.
119. Vivanco, I. and C.L. Sawyers, *The phosphatidylinositol 3-Kinase AKT pathway in human cancer.* Nat Rev Cancer, 2002. **2**(7): p. 489-501.
120. Osaki, M., M. Oshimura, and H. Ito, *PI3K-Akt pathway: its functions and alterations in human cancer.* Apoptosis, 2004. **9**(6): p. 667-76.
121. Pawson, T. and P. Nash, *Protein-protein interactions define specificity in signal transduction.* Genes Dev, 2000. **14**(9): p. 1027-47.
122. Maehama, T. and J.E. Dixon, *The tumor suppressor, PTEN/MMAC1, dephosphorylates the lipid second messenger, phosphatidylinositol 3,4,5-trisphosphate.* J Biol Chem, 1998. **273**(22): p. 13375-8.
123. Datta, S.R., et al., *Akt phosphorylation of BAD couples survival signals to the cell-intrinsic death machinery.* Cell, 1997. **91**(2): p. 231-41.
124. Zha, J., et al., *Serine phosphorylation of death agonist BAD in response to survival factor results in binding to 14-3-3 not BCL-X(L).* Cell, 1996. **87**(4): p. 619-28.
125. Ma, Y.Y., et al., *PIK3CA as an oncogene in cervical cancer.* Oncogene, 2000. **19**(23): p. 2739-44.
126. Shayesteh, L., et al., *PIK3CA is implicated as an oncogene in ovarian cancer.* Nat Genet, 1999. **21**(1): p. 99-102.
127. Samuels, Y., et al., *High frequency of mutations of the PIK3CA gene in human cancers.* Science, 2004. **304**(5670): p. 554.
128. Wu, G., et al., *Somatic mutation and gain of copy number of PIK3CA in human breast cancer.* Breast Cancer Res, 2005. **7**(5): p. R609-16.
129. Bachman, K.E., et al., *The PIK3CA gene is mutated with high frequency in human breast cancers.* Cancer Biol Ther, 2004. **3**(8): p. 772-5.
130. Price, J.T., et al., *Epidermal growth factor promotes MDA-MB-231 breast cancer cell migration through a phosphatidylinositol 3'-kinase and phospholipase C-dependent mechanism.* Cancer Res, 1999. **59**(21): p. 5475-8.

131. Hinton, C.V., L.D. Fitzgerald, and M.E. Thompson, *Phosphatidylinositol 3-kinase/Akt signaling enhances nuclear localization and transcriptional activity of BRCA1.* Exp Cell Res, 2007. **313**(9): p. 1735-44.
132. Takabatake, D., et al., *Tumor inhibitory effect of gefitinib (ZD1839, Iressa) and taxane combination therapy in EGFR-overexpressing breast cancer cell lines (MCF7/ADR, MDA-MB-231).* Int J Cancer, 2007. **120**(1): p. 181-8.
133. Chakrabandhu, K., S. Huault, and A.O. Hueber, *Distinctive molecular signaling in triple-negative breast cancer cell death triggered by hexadecylphosphocholine (miltefosine).* FEBS Lett, 2008. **582**(30): p. 4176-84.
134. Turner, N., et al., *Integrative molecular profiling of triple negative breast cancers identifies amplicon drivers and potential therapeutic targets.* Oncogene. **29**(14): p. 2013-23.
135. Zeng, Q., et al., *Treating triple-negative breast cancer by a combination of rapamycin and cyclophosphamide: an in vivo bioluminescence imaging study.* Eur J Cancer. **46**(6): p. 1132-43.
136. Lerma, E., et al., *Immunohistochemical heterogeneity of breast carcinomas negative for estrogen receptors, progesterone receptors and Her2/neu (basal-like breast carcinomas).* Mod Pathol, 2007. **20**(11): p. 1200-7.
137. Umemura, S., et al., *Increased phosphorylation of Akt in triple-negative breast cancers.* Cancer Sci, 2007. **98**(12): p. 1889-92.
138. Finn, R.S., et al., *Dasatinib, an orally active small molecule inhibitor of both the src and abl kinases, selectively inhibits growth of basal-type/"triple-negative" breast cancer cell lines growing in vitro.* Breast Cancer Res Treat, 2007.
139. Roskoski, R., Jr., *Src kinase regulation by phosphorylation and dephosphorylation.* Biochem Biophys Res Commun, 2005. **331**(1): p. 1-14.
140. Miller, C.T., et al., *Genomic amplification of MET with boundaries within fragile site FRA7G and upregulation of MET pathways in esophageal adenocarcinoma.* Oncogene, 2006. **25**(3): p. 409-18.
141. Wilson, L.K., et al., *pp60c-src tyrosine kinase, myristylation, and modulatory domains are required for enhanced mitogenic responsiveness to epidermal growth factor seen in cells overexpressing c-src.* Mol Cell Biol, 1989. **9**(4): p. 1536-44.
142. Twamley-Stein, G.M., et al., *The Src family tyrosine kinases are required for platelet-derived growth factor-mediated signal transduction in NIH 3T3 cells.* Proc Natl Acad Sci U S A, 1993. **90**(16): p. 7696-700.
143. Roche, S., et al., *DNA synthesis induced by some but not all growth factors requires Src family protein tyrosine kinases.* Mol Cell Biol, 1995. **15**(2): p. 1102-9.
144. Luttrell, D.K., L.M. Luttrell, and S.J. Parsons, *Augmented mitogenic responsiveness to epidermal growth factor in murine fibroblasts that overexpress pp60c-src.* Mol Cell Biol, 1988. **8**(1): p. 497-501.
145. Maa, M.C., et al., *Potentiation of epidermal growth factor receptor-mediated oncogenesis by c-Src: implications for the etiology of multiple human cancers.* Proc Natl Acad Sci U S A, 1995. **92**(15): p. 6981-5.
146. Benhar, M., et al., *Enhanced ROS production in oncogenically transformed cells potentiates c-Jun N-terminal kinase and p38 mitogen-activated protein kinase activation and sensitization to genotoxic stress.* Mol Cell Biol, 2001. **21**(20): p. 6913-26.

147. Karni, R., R. Jove, and A. Levitzki, *Inhibition of pp60c-Src reduces Bcl-XL expression and reverses the transformed phenotype of cells overexpressing EGF and HER-2 receptors.* Oncogene, 1999. **18**(33): p. 4654-62.
148. Cartwright, C.A., et al., *pp60c-src activation in human colon carcinoma.* J Clin Invest, 1989. **83**(6): p. 2025-33.
149. Jacobs, C. and H. Rubsamen, *Expression of pp60c-src protein kinase in adult and fetal human tissue: high activities in some sarcomas and mammary carcinomas.* Cancer Res, 1983. **43**(4): p. 1696-702.
150. Ottenhoff-Kalff, A.E., et al., *Characterization of protein tyrosine kinases from human breast cancer: involvement of the c-src oncogene product.* Cancer Res, 1992. **52**(17): p. 4773-8.
151. Rosen, N., et al., *Analysis of pp60c-src protein kinase activity in human tumor cell lines and tissues.* J Biol Chem, 1986. **261**(29): p. 13754-9.
152. Luttrell, D.K., et al., *Involvement of pp60c-src with two major signaling pathways in human breast cancer.* Proc Natl Acad Sci U S A, 1994. **91**(1): p. 83-7.
153. Muthuswamy, S.K. and W.J. Muller, *Activation of Src family kinases in Neu-induced mammary tumors correlates with their association with distinct sets of tyrosine phosphorylated proteins in vivo.* Oncogene, 1995. **11**(9): p. 1801-10.
154. Stover, D.R., et al., *Src phosphorylation of the epidermal growth factor receptor at novel sites mediates receptor interaction with Src and P85 alpha.* J Biol Chem, 1995. **270**(26): p. 15591-7.
155. Biscardi, J.S., et al., *Tyrosine kinase signalling in breast cancer: epidermal growth factor receptor and c-Src interactions in breast cancer.* Breast Cancer Res, 2000. **2**(3): p. 203-10.
156. Summy, J.M. and G.E. Gallick, *Src family kinases in tumor progression and metastasis.* Cancer Metastasis Rev, 2003. **22**(4): p. 337-58.
157. Dimri, M., et al., *Modeling breast cancer-associated c-Src and EGFR overexpression in human MECs: c-Src and EGFR cooperatively promote aberrant three-dimensional acinar structure and invasive behavior.* Cancer Res, 2007. **67**(9): p. 4164-72.
158. Sicheri, F. and J. Kuriyan, *Structures of Src-family tyrosine kinases.* Curr Opin Struct Biol, 1997. **7**(6): p. 777-85.
159. Das, J., et al., *2-aminothiazole as a novel kinase inhibitor template. Structure-activity relationship studies toward the discovery of N-(2-chloro-6-methylphenyl)-2-[[6-[4-(2-hydroxyethyl)-1- piperazinyl)]-2-methyl-4-pyrimidinyl]amino)]-1,3-thiazole-5-carboxamide (dasatinib, BMS-354825) as a potent pan-Src kinase inhibitor.* J Med Chem, 2006. **49**(23): p. 6819-32.
160. Srinivasan, D. and R. Plattner, *Activation of Abl tyrosine kinases promotes invasion of aggressive breast cancer cells.* Cancer Res, 2006. **66**(11): p. 5648-55.
161. Tryfonopoulos, D., et al., *Possible targets for dasatinib sensitivity in triple negative breast cancer.* . European Journal of Cancer Supplements, 2008. **6**(7, April 2008): p. 220.
162. Elsberger, B., et al., *Breast cancer patients' clinical outcome measures are associated with Src kinase family member expression.* Br J Cancer. **103**(6): p. 899-909.
163. Bernex, F., et al., *Spatial and temporal patterns of c-kit-expressing cells in WlacZ/+ and WlacZ/WlacZ mouse embryos.* Development, 1996. **122**(10): p. 3023-33.

164. Ulivi, P., et al., *c-kit and SCF expression in normal and tumor breast tissue.* Breast Cancer Res Treat, 2004. **83**(1): p. 33-42.
165. Maffini, M.V., et al., *Lack of c-kit receptor promotes mammary tumors in N-nitrosomethylurea-treated Ws/Ws rats.* Cancer Cell Int, 2008. **8**(1): p. 5.
166. Azoulay, S., et al., *KIT is highly expressed in adenoid cystic carcinoma of the breast, a basal-like carcinoma associated with a favorable outcome.* Mod Pathol, 2005. **18**(12): p. 1623-31.
167. Kim, M.J., et al., *Clinicopathologic significance of the basal-like subtype of breast cancer: a comparison with hormone receptor and Her2/neu-overexpressing phenotypes.* Hum Pathol, 2006. **37**(9): p. 1217-26.
168. Nalwoga, H., et al., *Expression of EGFR and c-kit is associated with the basal-like phenotype in breast carcinomas of African women.* Apmis, 2008. **116**(6): p. 515-25.
169. Kanner, S.B., et al., *Monoclonal antibodies to individual tyrosine-phosphorylated protein substrates of oncogene-encoded tyrosine kinases.* Proc Natl Acad Sci U S A, 1990. **87**(9): p. 3328-32.
170. Schaller, M.D., et al., *pp125FAK a structurally distinctive protein-tyrosine kinase associated with focal adhesions.* Proc Natl Acad Sci U S A, 1992. **89**(11): p. 5192-6.
171. Hanks, S.K. and T.R. Polte, *Signaling through focal adhesion kinase.* Bioessays, 1997. **19**(2): p. 137-45.
172. Schlaepfer, D.D., C.R. Hauck, and D.J. Sieg, *Signaling through focal adhesion kinase.* Prog Biophys Mol Biol, 1999. **71**(3-4): p. 435-78.
173. Weiner, T.M., et al., *Expression of focal adhesion kinase gene and invasive cancer.* Lancet, 1993. **342**(8878): p. 1024-5.
174. Weiner, T.M., et al., *Expression of growth factor receptors, the focal adhesion kinase, and other tyrosine kinases in human soft tissue tumors.* Ann Surg Oncol, 1994. **1**(1): p. 18-27.
175. Owens, L.V., et al., *Overexpression of the focal adhesion kinase (p125FAK) in invasive human tumors.* Cancer Res, 1995. **55**(13): p. 2752-5.
176. Cance, W.G., et al., *Immunohistochemical analyses of focal adhesion kinase expression in benign and malignant human breast and colon tissues: correlation with preinvasive and invasive phenotypes.* Clin Cancer Res, 2000. **6**(6): p. 2417-23.
177. Lu, Z., et al., *Epidermal growth factor-induced tumor cell invasion and metastasis initiated by dephosphorylation and downregulation of focal adhesion kinase.* Mol Cell Biol, 2001. **21**(12): p. 4016-31.
178. Sieg, D.J., et al., *FAK integrates growth-factor and integrin signals to promote cell migration.* Nat Cell Biol, 2000. **2**(5): p. 249-56.
179. Golubovskaya, V., et al., *Dual inhibition of focal adhesion kinase and epidermal growth factor receptor pathways cooperatively induces death receptor-mediated apoptosis in human breast cancer cells.* J Biol Chem, 2002. **277**(41): p. 38978-87.
180. Blume-Jensen, P. and T. Hunter, *Oncogenic kinase signalling.* Nature, 2001. **411**(6835): p. 355-65.
181. Trusolino, L. and P.M. Comoglio, *Scatter-factor and semaphorin receptors: cell signalling for invasive growth.* Nat Rev Cancer, 2002. **2**(4): p. 289-300.
182. Santoro, M.M., et al., *Constitutive activation of the RON gene promotes invasive growth but not transformation.* Mol Cell Biol, 1996. **16**(12): p. 7072-83.

183. Komada, M. and N. Kitamura, *The cell dissociation and motility triggered by scatter factor/hepatocyte growth factor are mediated through the cytoplasmic domain of the c-Met receptor.* Oncogene, 1993. **8**(9): p. 2381-90.
184. Rosen, E.M., S.K. Nigam, and I.D. Goldberg, *Scatter factor and the c-met receptor: a paradigm for mesenchymal/epithelial interaction.* J Cell Biol, 1994. **127**(6 Pt 2): p. 1783-7.
185. Engelman, J.A., et al., *MET amplification leads to gefitinib resistance in lung cancer by activating ERBB3 signaling.* Science, 2007. **316**(5827): p. 1039-43.
186. Lee, W.Y., et al., *Prognostic significance of co-expression of RON and MET receptors in node-negative breast cancer patients.* Clin Cancer Res, 2005. **11**(6): p. 2222-8.
187. Baselga, J. and S.D. Averbuch, *ZD1839 ('Iressa') as an anticancer agent.* Drugs, 2000. **60 Suppl 1**: p. 33-40; discussion 41-2.
188. von Minckwitz, G., et al., *A multicentre phase II study on gefitinib in taxane- and anthracycline-pretreated metastatic breast cancer.* Breast Cancer Res Treat, 2005. **89**(2): p. 165-72.
189. Albain, K., et al., *Open-label, phase II, multicenter trial of ZD1839 ('Iressa') in patients with advanced breast cancer.* Breast Cancer Research and Treatment, 2002. **76**(Suppl 1): p. A20.
190. Baselga, J., et al., *Phase II and tumor pharmacodynamic study of gefitinib in patients with advanced breast cancer.* J Clin Oncol, 2005. **23**(23): p. 5323-33.
191. Morelli, M.P., et al., *Sequence-dependent antiproliferative effects of cytotoxic drugs and epidermal growth factor receptor inhibitors.* Ann Oncol, 2005. **16 Suppl 4**: p. iv61-iv68.
192. Tubiana-Hulin, M., et al., *A multicenter, randomized, double-blind, parallel-group phase II study of gefitinib (IRESSA) or placebo in combination with docetaxel, as first-line treatment in patients with metastatic breast cancer. .* Breast Cancer Res Treat, 2007. **106: S69**.
193. Dennison, S.K., et al., *A phase II clinical trial of ZD1839 (Iressa) in combination with docetaxel as first-line treatment in patients with advanced breast cancer.* Invest New Drugs, 2007. **25**(6): p. 545-51.
194. Hoadley, K.A., et al., *EGFR associated expression profiles vary with breast tumor subtype.* BMC Genomics, 2007. **8**: p. 258.
195. Normanno, N., et al., *The MEK/MAPK pathway is involved in the resistance of breast cancer cells to the EGFR tyrosine kinase inhibitor gefitinib.* J Cell Physiol, 2006. **207**(2): p. 420-7.
196. Normanno, N., et al., *Breast cancer cells with acquired resistance to the EGFR tyrosine kinase inhibitor gefitinib show persistent activation of MAPK signaling.* Breast Cancer Res Treat, 2008. **112**(1): p. 25-33.
197. Pollack, V.A., et al., *Inhibition of epidermal growth factor receptor-associated tyrosine phosphorylation in human carcinomas with CP-358,774: dynamics of receptor inhibition in situ and antitumor effects in athymic mice.* J Pharmacol Exp Ther, 1999. **291**(2): p. 739-48.
198. Kaur, H., et al., *Toxicity and outcome data in a phase II study of weekly docetaxel in combination with erlotinib in recurrent and/or metastatic breast cancer (MBC).* J Clin Oncol, 2006. **24 (Suppl 18)**: p. Abstract 10623.
199. Dalle, S., et al., *Monoclonal antibodies in clinical oncology.* Anticancer Agents Med Chem, 2008. **8**(5): p. 523-32.

200. Goldstein, N.I., et al., *Biological efficacy of a chimeric antibody to the epidermal growth factor receptor in a human tumor xenograft model.* Clin Cancer Res, 1995. **1**(11): p. 1311-8.
201. Modi, S., et al., *A phase I study of cetuximab/paclitaxel in patients with advanced-stage breast cancer.* Clin Breast Cancer, 2006. **7**(3): p. 270-7.
202. Carey, L.A., et al., *TBCRC 001: EGFR inhibition with cetuximab added to carboplatin in metastatic triple-negative (basal-like) breast cancer.* J Clin Oncol, 2008. **26: May 20 supplement, abstr 1009**.
203. Lombardo, L.J., et al., *Discovery of N-(2-chloro-6-methyl- phenyl)-2-(6-(4-(2-hydroxyethyl)- piperazin-1-yl)-2-methylpyrimidin-4- ylamino)thiazole-5-carboxamide (BMS-354825), a dual Src/Abl kinase inhibitor with potent antitumor activity in preclinical assays.* J Med Chem, 2004. **47**(27): p. 6658-61.
204. Huang, F., et al., *Identification of candidate molecular markers predicting sensitivity in solid tumors to dasatinib: rationale for patient selection.* Cancer Res, 2007. **67**(5): p. 2226-38.
205. Hennequin, L.F., et al., *N-(5-chloro-1,3-benzodioxol-4-yl)-7-[2-(4-methylpiperazin-1-yl)ethoxy]-5- (tetrahydro-2H-pyran-4-yloxy)quinazolin-4-amine, a novel, highly selective, orally available, dual-specific c-Src/Abl kinase inhibitor.* J Med Chem, 2006. **49**(22): p. 6465-88.
206. Morgan, L., R.I. Nicholson, and S. Hiscox, *SRC as a therapeutic target in breast cancer.* Endocr Metab Immune Disord Drug Targets, 2008. **8**(4): p. 273-8.
207. Kowanetz, M. and N. Ferrara, *Vascular endothelial growth factor signaling pathways: therapeutic perspective.* Clin Cancer Res, 2006. **12**(17): p. 5018-22.
208. Khosravi Shahi, P., A. Soria Lovelle, and G. Perez Manga, *Tumoral angiogenesis and breast cancer.* Clin Transl Oncol, 2009. **11**(3): p. 138-42.
209. Linderholm, B.K., et al., *Significantly higher levels of vascular endothelial growth factor (VEGF) and shorter survival times for patients with primary operable triple-negative breast cancer.* Ann Oncol, 2009. **20**(10): p. 1639-46.
210. Ebos, J.M., et al., *Accelerated metastasis after short-term treatment with a potent inhibitor of tumor angiogenesis.* Cancer Cell, 2009. **15**(3): p. 232-9.
211. Deng, C.X. and R.H. Wang, *Roles of BRCA1 in DNA damage repair: a link between development and cancer.* Hum Mol Genet, 2003. **12 Spec No 1**: p. R113-23.
212. Drew, Y. and R. Plummer, *PARP inhibitors in cancer therapy: two modes of attack on the cancer cell widening the clinical applications.* Drug Resist Updat, 2009. **12**(6): p. 153-6.
213. Bryant, H.E. and T. Helleday, *Poly(ADP-ribose) polymerase inhibitors as potential chemotherapeutic agents.* Biochem Soc Trans, 2004. **32**(Pt 6): p. 959-61.
214. Dantzer, F., et al., *Involvement of poly(ADP-ribose) polymerase in base excision repair.* Biochimie, 1999. **81**(1-2): p. 69-75.
215. Wong, A.K., et al., *RAD51 interacts with the evolutionarily conserved BRC motifs in the human breast cancer susceptibility gene brca2.* J Biol Chem, 1997. **272**(51): p. 31941-4.
216. Boss, D.S., J.H. Beijnen, and J.H. Schellens, *Inducing Synthetic Lethality using PARP Inhibitors.* Curr Clin Pharmacol.
217. O'Shaughnessy, J., et al., *Efficacy of BSI-201, a poly (ADP-ribose) polymerase-1 (PARP1) inhibitor, in combination with gemcitabine/carboplatin (G/C) in*

patients with metastatic triple-negative breast cancer (TNBC): Results of a randomized phase II trial. J Clin Oncol 2009. **27:18s, 2009 (suppl; abstr 3)**

218. Brown, E.J., et al., *A mammalian protein targeted by G1-arresting rapamycin-receptor complex.* Nature, 1994. **369**(6483): p. 756-8.
219. Hay, N. and N. Sonenberg, *Upstream and downstream of mTOR.* Genes Dev, 2004. **18**(16): p. 1926-45.
220. O'Reilly, K.E., et al., *mTOR inhibition induces upstream receptor tyrosine kinase signaling and activates Akt.* Cancer Res, 2006. **66**(3): p. 1500-8.
221. Liu, T., et al., *Effect of mTOR inhibition on sensitivity of triple-negative breast cancer cells to epidermal growth factor inhibition.* J Clin Oncol, 2009. **Vol 27, No 15S (May 20 Supplement), 2009: 1055**.
222. Glynn, S.A., et al., *A new superinvasive in vitro phenotype induced by selection of human breast carcinoma cells with the chemotherapeutic drugs paclitaxel and doxorubicin.* Br J Cancer, 2004. **91**(10): p. 1800-7.
223. Roche, S., et al., *Development of a high-performance liquid chromatographic-mass spectrometric method for the determination of cellular levels of the tyrosine kinase inhibitors lapatinib and dasatinib.* J Chromatogr B Analyt Technol Biomed Life Sci, 2009.
224. Alban, A., et al., *A novel experimental design for comparative two-dimensional gel analysis: two-dimensional difference gel electrophoresis incorporating a pooled internal standard.* Proteomics, 2003. **3**(1): p. 36-44.
225. Chou, T.C. and P. Talalay, *Quantitative analysis of dose-effect relationships: the combined effects of multiple drugs or enzyme inhibitors.* Adv Enzyme Regul, 1984. **22**: p. 27-55.
226. Chou, T.C. and P. Talaly, *A simple generalized equation for the analysis of multiple inhibitions of Michaelis-Menten kinetic systems.* J Biol Chem, 1977. **252**(18): p. 6438-42.
227. Chou, T.C. and P. Talalay, *Analysis of combined drug effects: A new look at a very old problem.* Trends Pharmacol. Sci., 1983. **4**: p. 450 - 454.
228. Biosoft, *Calcusyn for Windows, Software for Dose Effect Analysis, Manual*. 1996 - 2005.
229. Chou, T.C., *The median-effect principle and the combination index for quantitation of synergism and antagonism*, in *Synergism and antagonism in chemotherapy*, T.C. Chou and D.C. Rideout, Editors. 1991, Academic Press: San Diego. p. pp. 61 - 102.
230. Chou, T.C. and J. Chou, *Dose-effect analysis with microcomputers: Quatitation of ED50, LD50, synergism, antagonism low-dose risk, receptor-ligand binding and enzyme kinetics.* 1987, Cambridge, UK: Manual and Software, Biosoft.
231. Chou, T.C., *Quantitation of synergism and antagonism of two or more drugs by computerised analysis.*, in *Synergism and antagonism in chemotherapy*, T.C. Chou and D.C. Rideout, Editors. 1991, Academic Press: San Diego. p. pp. 223 - 244.
232. Bland, J.M. and D.G. Altman, *Multiple significance tests: the Bonferroni method.* Bmj, 1995. **310**(6973): p. 170.
233. Konecny, G., et al., *Quantitative association between HER-2/neu and steroid hormone receptors in hormone receptor-positive primary breast cancer.* J Natl Cancer Inst, 2003. **95**(2): p. 142-53.

234. Chang, G.C., et al., *Molecular mechanisms of ZD1839-induced G1-cell cycle arrest and apoptosis in human lung adenocarcinoma A549 cells.* Biochem Pharmacol, 2004. **68**(7): p. 1453-64.
235. Peng, D., et al., *Anti-epidermal growth factor receptor monoclonal antibody 225 up-regulates p27KIP1 and induces G1 arrest in prostatic cancer cell line DU145.* Cancer Res, 1996. **56**(16): p. 3666-9.
236. Rimawi, M.F., et al., *Epidermal growth factor receptor expression in breast cancer association with biologic phenotype and clinical outcomes.* Cancer. **116**(5): p. 1234-42.
237. Magkou, C., et al., *Expression of the epidermal growth factor receptor (EGFR) and the phosphorylated EGFR in invasive breast carcinomas.* Breast Cancer Res, 2008. **10**(3): p. R49.
238. Nieto, Y., et al., *Prognostic significance of overexpression and phosphorylation of epidermal growth factor receptor (EGFR) and the presence of truncated EGFRvIII in locoregionally advanced breast cancer.* J Clin Oncol, 2007. **25**(28): p. 4405-13.
239. Hiwase, D.K., et al., *Dasatinib cellular uptake and efflux in chronic myeloid leukemia cells: therapeutic implications.* Clin Cancer Res, 2008. **14**(12): p. 3881-8.
240. Collins, D.M., et al., *Tyrosine kinase inhibitors potentiate the cytotoxicity of MDR-substrate anticancer agents independent of growth factor receptor status in lung cancer cell lines.* Invest New Drugs, 2009.
241. Maliepaard, M., et al., *Circumvention of breast cancer resistance protein (BCRP)-mediated resistance to camptothecins in vitro using non-substrate drugs or the BCRP inhibitor GF120918.* Clin Cancer Res, 2001. **7**(4): p. 935-41.
242. Hyafil, F., et al., *In vitro and in vivo reversal of multidrug resistance by GF120918, an acridonecarboxamide derivative.* Cancer Res, 1993. **53**(19): p. 4595-602.
243. Chu, I., et al., *Src promotes estrogen-dependent estrogen receptor alpha proteolysis in human breast cancer.* J Clin Invest, 2007. **117**(8): p. 2205-15.
244. O'Farrell, P.H., *High resolution two-dimensional electrophoresis of proteins.* J Biol Chem, 1975. **250**(10): p. 4007-21.
245. Marouga, R., S. David, and E. Hawkins, *The development of the DIGE system: 2D fluorescence difference gel analysis technology.* Anal Bioanal Chem, 2005. **382**(3): p. 669-78.
246. Unlu, M., M.E. Morgan, and J.S. Minden, *Difference gel electrophoresis: a single gel method for detecting changes in protein extracts.* Electrophoresis, 1997. **18**(11): p. 2071-7.
247. Otani, A., et al., *A fragment of human TrpRS as a potent antagonist of ocular angiogenesis.* Proc Natl Acad Sci U S A, 2002. **99**(1): p. 178-83.
248. Wakasugi, K., et al., *A human aminoacyl-tRNA synthetase as a regulator of angiogenesis.* Proc Natl Acad Sci U S A, 2002. **99**(1): p. 173-7.
249. Rubin, B.Y., et al., *Interferon induces tryptophanyl-tRNA synthetase expression in human fibroblasts.* J Biol Chem, 1991. **266**(36): p. 24245-8.
250. Berryman, M. and A. Bretscher, *Identification of a novel member of the chloride intracellular channel gene family (CLIC5) that associates with the actin cytoskeleton of placental microvilli.* Mol Biol Cell, 2000. **11**(5): p. 1509-21.

251. Qian, Y., et al., *Transaldolase deficiency influences the pentose phosphate pathway, mitochondrial homoeostasis and apoptosis signal processing.* Biochem J, 2008. **415**(1): p. 123-34.
252. Rual, J.F., et al., *Towards a proteome-scale map of the human protein-protein interaction network.* Nature, 2005. **437**(7062): p. 1173-8.
253. Zheng, X.M., et al., *Sequencing and expression of complementary DNA for the general transcription factor BTF3.* Nature, 1990. **344**(6266): p. 556-9.
254. Hirst, M., et al., *Human GMP synthetase. Protein purification, cloning, and functional expression of cDNA.* J Biol Chem, 1994. **269**(38): p. 23830-7.
255. Yuryev, A. and L.P. Wennogle, *Novel raf kinase protein-protein interactions found by an exhaustive yeast two-hybrid analysis.* Genomics, 2003. **81**(2): p. 112-25.
256. Ang, E.Z., et al., *Annexin-1 regulates growth arrest induced by high levels of estrogen in MCF-7 breast cancer cells.* Mol Cancer Res, 2009. **7**(2): p. 266-74.
257. Wang, J., et al., *Characterization of phosphoglycerate kinase-1 expression of stromal cells derived from tumor microenvironment in prostate cancer progression.* Cancer Res. **70**(2): p. 471-80.
258. Ray, R.B. and R. Steele, *Separate domains of MBP-1 involved in c-myc promoter binding and growth suppressive activity.* Gene, 1997. **186**(2): p. 175-80.
259. Shi, Z.Z., et al., *Mutations in the glutathione synthetase gene cause 5-oxoprolinuria.* Nat Genet, 1996. **14**(3): p. 361-5.
260. Rohde, M., et al., *Members of the heat-shock protein 70 family promote cancer cell growth by distinct mechanisms.* Genes Dev, 2005. **19**(5): p. 570-82.
261. Nirde, P., et al., *Heat shock cognate 70 protein secretion as a new growth arrest signal for cancer cells.* Oncogene. **29**(1): p. 117-27.
262. Alli, E., J.M. Yang, and W.N. Hait, *Silencing of stathmin induces tumor-suppressor function in breast cancer cell lines harboring mutant p53.* Oncogene, 2007. **26**(7): p. 1003-12.
263. Wanamaker, C.P. and W.N. Green, *Endoplasmic reticulum chaperones stabilize nicotinic receptor subunits and regulate receptor assembly.* J Biol Chem, 2007. **282**(43): p. 31113-23.
264. Cicchillitti, L., et al., *Comparative proteomic analysis of paclitaxel sensitive A2780 epithelial ovarian cancer cell line and its resistant counterpart A2780TC1 by 2D-DIGE: the role of ERp57.* J Proteome Res, 2009. **8**(4): p. 1902-12.
265. Papalouka, V., et al., *Muscle LIM protein interacts with cofilin 2 and regulates F-actin dynamics in cardiac and skeletal muscle.* Mol Cell Biol, 2009. **29**(22): p. 6046-58.
266. Salerno, M., et al., *Nm23-H1 metastasis suppressor expression level influences the binding properties, stability, and function of the kinase suppressor of Ras1 (KSR1) Erk scaffold in breast carcinoma cells.* Mol Cell Biol, 2005. **25**(4): p. 1379-88.
267. Natsumeda, Y., et al., *Two distinct cDNAs for human IMP dehydrogenase.* J Biol Chem, 1990. **265**(9): p. 5292-5.
268. He, Y., et al., *Identification of IMPDH2 as a tumor-associated antigen in colorectal cancer using immunoproteomics analysis.* Int J Colorectal Dis, 2009. **24**(11): p. 1271-9.

269. Blackwood, R.A. and J.D. Ernst, *Characterization of Ca2(+)-dependent phospholipid binding, vesicle aggregation and membrane fusion by annexins.* Biochem J, 1990. **266**(1): p. 195-200.
270. Liu, Q., et al., *[Expression of annexin I in human pancreatic cancer and the influence of its down-regulation on biology of this cancer].* Zhonghua Zhong Liu Za Zhi, 2007. **29**(10): p. 738-41.
271. Cao, Y., et al., *Loss of annexin A1 expression in breast cancer progression.* Appl Immunohistochem Mol Morphol, 2008. **16**(6): p. 530-4.
272. Konecny, G.E., et al., *Activity of the multikinase inhibitor dasatinib against ovarian cancer cells.* Br J Cancer, 2009. **101**(10): p. 1699-708.
273. Joly, E.C., et al., *TRiC-P5, a novel TCP1-related protein, is localized in the cytoplasm and in the nuclear matrix.* J Cell Sci, 1994. **107 (Pt 10)**: p. 2851-9.
274. Large, A.T., E. Kovacs, and P.A. Lund, *Properties of the chaperonin complex from the halophilic archaeon Haloferax volcanii.* FEBS Lett, 2002. **532**(3): p. 309-12.
275. Midorikawa, Y., et al., *Identification of genes associated with dedifferentiation of hepatocellular carcinoma with expression profiling analysis.* Jpn J Cancer Res, 2002. **93**(6): p. 636-43.
276. Skawran, B., et al., *Gene expression profiling in hepatocellular carcinoma: upregulation of genes in amplified chromosome regions.* Mod Pathol, 2008. **21**(5): p. 505-16.
277. Peters, D.G., et al., *Comparative gene expression analysis of ovarian carcinoma and normal ovarian epithelium by serial analysis of gene expression.* Cancer Epidemiol Biomarkers Prev, 2005. **14**(7): p. 1717-23.
278. Nibbe, R.K., et al., *Discovery and scoring of protein interaction subnetworks discriminative of late stage human colon cancer.* Mol Cell Proteomics, 2009. **8**(4): p. 827-45.
279. Ray, R.B., et al., *Human breast carcinoma cells transfected with the gene encoding a c-myc promoter-binding protein (MBP-1) inhibits tumors in nude mice.* Cancer Res, 1995. **55**(17): p. 3747-51.
280. Ejeskar, K., et al., *Introduction of in vitro transcribed ENO1 mRNA into neuroblastoma cells induces cell death.* BMC Cancer, 2005. **5**: p. 161.
281. Jiang, W., et al., *Constructing disease-specific gene networks using pair-wise relevance metric: application to colon cancer identifies interleukin 8, desmin and enolase 1 as the central elements.* BMC Syst Biol, 2008. **2**: p. 72.
282. Sartor, C.I., et al., *Role of epidermal growth factor receptor and STAT-3 activation in autonomous proliferation of SUM-102PT human breast cancer cells.* Cancer Res, 1997. **57**(5): p. 978-87.
283. Moasser, M.M., et al., *The tyrosine kinase inhibitor ZD1839 ("Iressa") inhibits HER2-driven signaling and suppresses the growth of HER2-overexpressing tumor cells.* Cancer Res, 2001. **61**(19): p. 7184-8.
284. Piechocki, M.P., et al., *Breast cancer expressing the activated HER2/neu is sensitive to gefitinib in vitro and in vivo and acquires resistance through a novel point mutation in the HER2/neu.* Cancer Res, 2007. **67**(14): p. 6825-43.
285. Neve, R.M., et al., *A collection of breast cancer cell lines for the study of functionally distinct cancer subtypes.* Cancer Cell, 2006. **10**(6): p. 515-27.
286. Yauch, R.L., et al., *Epithelial versus mesenchymal phenotype determines in vitro sensitivity and predicts clinical activity of erlotinib in lung cancer patients.* Clin Cancer Res, 2005. **11**(24 Pt 1): p. 8686-98.

287. Sharp, J.A., et al., *Identification and transcript analysis of a novel wallaby (Macropus eugenii) basal-like breast cancer cell line.* Mol Cancer, 2008. **7**: p. 1.
288. Hirata, A., et al., *HER2 overexpression increases sensitivity to gefitinib, an epidermal growth factor receptor tyrosine kinase inhibitor, through inhibition of HER2/HER3 heterodimer formation in lung cancer cells.* Cancer Res, 2005. **65**(10): p. 4253-60.
289. Krol, J., et al., *The transcription factor FOXO3a is a crucial cellular target of gefitinib (Iressa) in breast cancer cells.* Mol Cancer Ther, 2007. **6**(12 Pt 1): p. 3169-79.
290. Hegde, P.S., et al., *Delineation of molecular mechanisms of sensitivity to lapatinib in breast cancer cell lines using global gene expression profiles.* Mol Cancer Ther, 2007. **6**(5): p. 1629-40.
291. Crown, J., et al. *Lapatinib (L) plus Capecitabine (C) in HER2+ advanced breast cancer (ABC): report of updated efficacy and genearray data*. in *European Journal of Cancer Supplements*. 2007.
292. McKillop, D., et al., *Tumor penetration of gefitinib (Iressa), an epidermal growth factor receptor tyrosine kinase inhibitor.* Mol Cancer Ther, 2005. **4**(4): p. 641-9.
293. Mendelsohn, J. and Z. Fan, *Epidermal growth factor receptor family and chemosensitization.* J Natl Cancer Inst, 1997. **89**(5): p. 341-3.
294. Corkery, B., et al., *Epidermal growth factor receptor (EGFR) inhibition in triple-negative breast cancer (BrCa).* Jounal of Clinical Oncology, 2007. **25**(ASCO Annual Meeting Proceedings Part I): p. No. 18S.
295. Pegram, M.D., et al., *Rational combinations of trastuzumab with chemotherapeutic drugs used in the treatment of breast cancer.* J Natl Cancer Inst, 2004. **96**(10): p. 739-49.
296. Slamon, D., et al., *BCIRG 006: 2nd interim analysis phase III randomized trial comparing doxorubicin and cyclophosphamide followed by docetaxel (ACT) with doxorubicin and cyclophosphamide followed by docetaxel and trastuzumab (ACTH) with docetaxel, carboplatin and trastuzumab (TCH) in Her2neu positive early breast cancer patients.* San Antonio Breast Cancer Symposium, 2006. **abstr 52**.
297. Winer, E., et al., *Phase II multicenter study to evaluate the efficacy and safety of Tarceva (erlotinib, OSI- 774) in women with previously treated locally advanced or metastatic breast cancer.* Breast Cancer Research and Treatment, 2002. **76**: p. Abstract 445.
298. Kimura, F., et al., *Epidermal growth factor-dependent enhancement of invasiveness of squamous cell carcinoma of the breast.* Cancer Sci.
299. Sirohi, B., et al., *Platinum-based chemotherapy in triple-negative breast cancer.* Ann Oncol, 2008. **19**(11): p. 1847-52.
300. Chang, H.R., et al., *Preferential pathologic complete response (pCR) by triple-negative (-) breast cancer to neoadjuvant docetaxel (T) and carboplatin (C).* J Clin Oncol, 2008. **26: May 20 supplement; abstr 604**.
301. Carey, L.A., et al., *TBCRC 001: EGFR inhibition with cetuximab added to carboplatin in metastatic triple-negative (basal-like) breast cancer.* J Clin Oncol, 2008. **26: May 20 suppl; abstr 1009**(May 20 suppl; abstr 1009).
302. Cleator, S., W. Heller, and R.C. Coombes, *Triple-negative breast cancer: therapeutic options.* Lancet Oncol, 2007. **8**(3): p. 235-44.

303. Arslan, C., O. Dizdar, and K. Altundag, *Pharmacotherapy of triple-negative breast cancer.* Expert Opin Pharmacother, 2009. **10**(13): p. 2081-93.
304. Tian, X.S., et al., *Clinicopathologic and prognostic characteristics of triple-negative breast cancer.* Onkologie, 2008. **31**(11): p. 610-4.
305. Thike, A.A., et al., *Triple Negative Breast Cancer: Outcome Correlation With Immunohistochemical Detection of Basal Markers.* Am J Surg Pathol.
306. Liu, Y., et al., *Correlation effect of EGFR and CXCR4 and CCR7 chemokine receptors in predicting breast cancer metastasis and prognosis.* J Exp Clin Cancer Res. **29**: p. 16.
307. Cianfrocca, M. and L.J. Goldstein, *Prognostic and predictive factors in early-stage breast cancer.* Oncologist, 2004. **9**(6): p. 606-16.
308. Saez, R.A., W.L. McGuire, and G.M. Clark, *Prognostic factors in breast cancer.* Semin Surg Oncol, 1989. **5**(2): p. 102-10.
309. Boudny, V. and S. Nakano, *Src tyrosine kinase but not activated Ras augments sensitivity to taxanes through apoptosis in human adenocarcinoma cells.* Anticancer Res, 2003. **23**(1A): p. 7-12.
310. Vigneron, A., et al., *Src inhibits adriamycin-induced senescence and G2 checkpoint arrest by blocking the induction of p21waf1.* Cancer Res, 2005. **65**(19): p. 8927-35.
311. Irby, R.B., et al., *Activating SRC mutation in a subset of advanced human colon cancers.* Nat Genet, 1999. **21**(2): p. 187-90.
312. Sugimura, M., et al., *Mutation of the SRC gene in endometrial carcinoma.* Jpn J Cancer Res, 2000. **91**(4): p. 395-8.
313. Wang, N.M., et al., *No evidence of correlation between mutation at codon 531 of src and the risk of colon cancer in Chinese.* Cancer Lett, 2000. **150**(2): p. 201-4.
314. Nilbert, M. and E. Fernebro, *Lack of activating c-SRC mutations at codon 531 in rectal cancer.* Cancer Genet Cytogenet, 2000. **121**(1): p. 94-5.
315. Laghi, L., et al., *Lack of mutation at codon 531 of SRC in advanced colorectal cancers from Italian patients.* Br J Cancer, 2001. **84**(2): p. 196-8.
316. Irby, R.B. and T.J. Yeatman, *Role of Src expression and activation in human cancer.* Oncogene, 2000. **19**(49): p. 5636-42.
317. Mao, W., et al., *Activation of c-Src by receptor tyrosine kinases in human colon cancer cells with high metastatic potential.* Oncogene, 1997. **15**(25): p. 3083-90.
318. Mezquita, B., et al., *A novel intracellular isoform of VEGFR-1 activates Src and promotes cell invasion in MDA-MB-231 breast cancer cells.* J Cell Biochem. **110**(3): p. 732-42.
319. Guzman-Aranguez, A., et al., *Differentiation of human colon adenocarcinoma cells alters the expression and intracellular localization of annexins A1, A2, and A5.* J Cell Biochem, 2005. **94**(1): p. 178-93.
320. Shen, D., et al., *Decreased expression of annexin A1 is correlated with breast cancer development and progression as determined by a tissue microarray analysis.* Hum Pathol, 2006. **37**(12): p. 1583-91.
321. Patton, K.T., et al., *Decreased annexin I expression in prostatic adenocarcinoma and in high-grade prostatic intraepithelial neoplasia.* Histopathology, 2005. **47**(6): p. 597-601.
322. Xiao, G.S., et al., *Annexin-I as a potential target for green tea extract induced actin remodeling.* Int J Cancer, 2007. **120**(1): p. 111-20.

323. Wang, Y., et al., *Annexin-I expression modulates drug resistance in tumor cells.* Biochem Biophys Res Commun, 2004. **314**(2): p. 565-70.

LIST OF PUBLICATIONS AND PRESENTATIONS RELATED TO THIS RESEARCH

Publications:

1. **Epidermal growth factor receptor as a potential therapeutic target in triple-negative breast cancer.** B Corkery, J Crown, M Clynes, N O'Donovan. Annals of Oncology 2009 May; 20 (5):862-7; PMID: 19150933
    - **Annals of Oncology:** Impact Factor 4.875, ranked 23/132 oncology journals (Journal Citation Reports 2007, ISI)

Oral Presentations:

1. **Gefitinib enhances response to chemotherapy in triple-negative breast cancer (BrCa).** B Corkery, N O'Donovan, M Clynes, J Crown. Presented at **ECCO 14**, The European Cancer Conference, 23rd-27th September 2007, Barcelona, Spain.

Poster Presentations:

1. **Constitutive Activation of Src kinase as a Mechanism of Acquired Resistance to Dasatinib in Triple Negative Breast Cancer.** B. Corkery, J Crown, S. Roche, R. O'Connor, D. Tryfonopoulos, M. Clynes, N. O'Donovan. Absract 5066; Thirty-second Annual CTRC-AACR San Antonio Breast Cancer Symposium, Dec. 10-13, 2009.

2. **Gefitinib (G) synergistically potentiates the activity of carboplatin (P) and docetaxel (D) in triple negative breast cancer (TNBC).** B Corkery, N O'Donovan, M Clynes, J Crown. **33rd ESMO Conference,** Stockholm, September 12th-16th 2008.

3. **Preclinical evaluation of EGFR in triple negative breast cancer.** B Corkery, J Crown, M Clynes, N O'Donovan. **IACR Annual Meeting 2008**, Newcastle, Co. Down. February 29th-March 1st 2008.

4. **EGFR Inhibition in Triple-negative Breast Cancer Cell Lines.** B Corkery, N O'Donovan, M Clynes, J Crown. **IACR** (Irish Association for Cancer Research) **Annual Meeting 2007**, Cork March 2nd-3rd, 2007.

5. **Epidermal growth factor receptor (EGFR) inhibition in triple-negative breast cancer (BrCa).** B Corkery, N O'Donovan, M Clynes, J Crown. *Journal of Clinical Oncology*, **2007 ASCO Annual Meeting Proceedings** Part I. Vol 25, No. 18S (June 20 Supplement), 2007: 14071 (Abstract only)